Design of microfluidic flow cells for analysis of bacterial biofilms and identification of biofilm inhibitory strategies and compounds

Dissertation

zur Erlangung des Grades

Doktor der Naturwissenschaften

Am Fachbereich Biologie

der Johannes Gutenberg-Universität Mainz

Athanasios Gazanis

geb. am 18.04.1991 in Memmingen

Mainz, 2022

Dekan: Prof. Dr. Eckhard Thines

1. Berichterstatter: Prof. Dr. Ralf Heermann
2. Berichterstatter: [redacted]

Tag der mündlichen Prüfung: 23.09.2022

Eidesstattliche Erklärung

Ich versichere hiermit an Eides statt, dass die vorgelegte Dissertation von mir vollständig und ohne unerlaubte Hilfe angefertigt wurde. Des Weiteren erkläre ich, dass ich nicht anderweitig ohne Erfolg versucht habe, eine Dissertation einzureichen oder mich der Doktorprüfung zu unterziehen. Die folgende Dissertation liegt weder ganz, noch in wesentlichen Teilen einer anderen Prüfungskommission vor

Mainz, den 19.08.2022

Statutory Declaration

I declare that I have authored this thesis independently, that I have not used other than the declared sources/resources. As well I declare that I have not submitted a dissertation without success and not passed the oral exam. The present dissertation (neither the entire dissertation nor parts) has not been presented to another examination board.

Mainz, 19th August 2022

Table of content

Nomenclature

Deletion of genes are marked with a “Δ”. Integration of cassettes into the genome or resistance cassettes are marked with “::”. Antibiotic resistance is marked with a superscript R “Tet^R”. Promoter are marked with subscript P_{tral}.

Abbreviations

3D	Three-dimensional
A_{575}	Absorbance at 575 nm
A_{630}	Absorbance at 630 nm
A_{695}	Absorbance at 695 nm
ABC transporter	ATP binding cassette transporter
ABS	Acrylonitrile butadiene styrene
AHL	Acyl homoserine lactone
AHLs	Acyl homoserine lactones
ATP	Adenosine triphosphate
Br-HQNO	Brominated 2-Heptyl-4-hydroxyquinoline
CAD	Computer aided design
CAM	Computer aided manufacturing
cps	Counts per second
Cyclic AMP	Cyclic adenosine monophosphate
CF-PCR chip	Continuous flow polymerase chain reaction chip
CLSM	Confocal laser scanning microscope
CNC	Computerized numerical control
Cyclic-di-GMP	Cyclic diguanosine monophosphate
DAHS	Intermediate product of AHLs after catalysis by CeO_2 nanoparticles
DAHSL	Intermediate product of AHLs after catalysis by CeO_2 nanoparticles
DNA	Deoxyribonucleic acid
EPS	Extracellular polymeric substances
Fig.	Figure
HDPE	High density polyethylene
HPLC	High-performance liquid chromatography
HQNO	2-Heptyl-4-hydroxyquinoline
IC-CD	Ion chromatography – conductivity detection
IQS	Integrated quorum sensing
IR	Infrared
LC-ESI-QToF	Liquid chromatography-electrospray ionization-quadrupole time-of-flight
LC-HRMS	Liquid chromatography – High resolution mass spectrometry
LC-MS	Liquid chromatography – mass spectrometry
LSPR	Localized surface plasmon resonances
mAU	milli-Absorbance Units
MU	Miller Units
NMR	Nuclear magnetic resonance
NTA	Nitrilotriacetic acid
OD_{600}	Absorption at 600 nm
OLA	Oleylamine

ONPG	o-Nitrophenyl-β-D-galactopyranosid
OPPPs	Opportunistic premise plumbing pathogens
PAX peptides	Peptide-antimicrobial-*Xenorhabdus*
PC	Polycarbonate
PDMS	Polydimethylsiloxane
PE	Polyethylene
PES membranes	Polyethersulfone membranes
PETG	Polyethylene terephthalate
PLA	Polyactic acid
PMMA	Polymethyl methacrylate
PP	Polypropylene
PQS	*Pseudomonas* quinolone signal
PUR lacquer	Polyurethane lacquer
PVC	Polyvinylchloride
QQ	Quorum quenching
QS	Quorum sensing
RNA	Ribonucleic acid
ROS	Reactive oxygen species
RT	Room temperature
RTC	Real time clock
SCV	Small colony variants
SDS	Sodium dodecyl sulfate
TPU	Thermoplastic polyurethane
U.S.	United States of America
UPVC	Unplasticized polyvinyl chloride
USA	United States of America
USB	Universal serial bus
UV	Ultraviolet
X-Gal	5-bromo-4-chloro-3-indolyl-β-D-galactopyranoside

Summary

Bacterial biofilms are widespread and threaten health and the environment. Besides, biofilms cause severe financial losses in various industrial sectors. Biofouling, provoked by bacterial biofilms, is responsible for considerable damage, especially in the marine sector and drinking water supply systems. Due to the high tolerance against chemical agents as well as antibiotics by the bacteria present in a biofilm and the increasing antibiotic resistance, the demand for alternative solutions to treat bacterial biofilm formation is tremendous. Since biofilm formation is a consequence of bacterial communication named quorum sensing (QS), blocking this communication offers a promising non-biocidal alternative to classical treatments, a process termed quorum quenching (QQ). Thus, this work aimed to establish an effective tool to analyze the biofilm formation of marine and drinking water bacteria under native conditions and identify putative biofilm-preventing drugs as well as surfaces less susceptible to biofilm formation.

microfluidic flow cells are recommended for analyzing biofilms under native and realistic conditions. However, the analysis of biofilms could not be performed microscopically and macroscopically with the already available flow cell solutions. Therefore, as the first step of this work, prototypes of optimized microfluidic flow cells were designed and manufactured using CNC. These could be used for microscopic as well as macroscopic biofilm analyses.

It is already known that external factors such as the surfaces, the nutrient composition, and the bacterial community affect a bacterial biofilm. However, these studies were often only carried out with model organisms. The next step included the investigation of certain marine and drinking water bacteria. It was demonstrated that steel, in particular, positively influenced the biofilm formation of the marine bacterium *P. gallaeciensis*. A closer analysis of the composition of steel identified, among others, Fe^{2+} and Mn^{2+} as biofilm-inducing elements.

Furthermore, the studies on the influence of nutrient composition identified *B. nasdae* and *P. gallaeciensis* as producers of biofilm inhibiting and biofilm dispersing compounds, respectively. However, the chemical nature of these substances remains to be elucidated.

Entomopathogenic bacteria of the genera *Photorhabdus* and *Xenorhabdus* provide a large arsenal of secondary metabolites due to their complex life cycle. Therefore, these natural products were screened for the potential of biofilm inhibition leading to the identification of several compounds, such as phenylethylamides or xenofuranones, which inhibited the biofilm formation of several bacteria. Moreover, it could be shown that after the impregnation of plastic surfaces with selected compounds, the biofilm inhibiting effect did not diminish. Additionally, the phenylethylamides inhibited pyocyanin production in *P. aeruginosa*, which implied that the underlying mechanism could be QQ. As some natural products are known to act as QQ drugs, the potential QQ effect of natural products from entomopathogenic bacteria is discussed in this work.

Finally, classes of tungsten oxides and cerium oxides were investigated for their potential to inhibit biofilms. In this context, it was shown that the tungsten oxides exhibit a haloperoxidase-like function and photothermal activity. Furthermore, in applying the cerium oxides, besides the observable biofilm inhibition in Gram-negative bacteria, a novel mechanism of action was identified in *P. aeruginosa*. In this process, the HQNO was brominated, accompanied by reduced biofilm formation. It is assumed that tungsten oxides and cerium oxides also interfere with bacterial QS in Gram-negative bacteria.

In summary, the novel designed flow cells emerged to be highly suitable for future biofilm inhibitory drug research. Furthermore, different natural compounds and nanoparticle classes were identified as promising non-biocidal QQ drugs to prevent bacterial biofilm formation in various application areas in the future.

Zusammenfassung

Bakterielle Biofilme sind allgegenwärtig und bedrohen die Gesundheit als auch die Umwelt. Außerdem verursachen Biofilme in verschiedenen Industriezweigen schwere finanzielle Schäden. Biofouling, welches durch bakterielle Biofilme entsteht, ruft vor allem im maritimen Bereich und in Trinkwasserversorgungssystemen erhebliche Beeinträchtigungen hervor. Aufgrund der hohen Toleranz der im Biofilm vorhandenen Bakterien gegenüber chemischen Agenzien und Antibiotika, sowie der zunehmenden Antibiotikaresistenz, ist der Bedarf an alternativen Strategien, um bakterielle Biofilmbildung zu inhibieren, immens. Bakterielle Biofilmbildung ist eine Konsequenz von bakterieller Kommunikation, ein Prozess, der als „Quorum sensing“ (QS) bezeichnet wird. Die Unterbindung der bakteriellen Kommunikation, als „Quorum quenching“ (QQ) bezeichnet, bietet daher eine vielversprechende nicht-biozide Alternative zu klassischen Behandlungsmethoden. Ziel dieser Arbeit war es daher, ein effizientes Werkzeug zur Analyse der Biofilmbildung von marinen und Trinkwasserbakterien unter nativen Bedingungen zu entwickeln. Weiterhin sollten mögliche Wirkstoffe zur Vermeidung der Biofilmbildung sowie Oberflächen identifiziert werden, die für die Biofilmbildung weniger anfällig sind.

Die Analyse von Biofilmen unter naturnahen Bedingungen erfolgt üblicherweise in mikrofluidischen Durchflusszellen. Allerdings kann mit den herkömmlichen Durchflusszellen keine mikroskopische und makroskopische Biofilm-Analyse durchgeführt werden. Daher wurden im ersten Schritt dieser Arbeit Prototypen von optimierten mikrofluidischen Durchflusszellen entworfen und mittels CNC gefertigt. Diese wurden dann sowohl für die mikroskopische als auch die makroskopische Analyse verwendet.

Es ist bekannt, dass externe Faktoren wie Oberflächen, Nährstoffzusammensetzung des Mediums oder Bakteriengemeinschaft des Biofilms den Aufbau des Biofilms beeinflussen. Diese Studien wurden jedoch oft nur mit Modellorganismen durchgeführt. Daher wurden ausgewählte marine und Trinkwasserbakterien auf die Biofilmbildung unter verschiedenen Bedingungen untersucht. Es zeigte sich, dass vor allem Stahl die Biofilmbildung des Meeresbakteriums *P. gallaeciensis* positiv beeinflusst. Bei näherer Analyse der Zusammensetzung von Stahl wurden unter anderem Fe^{2+} und Mn^{2+} als Biofilm-induzierende Faktoren identifiziert.

Darüber hinaus wurden in den Untersuchungen zum Einfluss der Nährstoffzusammensetzung sowohl *B. nasdae* als auch *P. gallaeciensis* als Produzenten von biofilmhemmenden bzw. biofilmauflösenden Substanzen identifiziert. Die chemische Natur dieser Substanzen muss jedoch noch geklärt werden.

Entomopathogene Bakterien der Gattungen *Photorhabdus* und *Xenorhabdus* bieten aufgrund ihres komplexen Lebenszyklus ein großes Spektrum an verschiedenen Sekundärmetaboliten. Diese Naturstoffe wurden auf ihr Potenzial zur Biofilmhemmung hin untersucht, wobei unterschiedliche Verbindungen wie z.B. Phenylethylamide oder Xenofuranone identifiziert wurden, welche die Biofilmbildung verschiedener Bakterien inhibierten. Zudem konnte gezeigt werden, dass nach der Imprägnierung von Kunststoffoberflächen mit ausgewählten Substanzen die biofilmhemmende Wirkung nicht nachlässt. Ferner hemmten die Phenylethylamide die Pyocyaninproduktion in *P. aeruginosa*, was den Schluss zulässt, dass der zugrunde liegende Wirkmechanismus QQ sein könnte. Da bereits QQ-Naturstoffe bekannt sind, wird in dieser Arbeit die Möglichkeit eines potenziellen QQ-Wirkmechanismus von Naturstoffen aus entomopathogenen Bakterien diskutiert.

Weiterhin wurden verschiedene Klassen von Wolfram- und Ceroxiden auf ihr Potenzial zur Inhibierung von Biofilmbildung untersucht. Dabei zeigte sich, dass Wolframoxide eine Haloperoxidase-ähnliche Funktion und eine photothermische Aktivität ausüben. Bei der Anwendung der Ceroxide wurde neben der beobachteten Biofilmhemmung von Gram-negativen Bakterien auch ein neuartiger Wirkmechanismus auf *P. aeruginosa* identifiziert. Bei diesem Verfahren wurde das HQNO bromiert, was mit einer reduzierten Biofilmbildung einherging. Dies ließ die Vermutung zu, dass Wolfram- und Ceroxide ebenfalls das QS Gram-negativer Bakterien beeinflussen.

Zusammenfassend konnte im Rahmen dieser Arbeit gezeigt werden, dass die neuartig gestalteten Durchflusszellen für die zukünftige Entwicklung und Analyse von Biofilm-inhibierenden Wirkstoffen hervorragend geeignet sind. Weiterhin wurden verschiedene Naturstoffe und Nanopartikel-Klassen als vielversprechende nicht-biozide QQ-Wirkstoffe identifiziert, welche für die Inhibierung der bakteriellen Biofilmbildung in verschiedenen Anwendungsbereichen in Zukunft eingesetzt werden können.

1 Introduction

1.1 Bacterial biofilms – a complex way of life

1.1.1 Properties of bacterial biofilms

In nature, bacteria exist in two different lifestyles. These are the planktonic cells, which move freely, and the sessile counterparts, which together as a unit, form the so-called biofilm (Berlanga and Guerrero, 2016; Hall-Stoodley et al., 2004; van Gestel et al., 2015). The transfer process from one type of lifestyle to the other is bidirectional (McDougald et al., 2012). However, the biofilm lifestyle is the most widespread and successful way of life. Approximately up to 80% of the bacteria on earth are organized in biofilms (Flemming and Wuertz, 2019; Stoodley et al., 2002; Watnick and Kolter, 2000).

Unlike their free-swimming planktonic counterparts, bacteria in biofilms are mainly encountered on abiotic and biotic surfaces (Hall-Stoodley et al., 2004; Sweet et al., 2011; Yin et al., 2019). The transition between the surface and the liquid media offers perfect conditions for the adhesion and growth of the microorganisms (Donlan, 2002). In addition to the surface attachment, the bacteria are surrounded by a self-produced matrix consisting of extracellular polymeric substances (EPS) (Dunne, 2002; Muhammad et al., 2020; Roche et al., 2012). The EPS matrix mostly accounts for up to 90% of the total biofilm, while the embedded microorganisms represent only approximately 10% (Costerton et al., 1987; Flemming and Wingender, 2010). The EPS matrix not only ensures the stability and maintenance of the biofilm structure but also functions as a protective layer against external toxic agents, impacts, and forces (Flemming and Wingender, 2010; Penesyan et al., 2020; Sharma et al., 2019). Unlike planktonic cells, bacteria organized in biofilms can withstand extreme environments and survive under severe conditions due to the embedment in the EPS matrix (Van Houdt and Michiels, 2010; Yin et al., 2019). In fact, it is already widely known that the biofilm provides protection to bacteria from external influences such as extreme temperature, high pressure, lack of nutrients, high salt levels, UV exposure, high pH fluctuations, disinfectants, and treatment with various antibiotics (de Carvalho, 2017; Harrison et al., 2007; Hathroubi et al., 2017; Hoštacká et al., 2010; Hou et al., 2018; Kim and Chong, 2017; Marsden et al., 2017; Norwood and Gilmour, 2001; Peng et al.,

2002; Yin et al., 2019). Bacteria residing in a biofilm exhibit a 100 to 1000-fold increased resistance to antibiotics in contrast to their planktonic counterparts (Sharma et al., 2019). Moreover, the biofilm also shelters the bacteria from various predatory protozoa that ingest the bacteria and from various immunological response mechanisms of the host (Matz and Kjelleberg, 2005; Whiteley et al., 2001).

Besides the enhanced tolerances to environmental extremes, bacteria in biofilms also differ from planktonic cells in terms of gene expression (Costerton et al., 1995; Sánchez et al., 2019). In contrast to their planktonic counterparts, the expression of various genes is upregulated or downregulated in the bacteria embedded in the biofilm. The expression of genes coding, e.g., for the synthesis of secondary metabolites, the breakdown of iron or lipids, the transport of amino acids, or stress response, are upregulated in the biofilm. Genes that, in turn, are responsible for DNA repair appear to play a subordinate role in the biofilm, as they are downregulated (Berlanga and Guerrero, 2016; Guilhen et al., 2016; Nakamura et al., 2016; Rumbo-Feal et al., 2013).

A biofilm may consist of only one bacterial strain or several different bacterial species. Moreover, it is also likely that other organisms become part of a biofilm, such as archaea, algae, fungi, yeasts, and protozoa (Bogino et al., 2013; Costa-Orlandi et al., 2017; Muhammad et al., 2020; Raghupathi et al., 2018; Silva et al., 2014; Tomaras et al., 2003). The fact that a biofilm is composed of multiple cells frequently draws analogies to multicellular organisms (Penesyan et al., 2021). A certain division of labor can often be observed within a biofilm composed of multiple species. As a result, a surplus value is created for all participants since individual tasks, such as different metabolic pathways, do not have to be carried out by all. Single cells thus can specialize on one particular task and trade metabolites such as amino acids or various saccharides amongst each other rather than having to perform the burden of a double workload (Flemming et al., 2016; Fredrickson, 2015; van Gestel et al., 2015; Zelezniak et al., 2015). The consortium of the phototrophic cyanobacterium *Nostoc punctiforme* and the rock-growing fungus *Sarcinomyces petricola* is an exemplary case of a synergistic division of labor in a biofilm consisting of different organisms. Here, the bacteria supply the fungus with crucial nutrients, while the fungus, in return, distributes substantial metals obtained from the stone (Gorbushina and Broughton, 2009). Further, it might also be necessary that different types of metabolism are required in a biofilm since different electron acceptors are available due to spatial constraints. One example is the availability of oxygen in a biofilm. While the upper cell layers perform

aerobic metabolism, the sub-surface microorganisms, in turn, apply anaerobic metabolism. This kind of heterogeneity and division of labor is also known in biofilms consisting of only one species (Boles et al., 2004; Dragoš et al., 2018; Flemming et al., 2016; Kragh et al., 2016; von Ohle et al., 2010). Nevertheless, not only cooperation occurs between microorganisms in a biofilm, it also leads to competitive behavior. Using different tactics, the microorganisms attempt to prevent the competitors from gaining access to important nutrient sources or surfaces (Nadell et al., 2016; Rendueles and Ghigo, 2015). Therefore, the microorganisms strive to surpass the competition, e.g., by accelerated growth or by production of matrix components to prevent access to desired sectors (Pfeiffer et al., 2001; Schluter et al., 2015; Xavier and Foster, 2007). Furthermore, toxins and antibiotics have become more widespread as warfare strategies to keep the competition at bay and eliminate other species (Deschaine et al., 2018; Kobayashi and Ikemoto, 2019; Riley and Wertz, 2002; Schmitt and Breinig, 2006).

Even though biofilms can be beneficial and partly be used for new biotechnological applications, biofilms pose a significant threat to human health and generate high costs in various industrial fields such as food production, shipping, oil, water distribution systems, and medical facilities due to their tolerance of extreme conditions (Bott, 1998; Busscher and Der Mei, 1995; Galié et al., 2018; Garrett et al., 2008; Halabi et al., 2001; Kumar and Anand, 1998; Muhammad et al., 2020; Mukhi and Vishwanathan, 2022; Nemati et al., 2001; Yin et al., 2019). Furthermore, it is estimated that due to rising microbial resistance to antibiotics, the death toll will exceed 10 million annually by 2050 if alternative approaches are not considered (Rossi et al., 2020; Shallcross et al., 2015).

1.1.2 Initiation and development of bacterial biofilm formation and subsequent detachment

The regulation mechanisms that are responsible for initiating the formation of biofilms are diverse. Secondary messengers such as cyclic AMP and cyclic-di-GMP have a major role to contribute, in addition to different environmental parameters, such as extreme temperature, pH and oxygen levels, salt concentration, and UV irradiation. Moreover, bacterial communication, known as quorum sensing (QS), also has a

decisive influence on the formation of biofilms (Alotaibi and Bukhari, 2021; Amaning Danquah et al., 2020; Galié et al., 2018; Goller and Romeo, 2008; Hall-Stoodley et al., 2004; Lopez et al., 2010; Muhammad et al., 2020; O'Toole et al., 2000; Toyofuku et al., 2016).

Cyclic-di-GMP was initially identified in *Gluconoacetobacter xylinus* as an initiator of cellulose synthesis for the production of an extracellular cellulose matrix (Aloni et al., 1982; Cotter and Stibitz, 2007; Ross et al., 1987). Furthermore, cyclic-di-GMP was detected in other bacteria such as *Pseudomonas aeruginosa*, *Vibrio cholerae*, and *Salmonella enterica* and has been assigned a major role in the induction of biofilm formation (Hengge, 2009; Nair et al., 2017; Srivastava and Waters, 2012; Valentini and Filloux, 2016). In *P. aeruginosa*, cyclic-di-GMP leads to a reduction of motility of the bacteria as it binds to FleQ, which is a transcription factor that regulates the movement of flagella. Since flagellar rotation regulates the first step in biofilm formation in *P. aeruginosa*, biofilm initiation occurs (Baraquet and Harwood, 2013; Ha and O'Toole, 2015; Liang et al., 2007). Nevertheless, it is already known that cyclic-di-GMP intervenes and also acts in later phases of biofilm development. In *P. aeruginosa*, cyclic-di-GMP is indirectly involved in the final stage of biofilm development, referred to as dispersion (Ha and O'Toole, 2015; Nair et al., 2017; Roy et al., 2012; Yoon et al., 2002). As cyclic-di-GMP, cyclic AMP is a secondary messenger involved in the process of biofilm development. It was demonstrated in *P. aeruginosa* that cyclic AMP modifies the hydrophobicity of the cell surface, affecting the stage of the irreversible attachment. Moreover, it appears that cyclic AMP can affect the flagellar motor and thus regulate surface adhesion (Ono et al., 2014; Schniederberend et al., 2019).

The process of bacterial biofilm development can be split into five phases (Fig. 1.1). The first stage involves the reversible attachment of planktonic cells onto an aqueous surface. Irreversible adhesion subsequently occurs in the second step. During the third stage, the production of the extracellular matrix proceeds. This is followed by the maturation of the biofilm in the fourth phase and finally by the last step, referred to as detachment or dispersion (Berne et al., 2015; Hall-Stoodley et al., 2004; Hoffman et al., 2015; Limoli et al., 2015; Muhammad et al., 2020; O'Toole and Kolter, 1998; Rumbaugh and Sauer, 2020).

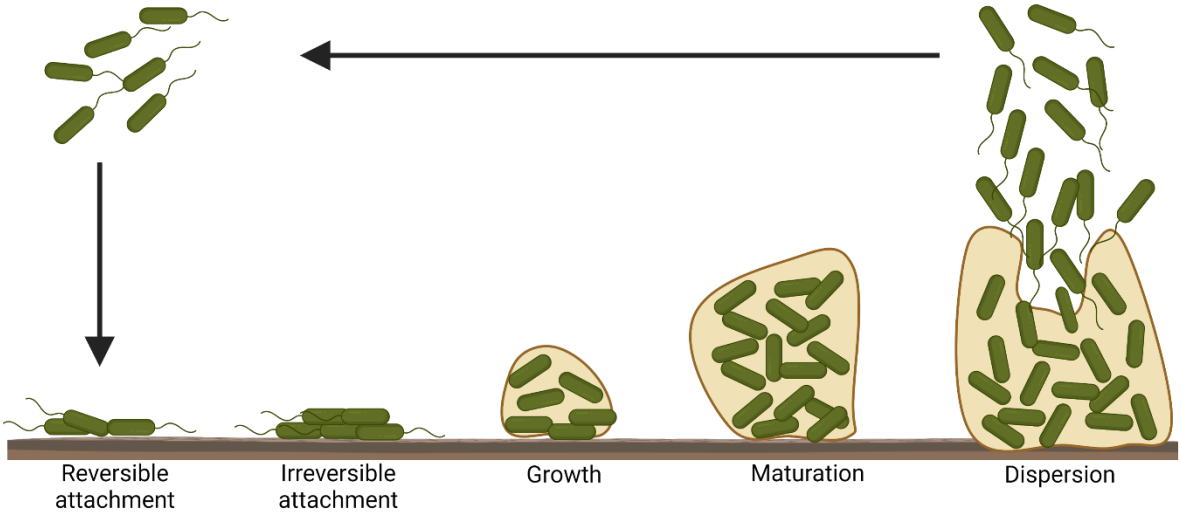

Fig. 1.1 The different steps of biofilm formation. Biofilm formation has five distinct steps: reversible attachment, irreversible attachment, growth, maturation, and dispersion. Modified from (Muhammad et al., 2020). Created with BioRender.com

Prior to the attachment of bacterial cells, however, a slight layer consisting of several molecules is formed on biotic and abiotic surfaces that are exposed to an aqueous solution, the so-called conditioning film (Bhagwat et al., 2021; Donlan, 2002; Loeb and Neihof, 1975; Muhammad et al., 2020; Tuson and Weibel, 2013). Such compounds may include various organic substances, for instance, polysaccharides, nucleic acids, lipids, proteins, glycoproteins, carbohydrates, amino acids, or exopolysaccharides (Ali et al., 2020; Bakker et al., 2004; Berman and Passow, 2007; Bhagwat et al., 2021; Compère et al., 2001; Jain and Bhosle, 2009; Rittle et al., 1990; Taylor et al., 1997). Those compounds may alter the surface tension, roughness, or even the chemical composition of the surface (Barth et al., 1989; Francius et al., 2017; Hogt et al., 1985; Oga et al., 1988; Xu and Logan, 2005). Thus, such conditioning films often represent an essential precondition for the formation of a complex microbial biofilm (Bhagwat et al., 2021; Cooksey and Wigglesworth-Cooksey, 1995).

The initial stage of biofilm generation commences with the attachment of planktonic cells to various surfaces. In this process, the bacteria might reach the surface either passively, such as by Brownian motion, deposition, or by the flow of the fluid, or actively, such as by, e.g., chemotaxis. The conditioning film on the surface can thereby provide a positive stimulus attracting the bacteria (Lawrence et al., 2015; Palmer et al., 2007; Porter et al., 2011; Vladimirov and Sourjik, 2009). Crucial for adhesion, however,

is the hydrophobicity of the material surface as well as the bacterial cell surface. This may differ from one bacterial genus to another, as it was shown that, e.g., *Streptococcus mutans* settles on surfaces with higher hydrophobicity, while, e.g., *Listeria monocytogenes* prefers to adhere to more hydrophilic surfaces (Chavant et al., 2002; Katsikogianni and Missirlis, 2004; Vacheethasanee et al., 1998; Yu et al., 2016). However, the adhering bacteria can detach at any time from the surface by own movement or by the shear forces of the fluid stream (Carniello et al., 2018; Li and Tang, 2009).

The second phase of biofilm development involves the irreversible attachment of the bacteria to the surfaces. Organelles such as flagella and pili or fimbriae are of key importance in this process. (Berne et al., 2015; Petrova and Sauer, 2012). In *L. monocytogenes*, mutants lacking flagella were shown to be unable to adhere to the surface during certain incubation durations, in contrast to the wild type (Vatanyoopaisarn et al., 2000). Besides it was observed that *Streptococcus pyogenes* in the absence of developed pili was unable to attach to the surface of human cells, such as mandelar epithelium or keratinocytes (Abbot et al., 2007; Beitelshees et al., 2018). Apart from flagella and fimbriae, however, non-fimbrial adhesins also participate in adherence to surfaces. In Gram-negative bacteria, non-fimbrial adhesins can be distinguished into two categories. First, non-fimbrial adhesins, which are released by a type 1 secretion system, and second, non-fimbrial adhesins, which are secreted by a type 5 secretion system (Berne et al., 2015; Chagnot et al., 2013; Gerlach and Hensel, 2007). Alongside the various adhesins, polysaccharides are also found to be involved in attachment to surfaces. Basically, these can be divided into capsular polysaccharides and extracellular polysaccharides. Briefly, capsular polysaccharides form a type of capsule which is affiliated with the bacterial cell surface. In contrast, extracellular polysaccharides are excreted into the environment (Berne et al., 2015; Guo et al., 2008; K.-J. Lee et al., 2013; Vozza et al., 2016; Whitney and Howell, 2013). For instance, in *P. aeruginosa*, the extracellular polysaccharides Pel and Psl take a significant part during the phase of attachment (Colvin et al., 2012). At this stage of biofilm development, QS additionally may have a tremendous impact on adherence (Abraham, 2016; Muhammad et al., 2020; Zhou et al., 2020).

Further, during the third phase of the biofilm process, the adherent bacterial cells initiate division, form so-called microcolonies, and produce the EPS (Muhammad et al., 2020; Toyofuku et al., 2016). In this regard, the extracellular polysaccharide Psl

has been shown to be instrumental in the organization of adherent cells into microcolonies in *P. aeruginosa* (Zhao et al., 2013). Along with polysaccharides, the EPS matrix also contains proteins, nucleic acids like extracellular DNA and RNA, lipids, lipopolysaccharides, and biopolymers such as humic substances. Humic matter is organic soil material, which can consist of proteins, carbohydrates, or lignin (Chatterjee and Chaudhuri, 2006; Flemming et al., 2016; Flemming and Wingender, 2010; Karygianni et al., 2020; Kelleher and Simpson, 2006; Poulin and Kuperman, 2021; Wingender et al., 1999). Furthermore, within the EPS matrix, flagella, pili, or fimbriae can be applied by the bacteria for stabilization reasons (Flemming and Wingender, 2010; Zogaj et al., 2001). However, depending on various environmental parameters, such as temperature or oxygen content, the EPS matrix composition may differ (Ahimou et al., 2007; Fang et al., 2013; Loustau et al., 2021; Toyofuku et al., 2016; Yawata et al., 2008). While mechanically stabilizing and shielding the bacteria from external extremes, the EPS matrix also serves as a water reservoir and carbohydrate store. In the EPS matrixes of, e.g., *Bacillus subtilis* and *P. aeruginosa*, water channels are incorporated to supply fresh nutrients to the cells and discard waste materials. Furthermore, nutrient-rich sources can be isolated and occupied through the EPS matrix. Additionally, a symbiotic relationship with animals and plants can be established and a genetic exchange among the microorganisms can occur. As a result, resistance genes to antibiotics, for instance, can be transferred via the EPS matrix (Acosta-Jurado et al., 2021; Costa et al., 2018; Flemming et al., 2007; Hu et al., 2019; Muhammad et al., 2020; Salama et al., 2016; Toyofuku et al., 2016; Yin et al., 2019).

The fourth phase of biofilm development is known as biofilm maturation. At this stage, strong global alterations in gene expression occur, as genes responsible for motility or the formation of adhesins and pili are down-regulated, and genes that promote sessile coexistence in a bacterial community, such as the transport of carbohydrates, are up-regulated (Beitelshees et al., 2018; Berlanga and Guerrero, 2016; Kostakioti et al., 2013; Muhammad et al., 2020). Up to 50% of proteins within the same bacterial species may differ between sessile cells embedded in a biofilm and the planktonic counterpart since a novel environment may arise within the biofilm and different concentrations of, e.g., nutrients, communication signals, or oxygen levels predominate (Sauer et al., 2002; Stewart and Franklin, 2008). Following the completion of biofilm maturation, the EPS matrix leads to spatially different gradients of nutrients and oxygen, which result in so-called heterogeneity and a particular division of labor within the bacterial cells

(Beitelshees et al., 2018; Penesyan et al., 2021; van Gestel et al., 2015). Once then the biofilm reaches a certain bulk, the exterior cell layer eventually departs from the mature biofilm (Dunne, 2002).

The final step in the process of biofilm growth is referred to as dispersion. At this stage, the bacterial cells depart the mature biofilm and head off to colonize new surfaces. Phenotypically, these cells differ from their sessile and planktonic counterparts (Chua et al., 2014; Singh et al., 2017; Uppuluri and Lopez-Ribot, 2016). Cell and particle detachment by mechanical impact, e.g., shear forces, can be passive. (Choi and Morgenroth, 2003; Loosdrecht et al., 1997). Beyond that, grazing is another cause of loss of biofilm mass. During this process, eukaryotic organisms and the biofilm-feeding protozoa nourish on the cells in the biofilm (Petrova and Sauer, 2016; Seiler et al., 2017; Stewart, 1993). Further reasons for a passive detachment include abrasion, erosion, and so-called sloughing. When abrasion occurs, parts of the biofilm become detached due to the collision of environmental particles. Conversely, in erosion, parts of the biofilm are removed by friction. The term sloughing describes the process where complete intact sections of the biofilm or even the entire biofilm is completely removed (Aqeel and Liss, 2022; Rochex et al., 2009; Rumbaugh and Sauer, 2020; Telgmann et al., 2004; Walter et al., 2013; Water Environment Federation, 2014). Contrary to this, dispersion refers to an active procedure in which the sessile cells abandon the biofilm due to environmental changes such as nutrient surplus, e.g., overflow of glutamate and iron, nutrient shortage, e.g., limitation of iron or carbon sources, increase of temperature, toxic product increase such as fermentation-formed acids, limitation of oxygen levels, pH-level changes or enzymatic degradation of the EPS matrix (Basu Roy and Sauer, 2014; Fleming and Rumbaugh, 2017; Gjermansen et al., 2010, 2005; Glick et al., 2010; Guilhen et al., 2017; Kaplan, 2010; Lanter et al., 2014; Lee and Yoon, 2017; Nguyen et al., 2015; Pettigrew et al., 2014; Reddinger et al., 2016; Serra and Hengge, 2014; Thormann et al., 2005; Uppuluri et al., 2010; Williamson et al., 2012). Additionally, the dispersion can also be initiated by internal signaling molecules, such as the concentration level of the secondary messenger cyclic-di-GMP within the biofilm or by the production of certain fatty acids (Davies and Marques, 2009; Dean et al., 2015; Dow et al., 2003; Kaplan, 2010; Marques et al., 2015; Wille and Coenye, 2020). Throughout this final stage of biofilm development, genes encoding motility, virulence, or EPS matrix degradation are upregulated, whereas genes responsible for adhesion and EPS matrix production are downregulated (Bridges et al., 2020; Kostakioti et al.,

2013; Pettigrew et al., 2014; Sauer et al., 2004; Toyofuku et al., 2016). However, dispersion from the mature biofilm, apart from the advantage of settlement on novel surfaces, also brings the disadvantage of surrendering certain attributes, such as tolerance to antimicrobial agents (Bester et al., 2005; Fleming and Rumbaugh, 2018; Rumbaugh and Sauer, 2020; Wille and Coenye, 2020). Nevertheless, detached bacteria often pose a threat, as dispersed cells from the biofilm often extend or intensify prevalent infections (Fleming and Rumbaugh, 2018; Marks et al., 2013). Cells of *P. aeruginosa* detached from the biofilm were capable of eliminating human macrophages, which are involved in phagocytosis, more efficiently than the planktonic variations (Chua et al., 2014).

1.2 Consequences of bacterial biofilms

1.2.1 Benefits of biofilms

Despite the risks, burdens, and threats, however, bacterial biofilms frequently find their use in biotechnological implementations due to their specific properties (Berlanga and Guerrero, 2016; Muhammad et al., 2020). For instance, biofilms can be grown in a controlled environment in specific bioreactors enabling the fermentation products generated by the biofilm cells, such as ethanol or lactic acid, to be subsequently obtained on a large industrial scale (Ercan and Demirci, 2015; Maksimova, 2014; Qureshi et al., 2005). Such special bioreactors are required to get access to particular bacterial compounds, as it could be demonstrated that, e.g., *Bacillus licheniformis* did not produce certain antimicrobial substances in liquid culture under shaking conditions but in special bioreactors within the biofilm (Morikawa, 2006; Yan et al., 2003). Another application sector suitable for deploying bacterial biofilms is sewage water processing and bioremediation. Due to their higher tolerance, the microorganisms within the biofilm help to degrade pollutants. Wastewater contains a large number of hazardous organic and inorganic compounds, which can be eliminated using technology that relies on biofilms. Frequently, bacterial metabolism is involved, which can break down the hazardous substances into harmless side products by using, e.g., specific enzymes. (Karigar and Rao, 2011; Naidoo and Olaniran, 2013; Turki et al., 2017; Van Dillewijn et al., 2009; Yamashita and Yamamoto-Ikemoto, 2014). Further applications

of bacterial biofilms can be found in agriculture. Due to their tolerance to drought, salt stress, or pH changes, biofilms offer several advantages and serve as biofertilizers. They increase the growth of the plants, thus improving the quality of the harvest. In addition, biofilms can act as a shield against pathogens (Das et al., 2017; Muhammad et al., 2020; Pandit et al., 2020; Premarathna et al., 2022).

1.2.2 Effects of bacterial biofilms on human health

Bacterial biofilms are, in fact, responsible for over 60% of bacterial infections and up to 80% of all chronic infections. In the USA alone, more than 1.7 million infections contracted in hospitals result from bacterial biofilms annually. It is evaluated that over 500.000 people die per year in the USA only due to the consequences of infections caused by bacterial biofilms (Fleming and Rumbaugh, 2017; Jamal et al., 2018; Lewis, 2001; Moscoso et al., 2009; Penesyan et al., 2021; Römling et al., 2014; VanEpps and Younger, 2016; Wi and Patel, 2018; Wolcott et al., 2010; Zhou et al., 2020). In many cases, infections caused by bacterial biofilms develop relatively slowly and cannot be controlled by antimicrobial treatments or the immune system (Vestby et al., 2020). Harmful biofilms mostly accumulate on the surfaces of medical devices or on living and dead host tissues (Dongari-Bagtzoglou, 2008; Guzmán-Soto et al., 2021; Koo et al., 2017; Wi and Patel, 2018). Such medical devices include, for example, pacemakers, catheters, contact lenses, orthopedic implants, heart valves, dental implants, breast implants, and tracheal tubes (Fig. 1.2) (Arciola et al., 2015; Beloin et al., 2017; Donlan, 2001; El-Ganiny et al., 2017; Guzmán-Soto et al., 2021; Jamal et al., 2018; Lebeaux et al., 2014; Murugan et al., 2016; Rieger et al., 2013; Santos et al., 2011; VanEpps and Younger, 2016; Veerachamy et al., 2014; Zimmerli and Sendi, 2017). The most abundant bacteria that can be encountered in biofilms on medical devices are *Enterococcus faecalis*, *Staphylococcus epidermidis*, *Staphylococcus aureus*, *Klebsiella pneumoniae*, and *P. aeruginosa*. Among the most frequent, particularly in developing countries, hospital-acquired infections, such as circulatory bloodstream infections, derive from *S. aureus* and *S. epidermidis*. Additionally, up to 2/3 of the bacterial infections that originate from implanted medical devices are the result of *Staphylococcus* species (M. Chen et al., 2013; Chessa et al., 2015; Darouiche, 2001; Donlan, 2001; Khatoon et al., 2018; Muhammad et al., 2020; Oliveira et al., 2018;

Rupp, 2014; Schroll et al., 2010; Zheng et al., 2018). *Staphylococcus* spec. are Gram-positive bacteria that often colonize human skin and mucosa (Baron, 1996; Rossi et al., 2020; Tong et al., 2015). Other infections and diseases that can arise due to colonization of bacterial biofilm on organs and tissues are, e.g., urethritis, osteomyelitis, endocarditis, bacterial vaginosis, cystic fibrosis, respiratory tract infections, otitis media, and oral diseases such as periodontitis and caries (Akyıldız et al., 2013; Filardo et al., 2019; Guzmán-Soto et al., 2021; Hamilos, 2019; Khatoon et al., 2018; Lebeaux et al., 2014; Masters et al., 2019; Muhammad et al., 2020; Southey-Pillig et al., 2005). For instance, in cystic fibrosis, a mutation in a gene encoding a transmembrane regulator leads to the formation of excessively thick and sticky mucus, which can subsequently be colonized by pathogenic bacteria. These include the bacteria *S. aureus*, *P. aeruginosa*, and the *Burkholderia cepacia* complex, with *P. aeruginosa* being crucial for chronic inflammation in later stages. It could be shown that epithelial cells affected by cystic fibrosis were significantly less capable of phagocytosis against *P. aeruginosa* than healthy epithelial cells (Bhagirath et al., 2016; Malhotra et al., 2019; Pier et al., 1997). In addition, *P. aeruginosa* also poses quite a threat in colonizing water-bearing pipes and forming biofilms in plumbing systems of hospitals, residential buildings, and office buildings. Together with *Mycobacterium avium*, *Legionella pneumophila*, *Acinetobacter baumanii*, *Aeromonas hydrophila*, *Stenotrophomonas maltophila*, and *Methylobacterium* spec., *P. aeruginosa* ranks among the so-called opportunistic premise plumbing pathogens (OPPPs), which can cause severe courses of bloodstream or respiratory infections such as bacterially provoked pneumonia or septicemia (Falkinham, 2015; Falkinham et al., 2015; Hayward et al., 2022; Kanamori et al., 2016; Loveday et al., 2014; Masaka et al., 2021; Szwetkowski and Falkinham, 2020). Pathogenic bacteria are also likely to spread directly on food or other surfaces that are involved in the food industry and form biofilms, meaning that diseases can be contracted by the consumption of bacterial biofilms (Camargo et al., 2017; Galié et al., 2018; Mizan et al., 2015). Besides, biofilms can also indirectly represent a health hazard. Due to colonization of, e.g., dental implants, corrosion might occur, and particles such as TiO_2 can eventually detach from the surface and cause inflammation in the oral cavity, e.g., peri-implantitis (Apaza-Bedoya et al., 2017; Mombelli et al., 2018; Noronha Oliveira et al., 2018).

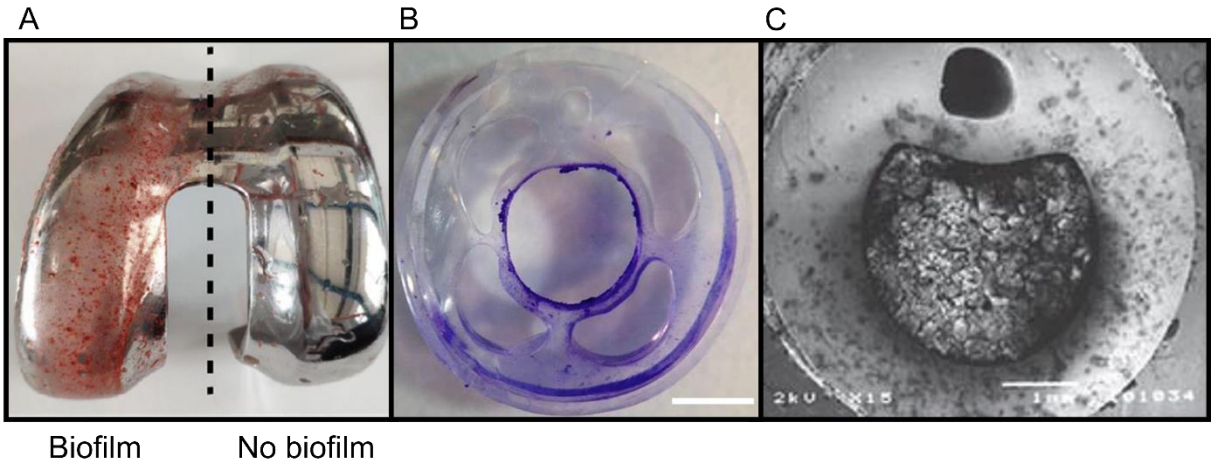

Fig. 1.2 Biofilm formation on various medical devices. (A) A knee prosthesis is covered on one side with biofilm. The biofilm was stained with Congo red. Modified from (Schoenmakers et al., 2021). (B) A prototype of a coated urinary catheter with biofilm presence. Modified from (Levering et al., 2016). (C) A cross-section of a silicone catheter. The interior area is exposed to biofilm. Modified from (Stickler, 2008).

1.2.3 Consequences of biofilms for the environment

Apart from endangering human health, biofilms also constitute an immense burden for a variety of environmental sectors (Muhammad et al., 2020; Vishwakarma, 2019). In aqueous environments, such as the marine one, biofilm formation can be the precursor to so-called biofouling (Fig. 1.3) (de Carvalho, 2018; Fletcher, 1994; Qian et al., 2022). Two types of fouling can be distinguished: microfouling and macrofouling. The former describes the attachment of, e.g., bacteria, microalgae, and diatoms. Macrofouling, on the other hand, refers to the attachment of larger organisms such as mussels, oysters, barnacles, or algae (Agostini et al., 2019; Cao et al., 2011; de Carvalho, 2018; Kanematsu and Barry, 2020). Bacteria of the *Rhodobacteriaceae* family, such as *Phaeobacter* spec., are well known to be primary colonizers of, e.g., harbor surfaces and thus able to initiate biofilm formation (Dang et al., 2008; de Carvalho, 2018; Garrity et al., 2015; Gram et al., 2015). Biofouling often occurs on man-made surfaces such as ship hulls or pipes (de Carvalho, 2018; Muhammad et al., 2020; Qian et al., 2022; Railkin, 2003). Due to fouling on hulls, surface roughness and friction are increased, resulting in additional fuel consumption to maintain the same speed. This, in turn, has a negative impact on the environment and climate change through increased CO_2 emissions (Demirel et al., 2017; Hakim et al., 2019; Schultz, 2007; Schultz et al., 2011). A further concern with biofouling on ship hulls is the spread of alien species, which

then compete with the native ones for special niches. Due to predation and competitiveness, the native ecosystem may no longer be in balance, impacting, therefore, the marine environment (Hakim et al., 2019; Minchin and Gollasch, 2003; Muhammad et al., 2020; Ulman et al., 2019).

However, biofouling can also pose issues on plastic surfaces. Fouling can impact the buoyancy of microplastics that are present in the ocean, causing the particles to sink and settle in the sediment. Another challenge of overgrown microplastics is the ingestion of the particles by, for example, oysters, which intend to feed on the bacteria and thus also indirectly ingest microplastics, which can have a negative effect on the metabolism and therefore lead to health concerns. Furthermore, microplastics can introduce alien species that pose a threat to native species due to transportation (Fabra et al., 2021; Kaiser et al., 2017; Lobelle and Cunliffe, 2011; Qian et al., 2022; Song et al., 2022).

Another major challenge associated with biofouling is the fouling of reverse osmosis membranes, which are used for the treatment and desalination of, e.g., wastewater and seawater (Fig. 1.3). Due to the microorganisms, clogging of the membrane can occur, which subsequently requires significantly more energy to purify the water or generally results in lower flow rates and reduced permeability. In addition, biofouling reduces the service lifetime of the membranes due to damages, requiring them to be exchanged more often. The formation of biofilms on such membranes is frequently initiated by *Sphingomonas* spec. (Abd El Aleem et al., 1998; Al-Abri et al., 2019; Bereschenko et al., 2010; Flemming, 2002; Maddah and Chogle, 2017; Matin et al., 2011).

Further environmental concerns caused by biofilms include microbially induced corrosion (Fig. 1.3). In this process, pipe materials such as metals or even concrete are damaged by the bacterial production of sulfuric acid or other corrosive metabolites or by electrons released from the metals. These kinds of damages can result in leakage of the pipe contents, causing an environmental hazard such as the 2006 Alaskan spill of 750,000 liters of oil due to biocorrosion. Another example of microbially induced corrosion is the 2015 leakage of 100,000 tons of methane (Chaudhari et al., 2022; Conley et al., 2016; Dou et al., 2021; Little et al., 2020).

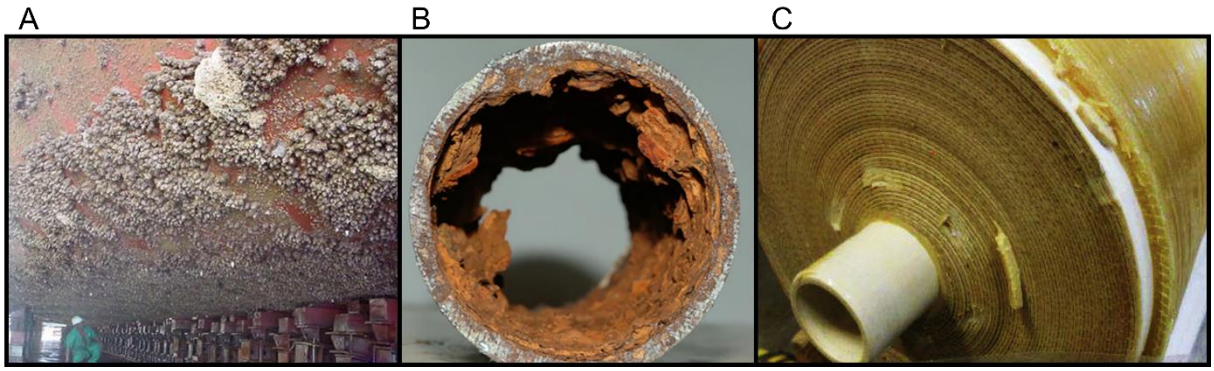

Fig. 1.3 Influence of biofilm and biofouling on a range of environmental domains. (A) A ship's hull affected by biofouling. The hull covered with barnacles was laid bare on the dry dock. Modified from (Callow and Callow, 2011). (B) A pipeline affected by microbially induced corrosion. The bacteria have contributed to the material damage. Modified from (Makhlouf and Botello, 2018). (C) A reverse osmosis membrane is subject to biofouling. Biofouling clogs the channels and results in dysfunctional membranes. Modified from (Voutchkov, 2017).

1.2.4 Economic consequences of biofilms

Besides affecting health and the environment, biofilms adversely impact healthcare and several industrial sectors in financial terms. Approximately the financial impact of biofilms globally is estimated to be almost $4,000 billion per year (Fig. 1.4) (Cámara et al., 2022; Hofer, 2022). In the U.S., up to 500,000 intravascular implant infections occur annually. For these, treatment costs can rise to as much as $56,000 per infection (M. Chen et al., 2013; Maki et al., 2006; Uçkay et al., 2009). In addition, hospital-acquired infections result in an approximate cost of over $11 billion in the U.S. alone (Römling et al., 2014; Wi and Patel, 2018). Collectively, the global healthcare system expense for infections attributed to biofilms approached $281 billion in 2017 (Cámara et al., 2022).

Apart from the healthcare system, other areas are also subject to biofilms, such as the food industry and water distribution (Cámara et al., 2022; Carrascosa et al., 2021; Chan et al., 2019; Fish et al., 2016; Galié et al., 2018). Thus, the estimated cost of an infection caused by OPPPs is about $500 million per year (Falkinham, 2015). Moreover, annual expenditures in the U.S. for foodborne pathogen infections are reported to be approximately $78 billion (Bai et al., 2021). Consumables in the EU

contaminated with *L. monocytogenes* cost the manufacturer about $30 million, including callback, transportation, and annihilation (Cámara et al., 2022).

Biofilms and biofouling generate high costs in the marine sector as well. In aquaculture, for example, biofouling leads to annual expenses of up to $3 billion (de Carvalho, 2018; Fitridge et al., 2012). In addition, fouled ship hulls require 15-20% more fuel to sustain velocity (Cámara et al., 2022; Farkas et al., 2020). Besides, biofouling on ship hulls costs the U.S. Navy roughly $56 million per year solely for the DDG-51 destroyer class (Schultz et al., 2011).

Latterly, the oil and gas sectors are also tormented by high financial burdens due to the formation of biofilms. Microbial-induced corrosion accounts for 20-30% of the corrosion cases in the oil and gas industry. Approximately 70-95% of leaking pipelines reportedly originate from microbial-induced corrosion (Cámara et al., 2022; de Carvalho, 2018; Skovhus et al., 2017). In total, corrosion contributes to two-thirds of the overall costs incurred by biofilm formation (Hofer, 2022).

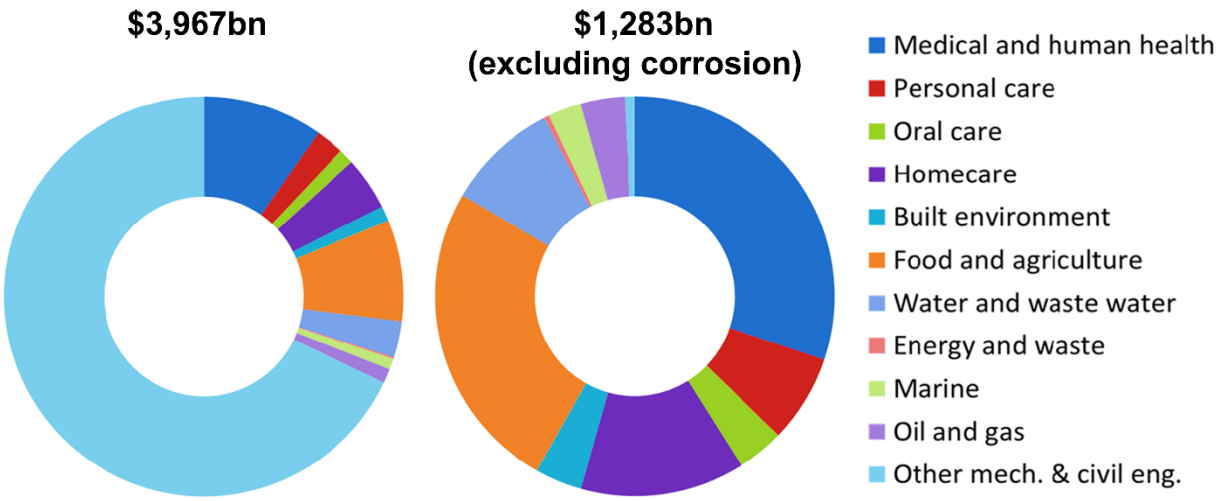

Fig. 1.4 The financial relevance of biofilms in different sectors. All affected sectors, including corrosion, are plotted on the left side of the pie charts. On the right side, the corrosion has been skipped for illustrative purposes. Modified from (Cámara et al., 2022).

1.3 Quorum sensing – the way of bacterial communication

The formation of bacterial biofilm is frequently regulated by cell-to-cell communication, referred to as QS. By means of QS, the entire bacterial population's behavior can be coordinated. Besides biofilm formation, these include, e.g., the production of secondary metabolites or the formation of common goods, bioluminescence, sporulation, the production of virulence factors, or even the generation of antibiotics. Initially, QS was studied based on the bioluminescence of the marine bacterium *Vibrio fischeri*. As QS is not lucrative for an individual bacterial cell, it only occurs above a threshold population cell density. The process of QS includes the synthesis, clearance, assembly, and sensing of extracellular signaling molecules, termed autoinducers (AIs). Receptors present in the bacteria can detect these signal molecules, thereby activating the expression of QS-controlled genes. Moreover, the expression of genes coding for the autoinducer synthase usually are also activated, resulting in an increased production and thus increased concentration levels of the signal molecules. Furthermore, bacteria can communicate not only within their own genus but often also across species, using different autoinducers. The QS systems among Gram-positive and Gram-negative bacteria are different, however, they have a similar mechanism and fulfill similar functions (Barnard et al., 2007; Bassler et al., 1994; Bassler and Losick, 2006; Bronesky et al., 2016; Coquant et al., 2020; de Kievit and Iglewski, 2000; Eickhoff and Bassler, 2018; Engebrecht et al., 1983; Liu et al., 2007; Miller and Bassler, 2001; Mukherjee and Bassler, 2019; Nealson et al., 1970; Ng and Bassler, 2009; Papenfort and Bassler, 2016; Pena et al., 2019; Rutherford and Bassler, 2012; Tobias et al., 2020; Waters and Bassler, 2005; Wu and Luo, 2021).

1.3.1 Quorum sensing in Gram-positive bacteria

In Gram-positive bacteria, peptides are used as AIs for QS. Initially, precursor peptides are produced by the ribosomes, which subsequently undergo various posttranslational modifications, such as isoprenylation, for e.g., improved stability (Le and Otto, 2015; Monnet and Gardan, 2015; Novick and Geisinger, 2008; Okada et al., 2017; Sturme et al., 2002; Verbeke et al., 2017). The peptide length can range from 5 to 17 amino acids. Furthermore, those peptides can be found in linear and cyclic forms (Bouillaut et al.,

2008; Okada et al., 2005; Rutherford and Bassler, 2012; Thoendel et al., 2011; Wu and Luo, 2021).

As the peptides are not membrane permeable, custom transporters are required. Consequently, release involves a membrane-bound ATP-binding cassette (ABC) transporter. In Gram-positive bacteria, the receptors consist of a two-component system featuring a membrane-bound histidine sensor kinase and a response regulator protein in the cytoplasm. Typical examples include the Fsr system in *E. faecalis* which is most likely responsible for the virulence and biofilm development, and the Agr system in *S. aureus*, which regulates pathogenesis. At a certain threshold, the peptides bind to the receptors, resulting in autophosphorylation of the histidine kinase. The phosphate group is then transferred to the response regulator protein. The phosphorylated response regulator protein then binds to the DNA and activates the expression of specific genes (Fig. 1.5). Additionally, self-induction occurs by activation of the genes encoding for precursors, transporters, receptors, and regulators. Moreover, peptides in *S. aureus* tend to show variability and have undergone evolution along with their corresponding receptors, enabling peptides from other strains to exhibit an inhibitory effect (Ali et al., 2022, 2017; Eickhoff and Bassler, 2018; Geisinger et al., 2009; Ji et al., 1995; Lyon et al., 2002; Michiels et al., 2001; Miller and Bassler, 2001; Monnet and Gardan, 2015; Ng and Bassler, 2009; Pinkston et al., 2011; Pomerantsev et al., 2009; Simon et al., 2007; Sturme et al., 2002; Verbeke et al., 2017; Waters and Bassler, 2005; Wu and Luo, 2021; Zschiedrich et al., 2016).

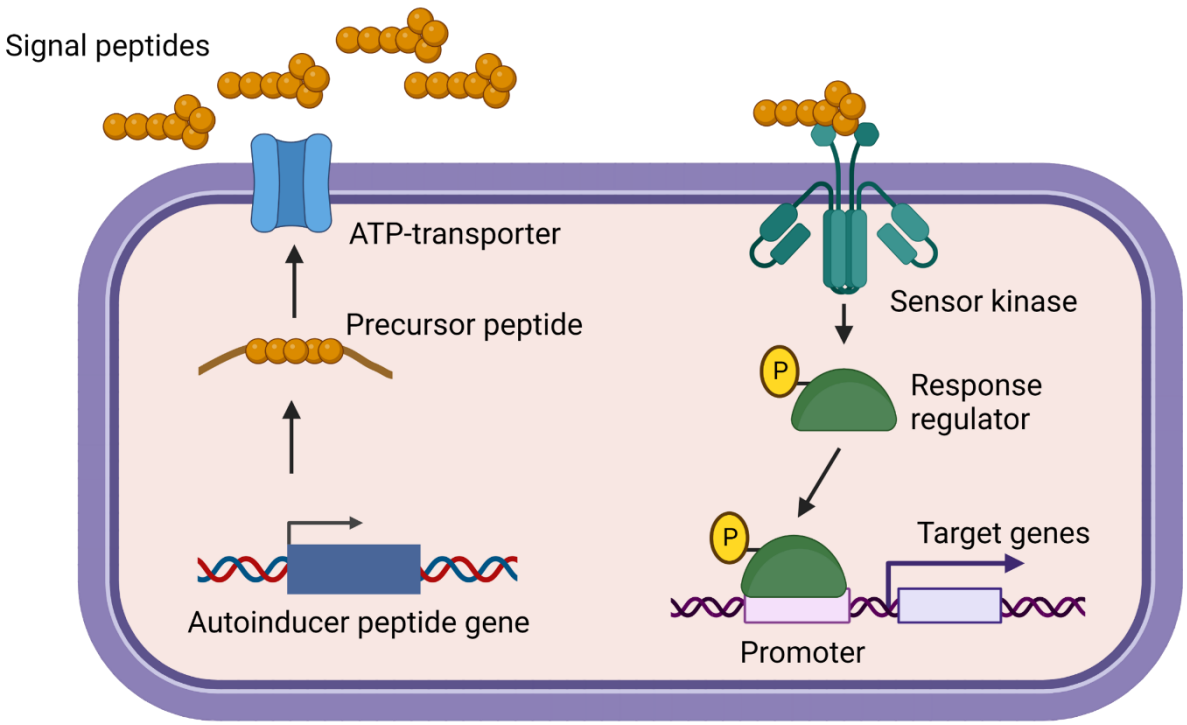

Fig. 1.5 The prototypical QS system of Gram-positive bacteria. In Gram-positive bacteria, peptides are used as signal molecules secreted by active export. When accumulated in the medium, the signal molecule is sensed by histidine sensor kinase. The sensor kinase then transfers the phosphoryl group to the cognate response regulator, which then binds to DNA and activates or deactivates the expression of specific genes. Modified from (Ng and Bassler, 2009; Sankar Ganesh and Ravishankar Rai, 2018). Created with BioRender.com

1.3.2 Quorum sensing in Gram-negative bacteria

In contrast to Gram-positive bacteria, the signaling molecules in Gram-negative bacteria belong largely to the category of so-called acyl homoserine lactones (AHLs). Those are characterized by an N-acylated homoserine lactone ring, which is linked to an acyl chain. The length of the chain may vary between 4 and 18 carbons, thus often influencing the stability. Moreover, various modifications at the C_3 position of the acyl chain might occur (Coquant et al., 2020; Galloway et al., 2011; Ng and Bassler, 2009; von Bodman et al., 2008; Wu and Luo, 2021).

QS-driven gene expression in Gram-negative bacteria often utilizes the regulatory LuxI/ LuxR system. It was first described in *V. fischeri*, and homologs were since then found in abundant different bacteria. In this process, the AHLs are synthesized by LuxI and subsequently released into the environment. Exceeding a certain autoinducer level

induces binding to the LuxR receptor with ensuing activation of specific genes (Fig. 1.6). Furthermore, activation of the genes encoding for the LuxI synthase and the LuxR receptor also takes place. Hence, a positive feedback loop is established, which is necessary for the synchronization within the bacterial population (Case et al., 2008; Coquant et al., 2020; Engebrecht and Silverman, 1984; Ng and Bassler, 2009; Parsek et al., 1999; Sifri, 2008; Verbeke et al., 2017).

Furthermore, LuxI synthases do not represent an exclusive way to synthesize AHLs. For example, in *Vibrio harveyi*, a LuxM synthase has been identified, which is not homologous to LuxI and is involved in the production of AHLs (Bassler et al., 1994, 1993; Ng and Bassler, 2009; Wu and Luo, 2021). In addition, bacteria also possess LuxR receptors without the corresponding LuxI synthase. Consequently, it is possible for bacteria to detect a signal molecule without synthesizing this substance on their own. These receptors are referred to as LuxR orphans or LuxR solos (Brameyer et al., 2014; Coquant et al., 2020; Hudaiberdiev et al., 2015; Patankar and González, 2009; Prescott and Decho, 2020; Subramoni and Venturi, 2009; Tobias et al., 2020).

However, there can be found bacteria that do not use AHLs for the QS system. For example, in the bacterial genus *Photorhabdus*, the QS system regulates cell clumping. For this purpose, *Photorhabdus luminescens* utilizes photopyrones as signal molecules, while *Photorhabdus asymbiotica*, a human-pathogenic bacterium, uses dialkylresorcinols. The photopyrones are synthesized by the synthase PpyS, while the dialkylresorcinols are produced by the *DarABC* operon (Brameyer, 2015; Brameyer and Heermann, 2016).

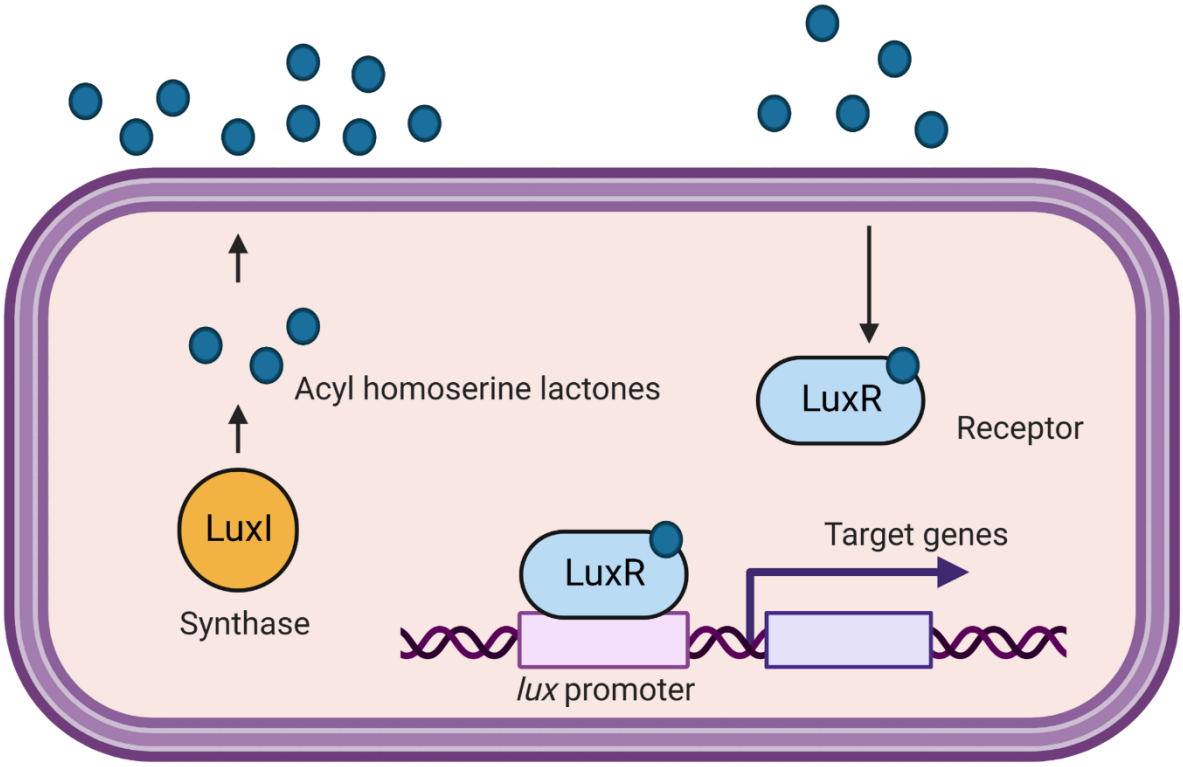

Fig. 1.6 The prototypical QS system of Gram-negative bacteria. LuxI synthase produces the acyl homoserine lactones, which diffuse out of the cell. At high accumulation, the AHLs bind to the LuxR receptor, which then binds to the promoter region of specific genes modulating gene expression. Modified from (Ng and Bassler, 2009; Sankar Ganesh and Ravishankar Rai, 2018). Created with BioRender.com

1.3.3 Quorum sensing in *Pseudomonas aeruginosa*

Besides the prototypical QS system of Gram-negative bacteria, the communication´s molecular mechanisms can deviate or be more complex. One example of a complex QS system is the Gram-negative opportunistic human pathogenic bacterium *P. aeruginosa*, which is frequently used as a model organism for biofilm formation (Ding et al., 2018; McDougald et al., 2008; Mulcahy et al., 2014; Tuon et al., 2022). Four diverse QS systems have been identified in *P. aeruginosa* until now, all of which are organized hierarchically (Fig.1.7) (J. Lee et al., 2013; Papenfort and Bassler, 2016).

Right at the top of the order is the *las* system. In this system, a LuxI/LuxR homolog is involved, which uses the 3-oxo-C_{12} homoserine lactone synthesized by LasI and sensed by LasR as a signal molecule. In addition to its own *lasI* synthase gene, the LasR-3-oxo-C_{12}-AHL complex activates the expression of *rhlI* and *rhlR*, which encode

the second *rhl* QS system. Furthermore, the expression of the genes *pqsABCDH* and *pqsR*, which encode the third PQS (*Pseudomonas* quinolone signal) QS system, are also induced. Finally, the fourth IQS (integrated quorum sensing) QS system is also affected by the *las* system if cultivation occurs in a rich medium. Additionally, the *las* system is involved in the formation of biofilm as well as being accountable for the production of virulence factors such as elastase, protease, and phospholipase C (Chugani and Greenberg, 2010; de Kievit, 2009; Déziel et al., 2004; Groleau et al., 2020; J. Lee et al., 2013; Lee and Zhang, 2015; Lee and Yoon, 2017; Malgaonkar and Nair, 2019; Papenfort and Bassler, 2016; Sakuragi and Kolter, 2007; Seed et al., 1995).

Similarly, the *rhl* system is also a LuxI/LuxR homolog. In this case, the signal molecule C_4-AHL is produced by the RhlI synthase and detected by the RhlR receptor. Likewise, that system is capable of autoinducing its own synthase *rhlI* gene, thus providing a loop. Furthermore, RhlR can inhibit the gene expression of *pqsABCDH* and *pqsR*, thereby blocking the PQS system. Besides biofilm formation, the *rhl* system is also involved in the production of further virulence factors, including rhamnolipids, phenazines, and pyocyanin (Cao et al., 2001; de Kievit et al., 2002; Ding et al., 2018; Groleau et al., 2020; Lau et al., 2004; Lee and Yoon, 2017; Malgaonkar and Nair, 2019; Mukherjee et al., 2017; Papenfort and Bassler, 2016; Soberón-Chávez et al., 2021; Ventre et al., 2003; Winson et al., 1995).

The third QS system is the PQS system. The signaling molecules here are not AHLs, but the 2-heptyl-3-hydroxy-4-quinolone (PQS). Quinolones are widely reported to have antibiotic properties, which in turn demonstrates that certain signaling molecules can fulfill multiple functions. Subsequently, the genes *pqsABCDE* encode for the synthesis of 2-heptyl-4-quinolone (HHQ), the precursor of PQS. Hydroxylation of HHQ is subsequently carried out with the enzyme PqsH, resulting in the formation of PQS. PQS binds to the receptor PqsR allowing the complex to activate the expression of several genes such as *rhlI* and *rhlR*. As a result, the PQS system acts as a link between the *rhl* and *las* QS systems. Moreover, the PQS system is considered responsible for biofilm formation and the synthesis of virulence factors (Allegretta et al., 2017; Cornforth and James, 1956; Heeb et al., 2011; Kostylev et al., 2019; Lee and Zhang, 2015; Lightbown and Jackson, 1956; Lin et al., 2018; McKnight et al., 2000; Papenfort and Bassler, 2016; Pesci et al., 1999; Pezzoni et al., 2015).

The fourth QS system, most recently described in *P. aeruginosa*, is known as IQS. This system can incorporate environmental stress into the QS network. The signal molecule consists of 2-(2-hydroxyphenyl)-thiazole-4-carbaldehyde and is synthesized by the expression of the gene cluster *ambBCDE*. Moreover, the IQS system is involved in the production of virulence factors such as pyocyanin, elastase, and rhamnolipids. In addition, under low phosphate conditions, the IQS system can replace the functions of the *las* system through the activation of IQS by the phosphate starvation protein PhoB (Eickhoff and Bassler, 2018; J. Lee et al., 2013; Lee and Zhang, 2015; Papenfort and Bassler, 2016).

Lastly, *P. aeruginosa* also carries a LuxR solo homolog, termed QscR, without corresponding synthase. This receptor has a broader ligand specificity and can therefore bind an array of AHLs such as C_8-AHL, C_{10}-AHL, 3-oxo-C_{10}-AHL, C_{12}-AHL, 3-oxo-C_{12}-AHL and C_{14}-AHL (Ding et al., 2018; Fuqua, 2006; Lee et al., 2006; Papenfort and Bassler, 2016).

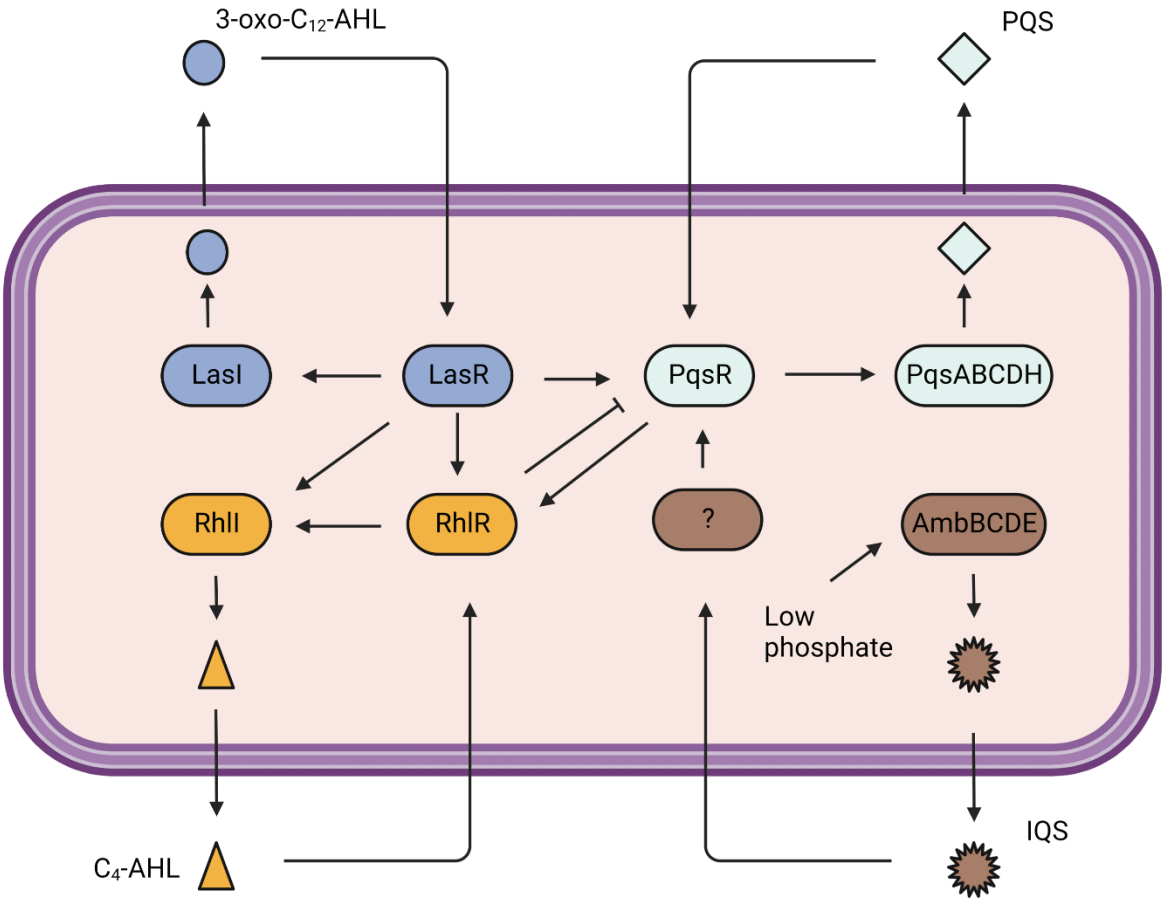

Fig. 1.7 QS in *Pseudomonas aeruginosa*. The QS system in *P. aeruginosa* contains four different mechanisms, which are arranged hierarchically. At the top is the Las system, which can control the other QS systems. Modified from (Papenfort and Bassler, 2016). Created with BioRender.com

1.4 Quorum quenching – the counterpart of quorum sensing

Due to the rising bacterial resistance to antibiotics, it is essential to explore alternatives. One option provides the interference of bacterial communication, known as quorum quenching (QQ). As there is no inhibition of bacterial growth, less selection pressure is applied, resulting in reduced resistance (Maeda et al., 2012; Paluch et al., 2020; Zhong and He, 2021).

QQ refers to a natural mechanism, which, however, has also found usage in various fields such as agricultural science, medicine, and various biotechnological applications (Bzdrenga et al., 2017; Dong et al., 2007; Grandclément et al., 2016).

There are several ways QQ can affect the QS system (Fig. 1.8). On the one hand, the synthesis of the autoinducer can be inhibited. On the other hand, inactivation or even

degradation of the signal molecule is another possible mechanism for QQ. While lactonases and acylases can degrade, e.g., AHLs, oxidases, and reductases merely modify the signal molecule. Further, blocking the transport of the signal molecule and using antagonists to prevent binding to the receptor is a further possible mechanism for QQ. Finally, prevention of signal transduction is another QQ approach, e.g., by blocking the formation of the signal molecule-receptor complex (Delago et al., 2016; Grandclément et al., 2016; Hornby et al., 2001; Lade et al., 2014; McInnis and Blackwell, 2011; Meschwitz et al., 2019; Ni et al., 2009; Paluch et al., 2020; Rampioni et al., 2014; Roy et al., 2010).

QQ thus represents a promising alternative for controlling bacterial infections and biofilms (F. Chen et al., 2013; Paluch et al., 2020; Zhou et al., 2020). The advantage of QQ is that no toxic substances are used, as has been the case in the past, and therefore bacterial growth is not affected. Furthermore, QQ might be an environmentally friendly alternative, which, unlike traditional methods, may not impact non-target organisms (Lade et al., 2014). In addition, using QQ exerts less selection pressure on the microorganisms than previous antimicrobial solutions (Beckmann et al., 2012; Maeda et al., 2012; Santhakumari and Ravi, 2019).

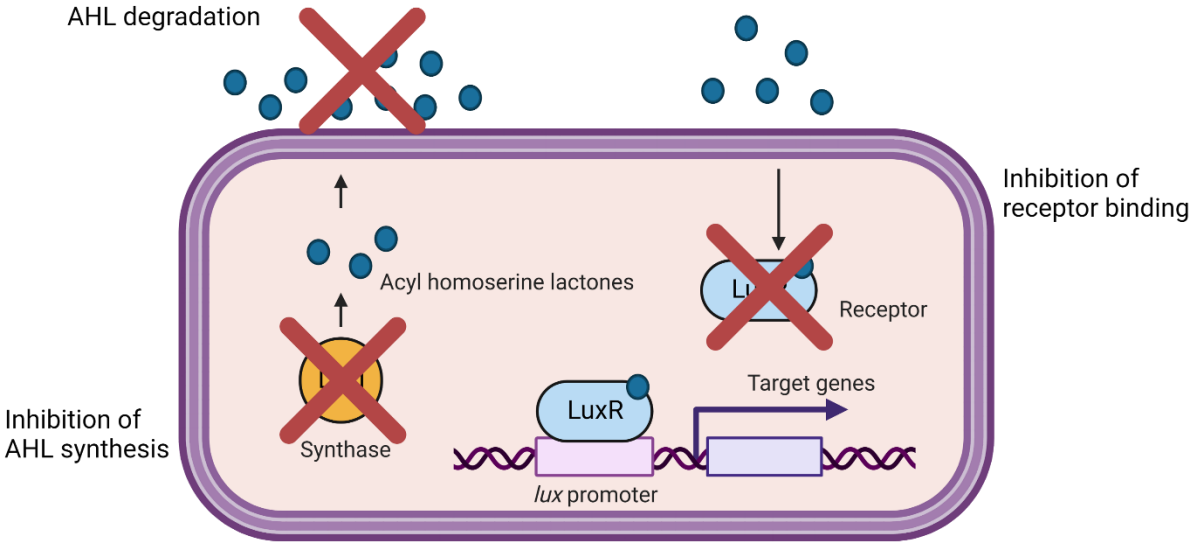

Fig. 1.8 Molecular mechanisms of QQ in Gram-negative bacteria. Either the production of the signal can be inhibited, the signal can be degraded, or an antagonist can prevent the signal molecule from binding to the receptor. Modified from (Paluch et al., 2020). Created with BioRender.com

1.5 Natural compounds from entomopathogenic bacteria as biofilm inhibitors

For the interruption of bacterial communication via QQ, natural substances often produced biologically as well as synthetically are applied (Carette et al., 2020; Paluch et al., 2020; Rossiter et al., 2017; Seghal Kiran et al., 2017).

The entomopathogenic bacteria of the genera *Photorhabdus* and *Xenorhabdus* belong to the family of the *Enterobacteriaceae* and display an extensive armory of secondary metabolites (Bode, 2009; Forst et al., 1997; Tobias et al., 2018). Besides, a wide range of biosynthetic gene clusters is projected in both genera for the synthesis of natural products, enabling the discovery of new active compounds (Bode, 2009; Chaston et al., 2011; Tobias et al., 2018).

Photorhabdus inhabits a symbiotic relationship with the nematode *Heterhorhabditis* (Waterfield et al., 2009), while *Xenorhabdus* is symbiotic with *Steinernema* nematodes (Han and Ehlers, 2000). During the infective juvenile phase, the nematodes infect the insects and deliver the bacteria into the hemocoel (Bode, 2009). Subsequently, the bacteria produce various natural compounds and toxins in order not only to kill the insect and to provide therefore nutrients but also to stop other competitive microorganisms from entering the carcass (Bode, 2009; Tobias et al., 2018). Once the nutrients are depleted, the nematodes reabsorb the bacteria and move on in search of further insects (Han and Ehlers, 2000; Tobias et al., 2016).

Since *Photorhabdus* features numerous LuxR solos, more than any further described bacterial genus (Brameyer, 2015; Brameyer and Heermann, 2016), and possesses a considerable repertoire of secondary metabolites (Bode, 2009), it can be assumed that *Photorhabdus* can sense and potentially influence the communication of various bacteria. Due to this fact, this work focused on the secondary metabolites from entomopathogenic bacteria.

1.6 Nanoparticles as a strategy to inhibit biofilm formation

Another promising novel approach to inhibit biofilms and thus reduce the harm to health is the use of nanotechnology. Based on the chemical and physical attributes, which are unique, as well as their antimicrobial characteristics, the effect of nanoparticles on microbial infections and bacterial surface settlement is under research. As a result, it is gaining more and more recognition in various fields, such as medicine, materials science, biomedical technology, and the food industry. For example, materials such as platinum, iron, silver, titanium, gold, and zinc are used extensively in biomedical diagnostics. Moreover, several metal oxide nanoparticles such as Fe_3O_4, ZnO, or even TiO_2 count among the most promising prospects. Furthermore, transition metal oxide nanoparticles such as FeO or CuO also exhibit a meaningful anti-bacterial activity (Alavi and Rai, 2019; Altaf et al., 2021; Asghar et al., 2020; Bhardwaj and Kaushik, 2017; Mirzaei et al., 2021; Paddle-Ledinek et al., 2006; Rau et al., 2017; Samuel and Guggenbichler, 2004; Shkodenko et al., 2020).

Apart from the above, there are first examples that nanoparticles can be applied to prevent bacteria directly or indirectly from communicating by using QQ (Elshaer and Shaaban, 2021; Hayat et al., 2019; Masurkar et al., 2012; Qais et al., 2018).

1.7 Scope of the thesis

Bacterial biofilms cannot only cause health hazards but also great damage to the environment. Furthermore, financial losses across different industrial sectors are substantial. The increasing antibiotic resistance results in a growing demand for alternatives. Moreover, to tackle biofilms, an analysis under realistic conditions is essential. Therefore, the main goal of this thesis is not only to develop a suitable microfluidic way to analyze biofilms microscopically and macroscopically but also to identify putative drugs for biofilm inhibition.

The first step should consist in designing and constructing optimized flow cells using CAD, compensating for the disadvantages of the microfluidic solutions already available in the state of the art. By using CNC milling, two different prototypes for microscopic and macroscopic biofilm analyses should be developed based on one precursor. Operating such a microfluidic system might provide a hint for further improvements and developments concerning process automatization.

As it is already known that different external factors can affect the formation of bacterial biofilm in model organisms and that the marine sector and drinking water supply heavily suffer from biofilms, the second part of this thesis should include the investigation of marine and drinking water bacteria involved in biofilm formation. For this purpose, the effect of nutrient composition, incubation period, surface materials, and the assembly of the biofilm itself should be analyzed. A closer examination of the constitution of the affected surface materials could provide insight into the extent to which bacterial biofilm formation may be accelerated by the commercial use of biofilm-prone surfaces.

Considering that in nature, the answer to biofilm formation is often already provided and that bacteria compete against each other, the next step should be the analysis of biofilm-forming bacteria from the marine and drinking water sectors regarding their ability to inhibit biofilms. Besides, it should be evaluated whether bacteria from these sectors are able to disperse an already existing biofilm. If an effect emerged to be evident, the properties of the potential agent should be analyzed, and the loss or retention of function should be documented using different procedures. This could provide further information on the nature of the respective candidate molecule.

As bacteria of the genera, *Photorhabdus* and *Xenorhabdus*, have a large repertoire of secondary metabolites due to their complex life cycles, the next step should include a screening of various natural products on their ability to inhibit biofilm in marine and drinking water bacteria. A variety of culture fluids from *Photorhabdus* and *Xenorhabdus* should be utilized for this purpose. Should compounds exhibit an effect on biofilm formation but no inhibiting or biocidal activity on planktonic cells, the virulence factor pyocyanin from *P. aeruginosa* should serve as a readout as this might give a hint on potential QQ as a putative molecular mode of action. In the case that natural substances that can inhibit biofilm formation could be discovered, it should be examined whether these substances retain an effect even after impregnation on plastic surfaces. A realistic drinking water simulation station should be used for this study. Additionally, a long-term experiment with pigment-coated plastic plates placed in the microfluidic setup could provide information on the durability of the impregnation.

The increasing application of nanoparticles to address biofilm formation should be explored as a further step by examining different tungsten oxide and cerium oxide nanoparticles as another biofilm suppression strategy. Should nanoparticles display an effect on biofilm formation but not affect planktonic cells, experiments with biosensors should provide insights into eventual QQ activity. In the case that QQ activity could be confirmed, the molecular mechanism should be enlightened by LC-MS analysis. Furthermore, the impact of nanoparticle-coated surfaces should be investigated.

2 Material and Methods

All chemicals used in this thesis had the highest degree of clarity and were labeled p.a. (pro analysis), which stands for analytically pure. Unless otherwise stated, the laboratory equipment and all the chemicals were obtained from Carl Roth (Karlsruhe), Merck (Darmstadt), or Thermo Fisher (USA).

2.1 Cultivation media and buffers used in this work

The cultivation media and the respective buffers used in this work are listed in Table 2.1.1.

Table 2.1.1 The cultivation media used in this work. The nutrient media were used both for cultivation of the bacteria and for biofilm formation.

Designation	Composition
LB	1% (w/v) tryptone, 0,5% (w/v) yeast extract, 1% (w/v) NaCl
2216	0,5% (w/v) peptone, 0,1% (w/v) yeast extract, 0,01% (w/v) $C_6H_5FeO_7$, 1,945% (w/v) NaCl, 0,59% (w/v) $MgCl_2$, 0,324% (w/v) Na_2SO_4, 0,18% (w/v) $CaCl_2$, 0,055% (w/v) KCl, 0,016% (w/v) $NaHCO_3$, 0,008% (w/v) KBr, 0,0034% (w/v) $SrCl_2$, 0,0022% (w/v) H_3BO_3, 0,0004% (w/v) sodium silicate, 0,00024% (w/v) NaF, 0,00016% (w/v) $(NH_4)NO_3$, 0,0008% (w/v) Na_2HPO_4
M1	0,5% (w/v) soy peptone, 0,3% meat extract
MM	1% (w/v) tryptone, 0,5% (w/v) yeast extract, 2,5% (w/v) NaCl
TSY	1,7% (w/v) casein peptone, 0,3% (w/v) soy peptone, 0,25% (w/v) glucose, 0,5% (w/v) NaCl, 0,25% (w/v) K_2HPO_4, 0,3% (w/v) yeast extract, pH = 7.0
RS	0,025% (w/v) K_2SO_4, 1% (w/v) $MgCl_2$, 1% (w/v) glucose, 0,01% (w/v) casamino acids, 0,5% (w/v) yeast extract, 0,3% (w/v) Tris, adjust pH with HCl to 7,3, after autoclaving addition of: 0,2% (v/v) trace element solution, 0,0005% (w/v) KH_2PO_4, 2 mM $CaCl_2$
Trace element solution for RS	0,04% (w/v) $ZnCl_2$, 0,2% (w/v) $FeCl_3$ x $6H_2O$, 0,01% (w/v) $CuCl_2$ x $2H_2O$, 0,01% (w/v) $MnCl_2$ x $4H_2O$, 0,01% (w/v) $Na_2B_4O_7$ x $10H_2O$, 0,01% (w/v) $(NH_4)_6Mo_7O_{24}$ x $4H_2O$
HD	1% (w/v) tryptone, 0,5% (w/v) yeast extract, 0,8% (w/v) NaCl, 0,5% (w/v) glucose, pH = 7
M9	0,4% (v/v) glucose, 1 mM $MgSO_4$, 0,3 mM $CaCl_2$, 0,75% (w/v) Na_2HPO_4, 0,3% (w/v) KH_2PO_4, 0,5% (w/v) NaCl, 0,5% (w/v) NH_4Cl

PBS	137 mM NaCl, 2,7 mM KCl, 10 mM Na_2HPO_4, 1,8 mM KH_2PO_4, pH = 7,4
Buffer Z	60 mM Na_2HPO_4, 40 mM NaH_2PO_4, 1 mM $MgSO_4$, 50 mM β-mercapto-EtOH

2.2 Bacterial strains and extracts used in this work

The bacterial strains used in this work and the resulting extracts are listed in Table 2.2.1.

Table 2.2.1 The microbes and the respective bacterial extracts used in this work.

Strain	Modification	Reference
Phaeobacter gallaeciensis DSM 26640	Wild type	(Ruiz-Ponte et al., 1998), (Buddruhs et al., 2013)
Phaeobacter inhibens DSM 16374	Wild type	(Martens et al., 2006), (Vandecandelaere et al., 2008), (Dogs et al., 2013)
Pseudomonas aeruginosa DSM 19882	Wild type	(He et al., 2004)
Staphylococcus aureus subsp. *aureus* DSM 11823	Wild type	(Schleifer and Kocur, 1973), (Wetzstein, 2005)
Sphingomonas adhaesiva DSM 7418	Wild type	(Yabuuchi et al., 1990), (Feng et al., 2018)
Sphingomonas pituitosa DSM 13101	Wild type	(Denner et al., 2001)
Brevundimonas nasdae DSM 100487	Wild type	(Li et al., 2004)
Brevundimonas diminuta DSM 7234	Wild type	(Segers et al., 1994)
Methylobacterium mesophilicum DSM 1708	Wild type	(Green and Bousfield, 1982)
Halotalea alkalilenta DSM 17697	Wild type	(Ntougias et al., 2007)
Halomonas aquamarina DSM 4739	Wild type	(Tindall, 2003)
Bacillus licheniformis DSM 1913	Wild type	(Gibson, 1944)
Exiguobacterium aurantiacum DSM 6209	Wild type	(Collins et al., 1983)

Agrobacterium tumefaciens A136	Lacking the Ti Plasmid; Insertion of pCF218-*traR* and pCF372-*traI*::*lacZ*; Tet^R, $Spec^R$	(Watson et al., 1975), (Zhu et al., 1998), (Tang et al., 2013)
Klebsiella pneumoniae subsp. *pneumoniae* DSM 4270	Wild type	(Spröer et al., 1999)
Escherichia coli DH10B MtaA-pCOLA-P_{ara}-P_{tacI}	Insertion of pCOLA with a P_{ara} and P_{tacI} promoter serving as a control	[redacted] (Goethe-Universität Frankfurt am Main)
Escherichia coli DH10B MtaA-pCX39	Insertion of pCX39 for the overproduction of secondary metabolite class xenortides	[redacted] (Goethe-Universität Frankfurt am Main)
Escherichia coli DH10B MtaA-pCX39	Insertion of pCX39 for the overproduction of secondary metabolite class of xenortides/tryptamines	[redacted] (Goethe-Universität Frankfurt am Main)
Escherichia coli DH10B MtaA-pCX4	Insertion of pCX4 for the overproduction of secondary metabolite class of nevaltophines	[redacted] (Goethe-Universität Frankfurt am Main)
Escherichia coli DH10B MtaA-pCX41	Insertion of pCX41 for the overproduction of secondary metabolite class of rhabdopeptides	[redacted] (Goethe-Universität Frankfurt am Main)
Escherichia coli DH10B MtaA-pCX41	Insertion of pCX41 for the overproduction of secondary metabolite class of rhabdopeptides/tryptamines	[redacted] (Goethe-Universität Frankfurt am Main)
Escherichia coli DH10B MtaA-pCX47	Insertion of pCX47 for the overproduction of secondary metabolite class of nematophines/tryptamines	[redacted] (Goethe-Universität Frankfurt am Main)
Escherichia coli DH10B MtaA-pCX65-pCX61	Insertion of pCX65 and pCX61 for the overproduction of secondary metabolite class of putrescines	[redacted] (Goethe-Universität Frankfurt am Main)
Escherichia coli DH10B MtaA-pCX71	Insertion of pCX71 for the overproduction of secondary metabolite class of leurhabdopeptides	[redacted] (Goethe-Universität Frankfurt am Main)
Photorhabdus luminescens subsp. *namnaonensis* PB45.5	Wild type	(Glaeser et al., 2017), (Machado et al., 2018)
Photorhabdus luminescens subsp. *namnaonensis* PB45.5 Δ*hfq*	Δ*hfq*	[redacted] (Goethe-Universität Frankfurt am Main)

Photorhabdus luminescens subsp. *namnaonensis* PB45.5 Δ*hfq* + pct83_145-147/1	Δ*hfq*; Production of secondary metabolite class of kollosins	[redacted] (Goethe-Universität Frankfurt am Main)
Photorhabdus luminescens subsp. *namnaonensis* PB45.5 Δ*hfq* + pct87_6/1	Δ*hfq*; Production of so far unknown secondary metabolites	[redacted] (Goethe-Universität Frankfurt am Main)
Photorhabdus luminescens subsp. *namnaonensis* PB45.5 Δ*hfq* + pct87_7/1	Δ*hfq*; Production of so far unknown secondary metabolites	[redacted] (Goethe-Universität Frankfurt am Main)
Photorhabdus luminescens subsp. *namnaonensis* PB45.5 Δ*hfq* + pct87_8-10/2	Δ*hfq*; Production of so far unknown secondary metabolites	[redacted] (Goethe-Universität Frankfurt am Main)
Photorhabdus luminescens subsp. *laumondii* TT01	Wild type	(Fischer-Le Saux et al., 1999)
Photorhabdus luminescens subsp. *laumondii* TT01 + *antJ*+++	Overexpression of *antJ*	[redacted] (Goethe-Universität Frankfurt am Main)
Photorhabdus luminescens subsp. *laumondii* TT01 Δ*antJ*	Δ*antJ*	[redacted] (Goethe-Universität Frankfurt am Main)
Photorhabdus luminescens subsp. *laumondii* TT01 Δ*hfq*	Δ*hfq*	[redacted] (Goethe-Universität Frankfurt am Main)
Photorhabdus luminescens subsp. *laumondii* TT01 Δ*hfq* pCEP-KM-*plu2670*	Δ*hfq*; Production of the secondary metabolite class of kolossins	[redacted] (Goethe-Universität Frankfurt am Main)
Photorhabdus luminescens subsp. *laumondii* TT01 Δ*hfq* pCEP-KM-*plu3130*	Δ*hfq*; Production of so far unknown secondary metabolites	[redacted] (Goethe-Universität Frankfurt am Main)
Photorhabdus luminescens subsp. *laumondii* TT01 Δ*hfq* pCEP-*plu1881*	Δ*hfq*; Production of the secondary metabolite class of glidobactins	[redacted] (Goethe-Universität Frankfurt am Main)
Photorhabdus luminescens subsp. *laumondii* TT01 Δ*hfq* pCEP-*plu3123*	Δ*hfq*; Production of the secondary metabolite class of ririwpeptides	[redacted] (Goethe-Universität Frankfurt am Main)
Photorhabdus luminescens subsp. *laumondii* TT01 Δ*hfq* pCEP-*plu3263*	Δ*hfq*; Production of the secondary metabolite class of GameXPeptides	[redacted] (Goethe-Universität Frankfurt am Main)

Xenorhabdus doucetiae DSM 17909	Wild type	(Tailliez et al., 2006)
Xenorhabdus doucetiae DSM 17909 Δ*hfq*	Δ*hfq*	[redacted] (Goethe-Universität Frankfurt am Main)
Xenorhabdus doucetiae DSM 17909 Δ*hfq* pBAD 70082	Δ*hfq*; Production of so far unknown secondary metabolites	[redacted] (Goethe-Universität Frankfurt am Main)
Xenorhabdus doucetiae DSM 17909 Δ*hfq* pBAD DC	Δ*hfq*; Production of the secondary metabolite class of phenylethylamides/tryptamides	[redacted] (Goethe-Universität Frankfurt am Main)
Xenorhabdus doucetiae DSM 17909 Δ*hfq* pBAD *gxpsA*	Δ*hfq*; Production of the secondary metabolite class of GameXPeptides	[redacted] (Goethe-Universität Frankfurt am Main)
Xenorhabdus doucetiae DSM 17909 Δ*hfq* pBAD XabA	Δ*hfq*; Production of the secondary metabolite class of xenoamicins	[redacted] (Goethe-Universität Frankfurt am Main)
Xenorhabdus doucetiae DSM 17909 Δ*hfq* pBAD XacA	Δ*hfq*; Production of the secondary metabolite class of xenoautocins	[redacted] (Goethe-Universität Frankfurt am Main)
Xenorhabdus doucetiae DSM 17909 Δ*hfq* pBAD_PAX-KM	Δ*hfq*; Production of the secondary metabolite class of PAX peptides	[redacted] (Goethe-Universität Frankfurt am Main)
Xenorhabdus doucetiae DSM 17909 Δ*hfq* pBAD_*xcnA*-KM	Δ*hfq*; Production of the secondary metabolite class of xenocoumacins	[redacted] (Goethe-Universität Frankfurt am Main)
Xenorhabdus doucetiae DSM 17909 Δ*hfq* pBAD_*xrdA*-KM	Δ*hfq*; Production of the secondary metabolite class of xenorhabdins	[redacted] (Goethe-Universität Frankfurt am Main)
Xenorhabdus nematophila DSM 3370	Wild type	(Thomas and Poinar, 1979)
Xenorhabdus nematophila DSM 3370 Δ*hfq*	Δ*hfq*	[redacted] (Goethe-Universität Frankfurt am Main)
Xenorhabdus nematophila DSM 3370 Δ*hfq* PAX	Δ*hfq*; Production of the secondary metabolite class of PAX peptides	[redacted] (Goethe-Universität Frankfurt am Main)
Xenorhabdus nematophila DSM 3370 Δ*hfq* PAX	Δ*hfq*; Production of the secondary metabolite class of PAX peptides	[redacted] (Goethe-Universität Frankfurt am Main)
Xenorhabdus nematophila DSM 3370 Δ*hfq* pCEP-KM-Xenoamicine	Δ*hfq*; Production of the secondary metabolite class of PAX peptides	[redacted] (Goethe-Universität Frankfurt am Main)
Xenorhabdus nematophila DSM 3370 Δ*hfq* pCEP-KM-Xenocoumacine	Δ*hfq*; Production of the secondary metabolite class of xenocoumacins	[redacted] (Goethe-Universität Frankfurt am Main)

Xenorhabdus nematophila DSM 3370 Δ*hfq* pCEP-KM-Xenortide	Δ*hfq*; Production of the secondary metabolite class of xenortides	[redacted] (Goethe-Universität Frankfurt am Main)
Xenorhabdus nematophila DSM 3370 Δ*hfq* pCEP-KM-Xenotetrapeptide	Δ*hfq*; Production of the secondary metabolite class of xenotetrapeptides	[redacted] (Goethe-Universität Frankfurt am Main)
Xenorhabdus szentirmaii DSM 16338	Wild type	(Lengyel et al., 2005)
Xenorhabdus szentirmaii DSM 16338 Δ*hfq*	Δ*hfq*	[redacted] (Goethe-Universität Frankfurt am Main)
Xenorhabdus szentirmaii DSM 16338 Δ*hfq* pCEP-KM-0346	Δ*hfq*; Production of the secondary metabolite class of GameXPeptides	[redacted] (Goethe-Universität Frankfurt am Main)
Xenorhabdus szentirmaii DSM 16338 Δ*hfq* pCEP-KM-0377	Δ*hfq*; Production of so far unknown secondary metabolites	[redacted] (Goethe-Universität Frankfurt am Main)
Xenorhabdus szentirmaii DSM 16338 Δ*hfq* pCEP-KM-1979	Δ*hfq*; Production of the secondary metabolite class of dipeptides	[redacted] (Goethe-Universität Frankfurt am Main)
Xenorhabdus szentirmaii DSM 16338 Δ*hfq* pCEP-KM-3397	Δ*hfq*; Production of the secondary metabolite class of rhabdopeptides	[redacted] (Goethe-Universität Frankfurt am Main)
Xenorhabdus szentirmaii DSM 16338 Δ*hfq* pCEP-KM-3460	Δ*hfq*; Production of the secondary metabolite class of szentiamides	[redacted] (Goethe-Universität Frankfurt am Main)
Xenorhabdus szentirmaii DSM 16338 Δ*hfq* pCEP-KM-3663	Δ*hfq*; Production of so far unknown secondary metabolites	[redacted] (Goethe-Universität Frankfurt am Main)
Xenorhabdus szentirmaii DSM 16338 Δ*hfq* pCEP-KM-3680	Δ*hfq*; Production of the secondary metabolite class of xenobactins	[redacted] (Goethe-Universität Frankfurt am Main)
Xenorhabdus szentirmaii DSM 16338 Δ*hfq* pCEP-KM-3942	Δ*hfq*; Production of the secondary metabolite class of rhabduscins	[redacted] (Goethe-Universität Frankfurt am Main)
Xenorhabdus szentirmaii DSM 16338 Δ*hfq* pCEP-KM-5118	Δ*hfq*; Production of the secondary metabolite class of jenamidins	[redacted] (Goethe-Universität Frankfurt am Main)
Xenorhabdus szentirmaii DSM 16338 Δ*hfq* pCEP-KM-*fclC*	Δ*hfq*; Production of the secondary metabolite class of fabclavins	[redacted] (Goethe-Universität Frankfurt am Main)
Xenorhabdus szentirmaii DSM 16338 Δ*hfq* pCEP-KM-*xfsA*	Δ*hfq*; Production of the secondary metabolite class of xenofuranones	[redacted] (Goethe-Universität Frankfurt am Main)
Xenorhabdus szentirmaii DSM 16338 Δ*hfq*-hmwp2	Δ*hfq*; Production of the secondary metabolite class of yersiniabactins	[redacted] (Goethe-Universität Frankfurt am Main)

2.3 Technical and craft techniques

2.3.1 Fabrication of the state-of-the-art flow cells, the *Panta Rhei* flow cells, and the *Panta Rhei* bracket

For the manufacturing of the current flow cells, the already existing design solutions were used as a guideline (Tolker-Nielsen and Sternberg, 2011). The previously described flow chambers, as well as the *Panta Rhei* flow cells (*Panta Rhei* D2 and *Panta Rhei* P) and the *Panta Rhei* bracket, were first created as technical drawings using the CAD program FreeCAD 0.18.4 (Machado et al., 2019). The design of the various components was then carried out using the same CAD software. The files were then transferred to the Tebis 4.0 software (Tebis – Technische Informationssysteme AG, Martinsried) in cooperation with Klaus Kunststofftechnik GmbH (Aitrach). Using this program, the individual parts were transferred to the CAM module of the Tebis 4.0 software (But, 2019) for further processing. The G code was then created to enable processing using a 5-axis P-T-F (10-10) CNC milling machine (HG GRIMME SysTech GmbH, Wiedergeltingen). The individual preforms were attached to the work board by means of vacuum during CNC milling. Unplasticized polyvinyl chloride (UPVC), polystyrene (PS), acrylonitrile butadiene styrene (ABS), and polycarbonate (PC) materials were used for the already common flow cells. Polyethylene (PE) and polypropylene (PP) were chosen to produce the *Panta Rhei* flow cells, and PE was selected for the *Panta Rhei* bracket. Using a plastic adhesive (3M, USA), different materials could be attached to the surface of the *Panta Rhei* D2. A silicone pad and screws (Bauhaus AG, Switzerland) were used to mount a plastic viewport to the *Panta Rhei* P cell. All polymer materials were provided by Klaus Kunststofftechnik GmbH. The milling components were manufactured with the approval of [redacted] and in collaboration with [redacted] and [redacted] from Klaus Kunststofftechnik GmbH in Aitrach.

2.3.2 Manufacturing of the peristaltic pump designed for the *Panta Rhei* system

A CP86 peristaltic pump with a NEMA 17 stepper motor and integrated UIM243 stepper motor controller (Gemke Technik GmbH, Ennepetal, Germany) was successfully used to create a peristaltic pump. The connections were then wired, and an external potentiometer (Conrad Electronic, Hirschau) was installed. Thus, the pump could be switched on, and a run could be initiated or terminated. In addition, the total speed was divided into a low-speed and a high-speed run by means of a further switch. The direction of flow was also adjustable from left to right or vice versa. The potentiometer was used to regulate the flow speed. A suitable synthetic enclosure was provided by Klaus Kunststofftechnik GmbH. Cutouts for the peristaltic pump and the respective connections were cut using a jigsaw (Robert Bosch GmbH, Stuttgart). A recess was also created for the installation of a cooling fan (Conrad Electronic, Hirschau) to ensure the proper ventilation of the stepper motor. The wiring was fixed inside the housing, and the cover was bolted together.

2.3.3 Assembly and commissioning of the *Panta Rhei* system

For the assembly of the components of the *Panta Rhei* system, a previously published method of a microfluidic system without the use of an air bubble trap was followed (Crusz et al., 2012). Two 1 L laboratory bottles (Schott AG, Mainz) were used to store the nutrient medium and to collect the already consumed medium. A borehole was cut in the lid of each bottle with a drilling machine (Robert Bosch GmbH, Stuttgart) to accommodate the tubing. A silicone pipe with an internal diameter of 3 mm and an outer diameter of 5 mm was inserted through the lid. A connector was used to join the end of another silicone hose. The opposite end was connected to the inlet of the *Panta Rhei* flow cell. A frame joint (Bauhaus AG, Switzerland) was used to adjust different angles when operating the *Panta Rhei* system. Therefore, one end was attached to a table, while the other end supported the *Panta Rhei* bracket. Rubber bands were used to attach the *Panta Rhei* flow cells to the *Panta Rhei* bracket. Another silicone tube was attached to the outlet of the flow cells, while the other end was connected to the peristaltic pump. Further silicone tubing led from the peristaltic pump to the vessel containing the spent media. Each tubing connection was equipped with tubing clamps to stop the flow of the culture medium. The silicone hoses, as well as the hose

accessories, were purchased from Bürkle GmbH (Bad Bellingen). To commission the complete *Panta Rhei* system, the bacteria and the surface necessary for the particular experiment were selected and placed in the *Panta Rhei* flow cells. Subsequently, the connection to the silicone tubing was carried out. The hose clamps were used to prevent the medium from leaking. Then the pump was switched on, the flow velocity and direction were set, and the respective experiment was executed. Finally, after the experiment was completed, the *Panta Rhei* flow cell was removed from the system. Beforehand, the hose clamps were provided to prevent the nutrient medium from spilling out. The *Panta Rhei* flow cells could be processed further in successive steps.

2.3.4 Design of the advanced *Panta Rhei* flow cells, the refined *Panta Rhei* Atlas, the BIAttiva *Panta Rhei* concepts and the associated block diagram

In the creation of the revised versions of the *Panta Rhei* flow cells and the *Panta Rhei* bracket (renamed to *Panta Rhei* Atlas), as well as the designs of the biofilm analyzer devices BIAttiva *Panta Rhei* Pente and BIAttiva *Panta Rhei* Pente^{thermo}, the CAD software FreeCAD 0.18.4 (Machado et al., 2019) was used. For the creation of the block diagram, the software tool Lucidchart (Lucid Software Inc., USA) (Sanford and Faulkner, 2018) was utilized.

2.3.5 Precutting and preparation of surfaces and common drinking water pipes for subsequent biofilm examination

The respective surfaces construction steel S235 (Bauhaus AG, Switzerland), polystyrene (PS), polycarbonate (PC), polyethylene tetraphtalate glycol (PETG) and polyethylene (PE) (Klaus Kunststofftechnik GmbH, Aitrach) were cut to a square, 1 cm^2 shape using a hacksaw (Scheppach GmbH, Ichenhausen) and a jigsaw (Robert Bosch GmbH, Stuttgart). The materials were then placed in 70% EtOH (v/v) for 24 h. The small plates were then dried under a clean bench (ibs tecnomara, Fernwald) and collected into previously autoclaved containers for further use.

The eight various drinking water pipes (Geberit AG, Switzerland) were provided by the Kebos Group in Munich. By utilizing a hacksaw and a jigsaw, slices were first cut, which were then trimmed into square 1 cm^2 pieces. The different materials were then placed in 70% EtOH (v/v) for 24 h. Under the clean bench, the pieces were then dried, and the outer side was taped using Parafilm (Bemis Company, USA) so that bacteria could only grow on the inner side of the tubes for later use. Storage was in vessels that had already been autoclaved.

2.3.6 CO_2-impregnation of the polymer platelets

For the coating of the plastic plates, already known methods (Mölders et al., 2018; Nikitin et al., 2003; von Schnitzler and Eggers, 1999) were considered. The selected plastic materials were HDPE T, PP, HDPE H, and TPU (Table 2.3.1). To briefly summarize, CO_2 was introduced to permeate the polymer surface of the platelets to enable the additive (silver nitrate, antibiotics, natural compounds) to be incorporated. During this process, only the upper layer of the material was impregnated, thus conserving resources. Furthermore, impregnation could be carried out at temperatures of approximately 40 °C, meaning that the stability of the respective additives was not affected. After the dwell time of the CO_2 containing the additive in the material had elapsed, the pressure was reduced to allow the CO_2 to be released, while the additive retained its position on the polymer surface. Impregnation was performed with and without EtOH as an entrainer. The entire CO_2-impregnation operation was carried out in close cooperation with [redacted] and [redacted] from Fraunhofer Institute for Environmental, Safety and Energy Technology UMSICHT in Oberhausen.

Table 2.3.1 The plastic discs used for CO_2-impregnation process in this thesis.

Material	Reference
HDPE T	[redacted] (Fraunhofer UMSICHT, Oberhausen)
PP	[redacted] (Fraunhofer UMSICHT, Oberhausen)
HDPE H	[redacted] (Fraunhofer UMSICHT, Oberhausen)
TPU	[redacted] (Fraunhofer UMSICHT, Oberhausen)

2.3.7 Extended-time experimentation to determine the efficiency of CO_2-impregnation

The HDPE T and PP plastic platelets impregnated with the Solvaperm Red pigment (Heubach GmbH, Langelsheim) as described above were disinfected with 70% EtOH (v/v) and placed in the *Panta Rhei* P flow cell. Beforehand, the platelets were photographed for a pre/post comparison (Samsung Electronics, South Korea). Then, the flow cells were connected to the *Panta Rhei* system, which was already filled with water. The long-term experiment was set for several months at a flow rate of 10 ml/h. The experiment was then stopped after eight months as loss of pigment impregnation was visually evident. The platelets were removed from the flow cells, and the intensity of the red coating was recorded by photography.

2.3.8 Assembly of the drinking water simulation setup

A simulation center was set up by Kebos Group in Munich to simulate the CO_2-impregnated platelets under realistic conditions. In the process, the simulation center was connected to the building's drinking water supply system to fill the 60 L system with drinking water. However, the simulation center could be operated completely self-sufficiently and independently of the building supply. By means of connection to the local network and remote control, the temperature, pressure, and water temperature could thus be monitored. A platelet adapter was designed and manufactured using 3D printing, which could hold up to 80 plastic discs. Furthermore, a special reactor with a

sight window was developed, which could accommodate the platelet adapter. Specific valves enabled the reactor to be installed in the simulation center and rapidly removed again. The valves also ensured the reactor was always filled with water and prevented the samples from drying out. A special insulated lockable suitcase was manufactured to transport the reactor to the laboratory in Mainz. The platelets were then analyzed as described in 2.5.7. After completion of each experiment, the reactor required elevated temperature and subsequent treatment with an H_2O_2 solution to be cleaned and prepared for the next experiment. The drinking water simulation of the impregnated specimen was carried out in close collaboration with [redacted] and [redacted] from Kebos Holding GmbH in Munich and Kebos Hygienic Solutions GmbH in Bergkirchen, respectively.

2.4 Synthetical methods

2.4.1 Tungsten oxides syntheses

The tungsten oxide nanoparticles used in this work were synthesized as previously published (Dören, 2022; Dören et al., 2021b). The synthesis was performed by [redacted] of the [redacted] at the JGU Mainz.

2.4.2 Ceroxide syntheses

The ceria nanoparticles used in this work were synthesized as previously published. The syntheses of CeO_2-EG, $BiCeO_2$-EG, CeO_2-HT and $BiCeO_2$-HT were performed by [redacted] of the [redacted] at JGU Mainz (Frerichs, 2020; Frerichs et al., 2020). The syntheses of CeO_2-SG and EP60A were carried out by [redacted] and [redacted] of the [redacted] at JGU Mainz (Jegel, 2022; Pütz, 2022). The syntheses of EP128a, EP132-400. EP157 and EP151 were accomplished by [redacted] of the [redacted] at JGU Mainz (Pütz, 2022; Pütz et al., 2022). The synthesis of CeO_2-FPEG was done by [redacted] of the [redacted] at JGU Mainz (Pfitzner, 2021). The synthesis of CeO_2-NTA was performed by [redacted] of the [redacted] at JGU Mainz (Jegel, 2022; Jegel et al., 2022). The synthesis of CeO_2-OLA was achieved by [redacted] of the [redacted] at JGU Mainz (Sarif, 2021; Sarif et al., 2022).

2.5 Microbiological methods

2.5.1 Cultivation of bacteria

Phaeobacter gallaeciensis, *Phaeobacter inhibens*, *Halotalea alkalilenta*, *Halomonas aquamarina* and *Exiguobacterium aurantiacum* were cultured aerobically at 30 °C in 2216 medium. *Pseudomonas aeruginosa*, *Staphylococcus aureus* and *Klebsiella pneumoniae* were grown aerobically at 30 °C in LB medium. *Sphingomonas adhaesiva*, *Sphingomonas pituitosa*, *Methylobacterium mesophilicum* and *Bacillus licheniformis* were aerobically cultivated at 30 °C in M1 medium. *Brevundimonas nasdae* and *Brevundimonas diminuta* were grown aerobically in TSY medium at 30 °C. *A. tumefaciens* A136 was cultured in LB medium supplemented with tetracycline (10 µg/ml) and spectinomycin (50 µg/ml) aerobically at 30 °C.

2.5.2 Secondary metabolite production and extract obtainment

To overproduce secondary metabolites, the strains of entomopathogenic *Xenorhabdus doucetiae*, *Xenorhabdus nematophila*, *Xenorhabdus szentirmaii, Photorhabdus luminescens* TT01 and *Photorhabdus luminescens* PB45.5 as well as the *Escherichia coli* strains (Table 2.2.1) were created and cultivated as previously published (Bode et al., 2019, 2015; Cai et al., 2017), followed by the preparation of the cell-free extracts. Briefly, the respective wild type bacteria as well as the generated mutants were cultured aerobically at 30 °C for 24 h in LB medium. Accordingly, 50 µg/ml kanamycin was added as an antibiotic for the mutant strains. Subsequently, to produce the respective secondary metabolites, the precultures were added to 100 ml LB at a final concentration of 0.1% (v/v). Moreover, the integrated promoter P_{ara} was induced using 0.1% arabinose (v/v). Aerobic incubation was performed for 48 h at 30 °C. Bacteria were then centrifuged in 50 ml Falcons (3500 x g, 30 min). The cell-free culture fluids were then freeze-dried and collected in 10 ml of distilled water. Until further use, the extracts were stored at -20 °C. The secondary metabolites production was carried out in collaboration with [redacted] from Goethe University, Frankfurt am Main.

2.5.3 Analysis of bacterial biofilm formation in 96-well microtiter plates using crystal violet staining

For the determination of biofilm formation in 96-well microtiter plates (Sarstedt AG & Co. KG, Nümbrecht) by crystal violet staining, previously published methods were followed (O'Toole, 2011; Zamora-Lagos et al., 2018). Briefly summarized, following incubation, bacteria were tapped out from the microtiter plate on paper towels. The plate was then washed for the removal of any remaining planktonic cells. Next, the microtiter plate was dried upside down in a laboratory fume hood for 20 minutes. Addition of an aqueous 1% (v/v) crystal violet solution to each well was then carried out. Crystal violet is suitable for staining the extracellular matrix of polysaccharides due to its property as a protein staining agent (Petrachi et al., 2017). Subsequently, incubation was performed for 30 minutes at room temperature. The crystal violet was then flopped out on paper tissues and the plate was washed twice each time in a tub of water to remove the unbound crystal violet. The microtiter plate was then dried upside down in a lab fume hood for at least 6 hours. Subsequently, 135 µl of 30% (v/v) acetic acid was added to the wells to allow the bound crystal violet to re-solve. If necessary, the microtiter plate containing the dried crystal violet was first photographed. After treatment with acetic acid, absorbance was measured at 575 nm in a Tecan Spark (Tecan Group AG, Switzerland). If required, the individual intensities of crystal violet staining were subsequently recorded photographically. Analysis was performed using Microsoft Excel 2019 (Microsoft Corp., USA) and Graphpad Prism 9.2.0 (Graphpad Software, USA).

2.5.4 Influence of nutrients on bacterial biofilm formation

Initially, the drinking water bacteria *S. adhaesiva*, *B. nasdae*, and *M. mesophilicum* and the marine bacteria *P. gallaeciensis*, *H. alkalilenta*, and *H. aquamarina* were cultured overnight in their respective cultivation medium. OD_{600} was then determined and adjusted to OD_{600} = 0.5, followed by centrifugation of the bacteria (2000 x g, 3 min) and discarding the culture fluid. The microorganisms were then washed in PBS buffer and centrifuged one more time (2000 x g, 3 min). PBS buffer was then discarded. The addition of the respective culture media, M1, MM, TSY, RS, HD, 2216, LB, and M9, was then performed and the cells were resuspended. 135 µl were dispensed into each

of ten wells of 96-well microtiter plates (Sarstedt AG & Co. KG, Nümbrecht). Plates were then sealed with Parafilm and aerobically cultured for 72 h at 30 °C. After incubation, the respective bacterial biofilm formation was analyzed as described in 2.5.3.

2.5.5 Analysis of the effect of incubation period on biofilm development

To assess the extent to which the incubation period can influence biofilm formation, the drinking water bacteria *S. adhaesiva*, *B. nasdae* and *M. mesophilicum* and the marine bacteria *P. gallaeciensis*, *H. alkalilenta* and *H. aquamarina* were cultured in microtiter plates for a period of 120 h and the biofilm was analyzed every 24 h to determine the effect on biofilm formation. For this purpose, precultures of the bacteria were prepared in their respective cultivation medium. OD_{600} was then measured and adjusted to 0.5. The bacterial cells were then centrifuged (2000 x g, 3 min) while the culture fluid was discarded. A wash step with PBS buffer was performed to remove the remaining culture fluids of the cultivation media. The bacterial cells were then centrifuged again (2000 x g, 3 min) and the buffer was discarded. The nutrient medium responsible for stimulating biofilm formation was now added, as previously found out, using 2.5.4. *S. adhaesiva* was resuspended in HD medium in this case. For *B. nasdae*, RS medium was used. *M. mesophilicum* and *H. alkalilenta* were both resuspended in TSY medium. 2216 medium was selected for *P. gallaeciensis* and *H. aquamarina*. Aerobic incubation was conducted at 30 °C for a total period of 120 h, during which biofilm formation progression was performed after 24 h, 48 h, 72 h, 96 h and 120 h, respectively, as described in 2.5.3.

2.5.6 Impact of different material surfaces on bacterial biofilm formation

After processing the materials as already described in 2.3.5, all materials were placed in separate wells of sterile 24-well microtiter plates (Sarstedt AG & Co. KG, Nümbrecht). *P. gallaeciensis* and *M. mesophilicum* were incubated overnight in the respective cultivation medium at 30 °C. OD_{600} was then measured and adjusted to 0.5 for a final volume of 1 ml. The bacterial cells were then centrifuged (2.000 x g, 3 min) and the culture fluid was discarded. To remove the remaining cultivation medium, the cells were washed in PBS buffer. Another centrifugation step was then performed (2.000 x g, 3 min) and the buffer was removed. *P. gallaeciensis* was resuspended in 2216 medium, while TSY medium was selected for *M. mesophilicum*. In each case, 1 ml of the bacterial suspension was added to the materials. In the case of *P. gallaeciensis*, incubation was performed for 72 h at 30 °C, while *M. mesophilicum* was cultured together with the materials at 30 °C for 144 h. The bacterial suspension was then introduced to the medium. After successful incubation, biofilm colonization on the materials was determined as adapted from previously published methods (Arnold, 2008). This was done by removing the bacteria from the wells and lifting out the individual materials using tweezers. The materials were then transferred to a new 24-well microtiter plate. The addition of 1 ml of distilled water to remove the planktonic cells was followed. The water was then withdrawn, and 1% (v/v) aqueous crystal violet solution was added. Incubation was held out for 30 minutes at room temperature. The crystal violet solution was thereafter removed, and the materials were washed twice with the addition of 1 ml of water each so that unbound crystal violet could be removed. After removal of the water, the materials were dried in a fume hood for 6 hours. Then, 1 ml of 30% (v/v) acetic acid was added to the materials to resolve the bound crystal violet. The acetic acid containing the crystal violet was transferred to 96-well microtiter plates and measured and analyzed in the plate reader as described in 2.5.3.

2.5.7 Biofilm formation on CO_2-impregnated polymer discs using crystal violet staining and confocal laser scanning microscopy (CLSM)

To investigate the effect of the impregnated additive against bacterial biofilm, the plastic platelets were impregnated using CO_2 as described in 2.3.6. Prior to using the plastic platelets, the entire *Panta Rhei* system was properly disinfected using 70% (v/v) EtOH at a flow rate of 100 mL/h. Sterile distilled water was then pumped through the system at the same flow rate to remove the remaining EtOH. Plastic platelets were then sterilized with 70% (v/v) EtOH and placed in the *Panta Rhei* P flow cells. A separate flow cell was used for each small platelet. One impregnated and one uncoated control platelet was used for each experimental run. The two *Panta Rhei* P flow cells were installed in parallel in the *Panta Rhei* system using Y-connectors (Bürkle GmbH, Bad Bellingen), allowing the same culture medium and pump to be used for both samples. *P. aeruginosa* was cultured overnight in LB medium at 30 °C and adjusted to an OD_{600} of 0.5 the following day. The bacterial cells were then centrifuged (2.000 x g, 3 min) and the culture fluid was collected. A washing step of the cells was performed using PBS. Finally, the cells were centrifuged one more time and the buffer was removed. The bacterial cells were resuspended in LB medium and added to the *Panta* Rhei P flow cells containing the plastic platelets by syringe. Bacteria were incubated in the flow cells at 30 °C without flow for 2 h, allowing them to attach to the surfaces. A flow rate of 5 ml - 8 ml was then set. After 72 h, the flow was stopped, and the plastic platelets were removed from the *Panta Rhei* P flow cells. The *Panta Rhei* system was disinfected with 70% (v/v) EtOH at a flow rate of 100 ml/h. Finally, the system was rinsed with sterile distilled water. For analysis by crystal violet, the method was performed as already described for the materials in 2.5.6. For quantification by CLSM, the removed plastic platelets were washed in water and then placed in 24-well microtiter plates. An addition of 1 ml of a SYTO9/propidium iodide solution (FILMTRACER LIVE/DEAD Biofilm Viability Kit, Invitrogen AG, USA) was carried out to stain the entire biofilm on the plastic platelet. The staining here was fluorescent, as SYTO9 can attach to the DNA of both live and already dead cells. Propidium iodide, in turn, can only pass into membranes that are already damaged and no longer functional. Together, these two fluorescent dyes are used to determine all cells as well as the respective live and dead ones (Deng et al., 2020). Incubation for 30 minutes at 30 °C was followed. Subsequently, the plastic plates were washed with water one more time to remove the unbound dyes. The plastic discs were then mounted on microscope

slides and the biofilm was analyzed using the LSM 880 microscope (Carl Zeiss AG, Oberkochen). A 40x water objective was used to do so. The excitation of SYTO9 was performed with an argon laser (Carl Zeiss AG, Oberkochen) (488 nm), while propidium iodide was visualized with a helium-neon laser (Carl Zeiss AG, Oberkochen) (543 nm). The images obtained were then analyzed using Zen blue software 3.1 (Carl Zeiss AG, Oberkochen) and ImageJ 1.53c (Schneider et al., 2012).

2.5.8 Impact of metal ions on biofilm formation of *P. gallaeciensis* using crystal violet staining and CLSM

To further determine whether metal ions stimulate biofilm formation of *P. gallaeciensis*, an overnight culture of *P. gallaeciensis* was prepared in 2216 medium at 30 °C. OD_{600} was then determined and adjusted to 0.5. The bacterial cells were centrifuged (2.000 x g, 3 min) and the culture fluid was withdrawn. This was followed by a wash step with PBS buffer. The cells were again centrifuged (2.000 x g, 3 min) and the buffer was removed. The bacteria were then resuspended in 2216 medium and 50 µM $FeCl_2$, $MnCl_2$, $CuCl_2$, $ZnCl_2$, $CoCl_2$, $CaCl_2$ were respectively added. Water was supplemented instead of the salts as a control. The bacterial suspensions were pipetted into 96-well microtiter plates and aerobically cultured for 72 h at 30 °C. After incubation, biofilm formation was performed as described in 2.5.3. For quantification by CLSM, slides were placed in petri dishes and covered with a *P. gallaeciensis* bacterial suspension adjusted to OD_{600} = 0.5. Additionally, 50 µM $FeCl_2$ and $MnCl_2$ were added, respectively. For the control, water was added. The analysis of the biofilm by CLSM was carried out as already described in 2.5.7.

2.5.9 Fluorescence microscopy of *P. gallaeciensis* biofilm grown in the *Panta Rhei* D2 flow cell

Initially, the *Panta Rhei* D2 flow cell was equipped with two microscope slides each. The flow cell was then connected to the *Panta Rhei* system. The system was then flushed and disinfected with 70% (v/v) EtOH at a flow rate of 100 ml/h. This was followed by washing with distilled sterile water. An overnight culture of *P. gallaeciensis* was set to an OD_{600} = 0.5 and washed with PBS buffer as described in 2.5.8. The

bacterial suspension was resuspended in 2216 medium and added to the *Panta Rhei* D2 flow cell using a syringe. No flow was set for 2 h at this point, allowing the bacterial cells to adhere to the surface. The *Panta Rhei* system was then set to a flow rate of 5 ml/h and the *Panta Rhei* D2 flow cell was positioned inside the *Panta Rhei* bracket at an angle of 90°. Incubation was performed in 2216 medium for 72 h at 30 °C. After incubation, SYTO9/propidium iodide was added using a syringe. This was followed by an incubation of 30 minutes without flow, allowing the dyes to enter the bacterial cells. A flow rate of 5 ml/h was then set again for 2 hours to remove the dyes. Then, the *Panta Rhei* D2 flow cell was decoupled and mounted on a Leica DMi8 fluorescence microscope (Leica Microsystems GmbH, Wetzlar). A FITC cube (Leica Microsystems GmbH, Wetzlar) (480 nm) was used to visualize SYTO9. For propidium iodide, a TXR cube (Leica Microsystems GmbH, Wetzlar) (560 nm) was utilized. Images were acquired using a Leica DFC9000GT digital camera (Leica Microsystems GmbH, Wetzlar). Analysis was carried out using the Leica application suite X 3.6.0.20104 software (Leica Microsystems GmbH, Wetzlar).

2.5.10 Impact of bacterial composition and primary colonizer on overall biofilm formation

To determine the extent to which the bacterial composition in the biofilm had an influence on the total biofilm formation, the drinking water bacteria *S. adhaesiva*, *B. nasdae*, and *M. mesophilicum* were each cultured individually and in a consortium. For the marine bacteria, this was repeated for *P. gallaeciensis*, *H. alkalilenta*, and *H. aquamarina*, each individually and in a composite. Bacteria were cultured overnight in their respective cultivation medium and associated conditions. Subsequently, the bacteria were washed with PBS as previously described in 2.5.8. The OD_{600} was set to 0.5. When culturing together in the consortium, only one-third of the bacterial cells were used from each of the three different bacterial species. The bacteria were pipetted into 96-well microtiter plates in the different assemblies. The drinking water bacteria were each cultured individually and in a consortium for 24 h at 30 °C in TSY medium. Then, 2216 medium was selected for the marine bacteria. Incubation was performed for 24 h at 30 °C. After incubation was complete, the biofilm was determined as described in 2.5.3. For the analysis of the influence of the primary colonizer on the total biofilm formation, *S. adhaesiva* and *B. nasdae* were used for the drinking water

bacteria. *P. gallaeciensis* and *H. alkalilenta* were applied for the marine bacteria. Preculture of the bacteria was adjusted to an OD_{600} = 0.25. After washing with PBS, *S. adhaesiva* or *B. nasdae* was resuspended in TSY medium. *P. gallaeciensis* and *H. alkalilenta*, respectively, were resuspended in 2216 medium. The bacterial suspension of *S. adhaesiva* or *B. nasdae* and *P. gallaeciensis* or *H. alkalilenta* was pipetted into 96-well microtiter plates and cultured for 6 h at 30 °C. Subsequently, the planktonic cells were removed by pipetting, leaving only the attached cells in each well. Then, the other bacterial species was adjusted to an OD_{600} = 0.25 and resuspended in the respective medium TSY or 2216 after washing in PBS. The bacterial suspension was then pipetted into the wells with the biofilm already present and incubated for further 6 h at 30 °C. Subsequently, the biofilm formation was determined using crystal violet as described in 2.5.3.

2.5.11 Effect of *P. gallaeciensis* culture fluid on biofilm formation of *Phaeobacter* spec. and *P. aeruginosa*

To identify whether the culture fluid of *P. gallaeciensis* influenced biofilm formation, a culture of *P. gallaeciensis* was first aerobically cultured in 2216 medium at 30 °C for 72 h. The cells were then centrifuged (2000 x g, RT, 10 Minutes) and the culture fluid was collected. The culture fluid was then filtered (0.22 µm) and stored at 4 °C for further use. Precultures of *P. gallaeciensis*, *P. inhibens*, and *P. aeruginosa* were prepared in the respective medium and cultivation conditions. Bacteria were then adjusted to an OD_{600} of 0.5 and washed in PBS. *P. gallaeciensis* and *P. inhibens* were then resuspended in the culture fluid of *P. gallaeciensis*. Resuspension in 2216 medium served as a control. The bacterial suspensions were pipetted into microtiter plates and incubated for 72 h at 30 °C. For *P. aeruginosa*, only 5% (v/v) of the culture fluid of *P. gallaeciensis* was used due to the increased salinity in 2216 medium. The addition of 5% (v/v) 2216 medium served as a control. The dilutions were performed in LB medium. 135 µl of the bacterial suspension was pipetted into microtiter plates each. The plate was incubated for 72 h at 30 °C. After incubation, the effect on biofilm formation was measured using the procedure described in 2.5.3.

2.5.12 Enrichment of the biofilm inhibiting molecule from *P. gallaeciensis* culture fluid.

The culture fluid of *P. gallaeciensis* was extracted as described in 2.6.1. After fractionation, as detailed in 2.7.1, 135 µl of a *P. aeruginosa* culture adjusted to OD_{600} = 0.5 in LB medium was added to each well containing the respective fractions. Incubation for 72 h at 30 °C proceeded. The biofilm was then analyzed as previously described in 2.5.3.

2.5.13 Effect of *B. nasdae* late stationary culture fluid on the own biofilm formation

A culture of *B. nasdae* was aerobically grown for 72 h in RS medium at 30 °C. Cells were then centrifuged (2.000 x g, RT, 10 min), and the culture fluid was collected and filtered (0.22 µm). The storage was done at 4 °C. A preculture of *B. nasdae* was subsequently prepared under the specific cultivation conditions and the culture was adjusted to an OD_{600} of 0.5. After the washing step with PBS, resuspension was performed in the culture fluid of *B. nasdae*. Resuspension in RS medium was also performed as a control. The bacterial suspensions were pipetted into 96-well microtiter plates and incubated for 72 h at 30 °C. The biofilm was then analyzed as described in 2.5.3.

2.5.14 Investigation of the biofilm disrupting effect of *B. nasdae* on the *B. diminuta* biofilm formation

First, *B. nasdae* was incubated in RS medium for 72 h at 30 °C. Subsequently, the cells were centrifuged (2.000 x g, RT, 10 min) and separated by filtration (0.22 µm). The culture fluid obtained was freeze-dried (Martin Christ Gefriertrocknungsanlagen GmbH, Osterode am Harz, Germany) in 50 ml Falcons. After completion of lyophilization, the dried culture fluid was concentrated 10x by the addition of water. Drying of only RS medium served as a control. A culture of *B. diminuta* set to OD_{600} = 0.5 in LB Medium as described in 2.5.8 was then grown in microtiter plates (135 µl) for 24 h at 30 °C. Subsequently, 1.35 µl of 10x concentrated *B. nasdae* culture fluid was added to each well containing *B. diminuta*. The addition of 10x concentrated RS medium functioned as a control. The microtiter plate containing the bacteria was then

incubated for an additional 24 h at 30 °C. The effect on the biofilm was subsequently analyzed as described in 2.5.3.

2.5.15 Treatment of *P. gallaeciensis* and *B. nasdae* culture fluid

To obtain an initial indication of the properties of the candidate molecules within the culture fluid of *P. gallaeciensis* and *B. nasdae*, the culture fluids were treated differently to be subsequently tested a further time for biofilm inhibitory activity. For *P. gallaeciensis*, the culture fluid was obtained as described in 2.5.11. For *B. nasdae*, the culture fluid was obtained as described in 2.5.14. Subsequently, the culture fluid was acidified with HCl to a pH of 1 or alkalized with NaOH to a pH of 13. After the acidic or alkaline treatment, the pH was neutralized again so that a falsified effect of pH on the biofilm could be excluded. In addition, the culture fluid of *P. gallaeciensis* and *B. nasdae* were each heated at 90 °C for 10 min or treated with proteinase K (400 µg/ml). Treatment with proteinase K involved overnight incubation at 56 °C followed by inactivation by heating at 75 °C for 20 minutes. Finally, the addition of the treated culture fluids and subsequent determination of the bacterial biofilm was performed as previously described in 2.5.11 and 2.5.13, respectively.

2.5.16 Biofilm inhibitory properties of secondary metabolites from entomopathogenic bacteria

To determine whether the secondary metabolites of entomopathogenic bacteria of the genera *Photorhabdus* and *Xenorhabdus* have a biofilm inhibitory effect, the extracts were prepared as described in 2.5.2. Then, 20 µl of the secondary metabolites were added to a well of a 96-well microtiter plate. Under a sterile bench, the extracts were then allowed to dry. Then, 50 µl of 70% (v/v) EtOH was added to the extracts to prevent contamination. The microtiter plate was dried one more time under a sterile bench until all EtOH was evaporated. The addition of only water served as a control. Dilutions of the extracts were prepared in water and also pipetted into the wells of the microtiter plate as described. Subsequently, 135 µl of the bacteria to be tested were added. Both drinking water and marine bacteria were used for these experiments consisting of *B. licheniformis*, *B. nasdae*, *S. adhaesiva*, *S. pituitosa*, *M. mesophilicum*, *P. aeruginosa*,

P. gallaeciensis, *P. inhibens*, *E. aurantiacum*, and *H. aquamarina*. Bacteria were cultured as described in 2.5.1 and then adjusted to an OD_{600} = 0.5 as described in 2.5.8. For *B. licheniformis* and *B. nasdae*, resuspension in RS medium and incubation at 30 °C for 72 h was performed. *S. adhaesiva* and *S. pituitosa* were resuspended in HD medium and incubated for 72 h at 30 °C. *M. mesophilicum* was resuspended in TSY medium and incubated for 7 days at 30 °C. *P. aeruginosa* was resuspended in LB medium and incubated for 72 h at 30 °C. *P. gallaeciensis*, *P. inhibens*, *E. aurantiacum*, and *H. aquamarina* were all resuspended in 2216 medium, respectively. For *P. gallaeciensis* and *P. inhibens*, incubation was performed at 30 °C for 72 h, whereas for *E. aurantiacum* and *H. aquamarina*, incubation was performed at 30 °C for 96 h. After the incubation process of the bacteria supplemented with secondary metabolites was completed, the determination of the biofilm was performed as described in 2.5.3.

2.5.17 Examination of the biofilm inhibitory effect of phenylethylamides/tryptamides in the *Panta Rhei* system

To produce phenylethylamides/tryptamides, the method already described in 2.5.2 was followed. Here, *Xenorhabdus doucetiae* DSM 17909 Δ*hfq* pBAD DC was cultured in a 20 L fermenter so that the secondary metabolites were produced on a large scale for later use in the *Panta Rhei* system. Cultivation of the bacteria without induction by 0.1% (v/v) arabinose served as a control. The *Panta Rhei* system was prepared as described in 2.5.9, and *P. aeruginosa* was set to an OD_{600} = 0.5 and added to the *Panta Rhei* D2 flow cell. Here, the bacteria were incubated for 30 min at 30 °C without flow. The secondary metabolites obtained from the previous step were now attached to the *Panta Rhei* system. The control, which was not induced, was connected to a second *Panta Rhei* system. Bacteria in the *Panta Rhei* D2 flow cells were incubated for 24 h at 30 °C. The flow rate was set to 8 ml/h. After incubation, the *Panta Rhei* D2 flow cells were disconnected from the *Panta Rhei* system and examined on a light microscope (Leica Microsystems GmbH, Wetzlar, Germany) using phase contrast. Images were acquired using a Leica DFC9000GT digital camera (Leica Microsystems GmbH, Wetzlar). Analysis was performed using the Leica application suite X 3.6.0.20104 software (Leica Microsystems GmbH, Wetzlar).

2.5.18 Quantification of pyocyanin production in *P. aeruginosa*

To investigate whether the secondary metabolites influence the QS system of *P. aeruginosa*, the intensity of the pyocyanin that was produced was quantified. A previously published method was used for this purpose (O'Loughlin et al., 2013). Briefly, *P. aeruginosa* was prepared as described in 2.5.16 and pipetted into the wells containing the respective secondary metabolite. The microtiter plate was then aerobically cultured for 24 h at 37 °C. Bacteria were separated by centrifugation (1.000 x g, 15 min), and the culture fluid was transferred to a new microtiter plate. A plate reader (Tecan Group AG, Switzerland) was utilized to measure the absorbance at 695 nm. If required, the individual intensities of the pyocyanin were subsequently recorded photographically. Analysis was performed using Microsoft Excel 2019 (Microsoft Corp., USA) and Graphpad Prism 9.2.0 (Graphpad Software, USA).

2.5.19 Examination of biofilm formation on drinking water pipes

The drinking water pipes to be tested were processed as described in 2.3.5. Then, for *P. aeruginosa*, the method was modified as in 2.5.6. Briefly, LB medium was used for the cultivation of *P. aeruginosa*. The bacteria were cultured on the surfaces for 72 h at 30 °C. Subsequently, the parafilm was removed from the covered outer surfaces, and the biofilm on the inner sides was analyzed as described in 2.5.6 and 2.5.3.

2.5.20 Investigation of the biofilm inhibitory effect of secondary metabolites impregnated on platelets under realistic conditions in the simulation center

The impregnated platelets were mounted in the simulation center by the Kebos Group in Munich. The bacteria *P. aeruginosa*, *S. adhaesiva*, *M. mesophilicum*, and *B. nasdae* were cultured in the appropriate media as described in 2.5.1. Cells were then washed in PBS and adjusted to a total OD_{600} = 0.01 in a volume of 15 ml. Bacterial cells were added to the simulation center and cultured in the system and on the platelets for 3 weeks at 30 °C. Monitoring of the experiments and setting of the correct parameters was performed by Kebos Group. After incubation was completed, the platelets were further processed, and the biofilm was analyzed as described in 2.3.8 and 2.5.7.

2.5.21 Analysis of the impact of tungsten oxides and cerium oxides on biofilm formation

For the assay of nanoparticles on bacterial biofilm, a previously published method was applied in a modified form (Frerichs et al., 2020; Opitz et al., 2022; Pütz, 2022). Briefly recapitulated, the bacteria *P. aeruginosa*, *K. pneumoniae*, *M. mesophilicum*, *P. gallaeciensis* and *S. aureus* were cultured as described in 2.5.1. Bacteria were then adjusted to an OD_{600} of 0.5. As explained in detail in 2.5.8, the bacteria were washed with PBS and then resuspended in the appropriate medium. For *P. aeruginosa*, *K. pneumoniae* and *S. aureus*, LB medium was applied. For *M. mesophilicum* and *P. gallaeciensis*, TSY and 2216 medium were used, respectively. Then, the nanoparticles were added accordingly. For the tungsten oxides, 0.1 mg/ml was used whereas for the cerium oxides, 28 µg/ml was included. No addition of nanoparticles served as a control. In addition, 32 mM KBr and 0.8 mM H_2O_2 were supplemented. 135 µl of the bacterial suspension were then pipetted into wells of microtiter plates along with the nanoparticles. This was followed by incubation for 72 h at 30 °C. Every 24 h, 0.8 mM H_2O_2 was supplemented. To identify whether an antibacterial effect of the tungsten oxides can be achieved by infrared, the method was performed similarly as previous described (Dören, 2022) but without the addition of KBr and H_2O_2. Furthermore, the bacterial cells in the plate reader were irradiated with an infrared beam at 950 nm every 30 minutes. No irradiation with infrared served as a control. After incubation was complete, biofilm analysis was performed as described in 2.5.3. Beforehand, the planktonic cells were quantified by measurement at 600 nm in the plate reader when necessary.

2.5.22 Preparation for the determination of the bromide equilibrium by addition of external NaBr

The test was carried out as already described (Pütz, 2022; Pütz et al., 2022).To determine whether bromination occurs on the homoserine lactones due to the nanoparticles, 30 µM external NaBr was supplemented to a *P. aeruginosa* culture adjusted to OD_{600} = 0.5 in LB medium. Furthermore, 0.8 mM H_2O_2 and 32 mM KBr were added. Additionally, 28 µg/ml cerium oxides were supplemented. The absence

of ceroxides served as a control. The bacteria were then incubated aerobically at 30 °C for 24 h. Cells were then centrifuged (2.000 x g, 5 min), and the culture fluid was filtrated (0.22 µm). The cell-free culture fluid was then shock frozen with liquid nitrogen (Linde plc, Ireland) and stored at -80 °C until further use.

2.5.23 Effect determination on *P. aeruginosa* biofilm formation by addition of 3-oxo-C_{12}-AHL, C_4-AHL and DAHSL

The test was carried out as already described (Pütz, 2022; Pütz et al., 2022). To examine the impact of the addition of 3-oxo-C_{12}-AHL, C_4-AHL, and DAHSL, these substrates were added at different concentrations (1 nM - 10 µM) to a *P. aeruginosa* culture adjusted to OD_{600} = 0.5 in LB medium. Subsequently, 135 µl of the bacteria were pipetted into 96-well microtiter plates along with the supplemented substrates. No substrate addition functioned as a control. The plate was then incubated at 30 °C for 72 h. Biofilm formation was then analyzed as previously described in 2.5.3.

2.5.24 Analysis of biofilm on cerium oxide coated materials using crystal violet and CLSM and quantification of pyocyanin formation by *P. aeruginosa*

To define the effect of cerium oxides embedded on the surfaces upon biofilm formation, previously published methods were applied in a modified manner (Frerichs, 2020; Frerichs et al., 2020; Jegel, 2022; Jegel et al., 2022; Sarif, 2021; Sarif et al., 2022). Briefly, an overnight culture of *P. aeruginosa* was prepared in LB medium as described in 2.5.1. OD_{600} was then set to 0.5 as previously described in 2.5.8. In each case, 1 ml of bacterial culture was pipetted into wells of a 24-well microtiter plate. When using a 6-well microtiter plate, 3 ml was used. In addition, 0.8 mM H_2O_2 and 32 mM KBr were supplemented. The respective cerium oxide-coated materials were placed in the wells. Uncoated surfaces served as controls. Incubation was performed for 72 h at 30 °C. Every 24 h, H_2O_2 was added to a final concentration of 0.8 mM. Subsequently, the planktonic cells were removed by washing with water. For crystal violet staining or analysis using CLSM, the method was performed as already described in 2.5.7. In the case of using an Axio Imager 2 microscope (Carl Zeiss AG, Oberkochen, Germany), SYTO9 was excited at 470 nm, while propidium iodide was excited at 558 nm. Zeiss

blue software 3.1 was used for the analysis. For the quantification of pyocyanin, similar procedures were followed as described above. However, aerobic incubation was performed at 37 °C. Bacterial culture was then removed from the wells of the microtiter plate and transferred to a microreaction tube (Eppendorf SE, Hamburg, Germany). The cells were centrifuged at 16000 x g for 2 minutes. The obtained culture fluid was then filtered (0.22 µm) and transferred to a 96-well microtiter plate. Quantification at 695 nm in the plate reader was used to determine the effect of cerium oxides on pyocyanin formation.

2.6 Extraction methods

2.6.1 Extraction of putative *P. gallaeciensis* secondary metabolites

For the preparation of 50 ml culture fluid of *P. gallaeciensis*, the method was performed as described in 2.5.11. The culture fluid was then shaken out three times in a separatory funnel with ethyl acetate. The hydrophilic phase was collected, and the hydrophobic phase was taken up in a rotary flask. For dilutions, LB medium was selected for the hydrophilic phase, and ethyl acetate was used for the hydrophobic phase. Using a rotary evaporator (Phoenix instrument GmbH, Garbsen), the hydrophobic phase was concentrated at approximately 1 ml. A vacuum concentrator was then used to evaporate the solvent. The weight of the substances obtained was then noted and the concentration was adjusted to 20 mg/ml using MeOH. The substances were stored at 4 °C until further use.

2.6.2 Extraction of homoserine lactones and supplemented DAHSL from *P. aeruginosa* culture fluid

For determination of the amount of homoserine lactones or the externally added 10 nM and 100 nM DAHSL (Pütz, 2022; Pütz et al., 2022) ([redacted] JGU Mainz), *P. aeruginosa* was first incubated at 30 °C for 24 h in the presence and absence of cerium oxides (28 µg/ml). Additionally, 0.8 mM H_2O_2 and 32 mM KBr were supplemented. The control for the external supply of DAHSL did not include the adding of the bacteria. Cells were then centrifuged at 2000 x g for 10 minutes. The culture fluid

was then filtered (0.22 µm). Using ethyl acetate, the culture fluid was shaken out three times in separating funnels. The hydrophilic phase was then discarded, and the hydrophobic phase was collected in round bottom flasks. Using a rotary evaporator, the contents were concentrated to approximately 1 ml and evaporated using a vacuum concentrator. Subsequently, 50% (v/v) MeOH was added. Further processing was carried out at the Bundesanstalt für Gewässerkunde in Koblenz in close collaboration with [redacted] and [redacted].

2.7 Analytical methods

2.7.1 HPLC fractionation of the *P. gallaeciensis* culture fluid

For fractionation, a previously published slightly modified method was followed (Guan et al., 2020). Briefly, a C18 column LiChrospher 100 RP-18 (Merck, Darmstadt) with a DAD Type G1315B Detector was used for fractionation in a 96-well microtiter plate. The temperature, which was set, equaled 20 °C, and the gradient started from 1% acetonitrile and 99% water to 100% acetonitrile. The run time was 25 minutes. The applied wavelength was 210 nm. Finally, for 3 minutes, only 100% acetonitrile was used. The individual fractions were all collected on one plate. Four different plates were created. Fractionation was carried out in cooperation with the IBWF in Mainz. The effect of each fraction contained in the wells was tested on *P. aeruginosa* as described in 2.5.16.

2.7.2 Reporter strain assays to quantify the effect of the nanoparticles on homoserine lactones

To determine whether the nanoparticles are capable of modifying homoserine lactones, a previously described method was followed (Tang et al., 2013). Briefly, *A. tumefaciens* A136 was used as the reporter strain, which cannot produce homoserine lactones as such but can sense long-chain homoserine lactones. Fusion of the *lacZ* gene to the *traI* gene results in the formation of the enzyme β-galactosidase upon detection of a long-chain homoserine lactone. Thus, by adding a cleavable substrate such as 5-bromo-4-chloro-3-indoxyl-β-D-galactopyranoside (X-Gal) or o-nitrophenyl-

β-D-galactopyranoside (ONPG), a color change can be achieved, which can then be photometrically quantified. For the tungsten oxides, 0.1 mg/ml nanoparticles were used in each case. In addition, 0.8 mM H_2O_2 and 32 mM KBr were supplied. Furthermore, external 5 µM 3-oxo-C_{12}-AHL was added. The aqueous mixture was then incubated for 12 h at room temperature. Then, the mixture was added to *A. tumefaciens* A136, which was previously adjusted to an OD_{600} of 1. 250 µg/ml of X-Gal was then supplemented. No addition of X-Gal served as a negative control. Aerobic incubation at 30 °C for an additional 8 h was performed. Bacteria were then centrifuged at 10.000 x g for 5 min. The culture fluid was transferred to 96-well microtiter plates and analyzed using a plate reader (Tecan AG, Switzerland) at 630 nm. For the cerium oxides, 28 µg/ml nanoparticles were used in each case. In addition, 10 µM external 3-oxo-C_{12}-AHL was applied in this case. After the addition of 0.8 mM H_2O_2 and 32 mM KBr, incubation was carried out at room temperature for 8 h. The same method was then used for the analysis by X-Gal as already described for the tungsten oxides. For analysis by ONPG, the nanoparticle-homoserine lactone mixture was added to *A. tumefaciens* A136, which was previously adjusted to an OD_{600} of 0.5. This was followed by incubation at 30 °C for 8 h. From each culture, 1 ml was then taken and centrifuged at 5000 x g for 5 min. After discarding the culture fluid, 1 ml of buffer Z was added. The cells were then resuspended in buffer Z. The use of buffer Z served as a negative control. The OD_{600} of the cells was then determined. This was followed by the addition of 100 µl of pure chloroform and 50 µl of 0.1% (v/v) SDS. The mixture was then shaken. The purpose of this was to allow the bacteria to lyse. This was followed by incubation of the mixture at 30 °C for 30 minutes. 160 µl of a 4 mg/ml ONPG solution was then added. Time was then measured until the samples turned yellow. To stop the reaction, 500 µl of a 1 M Na_2CO_3 solution was added to the mixture. The centrifugation of the cells was then performed at 16.000 x g for 2 min. Using a plate reader, the culture fluid was measured at 420 nm and 550 nm. The corresponding Miller units were then calculated using the following modified equation (Miller, 1972).

$$\text{Miller Units} = 1000 * \frac{OD420 - 1{,}75 * OD550}{t * V * OD600}$$

In this context, t represents the reaction time in minutes and V the reaction volume in ml.

2.7.3 IC-CD analysis for the calculation of the bromide level

The test was carried out as already described (Pütz, 2022; Pütz et al., 2022). Bromide concentrations of the culture fluids described in 2.5.22 were measured using a 940 Professional IC Vario Ion Chromatography (Metrohm AG, Switzerland) and an associated conductivity detector. A Metrosep A Supp 7 (250/4.0) column was adjusted to a flow rate of 700 µl/min to perform the separation. 50 µl of each sample was loaded, and the temperature was calibrated at 50 °C. The eluent fraction consisted of a 3.6 mM Na_2CO_3 solution, while the suppression fraction included a 250 mM H_3PO_4 solution. The total time was 50 minutes, while the exchange time was approximately 30 and 45 minutes. All samples were diluted 100-fold for better analysis. Bromide balancing was performed in close cooperation with [redacted] and [redacted] from the Bundesanstalt für Gewässerkunde in Koblenz.

2.7.4 LC-MS/MS analysis for the determination of homoserine lactones and DAHSL

The test was carried out as already described (Pütz, 2022; Pütz et al., 2022). To operate the LC system, an Agilent 1260 Infinity Series (Agilent Technologies, USA) was required. This was equipped with a pump and valve that could cut off the first two and last seven minutes of the measurement. A Poroshell 120 C18 column (3 x 50 mm, 2.7 µm) (Agilent Technologies, USA) was used at a flow rate of 0.3 ml/min for separation. 40 µl of each was injected and the temperature was adjusted to 40 °C. A mixture of Milli-Q water and acetonitrile in the ratio of 90:10 (v/v) was used for the elution phase. This was supplemented with 2 mM ammonium formate and 0.1% (v/v) formic acid. The gradient for LC was applied from a published method (Nürenberg et al., 2015). A mass spectrometer system (QqQ-LIT-MS, API 6500+ QTrap) (AB Sciex LLC, USA) was used. Electrospray ionization was used for the positive ion mode for 3-oxo-C_{12}-AHL. For DAHSL, the negative ion mode was utilized. Here, the ammonium formate was omitted, and pure acetonitrile was adopted for eluent B. LC-MS/MS analysis was performed in close collaboration with [redacted] and [redacted] from Bundesanstalt für Gewässerkunde in Koblenz.

2.7.5 Degradation assays and detection of intermediates using LC-HRMS

The test was carried out as already described (Pütz, 2022; Pütz et al., 2022). MilliQ water was used as the base for the degradation experiments. In addition, 30 mM NaBr, 25 µg/ml cerium oxides, and 5 µM substrate (3-oxo-C_{12}-AHL and HQNO, respectively) were added. 30 µM H_2O_2 was injected into the mixture so that the reaction could proceed. At certain time points, samples were repeatedly taken, and the reaction stopped immediately by $Na_2S_2O_3$ addition. Before injection, the nanoparticles had to be centrifuged for 15 minutes at 4 °C (15.000 rpm Mikro 220R (Andreas Hettich GmbH & Co. KG, Tuttlingen)). Calibration was performed using 100 nM C_6-AHL. To detect the substrate and the products formed, LC-HRMS was used. The same procedure was used as described in 2.7.4. The eluents were taken from the previously published method (Nürenberg et al., 2015). A TripleTOF 5600 (AB Sciex LLC, USA) together with electrospray ionization were utilized. Both positive and negative ion modes were applied. LC-HRMS analysis was performed in close collaboration with [redacted] and [redacted] at the Bundesanstalt für Gewässerkunde in Koblenz.

2.8 Bioinformatics methods

2.8.1 Identification of metal ion transporters in *P. gallaeciensis*

To investigate whether *P. gallaeciensis* is capable of taking up Fe^{2+} and Mn^{2+}, bioinformatic analysis was performed using the KEGG Genome Database (Kanehisa, 2000), which compares the individual pathways in the organism and assigns genes to the same function based on homologies to other known genes in different microorganisms.

3 Results

Due to the increasing antibiotic resistance in bacteria and the growing complications in health, environmental and economic sectors (Bowler et al., 2020; Muhammad et al., 2020; Cámara et al., 2022), it is necessary to find new antimicrobial agents against bacterial biofilms. Although dedicated flow cells (Tolker-Nielsen and Sternberg, 2014) for the analysis of biofilms and the effect of potential agents are available (Azeredo et al., 2017), these state-of-the-art flow cells have significant drawbacks in their entirety and applicability. For that reason, optimized microfluidic systems for the correct and easy analysis of bacterial biofilms are urgently needed. In addition, to treat and tackle biofilms, it is crucial to examine the conditions that cause marine as well as freshwater biofilms. Bacteria from these highly populated environments are frequently able to inhibit or disperse the biofilm of competing microorganisms (Nijland et al., 2010; Rehman and Leiknes, 2018; Simões et al., 2007). However, several species of marine and drinking water bacteria are still unexplored in terms of such capabilities. Entomopathogenic bacteria of the genera *Photorhabdus* and *Xenorhabdus* produce a variety of secondary metabolites with different characteristics during their life cycle (Bode, 2009). However, the influence of such secondary metabolites on bacterial biofilm formation is not well investigated to date. The use of nanoparticles to attack microorganisms are well known (Shkodenko et al., 2020), but it is still unexplored whether specific tungsten oxide or cerium oxide nanoparticles can interact with bacterial QS and thereby inhibit biofilm formation.

The points listed above must be thoroughly investigated to discover new antimicrobial agents and to be able to combat bacterial biofilms in the future.

3.1 *Panta Rhei* – an optimized microfluidic system for macroscopic and microscopic analysis of bacterial biofilms

It is indispensable to investigate biofilm analyses under native conditions since biofilms often form a complex structure dependent on the biological habitat (Dassanayake et al., 2020; Karygianni et al., 2020; Secchi et al., 2022). So-called microfluidic systems provide realistic conditions for cultivating and analyzing bacterial biofilms. An essential core component of such systems is a flow cell, in which the bacteria are placed for cultivation and to allow biofilm formation. Another component is a reservoir containing a fresh nutrient solution and another reservoir collecting the used medium. A highly precise peristaltic pump must provide the necessary flow within the microfluidic system and ensure fresh nutrients supply for the growing biofilm. The core components are connected by tubing (Azeredo et al., 2017; Behrens et al., 2020). However, the flow cells used to date have significant drawbacks, so one of the first steps in this thesis was to re-design and construct an optimized microfluidic system, which circumvents the disadvantages of the state-of-the-art flow cells.

3.1.1 State-of-the-art flow cells display major disadvantages

In order to analyze bacterial biofilms under realistic conditions, suitable and easy-to-use flow cells were required. For this purpose, the state-of-the-art was taken as a basis, and already known flow cells from previous studies were reproduced (Tolker-Nielsen and Sternberg, 2014). The flow cells were designed and scaled using a computer-aided-design (CAD) program (FreeCad 0.18.4) and then manufactured using a computer-aided-manufacturing (CAM) program (Tebis 4.0) as well as subtractive manufacturing like a 5-axis Computer Numerical Control (CNC) milling machine. Since bacteria from different habitats also prefer different cultivation conditions (Lear et al., 2021; McCaig et al., 2001; Vartoukian et al., 2010), different plastics (Fig 3.1.1) were used for fabrication based on their properties to ensure the appropriate environment. The plastics used were polyvinyl chloride (UPVC), polystyrene (PS), acrylonitrile butadiene styrene (ABS), and polycarbonate (PC). The different plastics differ significantly, e.g., in their operating temperature. For example, while ABS and PC are intended to be used at a starting temperature of -30 °C – -40 °C, PS can be used from -20 °C on, and UPVC from -15 °C and above (Klein, 2011).

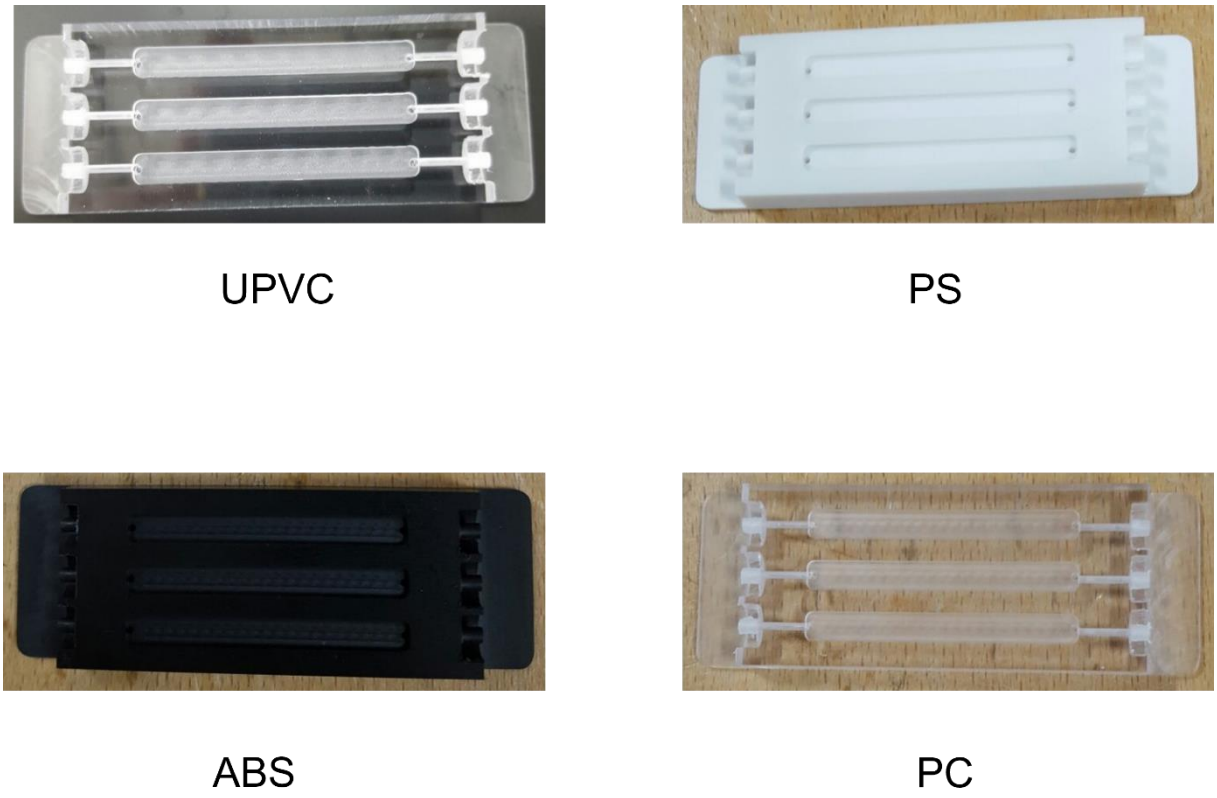

Fig. 3.1.1 Construction of state-of-the-art flow cells from different plastic materials. The shape of the flow cells was designed as indicated in previous studies. Subtractive manufacturing was then used to produce the flow cells with the specific sample chamber. The plastics used for manufacturing were unplasticized polyvinyl chloride (UPVC), polystyrene (PS), acrylonitrile butadiene styrene (ABS), and polycarbonate (PC).

However, when using these flow cells, it was noticed that due to the design, several disadvantages came along. First, since the bottom of the cells was not transparent, it was not possible to use a light microscope for further analyses because the light beam could not pass through. Therefore, the bacterial biofilm inside the flow cells could only be analyzed with the help of a special CLSM. Thus, a potentially failed experiment could not be validated before using elaborative and time-consuming microscopy. Additionally, when using these flow cells, it was found that there were increased complications with the flow velocity. Due to the selected height of the sample chamber and the tubing connections length, higher pressure within the sample chamber was increased, damaging the biofilm, or the tubing tore off at the connections. Another downside was that these flow cells could only be operated with the help of an additional

bubble trap. Without a bubble trap, air bubbles that entered the system could harm the entire biofilm and thus interfere with the entire experiment (Azeredo et al., 2017; Gómez-Suárez et al., 2001). In addition, macroscopic analysis of the bacterial biofilm was incompatible with these flow cells. Finally, the state-of-the-art flow cells enormously complicate the use of high throughput analyses due to the above-listed drawbacks.

3.1.2 The characteristics of the *Panta Rhei* flow cell variants

Since the conventional flow cells were not suitable for complete microscopic and macroscopic analyses of bacterial biofilms and other expensive flow cells available on the market also had significant limitations, such as the mandatory use of a bubble trap (Azeredo et al., 2017; Tolker-Nielsen and Sternberg, 2011), two optimized flow cell variants were designed and constructed after several trials and plenty of prototyping. These flow cell variants were named *Panta Rhei* D2 and *Panta Rhei* P (Fig. 3.1.2). The name *Panta Rhei* has been used only for personal use in this work; no legal claim is made to it. First, a plastic plate was manually cut into a square shape and then mounted for 5-axis CNC milling. Subtractive manufacturing was then used to produce prototypes for the two *Panta Rhei* variants. Machining with a CNC milling machine also offered the advantage of very high repeatability, which ensured that the scale was maintained to produce further *Panta Rhei* flow cells.

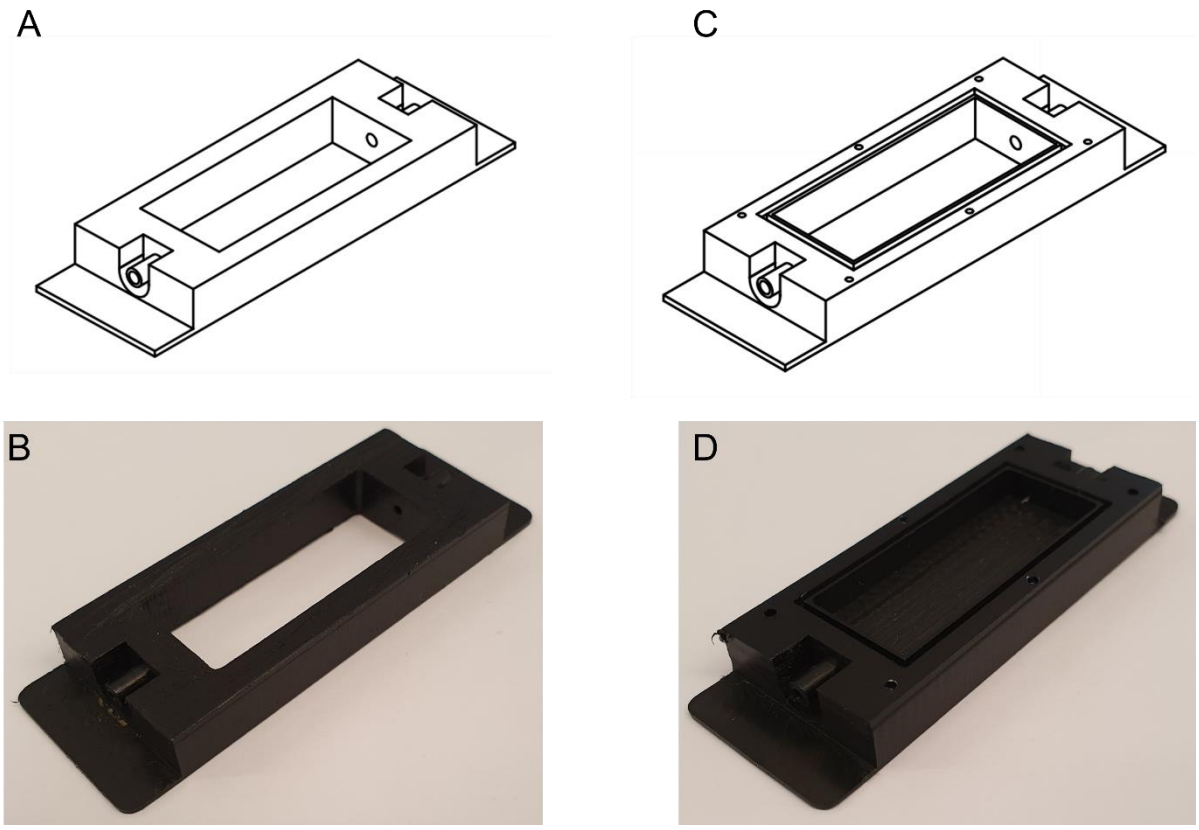

Fig. 3.1.2 Schematic representation of the optimized *Panta Rhei* flow cell variants. (A) Technical drawing of the *Panta Rhei* D2 flow cell. (B) The *Panta Rhei* D2 flow cells are manufactured with a 5-axis CNC milling machine. (C) Technical drawing of the *Panta Rhei* P flow cell. (D) The *Panta Rhei* P flow cells are manufactured with a 5-axis CNC milling machine. The two flow cell variants share the same point of origin since they both match the dimensions of a specimen carrier, which makes them applicable to all variants of microscopes.

These two *Panta Rhei* flow cell variants have a lot of features in common and differ only in several points. Both *Panta Rhei* flow cell modifications consist of polyethylene (PE) or polypropylene (PP) and share the exact same dimensions, matching the size of microscope slides. This feature and the handles on each frontside and backside of the flow cells ensure compatibility for different microscopes. While choosing the materials for those two modifications, the focus was on durability, sustainability, and reusability. Since it is already known that polypropylene is autoclavable and therefore used in medical technology (Lan et al., 2013), has low cost, and is physically versatile (Zaferani, 2018), the decision was consequential towards the choice of the plastic material. In parallel, the operating temperature of PP ranges from -5 - 100 °C, which means that different cultivating conditions can be simulated with the aid of this material (Klein, 2011). Additionally, both variants show the same extended inlets and outlets, which can be connected to a different kind of tubing material, e.g., silicone or polyvinyl

chloride (PVC), to ensure the supply of fresh nutrient solutions inside the sample chamber and remove the used nutrients. Due to the lengthening of the connections, the problem of sliding off the tubing could thereby be addressed. To counteract the pressure and shear forces, the height of the sample chamber was elevated (8 mm), and the diameter of the connections was widened (2,5 mm).

Using the following Bernoulli-equation (Alexander, 2017; Qin and Duan, 2017):

$$p_1 + \frac{1}{2}\rho v_1^2 + \rho g h_1 = p_2 + \frac{1}{2}\rho v_2^2 + \rho g h_2$$

where p stands for pressure, ρ represents the density of the fluid, v is the velocity of the fluid, g represents the gravitational acceleration, and h is the elevation and furthermore using the following equation (Killer et al., 2019):

$$p = \frac{F}{A}$$

where p represents the pressure, while F is the force and A is the area, the pressure could be reduced, while at the same time the surface area was expanded. Furthermore, the enlargement of the sample chamber height had the advantage that no bubble trap was necessary for the system anymore. Due to the height, indrawn air bubbles during an experiment were trapped at the cover side and did not interfere with the biofilm growing on the base of the *Panta Rhei* flow cells.

Although sharing the basic structure, the two modifications differ in their usability. The *Panta Rhei* D2 cell was designed basically with no sample chamber at the top and bottom so that the core of the cells is accessible. This feature creates opportunities to attach different surfaces to the *Panta Rhei* D2 flow cell and thus perform individual experiments. While using a specific glue for plastic attachment (3M, USA), the surfaces are also detachable and re-attachable. Therefore, a micro- and macroscopic analysis of the biofilm structure is possible. In the *Panta Rhei* P flow cell, the sample chamber is attached to the bottom, and the top cover is missing. Therefore, a groove and screw holes were placed to attach a transparent top cover. This allows the opportunity to put several samples with different geometry inside the sample chamber, then seal the top cover and perform macroscopic biofilm analyses.

In summary, the *Panta Rhei* flow cells were not only designed and constructed to overcome the limitations and disadvantages of already known devices but also to combine their advantages.

3.1.3 The *Panta Rhei* flow cells can be operated at different angles

As previously listed, *Panta Rhei* flow cells were designed to eliminate the need for a bubble trap due to the raised sample chamber, among other features.

In addition, the attached retaining elements not only allowed the attachment of the cells to a microscope stage but also to a specially manufactured bracket, which, in combination with a frame joint, allowed the *Panta Rhei* flow cells to be used at different angular settings and inclinations. As no other flow cells with the characteristics to adjust the angle exist, a special bracket was designed and manufactured to design the cells for space-saving high throughput analyses.

First, a cuboid-shaped piece of plastic was cut to size manually. This was followed by clamping onto the CNC milling machine and subsequent machining (Fig. 3.1.3A; 3.1.3B). The *Panta Rhei* holder was designed to accommodate at least two or more *Panta Rhei* flow cells (Fig. 3.1.3C). With the help of elastic bands, the *Panta Rhei* flow cells could then be attached to or removed from the *Panta Rhei* bracket (Fig. 3.1.3D).

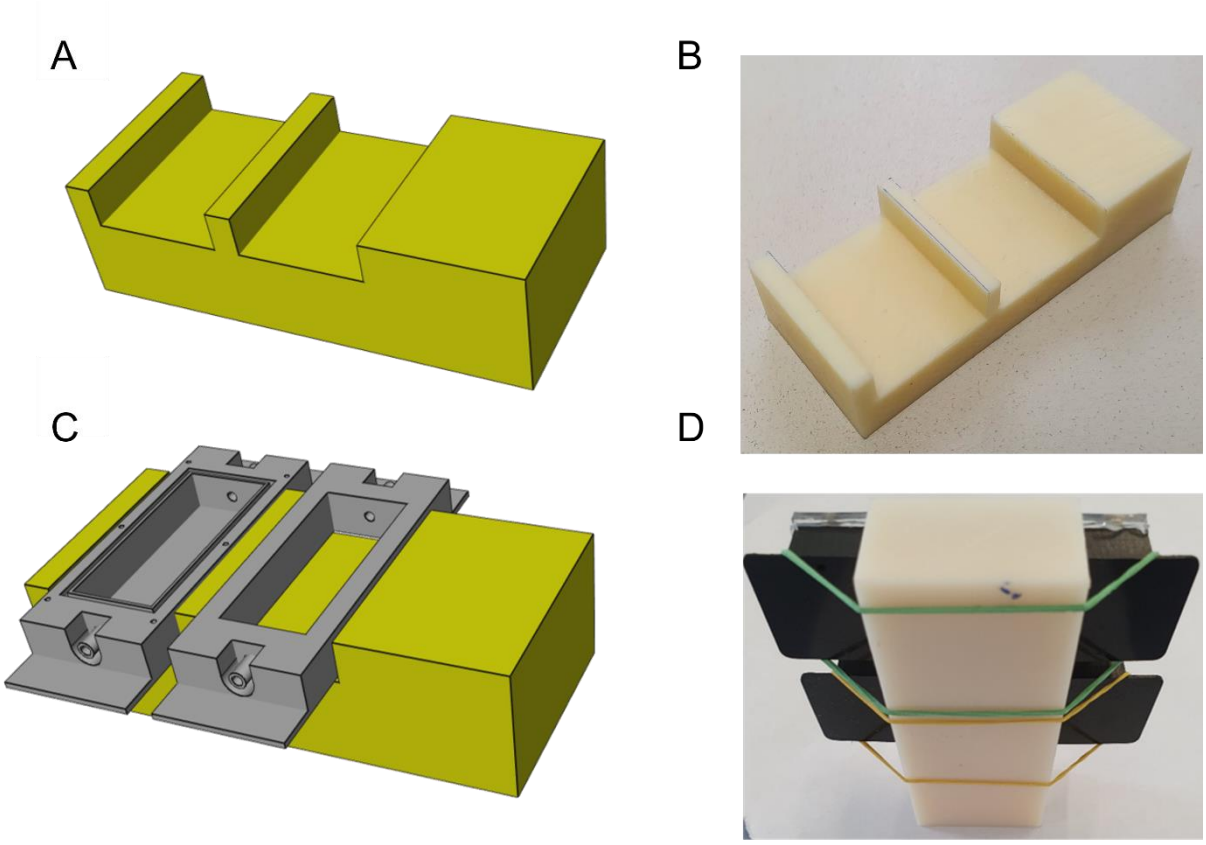

Fig. 3.1.3 The *Panta Rhei* bracket containing the *Panta Rhei* flow cells D2 and P. (A) The CAD construction of the *Panta Rhei* bracket holds two or more *Panta Rhei* flow cells. (B) The *Panta Rhei* bracket after manufacturing by a 5-axis CNC milling machine. (C) Two or more *Panta Rhei* flow cell variants can be mounted on the *Panta Rhei* bracket. (D) Elastic bands are used to attach the flow cells to the bracket.

The *Panta Rhei* flow cells could thus be operated between 0° - 180° using the *Panta Rhei* bracket in combination with a frame joint. This allowed the bacteria to be placed in the sample chamber at a horizontal position of 0°. Once the bacteria had adhered to the surface, the operation could be performed vertically at 90°. This offered the additional advantage that the growing biofilm did not interfere with any air bubbles that might have been penetrated. Based on their properties, the air bubbles float to the top and are carried away by the peristaltic pump (Fig. 3.1.4).

Moreover, the adjustable angles made it possible to simulate different situations. The *Panta Rhei* flow cells could hence also function as a trickle flow reactor. An angle of 10° - 20° resulted in an evenly distributed liquid film on the surface. This led to optimal growth at the air-liquid interface.

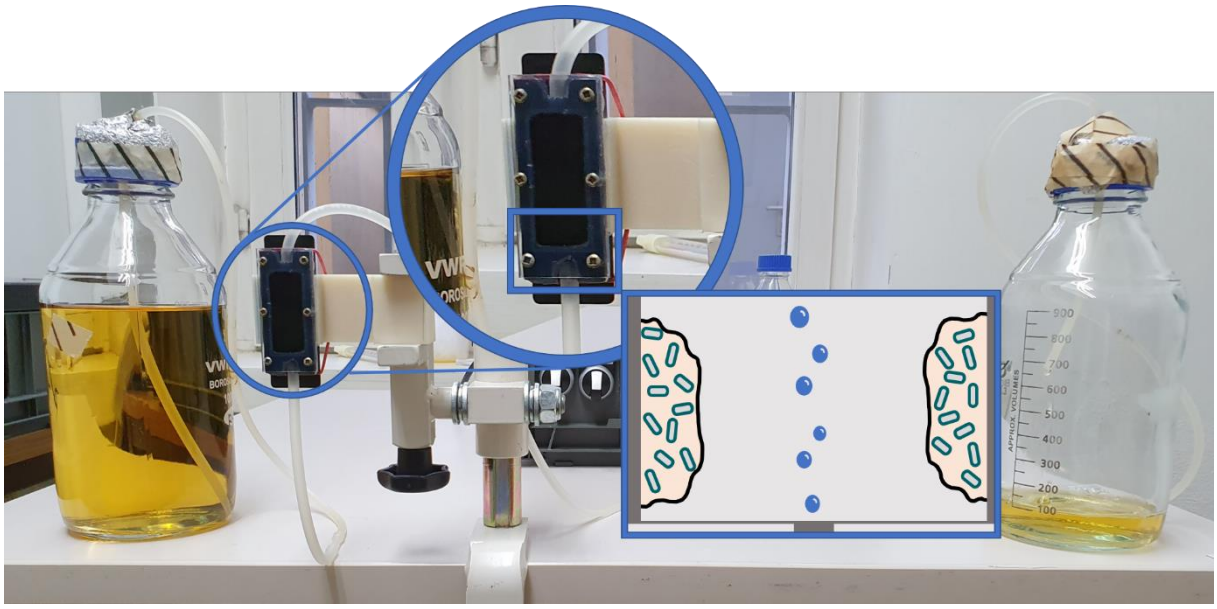

Fig. 3.1.4 Presentation of the *Panta Rhei* microfluidic system using the *Panta Rhei* bracket and the *Panta Rhei* P flow cell. A container with fresh nutrient solution (left side) is connected via tubing to the *Panta Rhei* P flow cell, vertically mounted on the *Panta Rhei* bracket. Due to the angular settings, penetrated air bubbles can be carried away by the connected peristaltic pump without interfering with the grown biofilm inside the sample chamber. The second reservoir (right side) collects the already used-up medium.

3.1.4 The *Panta Rhei* D2 flow cells assure versatility in the selection of surfaces

As described before, the two variants of the *Panta Rhei* flow cells are similar in design but differ significantly in their function. Since there was no system commercially available having two distinct surfaces that could be analyzed with only one flow cell, the *Panta Rhei* D2 flow cell was developed and built for these purposes.

As the focus for the conception of the *Panta Rhei* D2 flow cell was mainly on the flexible use of different surfaces, this flow cell was constructed without an attached lid and base. As a result, the flow cell was designed to be both simple and highly functional. By providing a free choice of surface materials, the *Panta Rhei* D2 flow cell could be used to design an individual experiment without being restricted by the choices offered. Various materials such as glass, plastics, or even metals could be used on both the bottom and the top of the *Panta Rhei* D2 flow cell (Fig. 3.1.5). Surfaces could be attached and removed at any time with the aid of a unique plastic adhesive. Furthermore, the possibility of operation at 90° allowed a biofilm to grow on both surfaces simultaneously without air bubbles hindering these biofilms.

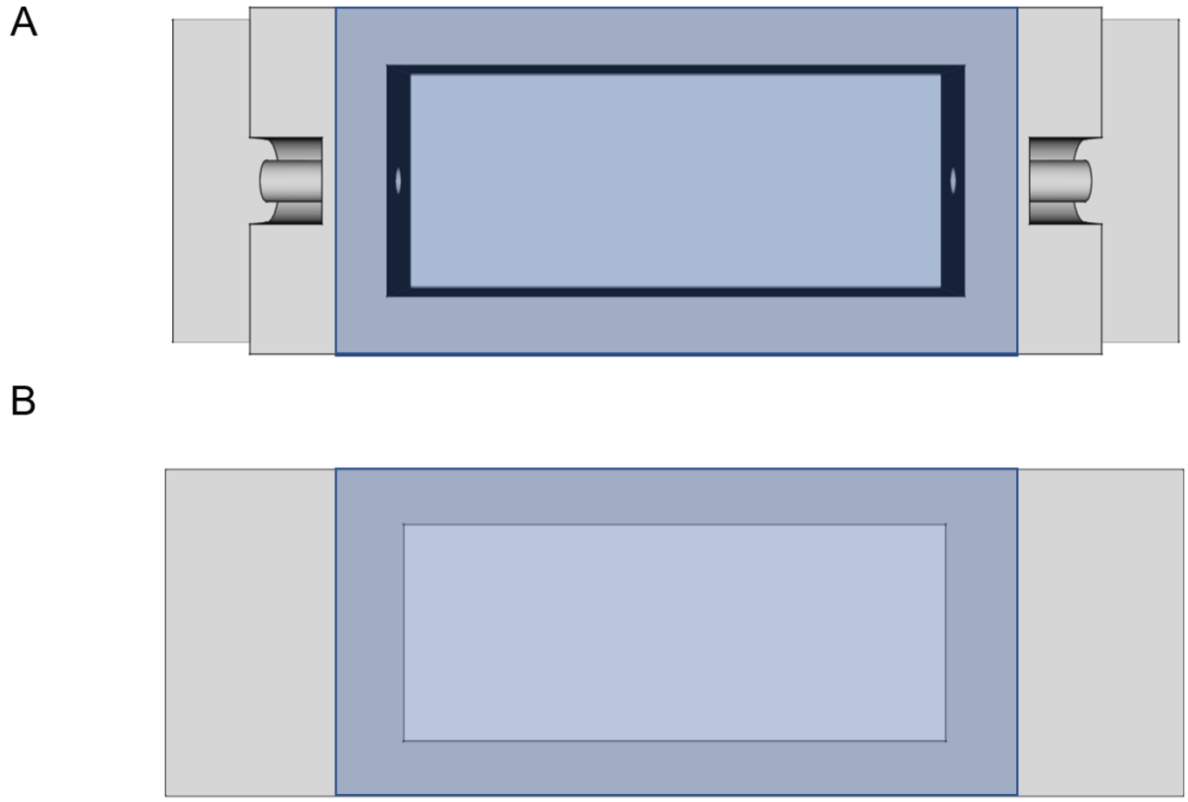

Fig. 3.1.5 The *Panta Rhei* D2 flow cell with attached variable surfaces on top (A) and on the bottom (B). The *Panta Rhei* D2 flow cell design permits the selection of various surface materials. Since the lid and the bottom are not present in this variant, individual materials can be matched to the flow cell. Consequently, a broad spectrum of experiments can be performed using the *Panta Rhei* D2 flow cell. The blue area of the cells indicates the materials and surfaces that are versatile and therefore suitable for different experimental applications.

As shown in Fig. 3.1.6A, it was feasible to use traditional light microscopy with the *Panta Rhei* D2 flow cell. By placing transparent surfaces such as glass on both sides of the *Panta Rhei* D2 flow cell, the beam of light and laser could cross through the flow cell and thus complete the respective analysis.

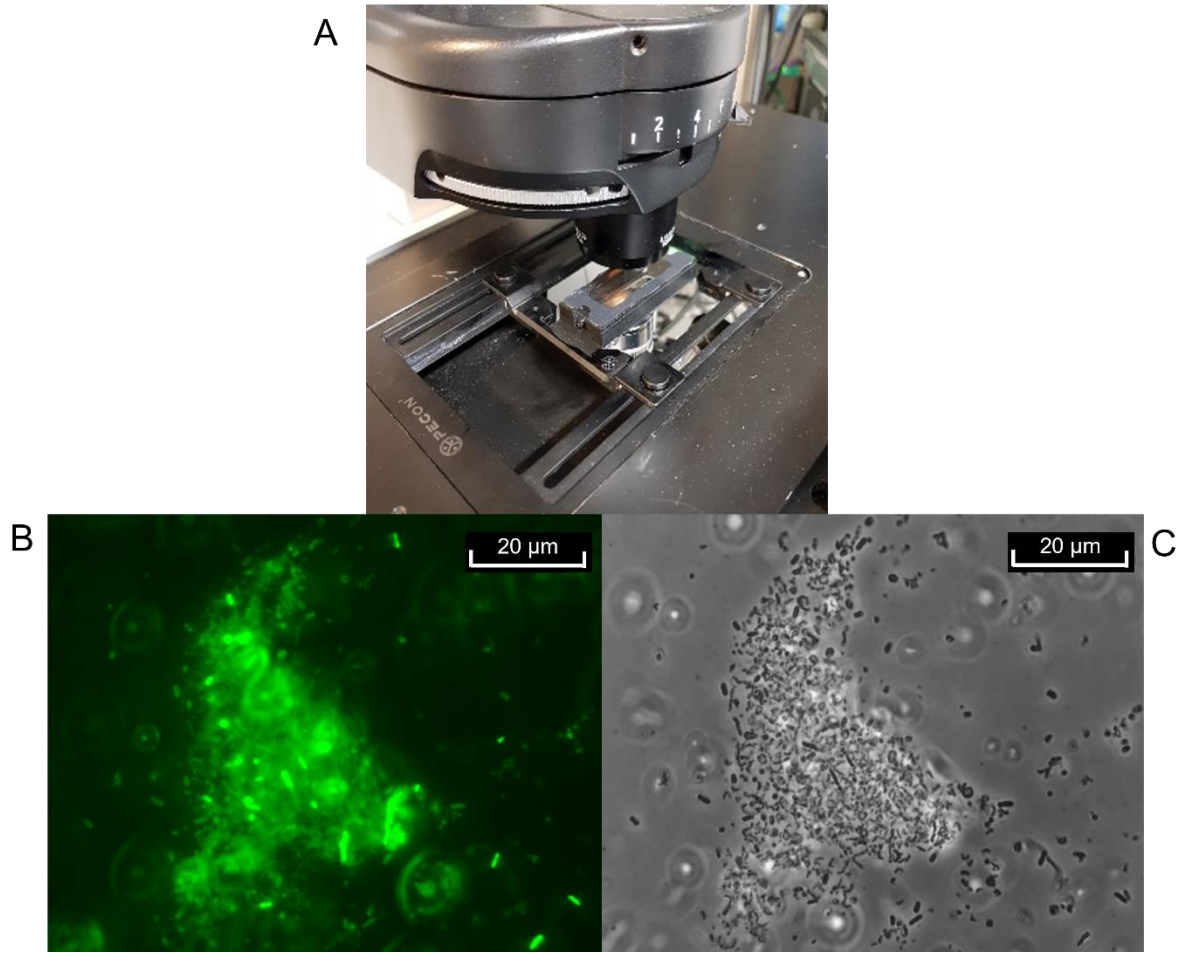

Fig. 3.1.6 Visualization of *P. gallaeciensis* biofilm in the *Panta Rhei* D2 flow cell. (A) The *Panta Rhei* D2 flow cell is mounted onto a fluorescence microscope specimen stage. Due to the transparent surfaces on the top and the bottom, the light beam can pass through the cell. The bacteria, *P. gallaeciensis*, were cultivated in marine medium 2216 for 72 h under constant flow at 30 °C. The attached bacteria were stained with SYTO9 and propidium iodide for 30 minutes at 30°C and made visible using (B) fluorescent microscopy and (B) phase contrast microscopy.

To determine whether the *Panta Rhei* D2 flow cell was functional, the biofilm formation of *P. gallaeciensis* was analyzed. *P. gallaeciensis* is a marine bacterium of the clade *Rhodobacteriaceae*, which is known as a primary colonizer in diverse marine biofilms like ship bodies, an effect that can cause substantial economic loss (de Carvalho, 2018; Gram et al., 2015; Rabus, 2014). For the biofilm assays, the bacteria were grown under a constant flow of 5 ml/h for 72 h in the marine medium 2216 at 30 °C. The cells were then stained with SYTO9 and propidium iodide for 30 minutes at 30 °C. It is apparent from Fig. 3.1.6B and Fig. 3.1.6C that the bacteria could perform biofilm under a constant flow in the *Panta Rhei* D2 flow cell. The planktonic cells were washed away,

leaving the biofilm attached to the surface. Additionally, it could be observed that almost all cells were alive. Consequently, this proved that the *Panta Rhei* D2 flow cell was fully functional and perfectly designed for live cell biofilm imaging analyses.

3.1.5 The *Panta Rhei* P flow cells enable the investigation of external specimen

Given that the flow cells available on the commercial market were either not designed for external sample or surface analysis, not compatible with every external sample geometry, or only compatible with predetermined external sample shapes, the design and engineering of the *Panta Rhei* P flow cell was focused on those features.

The basic structure of both *Panta Rhei* versions is very similar, and the fabrication is almost identical except for a few additional steps. However, in contrast to the *Panta Rhei* D2 flow cell, only the cover is absent in the *Panta Rhei* P flow cell. The bottom was not removed from the beginning in this variant. In addition, the *Panta Rhei* P flow cell has screw holes and a groove on the top to attach a transparent lid. Thus, a time-consuming experiment can be constantly observed from the outside.

To evaluate the functionality of the *Panta Rhei* P flow cells, uncoated and silver nitrate-coated HDPE discs were tested for *P. aeruginosa* biofilm. *P. aeruginosa* is a potent biofilm-forming soil bacterium that occurs in various habitats such as drinking water distribution systems (Mena and Gerba, 2009). Therefore, it is also commonly used as an indicator strain as it can cause severe pulmonary infections (Van Delden and Iglewski, 1998). Moreover, it is already well known that silver exhibits an antimicrobial effect (Kim et al., 2007), therefore serving as a control.

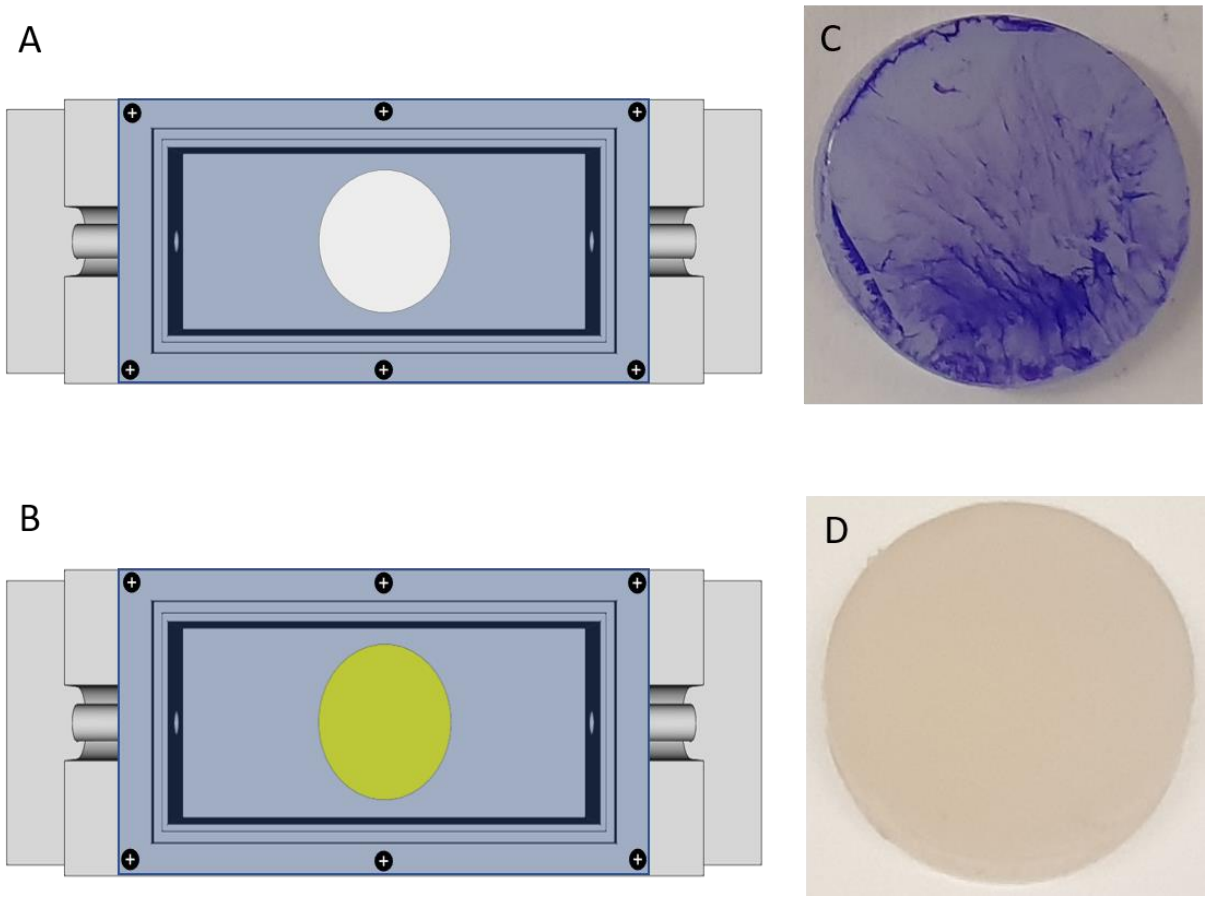

Fig. 3.1.6 Presentation of the non-coated and silver nitrate-coated sample discs. *P. aeruginosa* biofilm was grown for 72 h under a constant flow of 5 ml/h at 30 °C in LB medium on non-coated (A) and silver nitrate-coated (B) sample discs placed inside the *Panta Rhei* P flow cell. The discs were then removed from the flow cells, and the attached bacteria were stained with 1% (w/v) crystal violet. The non-coated sample disc (C) served as a positive control. The silver nitrate-coated sample disc (D) revealed the effect of the inorganic chemical on the bacterial biofilm. The blue area indicates the transparent lid for observation of the experiment.

For the biofilm assays, the discs were placed in separate *Panta Rhei* P flow cells (Fig. 3.1.6A; Fig. 3.1.6B). The bacteria were then placed inside the sample chamber of the *Panta Rhei* P cells. Then, the lid was attached to the top of the respective cell, and the bacteria were cultivated in the cells for 72 hours under a constant flow of 5 ml/h. After crystal violet staining, it was observed that the uncoated disk (Fig. 3.1.6C) did not inhibit biofilm formation. In contrast, the silver nitrate-coated disk (Fig. 3.1.6D) did since no biofilm could be observed on the coated discs.

Furthermore, confocal laser scanning microscopy (CLSM) was used to visualize the biofilm of *P. aeruginosa* on the discs to confirm the macroscopic results observed with

crystal violet. Biofilms were again grown for 72 h at 30° C under a constant flow of 5 ml/h in two separate *Panta Rhei* P flow cells. After removing the sample discs, the attached bacteria on the discs were stained with SYTO9 and propidium iodide. This fluorescent live-dead dye stains all the cells in the biofilm (Deng et al., 2020). Compared to the non-coated disc (Fig. 3.1.7A), the silver nitrate-coated disc (Fig. 3.1.7B) inhibited the bacterial biofilm completely. What stands out in Fig. 3.1.7 is the contrast between the biofilm thickness of the two samples. The non-coated disc showed a biofilm with a thickness of roughly 12 µm, whereas no biofilm was detected on the silver nitrate-coated disc.

In summary, these experiments proved that the Panta Rhei P flow cell is fully functional and practical for analyzing external samples or surfaces, e.g., on their property to repel biofilm formation.

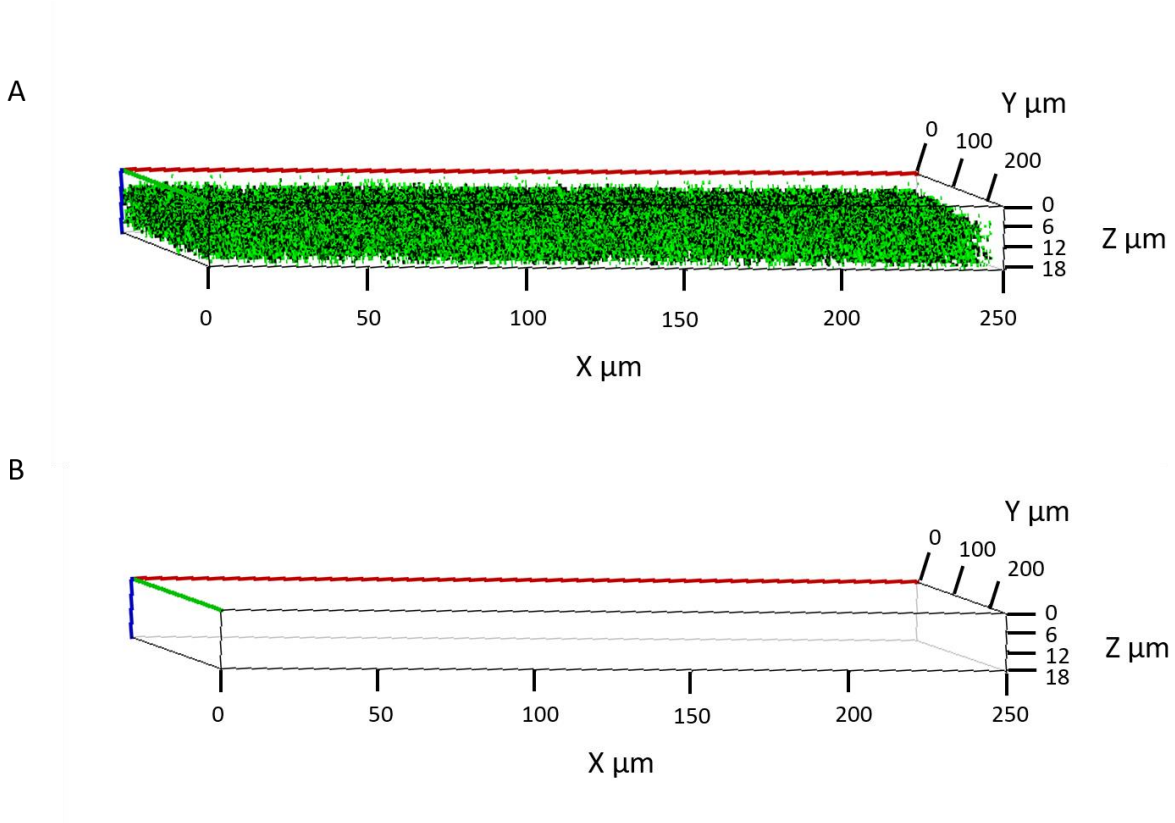

Fig. 3.1.7 The effect of silver nitrate-coating on biofilm formation of *P. aeruginosa*. Confocal laser scanning microscopy (CLSM) of *P. aeruginosa* biofilm grown in LB broth. The bacteria were grown for 72 h under constant flow at 30 °C on non-coated and coated sample discs. The non-coated disc (A) served as a positive control. After removal of the planktonic cells, the remaining bacteria attached to the membranes were stained with SYTO9 and propidium iodide for 30 minutes at 30 °C. The effect of the incorporated silver nitrate (B) on the biofilm was then analyzed by CLSM.

3.1.6 The evolution of the *Panta Rhei* flow cells into an automated biofilm analyzing system

The previous results have already shown that *Panta Rhei* D2 and *Panta Rhei* P represent optimized variants of flow cells, which could cover the needs of a complete macroscopic and microscopic analysis of bacterial biofilm and overcome the limitations of previous commercially available flow cells. However, the question arose whether the entire biofilm analysis process could also be automated significantly and, therefore, would also be suitable for screenings. Since such a system does not exist yet for biofilm analysis, the next task of this work was to design an automated all-in-one biofilm-analyzer system.

Therefore, the design of the two flow cell variants, *Panta Rhei* D2 and *Panta Rhei* P, was initially revised. For easier handling, both cells were upgraded modularly with a clip-on system. As shown in Fig. 3.1.8A, the *Panta Rhei* D2 flow cell was designed with a frame for the bottom and the lid. The respective surfaces could thus be snapped into the cells. In addition, a snap-in feature was developed that provided a space-saving option for multiple flow cells to be used simultaneously. The same development was applied to the *Panta Rhei* P flow cell (Fig. 3.1.8B).

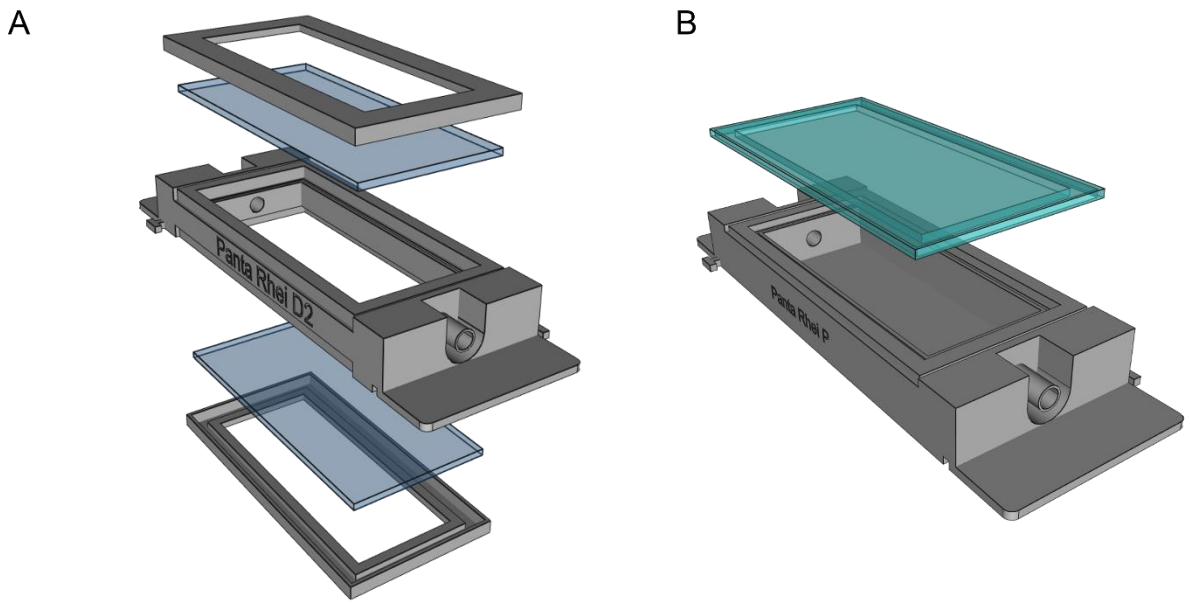

Fig. 3.1.8 The revised *Panta Rhei* flow cells. (A) Exploded drawing of the *Panta Rhei* D2 flow cell. The frames for the bottom and the lid, respectively, can clamp a surface. (B) Exploded drawing of the *Panta Rhei* P flow cell. The transparent lid is clicked onto the upper side of the cell for sealing.

A further step towards automated design involved the customization of the *Panta Rhei* bracket. Here, a retainer was redesigned from scratch. However, particular focus was given to preserving the ability to clamp the *Panta Rhei* flow cells via the retaining elements. The modified *Panta Rhei* bracket was renamed *Panta Rhei* Atlas. The *Panta Rhei* Atlas is presented in Fig. 3.1.9. The *Panta Rhei* Atlas has been specifically designed with a notch to insert single or stacked *Panta Rhei* flow cells. Furthermore, pivots have been developed on the sides, which stepper motors can automatically control, so adjustment of different angle settings is always possible. Furthermore, a frame joint was no longer required due to the incorporated base plate.

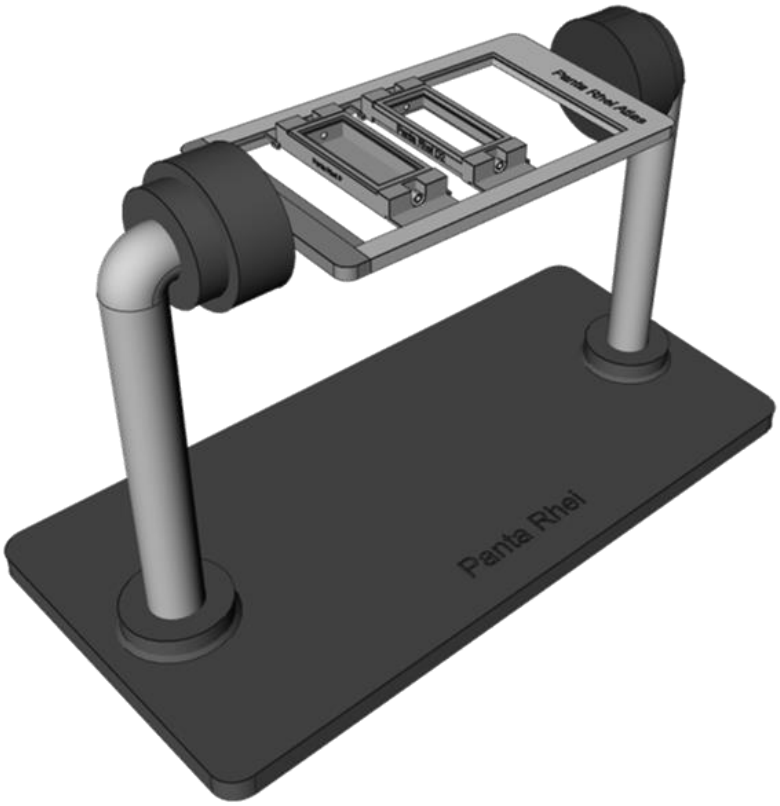

Fig. 3.1.9 The redesigned *Panta Rhei* Atlas carrying *Panta Rhei* flow cells. The *Panta Rhei* Atlas was supplied with a special groove to accommodate one or more *Panta Rhei* flow cells. With the help of the swivel joints on the sides, control by a stepper motor is enabled. An operation in combination with a frame joint was not necessary for the angular settings.

A circuit design was required to enable a system to operate in an automated process. Fig. 3.1.10 illustrates a simplified version of the designed block diagram for the *Panta Rhei* system. A microcontroller is the system´s core, which can perform different tasks. To use the system, a power supply, a voltage regulator, and appropriate switching elements are required. A real-time clock (RTC) can schedule the process steps. A thermal sensor monitors the temperature and transmits the data to the microcontroller. A heating element or a fan is activated accordingly in case of temperature deviations. The microcontroller also drives two stepper motors. One is responsible for adjusting the angular gradient, while the other stepper motor controls the integrated peristaltic pump. For interactivity, the system is also equipped with a USB port. A touchscreen display also supports proper operability. With the help of the ethernet adapter, access is also possible via the network.

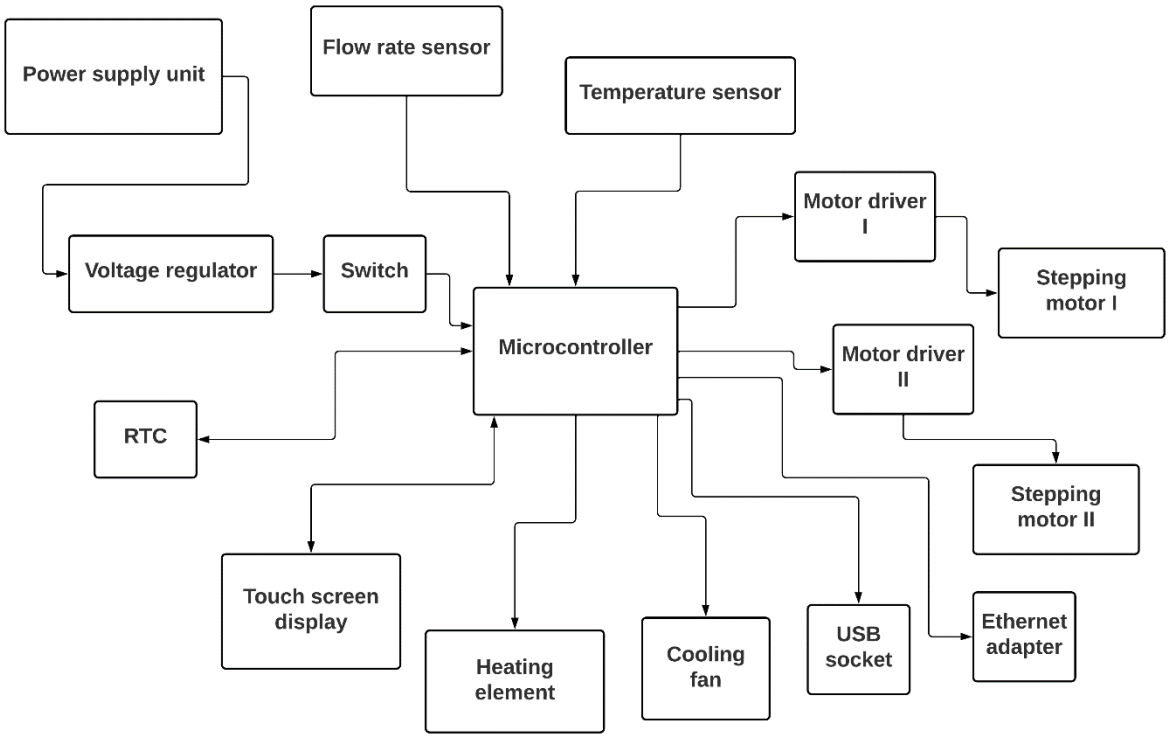

Fig. 3.1.10 Simplified block diagram of the *Panta Rhei* biofilm analyzer system. To control an automated *Panta Rhei* system, a central microcontroller is required. This is supplied with electricity by a power supply unit. The connection of a touch display enables the input of desired parameters. The ethernet adapter allows access to the system through the network. The first stepper motor controls the angular inclination of the *Panta Rhei* Atlas and thereby the *Panta Rhei* flow cells. The second sensor controls an integrated peristaltic pump and thus the supply of nutrient solution to the *Panta Rhei* flow cells. An associated flow sensor allows the adjustment of the flow rate. An additional temperature sensor enables control of the cultivation temperature. Finally, a heating element and a fan regulate the set temperature.

Additionally, a housing was sketched so that the components of the *Panta Rhei* system could interact with each other in the form of an all-in-one device close to one another. Fig. 3.1.11 shows two concepts for the *Panta Rhei* device. Among them, the so-called BIAttiva Pente device (Fig. 3.1.11A) differs from the BIAttiva Pente^{thermo} (Fig. 3.1.11B) only in the absence or presence of the temperature incubation control. Instead, the BIAttiva Pente^{thermo} has an additional incubation chamber with an associated heating element and fan. In this case, the *Panta Rhei* flow cells can be retracted, and the temperature is kept stable by closing the shutters.

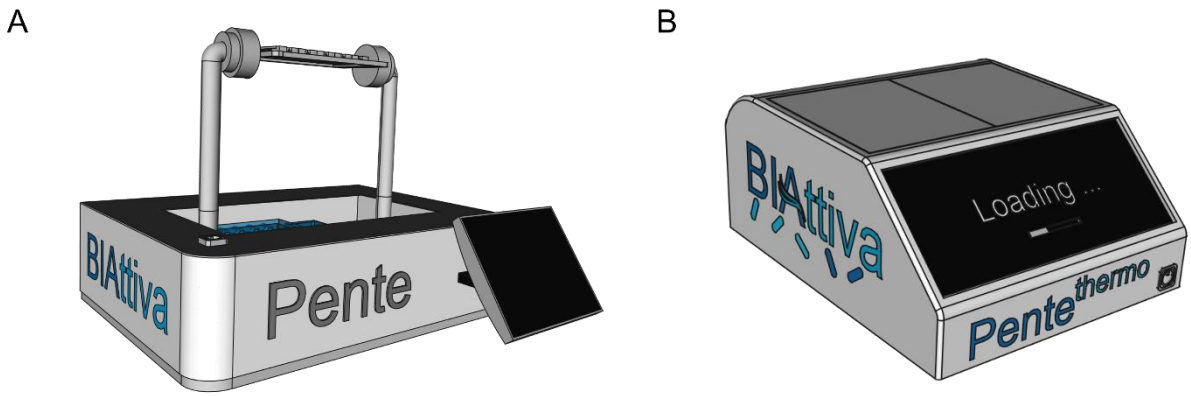

Fig. 3.1.11 Schematic illustration of potential variants BIAttiva Pente without (A) and BIAttiva Pente^{thermo} with (B) temperature regulation of an all-in-one microfluidic *Panta Rhei* device to analyze bacterial biofilm. The individual components of the *Panta Rhei* system, such as the *Panta Rhei* flow cells, the *Panta Rhei* Atlas, the associated stepper motors, sensors, and the peristaltic pump and the microcontroller for operation, are installed in a corresponding enclosure. A suitable touch display is used for the operation and setting of parameters.

Taken together, two different variants of flow cells could be designed and manufactured in this thesis. Due to the design, the limitations of the already common flow cells, which were identified during the production and usage of these, could be circumvented. Furthermore, with the help of a manufactured *Panta Rhei* bracket, it was possible to operate the cells without a bubble trap, as common flow cells have to use. Moreover, operation at an angle of 90° could be achieved. This enabled the simultaneous cultivation of bacterial biofilm on two different surfaces. In addition, the results demonstrate that microscopic and macroscopic analysis, such as examination by CLSM or crystal violet staining, is applicable with the *Panta Rhei* flow cells. With the design of a complete *Panta Rhei* system, including different housings and the development of an accompanying block diagram, new standards could be set regarding biofilm analysis on a large scale.

The optimized microfluidic flow-through system designs with the file number DE 10 2020 130 870.1 were submitted to the German Patent and Trademark Office and have already been accepted as a patent.

3.2 Various environmental conditions contribute to the formation of bacterial biofilms

Bacteria form biofilm under a wide variety of circumstances and in a broad range of environments (Yin et al., 2019), which provides many advantages for the bacteria (Santos et al., 2018), but also poses increased threats to the environment, industry, and public health (Muhammad et al., 2020). Although some factors are known to initiate or minimize biofilm generation, these studies mainly deal with model organisms such as *P. aeruginosa* (Toyofuku et al., 2016). However, the observed effects do not often reflect the general nature of all the bacteria in biofilms (Flemming, 2020). Thus, the factors affecting bacteria found in drinking water or marine biofilms remain largely unexplored, and biofilm formation in those sectors remains a major challenge.

As bacterial biofilm formation in the marine sector and the drinking water supply cause significant financial and health problems (Chaves Simões and Simões, 2013; de Carvalho, 2018; Fish et al., 2016), the objective of this work was to investigate which conditions stimulate the bacteria that can be found in biofilms from the marine sector and the drinking water supply into forming biofilms, as well as the factors that prevent or diminish the development of biofilms. Therefore, the influence of the nutrient composition and the incubation period was investigated. In addition, different surfaces were examined for their effect on biofilm formation. Furthermore, the bacterial composition and the associated biofilm development were analyzed.

3.2.1 Nutrient composition and incubation time span impact biofilm formation of marine and drinking water bacteria

Since the nutrient supply in the marine environment and the drinking water system may fluctuate and thus the intensity of the biofilm formation may vary from time to time (Dai et al., 2022; Douterelo et al., 2016; Salgar-Chaparro et al., 2020), it was necessary to investigate first to what extent the nutrient composition contributes to the bacterial biofilm formation. Furthermore, biofilm formation frequently depends on the duration of incubation as well as on the nutrients (Guzmán-Soto et al., 2021). Thus, the extent to which biofilm formation depends on different incubation periods was also part of the investigation. Therefore, bacteria from the marine area and the drinking water supply

were selected that either initiate the biofilm formation or are involved in the formation of the biofilm. The marine bacteria *P. gallaeciensis*, *H. alkalilenta*, and *H. aquamarina* were selected for this study. *Phaeobacter* belongs to the *Roseobacter* clade, which are primary colonizers of marine surfaces (de Carvalho, 2018; Zhao et al., 2016). *H. alkalilenta* and *H. aquamarina* belong to the *Oceanospirillales* family, well-known to be involved in the development of marine biofilms (de la Haba et al., 2014; Mouchka et al., 2010; Tahrioui et al., 2013; Vaksmaa et al., 2021). Regarding drinking water bacteria, *S. adhaesiva*, *M. mesophilicum*, and *B. nasdae* were investigated for biofilm formation. *S. adhaesiva* belongs to the *Sphingomonas* spec., which are responsible for colonizing reverse osmosis membranes (Bereschenko et al., 2010; de Vries et al., 2019). *M. mesophilicum* belongs to the *Methylobacterium* spec., which are considered OPPPs (Szwetkowski and Falkinham, 2020). *B. nasdae* belongs to the *Brevundimonas* spec., which are opportunistic pathogens (Ryan and Pembroke, 2018) and can be found in drinking water distribution systems (Zhu et al., 2020).

First, the different bacteria were cultured along with various nutrient compositions for a constant incubation time of 72 h at 30 °C. Subsequently, the biofilms were analyzed using crystal violet staining. The cultivation media differ significantly in their composition, as, for example, the M1 and TSY media contain a high peptone content. The medium M9, on the other hand, is notable for its deficient nutrient level. The HD medium contains a higher level of glucose. The media 2216 and MM display a high salt content, with 2216 featuring a higher salt variation, while MM contains only NaCl. In particular, various trace elements are present in the RS medium. The media selection was made to identify the influence of different components on biofilm formation.

Fig. 3.2.1 shows the comparison of the different nutrient solutions on the biofilm development of the respective bacteria. Regarding the drinking water bacteria, Fig. 3.2.1A clearly demonstrates that not all nutrient media led to a similarly strong biofilm formation. *S. adhaesiva* exhibited the strongest biofilm generation in HD medium (A_{575} = 3.42), while the weakest was observed with M9 medium (A_{575} = 0.74). *B. nasdae* showed strong biofilm formation in RS medium (A_{575} = 2.75), TSY medium (A_{575} = 2.61) and HD medium (A_{575} = 2.15), and the lowest values were observed with 2216 medium (A_{575} = 0.93) and M9 (A_{575} = 0.91). *M. mesophilicum* was particularly distinguished by developing a significantly lower biofilm in contrast to *S. adhaesiva* and *B. nasdae*. The highest biofilm formation was achieved in TSY medium (A_{575} = 1.57). Similarly, little

biofilm formation was detected in 2216 medium (A_{575} = 0.31) and M9 medium (A_{575} = 0.29).

In summary, it was observed that cultivation media with higher content of glucose, peptone, or trace elements enhanced biofilm formation in drinking water bacteria.

Fig. 3.2.1B depicts the effect of different nutrients on biofilm formation in the marine environment. Once more, it was noticed that not all nutrient media had the same effect on biofilm development. While *H. alkalilenta* reached a biofilm of at least A_{575} = 2.6 in all tested nutrient solutions, this effect could not be observed for *H. aquamarina* and *P. gallaeciensis*. The HD, LB, and M1 media resulted in low biofilm formation for *H. aquamarina* and *P. gallaeciensis*. The greatest increase in biofilm was obtained in medium 2216. Here, *P. gallaeciensis* achieved a value of A_{575} = 1.98 and *H. aquamarina* a value of A_{575} = 1.28. The results indicated that biofilm formation and nutrient composition are probably correlated. It was noted that, in addition to the high salt content, the variety of different salts also impacted biofilm formation in marine bacteria. Cultivation media with a high glucose and peptone content resulted in less biofilm formation in marine bacteria.

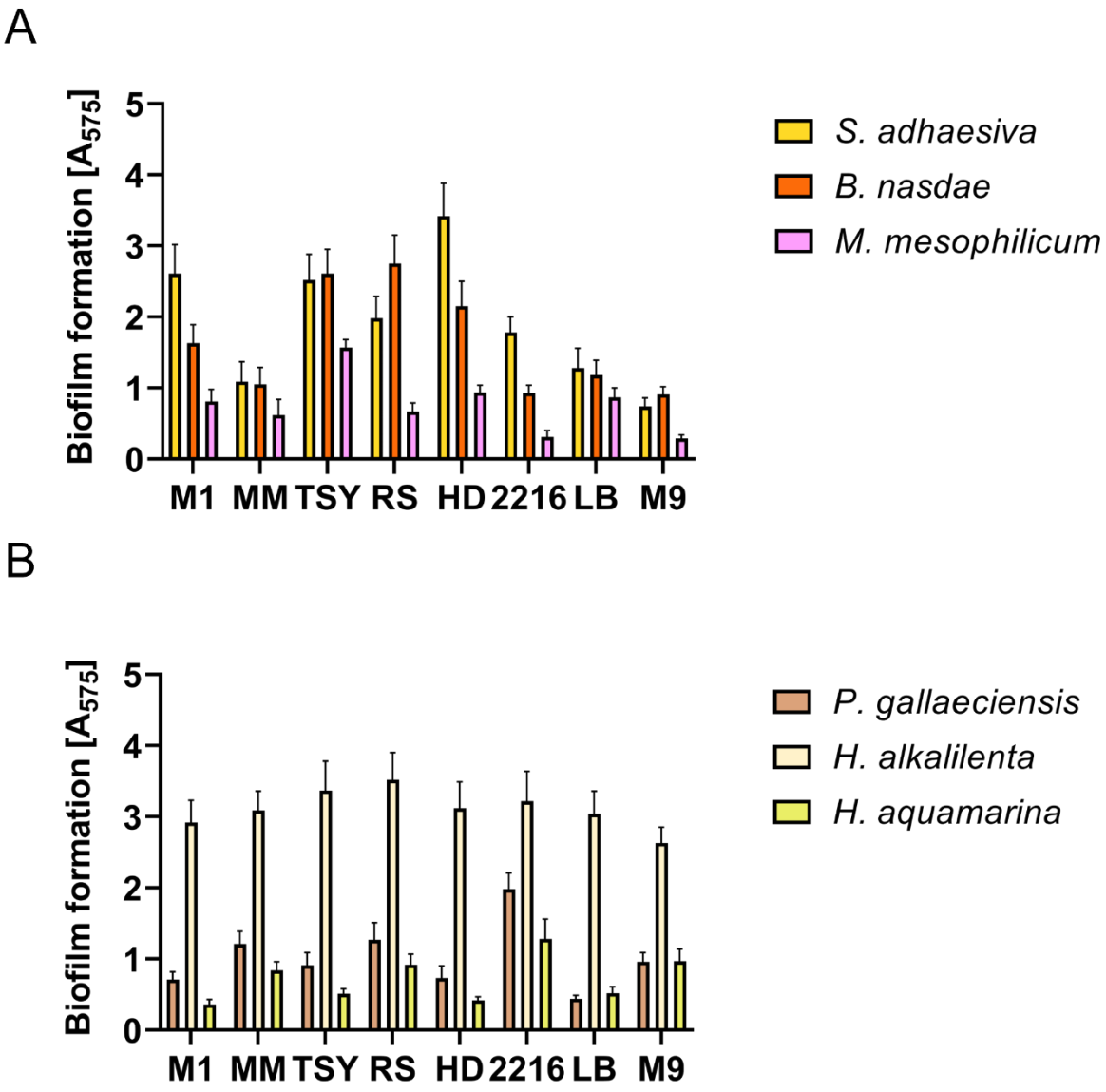

Fig. 3.2.1 The influence of nutrient composition on bacterial biofilm formation. Drinking water bacteria *S. adhaesiva*, *B. nasdae*, and *M. mesophilicum* (A) and marine bacteria *P. gallaeciensis*, *H. alkalilenta*, and *H. aquamarina* (B) were incubated in various cultivation media M1, MM, TSY, RS, HD, 2216, LB and M9 for 72 h at 30 °C. Then, biofilm analysis was quantified using crystal violet staining. Error bars represent the standard deviation of three biologically independently performed experiments.

To examine the degree to which the incubation time affected biofilm formation, the bacteria from the drinking water and the marine habitat, which were also tested for biofilm formation in the different nutrient media, were cultivated for different time periods in the respective medium they showed highest biofilm formation. The various time points 24 h, 48 h, 72 h, 96 h, and 120 h were selected accordingly. Following the respective time points, crystal violet staining was performed and quantified.

Fig. 3.2.2 clearly depicts the effect of the different incubation periods on the biofilm. As it can be observed in Fig. 3.2.2A, the biofilm formation of the drinking water bacteria differed significantly with continuous incubation. *S. adhaesiva* exhibited maximum biofilm intensity after 72 h (A_{575} = 3.42), which did not significantly change after 96 h and 120 h of incubation. Surprisingly, an unexpected observation was made regarding the biofilm formation of *B. nasdae*. The maximum biofilm formation (A_{575} = 3.57) was observed after 48 h. However, the biofilm gradually decreased with ongoing incubation times, resulting in the detection of only about 55% of the biofilm at 120 h (A_{575} = 1.94), in contrast to 48 h. For *M. mesophilicum*, the results pointed to a slow but steady biofilm increase as the incubation period progressed. Fig. 3.2.2B displays the results of biofilm development of the marine bacteria at different time lengths. The biofilm of *H. alkalilenta* reached a strong biofilm formation after 48 h (A_{575} = 3.47). The value of the biofilm hardly changed as incubation proceeded. The results observed for *H. aquamarina* indicated that the biofilm increased with time as incubation progressed. The peak value of biofilm was reached after 120 h (A_{575} = 1.87). Moreover, a surprising observation was made in *P. gallaeciensis*. Here, the highest value of biofilm was detected after only 24 h (A_{575} = 2.97). The biofilm development decreased after progressive incubation so that after 120 h (A_{575} = 1.29), only about 45% of the biofilm could be detected. These results indicated that the length of the incubation period could be crucial for bacterial biofilm formation.

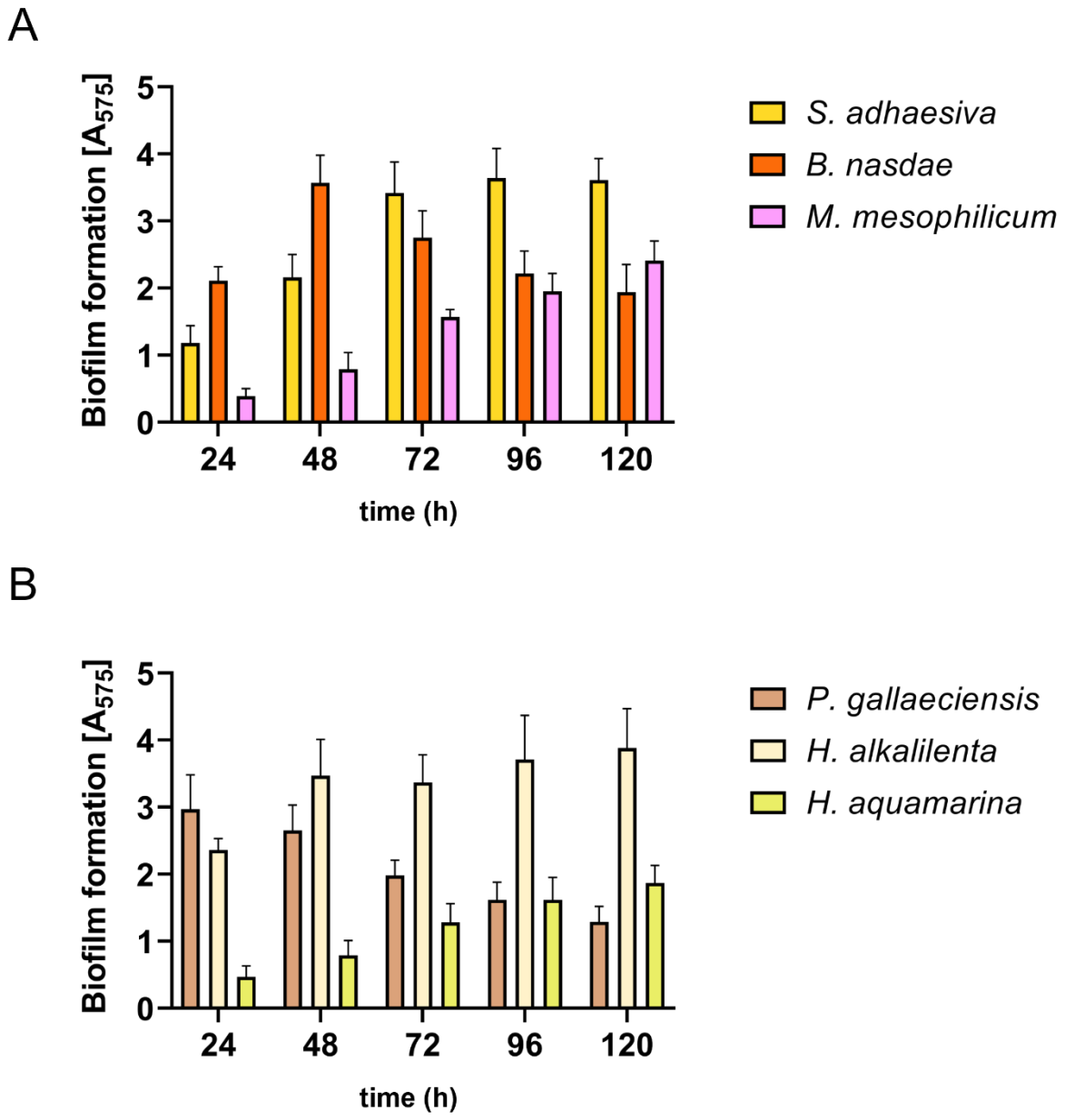

Fig. 3.2.2 The effect of varying incubation periods on bacterial biofilm formation. Drinking water bacteria *S. adhaesiva*, *B. nasdae*, and *M. mesophilicum* (A) and marine bacteria *P. gallaeciensis*, *H. alkalilenta*, and *H. aquamarina* (B) were incubated for different incubation periods before biofilm formation was quantified. Five different time points were chosen for that study (24 h, 48 h, 72 h, 96 h, and 120 h). *S. adhaesiva* was cultivated in HD medium, *B. nasdae* was incubated in RS medium, and *M. mesophilicum* was cultivated in TSY medium. The marine bacteria *P. gallaeciensis* and *H. aquamarina* were cultivated in 2216 medium, whereas *H. alkalilenta* was incubated in TSY medium. After each time point, the biofilm formation was analyzed using crystal violet solution. The standard deviation of three biologically independently performed experiments is represented by error bars.

3.2.2 Different surface materials have an impact on bacterial biofilm development

Since it was shown that the composition of the nutrients, as well as the incubation time, affected the biofilm formation of marine and drinking water bacteria, the influence of various surface materials was tested. Different materials, such as steel and different plastics, are commonly used in the marine environment (Vukelic et al., 2021; Dhandapani et al., 2022; Oluniyi Solomon and Palanisami, 2016; Dang and Lovell, 2016) and in the drinking water supply systems (Allion et al., 2011), so it was essential to examine whether different materials could be used to expose different bacteria to the respective surface materials in order to determine their impact on biofilm formation. The materials S235 steel, PE, PETG, PC, and PS were used accordingly, as shown in Fig. 3.2.3.

Fig. 3.2.3 The materials examined on the effect of biofilm formation. The different types of materials were cut to a square shape and analyzed for their impact on biofilm formation. From left to right: S235 steel, PE, PETG, PC, and PS.

First, the individual materials were cut into squares and then placed among the bacteria. *P. gallaeciensis* was used as a representative for marine bacteria, and *M. mesophilicum* was used as an example for the drinking water bacteria. *P. gallaeciensis* was incubated together with the materials for 72 h at 30 °C in 2216 medium, while *M. mesophilicum* was cultured on the materials for 144 h at 30 °C in TSY medium. The evaluation was then performed by staining the materials with crystal violet and photometric analysis at 575 nm.

The results for the biofilm formation of *M. mesophilicum* and *P. gallaeciensis* on the various substrates are shown in Fig. 3.2.4. For *M. mesophilicum*, the highest biofilm formation was detected on PS (A_{575} = 1.07), and the lowest biofilm formation was detected on steel (A_{575} = 0.29). For PETG (A_{575} = 0.61), PC (A_{575} = 0.55) and PE (A_{575}

= 0.42), moderate biofilm formation was observed. Surprisingly, in the case of *P. gallaeciensis*, very strong biofilm formation was detected on steel (A_{575} = 4.48). However, on the plastic surfaces, the biofilm development was distinctly weaker. The polymer that exhibited the strongest biofilm formation among the plastics was PS (A_{575} = 1.61). The biofilm on steel, however, amounted to roughly 280% of the biofilm on PS.

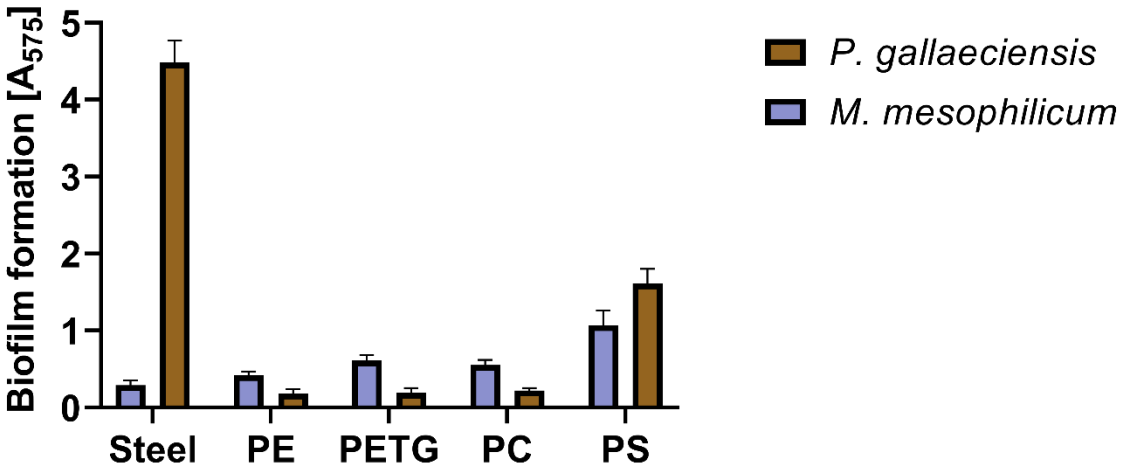

Fig. 3.2.4 Influence of different material surfaces on the biofilm formation of *P. gallaeciensis* and *M. mesophilicum*. *P. gallaeciensis* was cultivated with the materials for 72 h at 30 °C in 2216 medium. *M. mesophilicum* was incubated together with the materials for 144 h at 30 °C in TSY medium. The standard deviation of three biologically independently performed experiments is represented by error bars.

Since exceptionally strong biofilm formation was observed on steel in *P. gallaeciensis*, the composition of structural steel was examined to identify a putative content of the material that triggered biofilm formation. Iron and manganese were found to be present in higher proportions (Schäfer et al., 2015). Accordingly, the next focus was on examining the effect of bivalent Fe^{2+} and Mn^{2+} ions on the biofilm formation of *P. gallaeciensis*. Additionally, the investigation also included other bivalent metal cations, such as Cu^{2+}, Zn^{2+}, Co^{2+}, and Ca^{2+}.

Fig. 3.2.5 demonstrates the effect of the bivalent cations on the biofilm formation of *P. gallaeciensis*. In particular, Fe^{2+} increased the biofilm by about 26%. For Mn^{2+}, an approximately 22% increase could be observed. In contrast, Zn^{2+} decreased biofilm formation by approximately 10%, while Cu^{2+} exhibited a reduction of about 40%. Ca^{2+} appeared to have no significant effect on the biofilm.

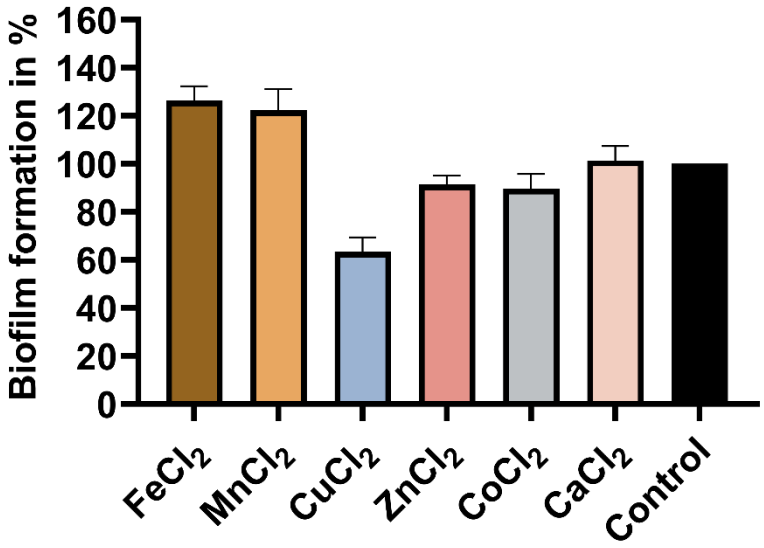

Fig. 3.2.5 Effect of metal cations on biofilm formation of *P. gallaeciensis*. The various metal cations were added to *P. gallaeciensis* at a final concentration of 50 µM. Bacteria were then cultivated for 72 h at 30 °C in 2216 medium. The biofilm was then detected and quantified using crystal violet staining. The error bars symbolize the standard deviation of three independently performed biologically replicates.

To confirm and visualize the effect of Fe^{2+} and Mn^{2+}, CLSM was performed. Fe^{2+} and Mn^{2+} were added to the bacteria, while no addition of metal cations served as a control. After incubation and removal of the planktonic cells, the bacteria were stained on the surface with SYTO9 and propidium iodide. This method allowed the detection of all bacteria within the biofilm.

The results of CLSM analysis of the biofilm of *P. gallaeciensis* with and without the addition of Fe^{2+} and Mn^{2+} can be seen in Fig. 3.2.6. It could be observed that without the addition of metal cations (Fig. 3.2.6A), the bacteria (green fluorescence) colonized the surface uniformly, although non-colonized areas (white spots) were also clearly visible. However, with the addition of Mn^{2+} (Fig. 3.2.6B) or Fe^{2+} (Fig. 3.2.6C), it was obvious that the colonized areas became denser, and the non-colonized areas were strongly diminished.

Furthermore, bioinformatics analysis revealed that *P. gallaeciensis* exhibits specific transporters for Mn^{2+} and Fe^{2+}.

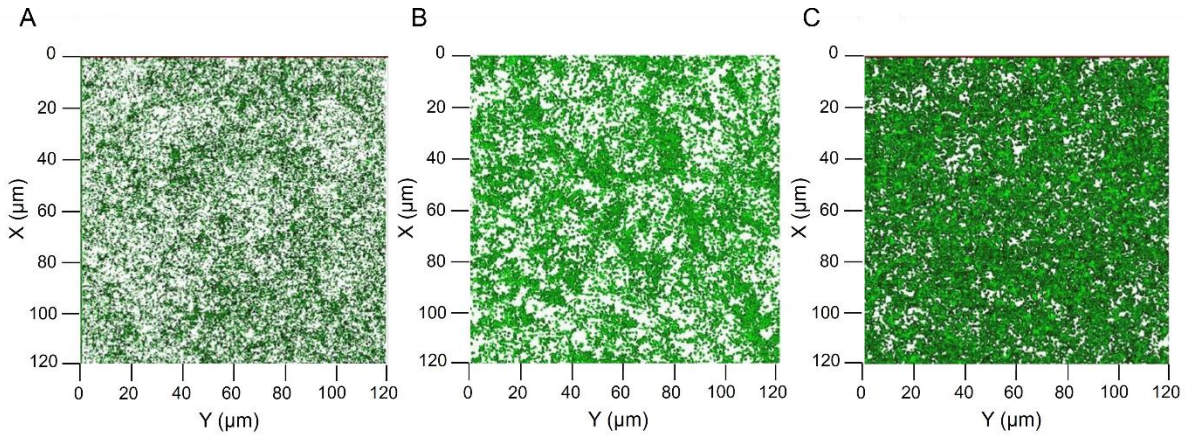

Fig. 3.2.6 CLSM analysis of the effect of Fe^{2+} and Mn^{2+} on the biofilm of *P. gallaeciensis*. Bacteria were incubated without addition (A), with the addition of Mn^{2+} (B) and Fe^{2+} (C) for 72 h in 2216 medium at 30 °C. Subsequently, the attached bacteria were stained with SYTO9 and propidium iodide and then analyzed on CLSM.

These obtained results demonstrated that the surface material had a very significant contribution to the biofilm formation of *M. mesophilicum* and *P. gallaeciensis*. In addition, it was also observed that Fe^{2+} and Mn^{2+} strongly enhanced the biofilm formation of *P. gallaeciensis*. Moreover, it was found that this organism contains specific transporters for manganese and iron.

3.2.3 Mixed species composition strongly affects biofilm intensity

Both nutrient composition and incubation time, as well as surface material, were identified to influence biofilm formation. In nature, bacterial biofilms are often composed of several bacterial species rather than just one (Guillonneau et al., 2018; Schwering et al., 2013). For that reason, the extent to which the biofilm composition affects biofilm strength was also investigated.

The drinking water bacteria, as well as the marine bacteria, were cultivated individually and together in a consortium. As a representative for the drinking water bacteria, *S. adhaesiva*, *B. nasdae*, and *M. mesophilicum* cultivated in TSY medium were selected. Representatives of the marine bacteria were *P. gallaeciensis*, *H. alkalilenta*, and *H. aquamarina* grown in the 2216 medium. The respective bacterial cell count was adjusted to a starting OD_{600} of 0.5 and cultivated at 30 °C for 24 h in the appropriate

media. When cultivating collectively in a mixed species consortium, only one-third of each bacterial species was used to set the starting OD_{600} of 0.5 as well. After 24 h, the biofilm was stained with crystal violet and quantified.

The influence of bacterial mixed species composition on the biofilm formation is shown in Fig. 3.2.7. Regarding the drinking water bacteria (Fig. 3.2.7A), it can be noticed that after 24 h, *B. nasdae* developed the strongest biofilm when cultivated separately (A_{575} = 1.91). On the other hand, *M. mesophilicum* produced the weakest biofilm when cultivated by itself (A_{575} = 0.39). However, it was observed that the highest biofilm formation (A_{575} = 2.78) of this experimental setup was detected when the bacteria were cultivated together in the consortium. Considering the marine bacteria (Fig. 3.2.7B), it was observed that, when separately cultivated, *P. gallaeciensis* (A_{575} = 2.97) and *H. alkalilenta* (A_{575} = 2.48) both formed a strong biofilm. In contrast, *H. aquamarina* formed a weaker biofilm (A_{575} = 0.47). It was also observed for the marine bacteria that joint cultivation in a consortium (A_{575} = 3.81) significantly boosted biofilm development. In summary, a stronger overall biofilm formation was observed in the drinking water and marine consortium. However, since only one-third of the respective bacteria were added at the beginning of the experiment, a purely additive effect on the biofilm formation can be excluded with a high grade of likelihood.

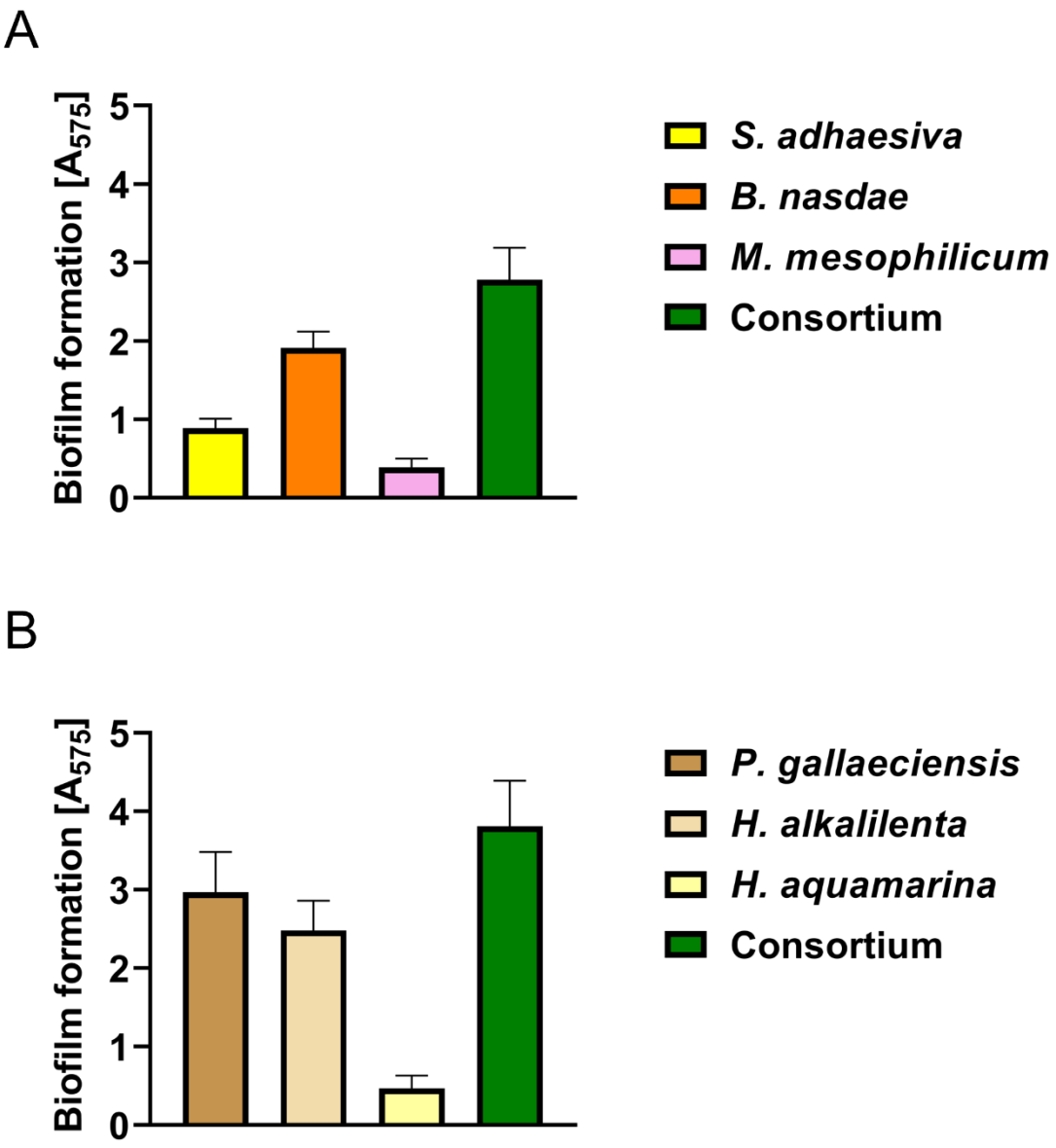

Fig. 3.2.7 The biofilm formation of marine and drinking water bacteria cultivated both individually and collectively as a consortium. (A) Drinking water bacteria were cultured both individually and together as a consortium for 24 h at 30 °C in TSY medium. (B) Marine bacteria were cultured both individually and as a consortium for 24 h at 30 °C in 2216 medium. Biofilm analysis and quantification were performed by crystal violet staining. The error bars represent the standard deviation of three independently performed biological replicates.

Based on the finding that a bacterial consortium could promote biofilm formation, the extent to which the strength of the biofilm was dependent on the initial colonization of the surface by a particular bacterial species within the consortium was investigated.

For that purpose, *S. adhaesiva* and *B. nasdae* were used as representatives for drinking water bacteria. The consortium of marine bacteria analyzed was composed of

P. gallaeciensis and *H. alkalilenta*. Both bacterial species were cultivated together in a consortium. However, the primary colonizer in each case was exchanged to analyze the degree of altered biofilm development. This was accomplished by adding the bacteria with a time delay. The designated primary colonizer was added to the incubation wells at the beginning and cultivated for 6 h at 30 °C. Subsequently, the second bacterial species was added to the previous culture. Together, both species were incubated as a consortium for additional 6 h before the biofilm strength was analyzed and quantified.

Fig. 3.2.8 shows the effect of the respective primary colonizer on the intensity of the biofilm. The choice of the primary colonizer in the case of drinking water bacteria (Fig. 3.2.8A) was observed to have a tremendous effect on biofilm formation. By selecting *S. adhaesiva* as the primary colonizer (A_{575} = 1.12), a significantly higher biofilm formation was observed. In contrast, using *B. nasdae* (A_{575} = 0.61) first, the biofilm formation was 45% weaker. Similar results were obtained for the experiments with the marine bacteria (Fig. 3.2.8B). A more intense biofilm was obtained in the case when *P. gallaeciensis* was applied as the primary colonizer. On the other hand, *H. alkalilenta* as the primary colonizer resulted in a 30% lower biofilm development. These data showed that, within a mixed species population, the primary colonizer of the surface is crucial for the development of a distinct biofilm.

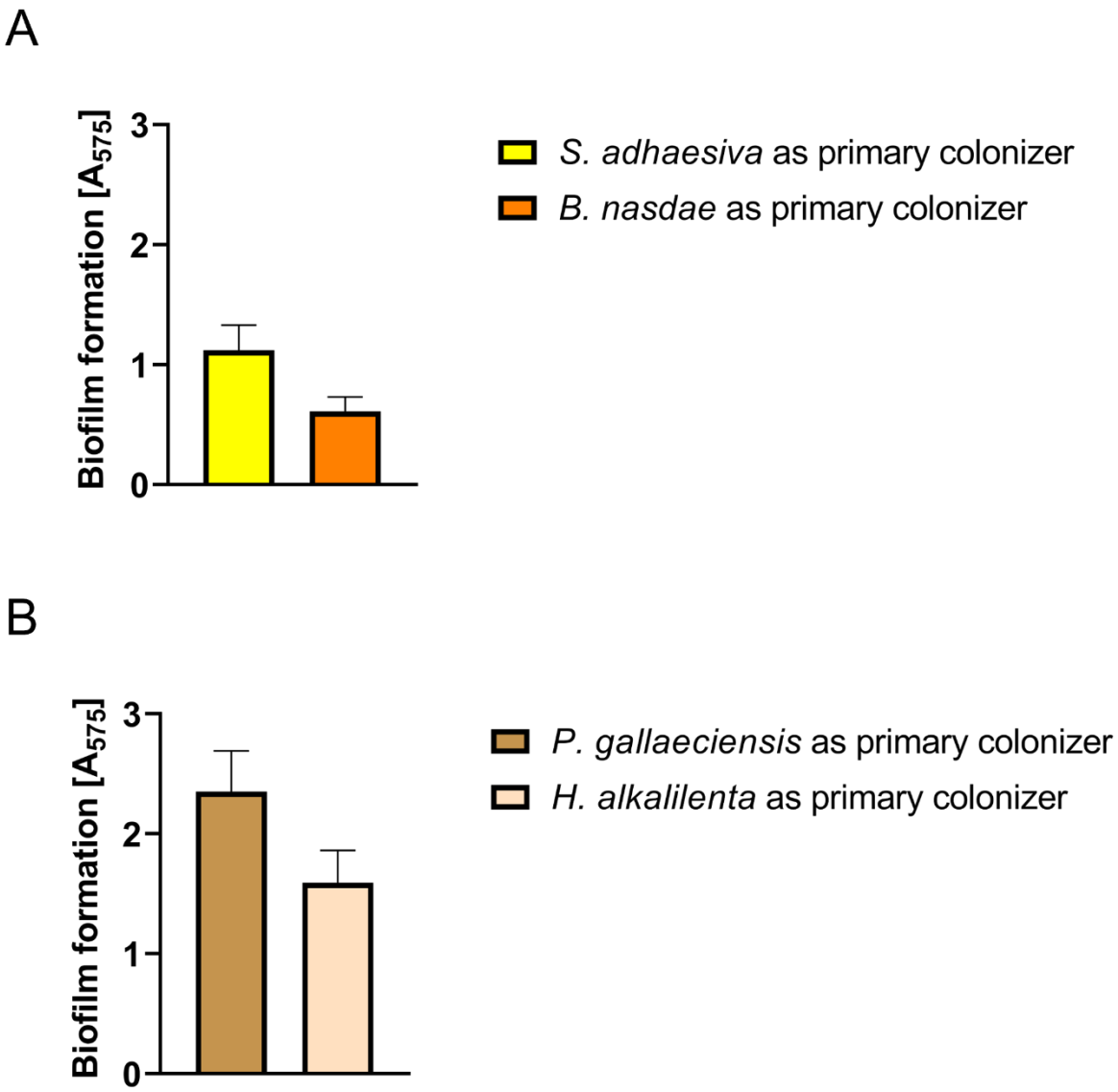

Fig. 3.2.8 Impact of the primary colonizer on the development of a mixed species biofilm. *S. adhaesiva* and *B. nasdae* (A) or *P. gallaeciensis* and *H. alkalilenta* (B) were cultured together in a consortium. The respective primary colonizer was solely cultivated for 6 h at 30 °C, and the second bacterial species was subsequently added. Cultivation was then carried out for a further 6 h at 30 °C before the biofilm formation was analyzed and quantified using crystal violet staining. The error bars symbolize the standard deviation of three biologically independently performed experiments.

In summary, all these data demonstrated that bacterial biofilm formation depends on several factors. It was observed that the nutrient composition and the incubation period have a strong impact on biofilm development. Additionally, it could be shown that the surface is also crucial for biofilm development. Furthermore, in the case of *P. gallaeciensis*, it was shown that the metal cations Fe^{2+} and Mn^{2+} boosted the biofilm formation. Moreover, it was observed that the bacterial composition of the biofilm is

relevant for its intensity, and the initial species colonization process contributes immensely to the development of a mixed species biofilm.

3.3 Marine and drinking water bacteria produce compounds that inhibit bacterial biofilm formation and trigger biofilm dispersion

Bacterial biofilms in marine and drinking water environments frequently pose enormous financial damage or severe health hazards (de Carvalho, 2018; Masaka et al., 2021). Solutions for these problems often involve the use of toxic surfaces to prevent the formation of biofilms. Moreover, biofilms that have already accumulated can be removed eventually only physically or with the application of chemicals (Roy et al., 2018; Uneputty et al., 2022). This usually requires not only enormous financial resources but additionally burdens the environment (Fish and Boxall, 2018; Schultz et al., 2011; Vats et al., 2022).

Bacteria have evolved a large arsenal of weapons to repel or eliminate rival microorganisms. Among others, they developed the possibility of preventing other bacteria from forming biofilms, e.g., by interfering with the QS system of the respective competitor (Rehman and Leiknes, 2018; Romero et al., 2011). Another strategy is to disrupt existing biofilms, e.g., by initiating biofilm dispersion (Cooke et al., 2020; Davies and Marques, 2009). However, many potential contenders have not yet been explored.

Identifying bacteria from the marine and drinking water sectors capable of inhibiting biofilm formation and dispersing existing biofilms was one part of this thesis.

3.3.1 A compound derived from *P. gallaeciensis* inhibits bacterial biofilm development

Since it was observed that the biofilm formation of *P. gallaeciensis* decreased when the incubation period was progressed, it was possible that the bacteria produced specific molecules inducing biofilm dispersion. To investigate this, the culture fluid of *P. gallaeciensis* was tested on the biofilm development of the bacteria itself as well as on their marine conspecific *P. inhibens*. For that purpose, *P. gallaeciensis* was cultured for 72 h at 30 °C in 2216 medium, and the cells were subsequently centrifuged. The culture fluid was collected and filtrated. The culture fluid was then added to *P. gallaeciensis* or *P. inhibens*, respectively. No supplementation of culture fluid served as a control. After incubation at 30 °C for 72 h, biofilm formation was visualized and quantified by crystal violet staining (Fig. 3.3.1).

Both the biofilm of *P. gallaeciensis* itself decreased by up to 80%, and the biofilm of *P. inhibens* dropped by up to 85%.

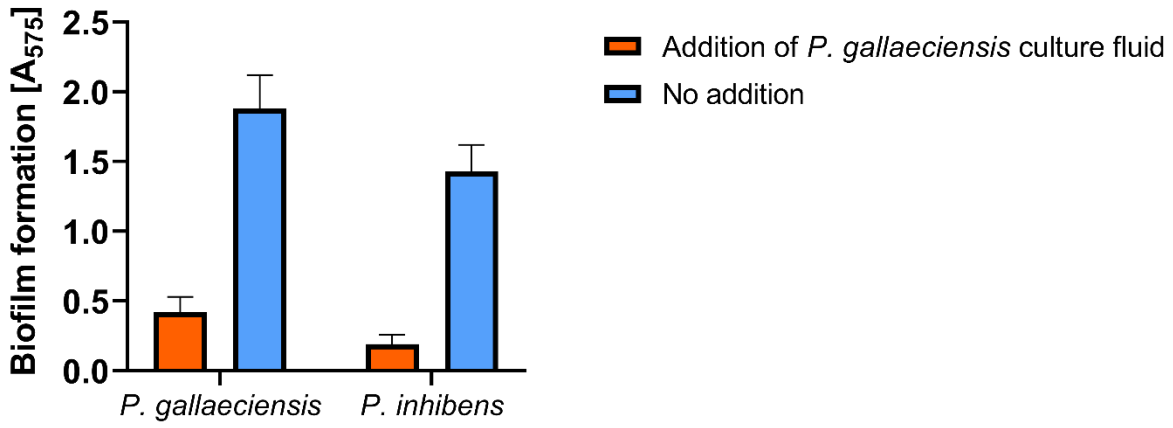

Fig. 3.3.1 Influence of *P. gallaeciensis* culture fluid on biofilm formation of *P. gallaeciensis* and *P. inhibens*. The culture supernatant of *P. gallaeciensis* was collected and filtered. The culture fluid was then added to *P. gallaeciensis* itself, and *P. inhibens* and biofilm formation was analyzed using crystal violet staining after incubation of 72 h at 30 °C. The error bars symbolize the standard deviation of three independently performed biological replicates.

As the culture fluid of *P. gallaeciensis* showed a strong inhibiting effect on the biofilm formation of *Phaeobacter* spec., the next task was to also test the culture fluid on biofilm formation of non-marine bacteria. For that, *P. aeruginosa* was selected as representative since it not only colonizes drinking water systems but, as a human pathogen, can also cause considerable damage to health (Masaka et al., 2021). To exclude growth effects caused by the high osmolarity due to the high salt level of the 2216 medium, a considerably lower concentration of 5% culture fluid was used for the experiments. The addition of 5% 2216 medium provided an internal control.

Fig. 3.3.2 depicts the effect of the *P. gallaeciensis* culture fluid on *P. aeruginosa* biofilm formation. Remarkably, with the addition of 5% 2216 medium, the extracellular matrix was clearly visible after centrifugation (Fig. 3.3.2A). Since bacterial cells could not be pelleted despite centrifugation, this was the first visual indication that the biofilm matrix was not affected by the 2216 medium. In contrast, no clearly distinct extracellular matrix could be detected after centrifugation upon the addition of 5% culture fluid (Fig. 3.3.2B). It was observed that the bacterial cells were pelleted after centrifugation without clearly visual observation of a biofilm matrix. In addition, the biofilm of *P.*

aeruginosa was reduced by approximately 25% compared to the controls (Fig. 3.3.2C). An effect of the 2216 medium could thus be excluded.

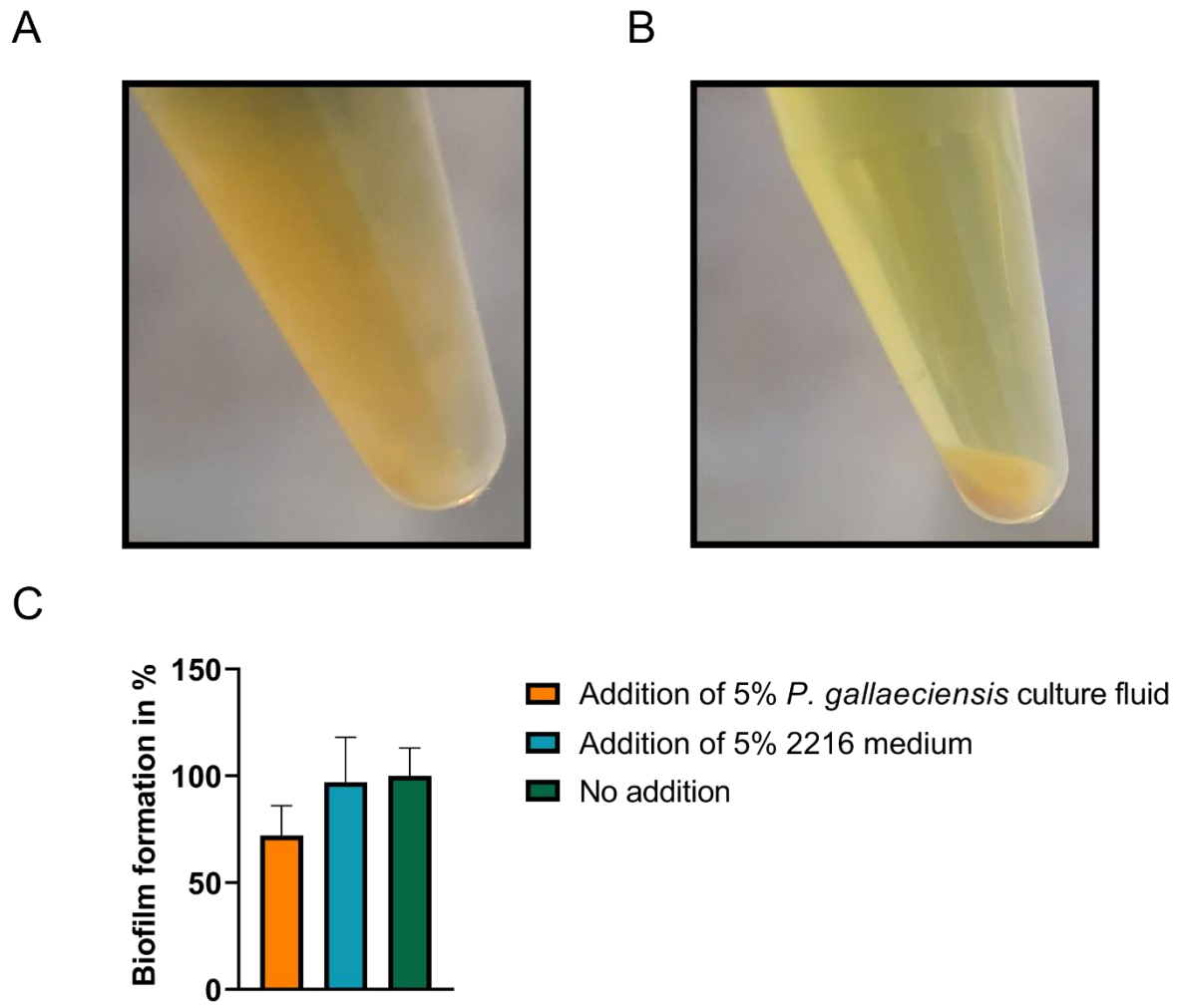

Fig. 3.3.2 Biofilm formation of *P. aeruginosa* upon addition of the culture fluid of *P. gallaeciensis*. (A) The addition of 5% 2216 medium served as an internal control. (B) The concentration of 5% culture fluid was added to *P. aeruginosa*. (C) The effect on biofilm formation was analyzed and quantified by crystal violet staining after 72 h of incubation. The error bars symbolize the standard deviation of three biologically independently performed experiments.

The potential molecule was to be tested for stability since an apparent effect of the culture fluid on *P. aeruginosa* was detected. To obtain a more accurate impression, the culture fluid was treated in different assays to evaluate the retention or loss of the biofilm inhibitory effect. Therefore, the culture fluid was treated with heat and proteinase K. Additionally, the sample was alkalized or acidified. It is known that exposure to heat can denature proteins that are not heat resistant (Bischof and He,

2005). In addition, proteases such as proteinase K can hydrolyze peptide bonds and thus degrade proteins (Skowron et al., 2020). Furthermore, polymers with pH-sensitive bonds are susceptible to structural changes and degradation with altering pH (Kocak et al., 2017; Ofridam et al., 2021). Thus, the aim was to obtain an indication of the molecule's chemical structure by applying the different treatments.

Fig. 3.3.3 shows the results of the different treatments of the culture fluid of *P. gallaeciensis* and the impact on biofilm formation in *P. aeruginosa*. Notably, none of the selected treatments altered the effect on biofilm formation since the influence of biofilm reduction could still be observed. Thus, the candidate compound appeared to tolerate the acidic or basic treatments. Therefore, it is highly likely that the molecule in question does not possess any pH-labile bonds. Moreover, the potential molecule appeared to be heat stable, as no loss of function was observable after heat treatment. Additionally, as the effect remained unchanged when also treated with proteinase K, one might assume that the putative molecule might not be a protein.

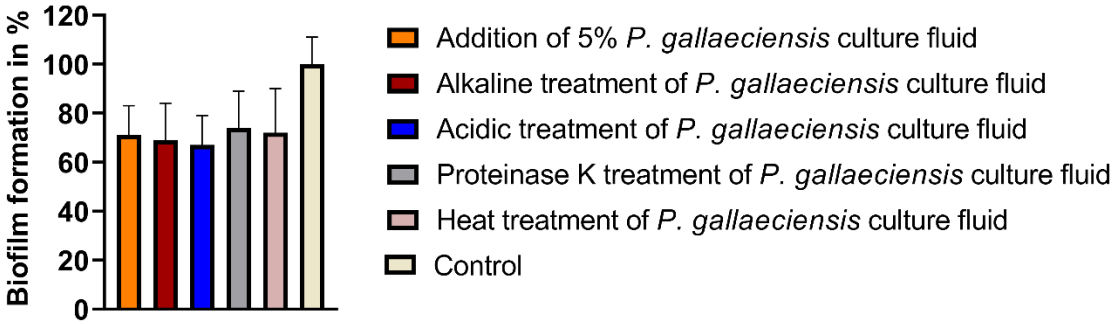

Fig. 3.3.3 Treatment of the culture fluid to test the stability of the potential molecule in biofilm inhibitory activity of *P. aeruginosa* biofilm. The culture fluid underwent acidic and alkaline treatment. In addition, proteinase K and heat treatment were performed. The addition of only 5% 2216 medium served as a control. The standard deviation of three biologically independently performed experiments is represented by error bars.

To gain more information about the chemical nature of the potential biofilm inhibiting compound, the hydrophobic compounds of the *P. gallaeciensis* culture fluid were extracted with 100% ethyl acetate in a 1:1 ratio and then evaporated in a rotary evaporator. Since the hydrophilic phase could barely show a biofilm inhibiting effect (Fig. S.1), the main focus was set on the hydrophobic phase since, in this phase, the biofilm of *P. aeruginosa* was reduced by approximately 25%. Therefore, the potential

molecules in the hydrophobic phase were suspended in MeOH, and the molecules were separated by HPLC and fractionated. To each fraction, 135 µl of a *P. aeruginosa* culture with an OD_{600} of 0.5 was then added. After incubation at 30 °C for 72 h, the effect of each fraction on biofilm formation was determined by crystal violet staining.

Fig. 3.3.4A illustrates the influence of the fractions on the biofilm formation of *P. aeruginosa*. A strong negative effect on biofilm formation could be detected with fraction A5. The reduction was about 45% in contrast to fraction H1, representing the control. The neighboring fractions A4 and A6 also exhibited a slight impact of 20% and 10%, respectively. Fig. 3.3.4B illustrates the preparative chromatogram. Several hydrophobic substances could be separated from the culture fluid of *P. gallaeciensis*. The highest peak at approximately 1 min correlates with fraction A5, which exhibited a biofilm inhibitory effect in *P. aeruginosa*.

A

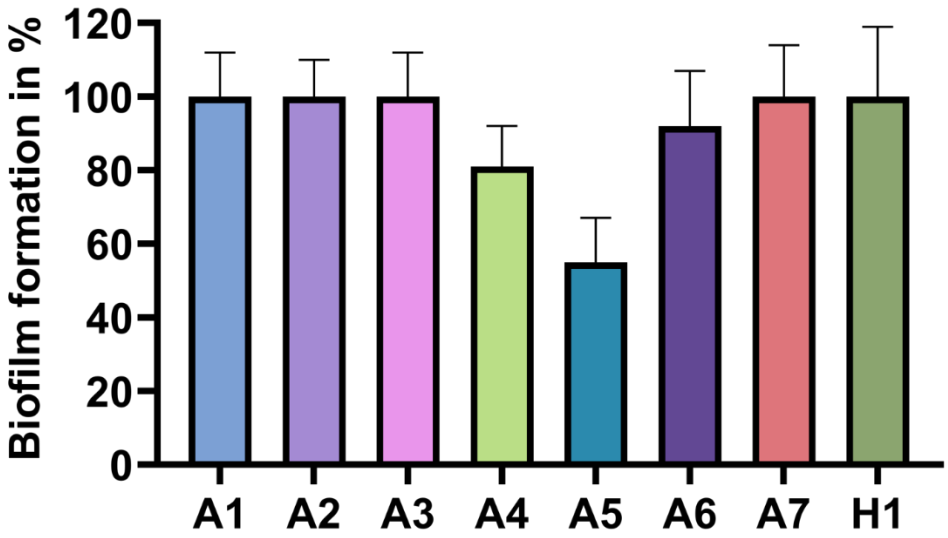

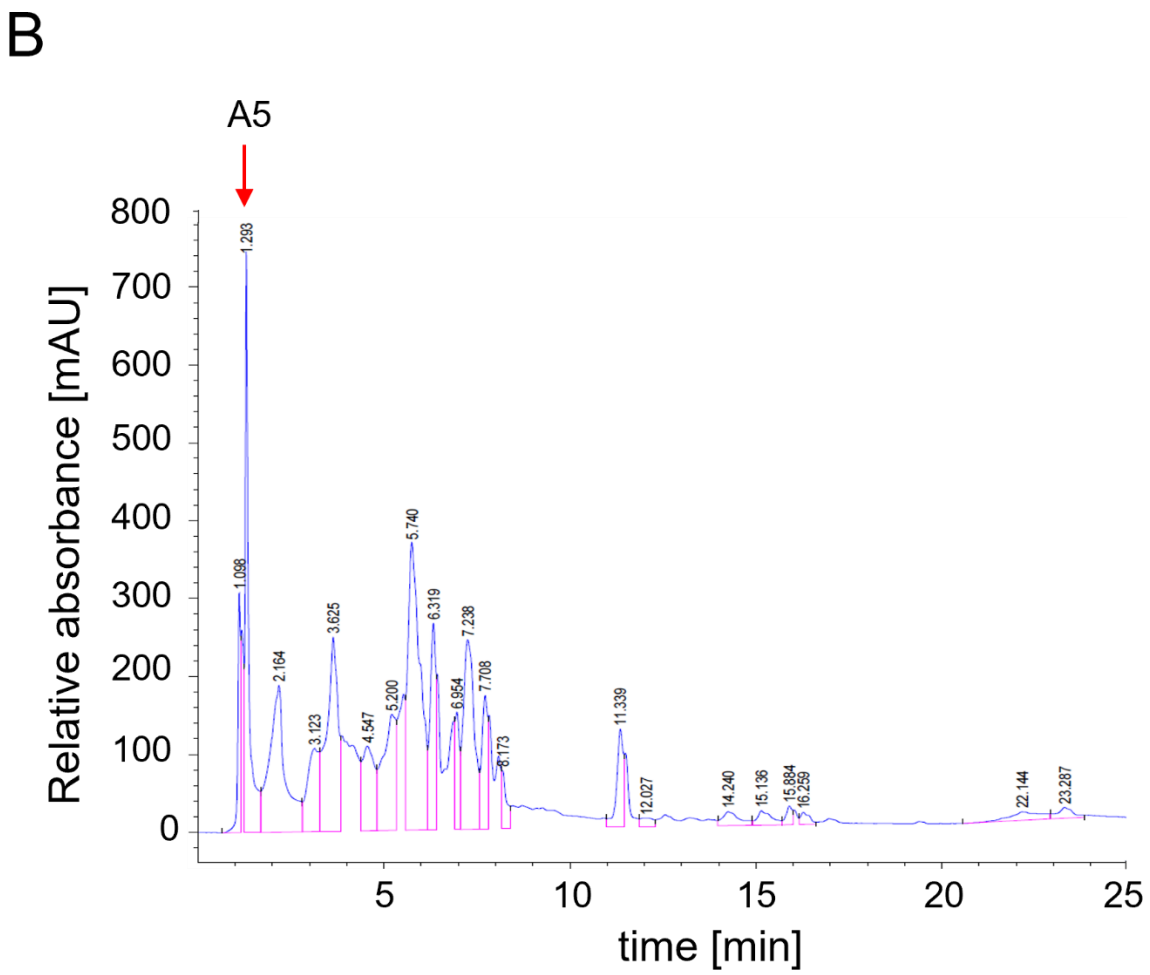

Fig. 3.3.4 The fractionation of the hydrophobic compounds in *P. gallaeciensis* culture fluid and the effect on *P. aeruginosa* biofilm formation. The hydrophobic molecules in the culture fluid of *P. gallaeciensis* were fractionated on a reverse phase C18 column into 92 sections via HPLC. (A) *P. aeruginosa* was placed in each well, incubated at 30 °C for 72 h, and the effect on biofilm formation was examined and quantified using crystal violet staining for each separate fraction. H1 served as a control without fractionation parts. (B) The preparative chromatogram is in blue with the respective peaks. The A5 fraction is highlighted with an arrow. The maximum of each peak is labeled with the corresponding time. The associated compounds are marked in pink. The wavelength applied was 210 nm. The error bars symbolize the standard deviation of three biologically independently performed experiments.

3.3.2 *B. nasdae* induces biofilm dispersal

Among the drinking water bacteria, it was noticed that the biofilm formation of *B. nasdae* started to increase after 48 h but rapidly declined again after 72 h. Therefore, the idea came up that a specific molecule produced by the bacteria in the late growth phase of the biofilm could be responsible for these effects. To verify this, the culture fluid of *B. nasdae* was screened for dispersal effects on its own biofilm formation. Briefly, *B. nasdae* was incubated at 30 °C for 72 h. Subsequently, the cells were removed by centrifugation, and the collected culture fluid was filtrated. The culture fluid was then added to *B. nasdae*, and after 72 h of incubation, the effect on the biofilm formation was analyzed using a crystal violet assay.

It could be observed that the biofilm was reduced by up to 30% after adding the *B. nasdae* culture fluid (A_{575} = 1.97) compared to the control without addition (A_{575} = 2.78) (Fig. 3.3.5).

Fig. 3.3.5 Impact of *B. nasdae* culture fluid on its own biofilm development. The culture fluid of *B. nasdae* was centrifuged and filtrated after 72 h of cultivation. Then, the culture fluid was added to *B. nasdae* to observe the effect on the biofilm. After further 72 h of cultivation, the biofilm was quantified using crystal violet staining. The standard deviation of three biologically independently performed experiments is represented by the error bars.

It was shown that the culture fluid of *B. nasdae* exhibited biofilm-reducing properties, so the intention was to investigate whether the culture fluid could also disperse a pre-existing biofilm. The conspecific bacterium *Brevundimonas diminuta* was used to

analyze this purpose. *B. diminuta* is a Gram-negative bacterium known for its colonization of water distribution systems and, due to its size, can exhibit aerosol-like properties (Chattopadhyay et al., 2017). First, after 72 h incubation, the culture fluid of *B. nasdae* was freeze-dried after filtration. Upon completion of lyophilization, water was added accordingly so that a 10x concentrated culture fluid was obtained. Freeze-dried 10x concentrated medium served as a control. Then, *B. diminuta* was cultured for 24 h in LB medium. The 10x concentrated culture fluid or only the 10x concentrated culture medium was thereafter provided to *B. diminuta*. After cultivation for another 24 h, the planktonic cells were removed, and the attached cells were stained with crystal violet. The analysis was conducted at 575 nm.

As can be seen in Fig. 3.3.6, the additional 10x concentrated culture fluid of *B. nasdae* caused a roughly 40% decrease in the pre-existing biofilm of *B. diminuta*. Consequently, it was shown that a potential molecule within the culture fluid of *B. nasdae* could initiate biofilm dispersion.

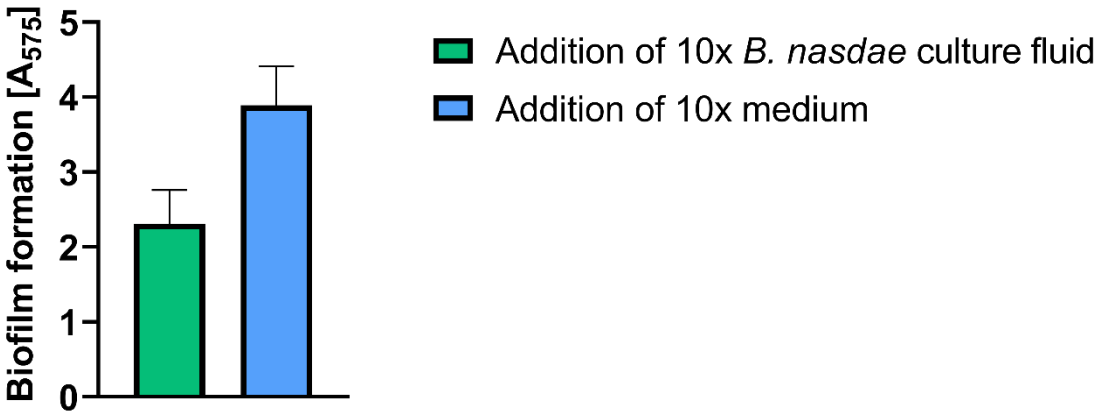

Fig. 3.3.6 Influence of the 10x concentrated culture fluid of *B. nasdae* on the pre-existing biofilm of *B. diminuta*. The culture fluid of *B. nasdae* was freeze-dried after centrifugation and filtration. After lyophilization was completed, a 10x concentrated culture fluid was adjusted with water. Freeze-drying of medium only served as a control. *B. diminuta* was incubated for 24 h in LB medium at 30 °C. The 10x concentrated culture fluid was then supplemented. The impact on the biofilm was evaluated using crystal violet. The standard deviation of three biologically independently performed experiments is represented by the error bars.

To obtain a greater insight into the potential chemical nature of the biofilm dissolving molecule, the culture fluid of *B. nasdae* was treated with proteinase K and subjected to heating. It was then added to the pre-existing biofilm of *B. diminuta* so that either retention or loss of the biofilm dissolving activity was evaluated.

Surprisingly, both proteinase K and heat were able to terminate the observed effect on the biofilm (Fig. 3.3.7). Thus, it could be shown that the potential molecule in the culture fluid could be inactivated by proteinase K and did not withstand intense levels of heat so that the molecule might be of protein nature.

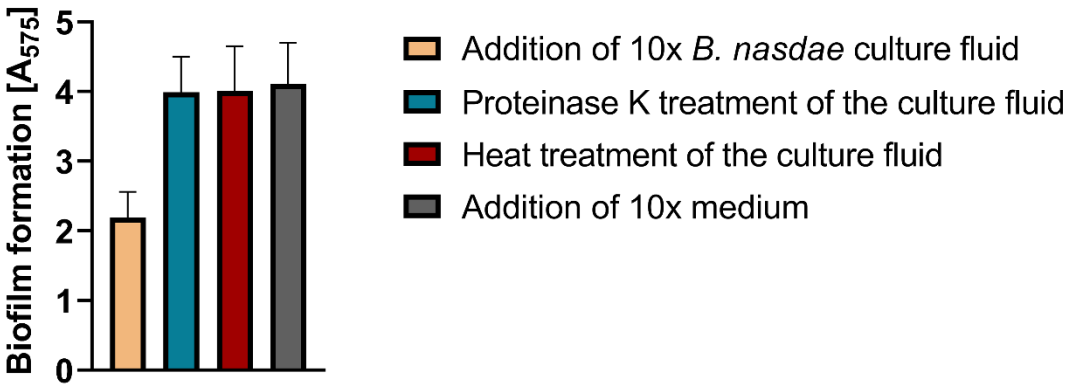

Fig. 3.3.7 Treatment of the culture fluid to test the sustained effect on biofilm dispersion. The culture fluid was exposed to Proteinase K and heating. The addition of a 10x concentrated medium served as a control. The standard deviation of three biologically independently performed experiments is represented by error bars.

Summarizing the results, two bacteria were identified that either inhibited bacterial biofilm or induced dispersion. In the area of marine bacteria, it was shown that *P. gallaeciensis* generated a putative molecule in the culture fluid, which demonstrated an inhibiting effect on *P. aeruginosa* biofilm formation as well. Furthermore, it was shown that the candidate molecule could not be inhibited by treatments with acids, bases, proteinase K, or heat. For this reason, it is assumed that the putative molecule can be neither a protein nor a polymer with pH-sensitive compounds. Additionally, *B. nasdae* was identified as a source of a potential compound in drinking water that initiated biofilm dispersion in *B. diminuta*. Furthermore, it could be illustrated that the

potential agent was either inactivated by proteinase K or heat. It can therefore be concluded that the candidate molecule is highly likely a protein.

3.4 Surfaces coated with secondary metabolites of entomopathogenic bacteria as novel anti-biofilm strategy

Bacteria of the genera *Photorhabdus* and *Xenorhabdus* belong to the entomopathogenic bacteria and display a complex life cycle, colonizing different hosts and changing between pathogenicity and symbiosis. During this life cycle, a wide range of secondary metabolites are produced to combat or repel, among others, a full range of microorganisms such as bacteria or fungi (Bode, 2009; Parihar et al., 2022; Tobias et al., 2018). Although it is known that many secondary metabolites have antibiotic, biostatic or antifungal effects (Booysen and Dicks, 2020; Chacón-Orozco et al., 2020), it is currently not investigated whether these substances also have a biofilm inhibitory effect without effectively eliminating other bacteria, especially in water environments.

In the marine sector and in drinking water supplies, bacterial biofilms not only cause economic losses but also endanger the health and the environment in particular (Cámara et al., 2022; de Carvalho, 2018; Masaka et al., 2021; Muhammad et al., 2020).

This thesis investigated whether secondary metabolites from entomopathogenic bacteria can prevent the formation of biofilm in bacteria originating from the marine environment or drinking water supply. Furthermore, it should be evaluated whether surfaces coated with those secondary metabolites can lead to a reduction of bacterial biofilm.

3.4.1 Secondary metabolites from *Photorhabdus* spec. and *Xenorhabdus* spec. inhibit biofilm formation of bacteria from marine environments and drinking water distribution systems

To determine whether the secondary metabolites from *Photorhabdus* and *Xenorhabdus* have biofilm inhibitory properties, different Δ*hfq* and wild-type strains of *P. luminescens*, *X. szentirmaii*, *X. nematophila*, and *X. doucetiae* were used. However, several Δ*hfq* strains possessed a promoter upstream of specific secondary metabolite biosynthesis gene clusters, so their expression could be induced by arabinose.

A

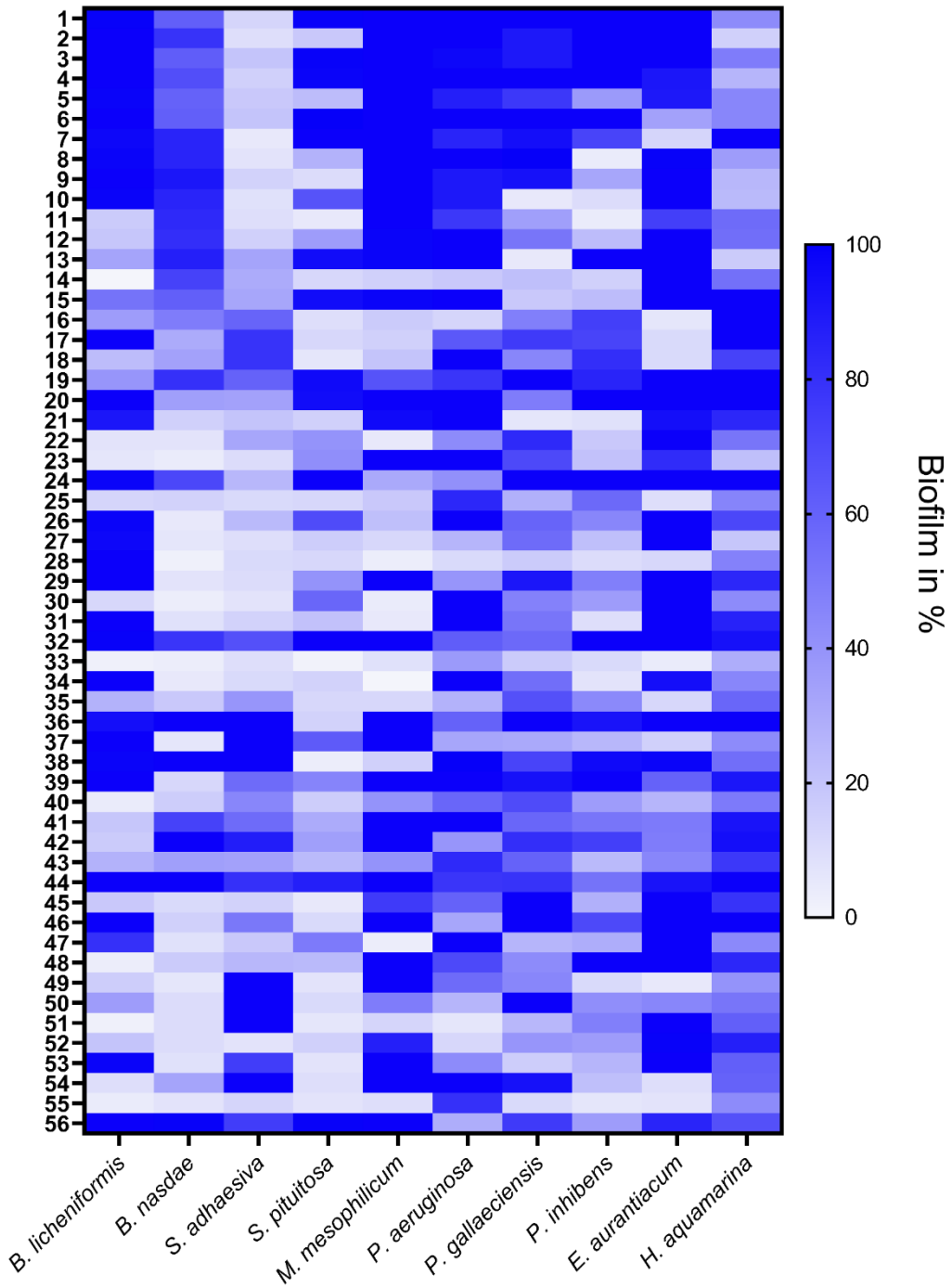
1
2
3
4
5
6
7
8
9
10
11
12
13
14
15
16
17
18
19
20
21
22
23
24
25
26
27
28
29
30
31
32
33
34
35
36
37
38
39
40
41
42
43
44
45
46
47
48
49
50
51
52
53
54
55
56
B. licheniformis
B. nasdae
S. adhaesiva
S. pituitosa
M. mesophilicum
P. aeruginosa
P. gallaeciensis
P. inhibens
E. aurantiacum
H. aquamarina
100
80
60
40
20
0
Biofilm in %

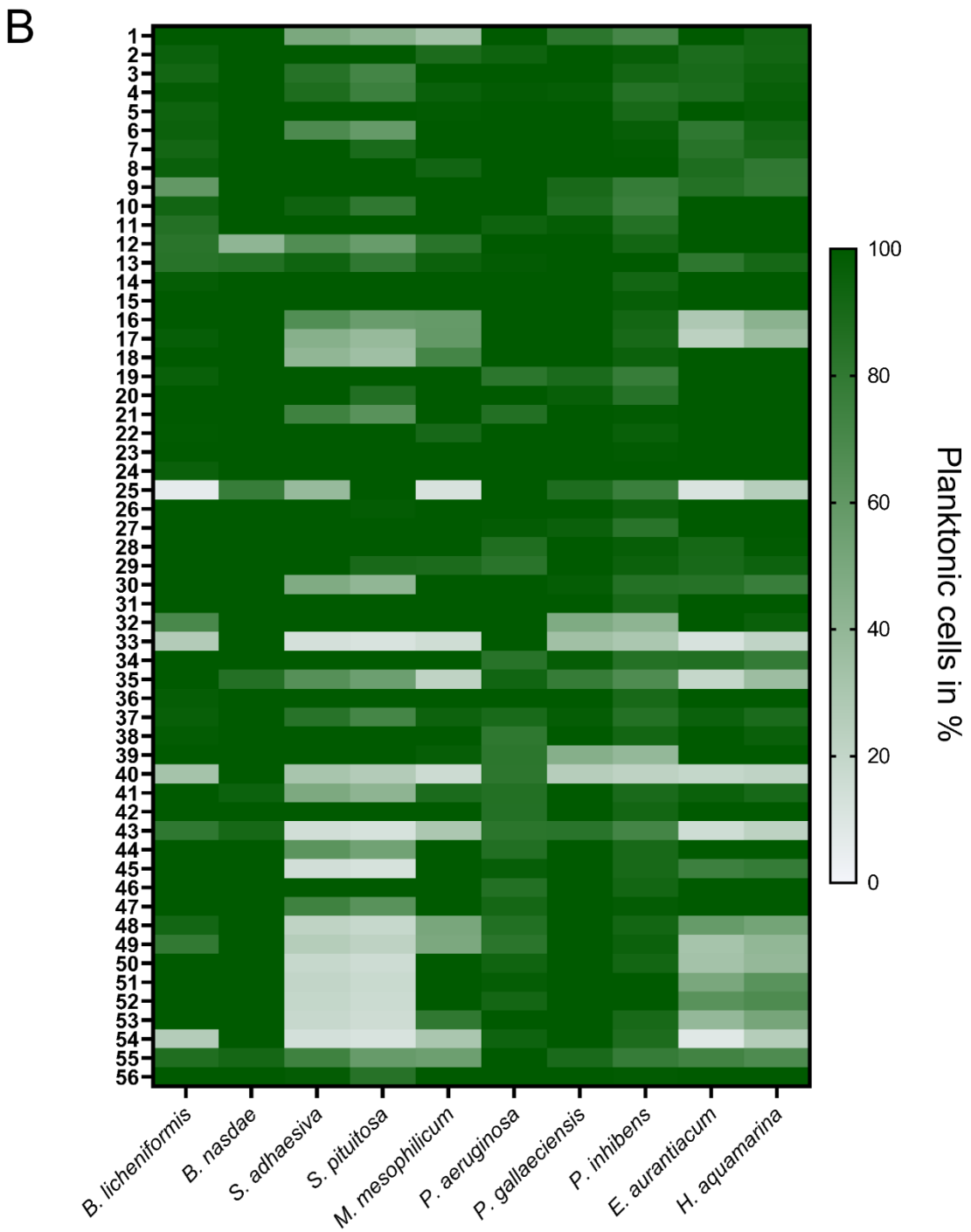

Fig. 3.4.1 The effect of the secondary metabolites from *Photorhabdus* and *Xenorhabdus* strains on biofilm formation of bacteria from marine environments and water distributions. The culture fluids of each *Photorhabdus* or *Xenorhabdus* strain were added to the biofilm-forming bacteria, and then the effect on the respective biofilm (A) and optical density (B) was analyzed. *B. licheniformis* and *B. nasdae* were cultivated in RS medium for 72 h at 30 °C. *S. adhaesiva* and *S. pituitosa* were grown in HD medium for 72 h at 30 °C. *M. mesophilicum* was cultivated in TSY medium for 7 days at 30 °C. *P. aeruginosa* was cultured in LB medium for 72 h at 30 °C. *P. gallaeciensis*, *P. inhibens* were incubated in marine medium 2216 for 72 h at 30 °C. *E. aurantiacum* and *H. aquamarina* were cultivated in marine medium 2216 for 96 h at 30 °C.

Since biofilm formation in the marine sector and in drinking water supplies leads to significant financial as well as health problems (de Carvalho, 2018; Masaka et al., 2021; Muhammad et al., 2020), the focus was put on biofilm-forming bacteria from these sectors. *B. licheniformis*, *B. nasdae*, *S. adhaesiva*, *S. pituitosa*, *M. mesophilicum*, and *P. aeruginosa* are biofilm-forming bacteria found in drinking water supplies (Bereschenko et al., 2010; de Vries et al., 2019; El-Liethy et al., 2018; Szabo et al., 2017; Szwetkowski and Falkinham, 2020; Zhu et al., 2020). *P. gallaeciensis* and *P. inhibens* belong to the *Roseobacter* clade, which are considered primary colonizers of surfaces in marine environments (de Carvalho, 2018; Zhao et al., 2016). *E. aurantiacum* and *H. aquamarina* are also classified as biofilm-forming bacteria occurring in the marine zone (Inbakandan et al., 2010).

First, the cell-free culture fluids of the individual *Photorhabdus* and *Xenorhabdus* strains were added to the respective biofilm-forming bacteria. After incubation of the bacteria from the marine area and the drinking water supply, the effect of the culture fluids was analyzed using crystal violet assays. A prior absorbance measurement at 600 nm provided information about the planktonic cell count.

Fig. 3.4.1A provides that several culture fluids influenced the bacterial biofilm. All substances that showed an effect on several bacteria are remarkable. For example, culture fluid 28 (phenylethylamides/tryptamides) was effective on the biofilm formation of all marine bacteria and almost all drinking water bacteria. For *B. nasdae* and *M. mesophilicum*, less than 10% of the original biofilm was left. For *S. adhaesiva*, *S. pituitosa*, *P. aeruginosa*, *P. gallaeciensis*, *P. inhibens* and *E. aurantiacum*, the biofilm was reduced by up to 80%. The addition of water instead of culture fluid served as a control. Although a decrease in biofilm was observed in compound 28, the planktonic cell number did not decrease, as seen in Fig. 3.4.1B.

Furthermore, culture fluid 55 (xenofuranones) also exhibited a biofilm-reducing effect for a total of 9 bacteria. Except for *P. aeruginosa* and *H. aquamarina*, the biofilm of the other bacteria was reduced by up to 90%. Surprisingly, culture fluid 55 also displayed an effect on the cell count of, e.g., *S. pituitosa* and *M. mesophilicum*. In this case, the cell count was reduced by up to 40%.

Additionally, culture fluids were detected that had an effect on biofilm formation but at the same time also significantly reduced the cell count. Culture fluid 52 (rhabduscin), for example, decreased the biofilm of *S. pituitosa* by about 75%, but the addition of this

culture fluid also reduced the number of cells by up to 75%. The effect thus appeared to be non-biofilm specific, but the effect might be due to a classical antimicrobial mode of action.

Surprisingly, culture fluids such as culture fluid 33 (xenocoumacin) were also identified, which reduced biofilm in most bacteria screened due to a decline in cell count, but reduced biofilm in *B. nasdae* and *P. aeruginosa* without concurrently greatly affecting cell count.

The structures of the most promising compounds with an impact on biofilm formation are summarized in Fig. 3.4.2.

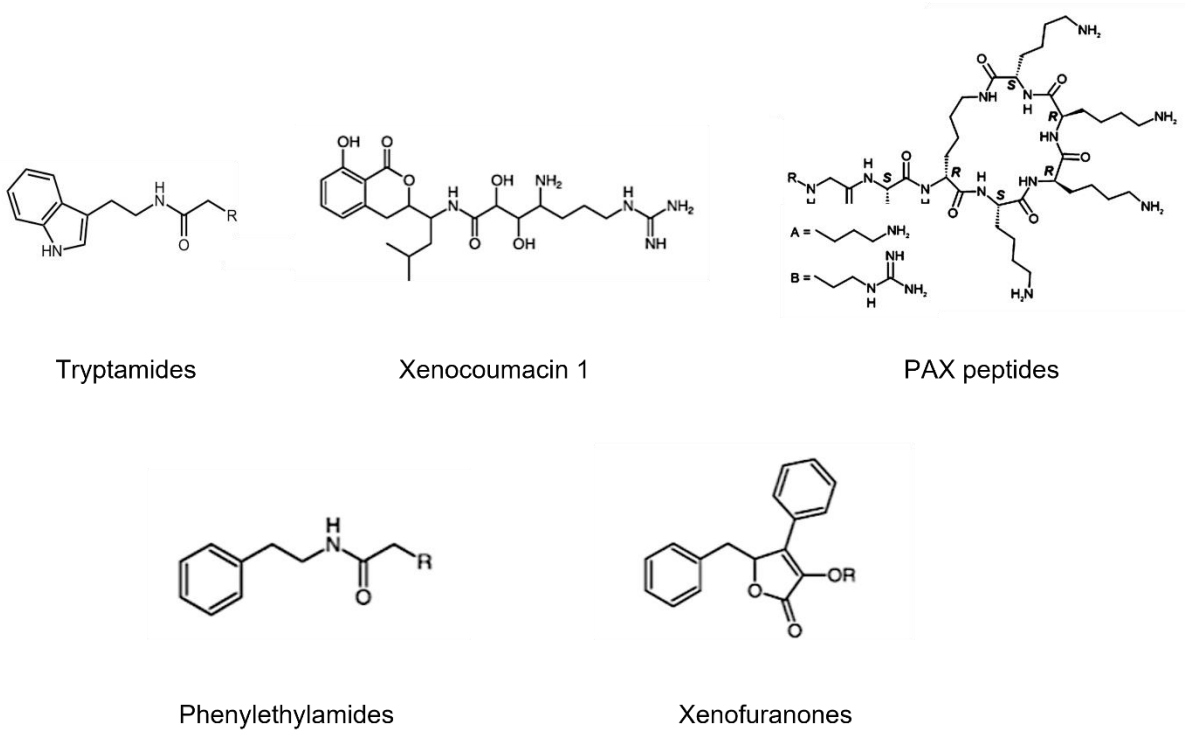

Fig. 3.4.2 The secondary metabolites from *Xenorhabdus* spec. with the most promising effect on non-biocidic inhibition of bacterial biofilms. The compounds were produced in *Xenorhabdus* spec. and evaluated for their biofilm inhibitory activity in different marine and drinking water bacteria. The structural formulas were provided by [redacted], Goethe-Universität Frankfurt. Modified from (Bode et al., 2017; Brachmann et al., 2006; Fuchs et al., 2011; Park et al., 2009).

Subsequently, to determine whether the substances also demonstrate an effect on biofilm formation in diluted form, compounds that already had a strong effect in Fig. 3.4.1 were diluted 1:10 or 1:100 and underwent testing.

As can be seen in Fig. 3.4.3A, the phenylethylamides/tryptamides still exhibited an effect on the biofilm formation of *P. aeruginosa* even in diluted conditions. At a dilution of 1:100, the biofilm was still reduced by up to 55%. The results, as shown in Fig. 3.4.3B, indicate that the xenofuranones in diluted dosage also had a strong effect. When tested on the biofilm of *P. gallaeciensis*, a level of reduction of around 80% was observed at the 1:10 dilution. The 1:100 dilution further diminished the biofilm by up to 70% compared to the control. This suggested a highly effective biofilm-inhibiting effect also at low concentrations.

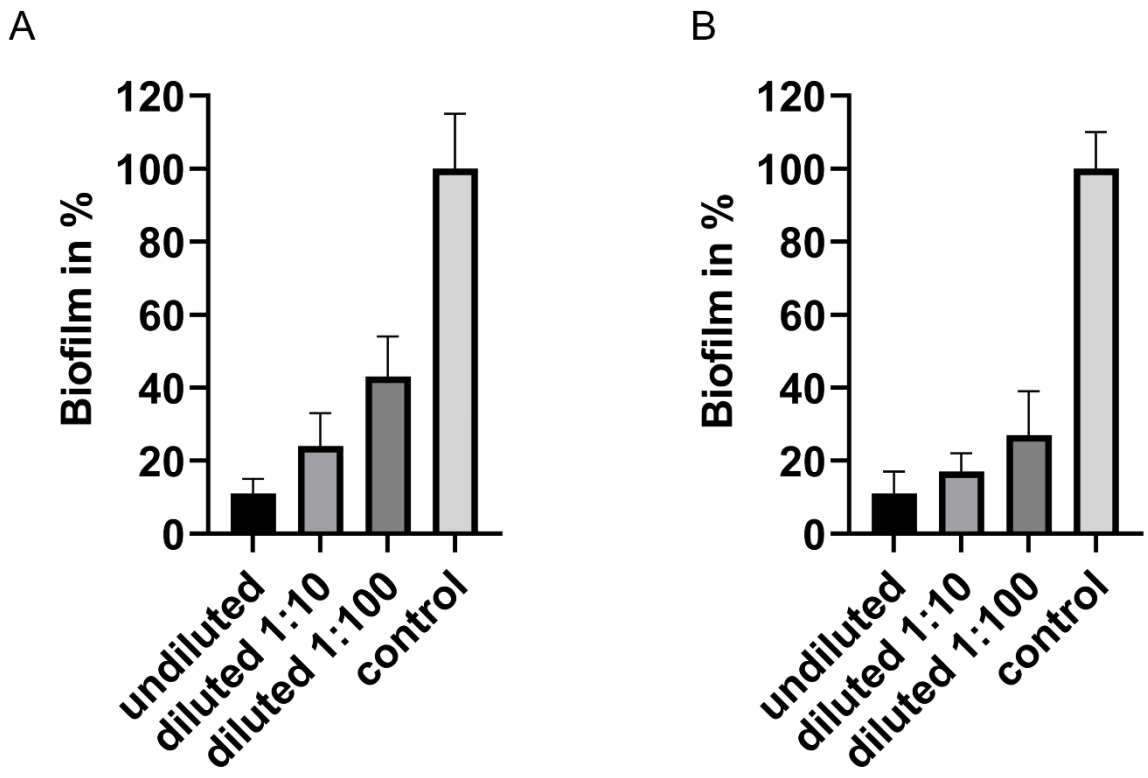

Fig. 3.4.3 The effect of secondary metabolites produced by entomopathogenic bacteria on bacterial biofilm formation at different dilutions. (A) The effect of compound 28 (phenylethylamides/tryptamides) in undiluted and 1:10 and 1:100 dilutions on *P. aeruginosa* biofilm. (B) The effect of substance 55 (xenofuranones) in undiluted and 1:10 and 1:100 diluted form on the biofilm of *P. gallaeciensis.* The standard deviation of three biologically independently performed experiments is represented by error bars.

Furthermore, light microscopic images were taken to confirm the obtained results of the biofilm inhibitory effect of the compounds and to obtain a visual image of the biofilm.

Initially, *X. doucetiae* Δ*hfq* pBAD-DC was used to produce compound 28 at a large scale in a fermenter vessel. Here, arabinose was used to activate the promoter and,

therefore, expression of the downstream located genes. No addition of arabinose served as a control. Cells were then centrifuged, and the culture fluid was filtered. The *Panta Rhei* microfluidic system was then used to observe the effect of the compound on the biofilm of *P. aeruginosa* under a constant flow of 8 ml/h.

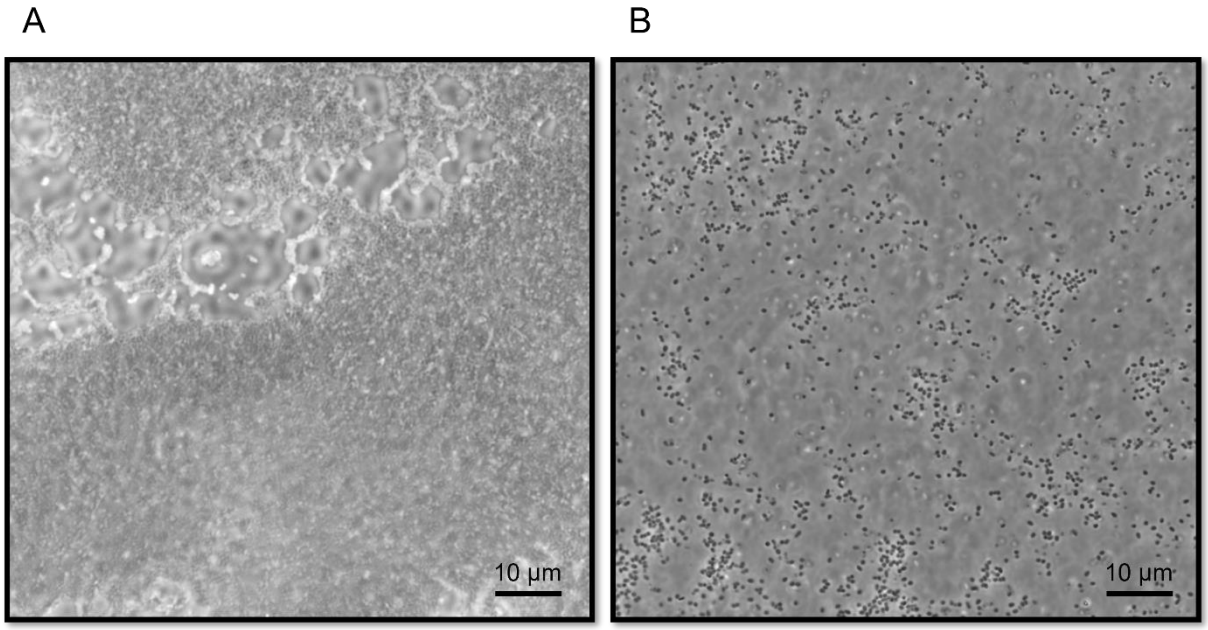

Fig. 3.4.4 The effect of phenylethylamides/tryptamides on bacterial biofilm formation of *P. aeruginosa* in the *Panta Rhei* microfluidic system. *X. doucetiae* Δ*hfq* pBAD-DC was cultured separately without addition (A) and with addition (B) of arabinose. The culture fluid was then used to perfuse *P. aeruginosa*, which was placed in the sample chamber of *Panta Rhei* D2 for 24 h. The effect was then examined by phase contrast microscopy.

After 24 h, it was observed that the culture fluid, which did not result from arabinose induction (Fig. 3.4.4A), hardly affected the biofilm formation of *P. aeruginosa*. The surface was uniformly colonized by the bacterial biofilm. However, the situation looked different when the expression of the phenylethylamides/tryptamides biosynthesis genes was induced (Fig. 3.4.4B). The culture fluid containing the synthesized molecules caused *P. aeruginosa* to barely colonize the surface. Sporadically, adherent bacteria can be observed on the surface but to a much lower content compared to the situation without phenylethylamides/tryptamides. This confirmed the results obtained concerning the in-batch biofilm inhibiting effect of the phenylethylamides/tryptamides.

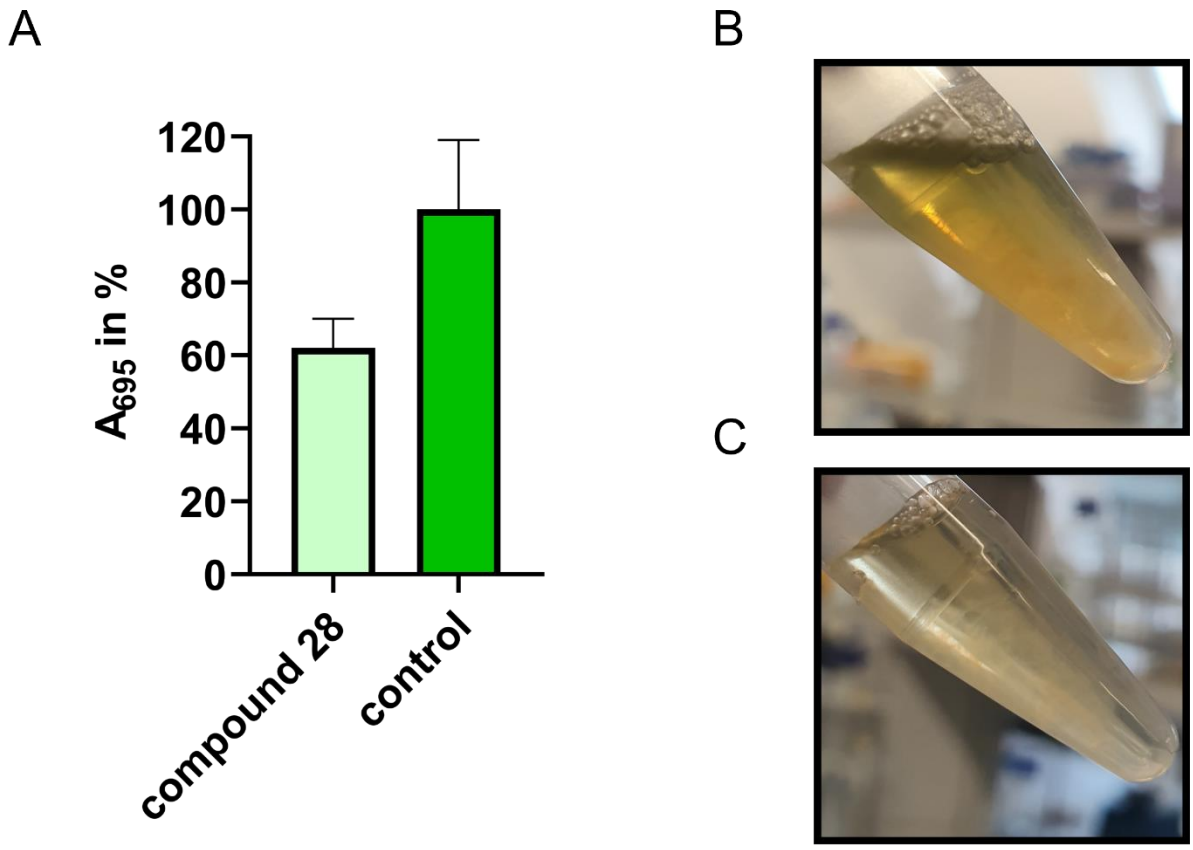

Fig. 3.4.5 The effect of compound 28 on pyocyanin production by *P. aeruginosa*. The variation in the absorbance (A) of pyocyanin of *P. aeruginosa* was measured at 695 nm following the incubation at 37 °C for 24 h and subsequent centrifugation of the cells. Incubation of *P. aeruginosa* was performed without addition (B) and with addition (C) of 15% compound 28. The standard deviation of three biologically independently performed experiments is represented by the error bars.

Since bacterial biofilm formation often results from the principle of QS, i.e., bacterial communication (Subramani and Jayaprakashvel, 2019), it was necessary to investigate whether the biofilm-inhibiting effect of compound 28 can be attributed to an inhibition of the QS system, resulting in so-called QQ (Turan and Engin, 2018).

However, since *P. aeruginosa* is not only a very well-studied model organism regarding QS (Kostylev et al., 2019), but the biofilm also decreased rapidly after the addition of substance 28, this was the organism chosen for further investigations. *P. aeruginosa* produces a green pigment termed pyocyanin. This pigment is a virulence factor, and the expression of the respective genes is under the control of the QS system (O'Loughlin et al., 2013). Thus, pyocyanin production was used as a readout to investigate whether compound 28 blocks QS.

First, *P. aeruginosa* was aerobically cultured for 24 h at 37 °C with and without the addition of compound 28. Next, the cells were removed from the medium by centrifugation. Then, the culture supernatant was filtered, and pyocyanin was detected and quantified by measuring the absorption of the filtrated culture fluid at 695 nm.

In contrast to the control with no secondary metabolite, the addition of substance 28 to the *P. aeruginosa* culture reduced the pyocyanin by up to 40% (Fig. 3.4.5A). Furthermore, the greenish color of the pyocyanin after cultivation was already detectable visually (Fig. 3.4.5B). However, after the addition of substance 28, the greenish color was significantly reduced (Fig. 3.4.5C). This indicated that substance 28 might influence the QS system of *P. aeruginosa*.

3.4.2 Secondary metabolite-coated plastic materials lead to a reduction in biofilm formation of *P. aeruginosa*

As it was demonstrated that secondary metabolites from entomopathogenic bacteria of the genera *Photorhabdus* and *Xenorhabdus* were able to reduce the biofilm formation of marine and drinking water bacteria, the next task was to apply these secondary metabolites to particularly biofilm-prone materials such as drinking water pipes in order to inhibit biofilm development for applications.

First, commercial drinking water pipes were investigated for their overall susceptibility to the bacterial biofilm of *P. aeruginosa*. *P. aeruginosa* belongs to the so-called OPPPs, and biofilm accumulation in the potable water sector causes serious economic and health problems (Falkinham et al., 2015).

The first step was to cut the commercial tubes into 1 cm^2 squares using a metal saw. The outside of the tube pieces was then taped so that only the internal side that was to be investigated would be colonized by bacteria. *P. aeruginosa* was then applied to the pipe segments and incubated at 30 °C for 72 h. The biofilm formation was then analyzed using a 1% (v/v) aqueous crystal violet solution. Subsequently, analysis was carried out after the sealants had been removed.

The results are depicted in Fig. 3.4.6. In this study, it was discovered that commercial drinking water pipes differ significantly in their sensitivity to biofilm infestation. The least biofilm was exhibited by G6 (A_{575} = 0.38). The most severe biofilm formation, and thus approximately 450% more biofilm than G6, was exhibited by G7 (A_{575} = 1.72).

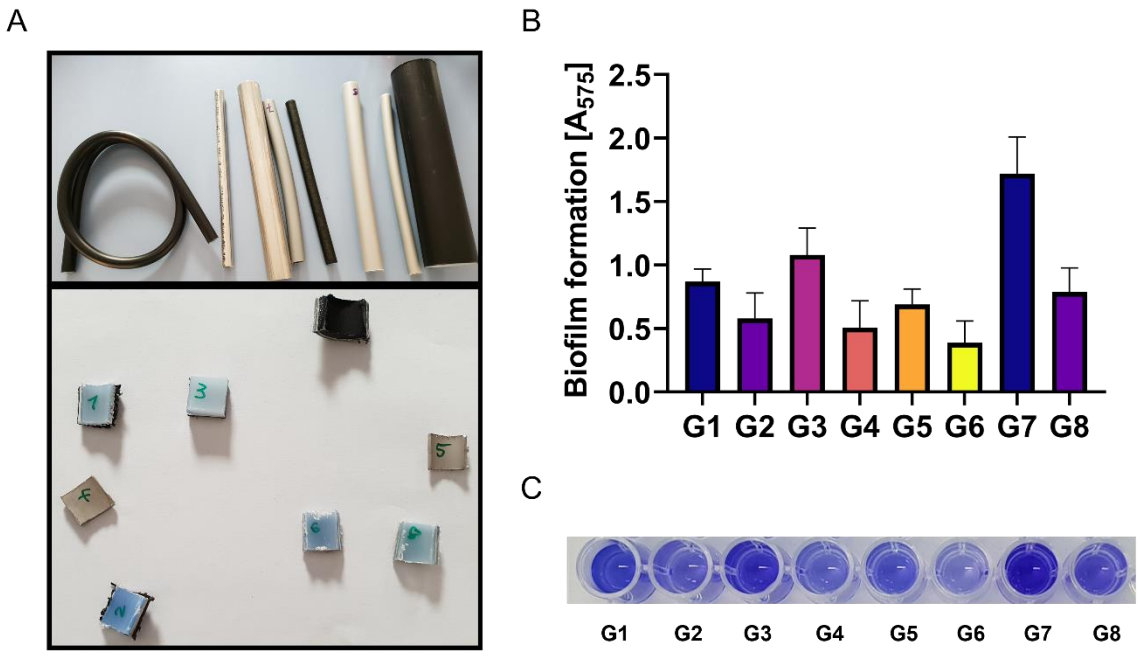

Fig. 3.4.6 Susceptibility of commercial domestic water pipes towards biofilm formation by *P. aeruginosa*. (A) Plastic pipes were sawed into 1cm^2 squares for analysis. (B) *P. aeruginosa* was cultured on the plastics for 72 h at 30 °C. Planktonic cells were then removed, and the remaining biofilm was stained with crystal violet solution. (C) After the unbound crystal violet was washed out, the remaining crystal violet was re-solubilized with 30% (v/v) acetic acid. The analysis was then performed by absorbance measurement at 575 nm. The standard deviation of three biologically independently performed experiments is represented by the error bars.

After commercial drinking water pipes were identified as prone to bacterial biofilm colonization, the research focused on finding suitable materials that closely resembled the materials incorporated in the pipes. Therefore, four different materials were selected, also used in potable water tubes (Tab. 3.4.1).

Tab. 3.4.1 The materials examined for the coating trials. The table contains the four selected materials to proceed with the coating studies.

Material	Properties
HDPE T	Semi-crystalline thermoplastic (Klein, 2011)
PP	Semi-crystalline thermoplastic (Klein, 2011)
HDPE H	Semi-crystalline thermoplastic (Klein, 2011)
TPU	Thermoplastic elastomer (Klein, 2011)

To verify the effectiveness of the coating, an antibiotic was initially applied to the material to demonstrate the proof of the concept. Tetracycline was selected for this procedure as a representative (Chu et al., 2013). Since it is known that tetracycline has antibiotic effects (Liaqat et al., 2009), an impact on biofilm formation would be assumed. The advantage of using tetracycline for this purpose was that the successful impregnation of the materials could be directly evaluated due to its yellow color (Egbuna, 2019). In the process of the trials, however, the TPU material proved unsuitable for this intended application. Although the coating worked in general, the characteristics of the material were not suitable for prolonged studies with bacteria. After incubation with *P. aeruginosa* for 72 h, the produced pyocyanin colored the TPU material green. This indicated that although the material coating worked, it was inadequate in the setting with bacterial solutions.

However, the remaining three materials were suitable for investigation in the presence of bacterial cultures. First, the individual plates were coated with CO_2 impregnation. This was done without an entrainer and with EtOH as an impregnating agent. After successful impregnation, the discs were placed in the *Panta Rhei* P flow cell and overlaid with bacterial culture. Subsequently, the biofilm was incubated for 72 h under a constant flow of 8 ml/h. After incubation, the discs were stained with crystal violet and analyzed at 575 nm.

Fig. 3.4.7 presents the results of the coating of the discs with the antibiotic tetracycline. Surprisingly, the coating on the HDPE H material showed little effect on the biofilm either with an entrainer or without an entrainer. The coating of the material HDPE T showed a reduction of bacterial biofilm up to 85% without using an entrainer and about 75% with EtOH use. The PP material also affected the biofilm as biofilm formation was reduced by approximately 80% without entrainer, and a reduction of approximately

65% was obtained with EtOH. The effects were slightly stronger without entrainer. Therefore, this showed that the CO_2 impregnation technique was effective.

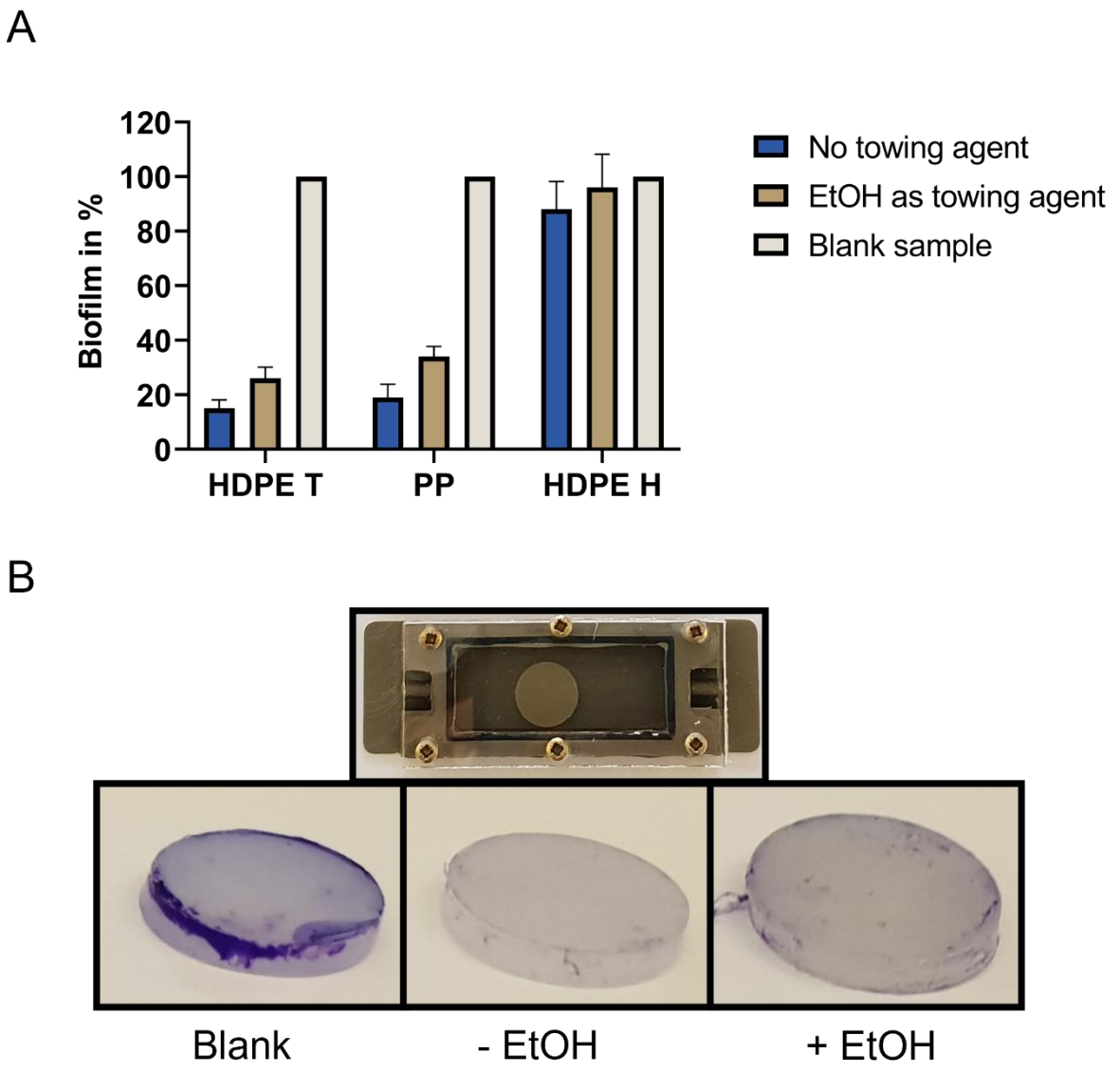

Fig. 3.4.7 Coating of tubing materials with tetracycline using CO_2 impregnation. (A) The different materials, HDPE T, PP, and HDPE H, were coated using CO_2 impregnation. Both no towing agent and EtOH as entrainer were used. This was followed by incubation with *P. aeruginosa*. (B) After incubation of the HDPE T disc in the *Panta Rhei* system, staining with crystal violet and analysis at 575 nm was performed. The standard deviation of three biologically independently performed experiments is represented by error bars.

After a successful proof of principle using the antibiotic, the next goal was to incorporate the secondary metabolites from *Photorhabdus* and *Xenorhabdus* into the targeted materials. As the material HDPE H did not display any particular effect, the main focus was placed on the remaining two materials, HDPE T and PP. Impregnation of both materials was carried out for substance 28, which had already been successfully evaluated for biofilm inhibition. Both impregnation methods were also applied here, with and without entraining agent. After impregnation, the discs were placed in the *Panta Rhei* P flow cell and incubated with *P. aeruginosa* at a constant flow rate of 8 ml/h at 30 °C. Then, the platelets were analyzed by both crystal violet and CLSM. For microscopy, a SYTO9/propidium iodide mixture was added to the cells and incubated for 30 min at 30 °C.

As shown in Fig. 3.4.8A, both impregnation methods had a negative effect on the biofilm formation of *P. aeruginosa*. Additionally, both materials were less accessible for effective biofilm formation. In the case of PP, a reduction of 70% was observed without an entraining agent. The variant using EtOH as an entraining agent achieved an 80% reduction. For HDPE T, the effects observed were stronger. For the variant without entrainer, the biofilm was decreased by 80%. The platelet impregnated EtOH as an entraining agent showed a 90% reduction. The platelets produced with EtOH as an entrainer exhibited slightly stronger effects by 10%.

The crystal violet and CLSM analysis results are shown in Fig. 3.4.8B. It could be observed that the PP blank sample was completely overgrown by the biofilm, as can be seen from the blue color of the crystal violet. In contrast, the biofilm hardly affected the phenylethylamides/tryptamides impregnated sample. The CLSM data reflected the same results. While the blank sample contained an approx. 40 µm thick biofilm layer, only a very thin biofilm layer was detected on the coated plate, which did not cover the entire surface.

The use of secondary metabolite impregnation, therefore, created a functional antibiofilm surface.

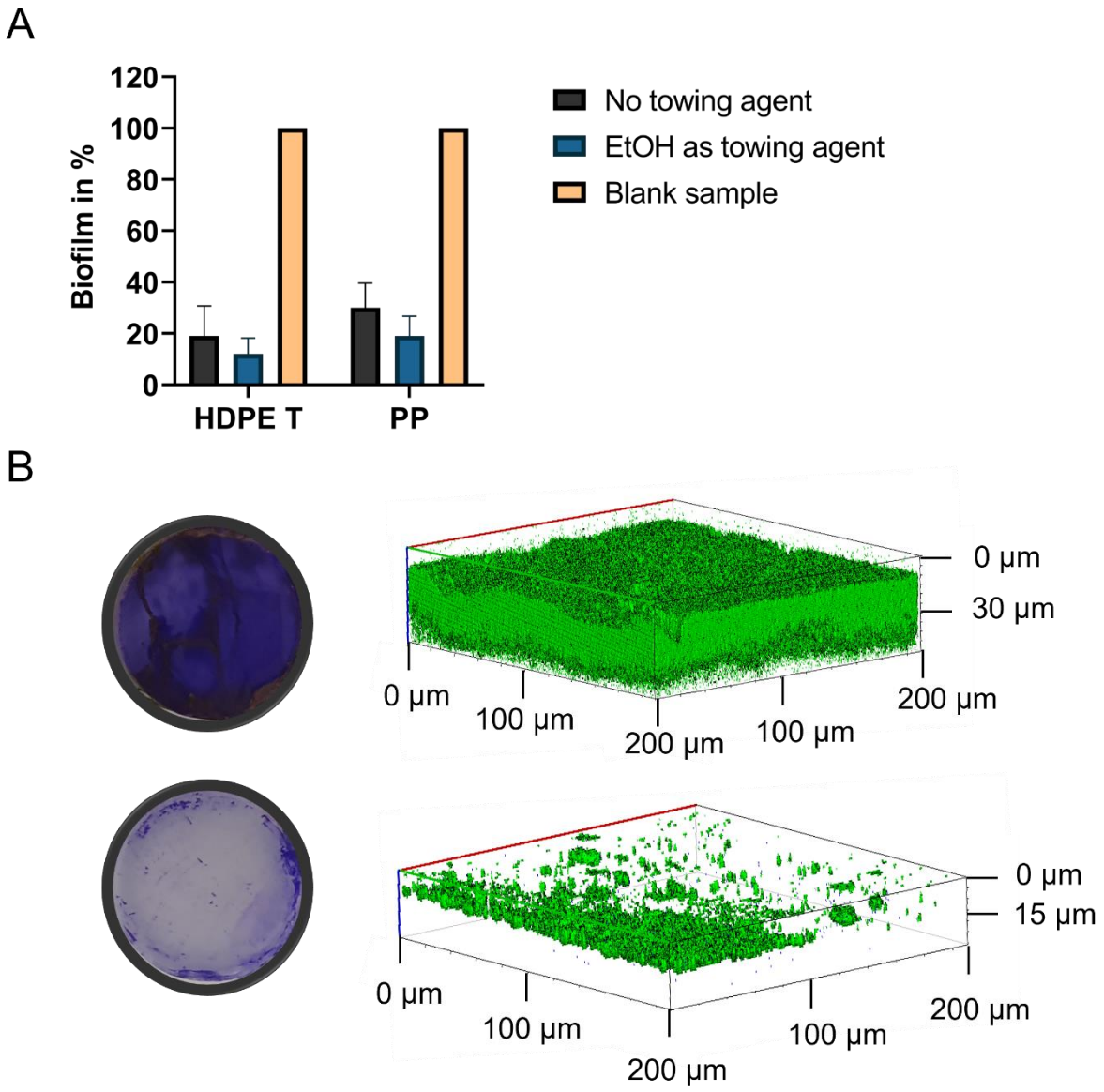

Fig. 3.4.8 The effect of the impregnated phenylethylamides/tryptamides on biofilm formation of *P. aeruginosa*. (A) *P. aeruginosa* was incubated along with the platelets for 72 h at 30 °C in the *Panta Rhei* P flow cell under a constant flow of 8 ml/h. Disks were impregnated with and without EtOH. (B) Analysis of the phenylethylamides/tryptamides impregnated PP and the blank sample was done by crystal violet and CLSM. The standard deviation of three biologically independently performed experiments is represented by the error bars.

3.4.3 Impregnated surfaces show long-term durability and inhibit bacterial biofilm under natural conditions

Once it had been confirmed that CO_2 impregnation was adequate and that secondary metabolites could thus be introduced onto the surface, it was investigated how long it takes for the substance introduced into the material to be leached out. The pigment Solvaperm Red from Clariant AG in Switzerland was selected for this purpose. Solvaperm Red is a red/ orange pigment that is clearly visible when successfully impregnated into the material (Prokein et al., 2021).

A long-term experiment was carried out for this study. The two materials, HDPE T and PP, were impregnated with Solvaperm Red and transferred into the *Panta Rhei* P flow cell after coating. The *Panta Rhei* flow cell was then operated for eight months at a constant flow rate of 10 ml/h with water.

Fig. 3.4.9 presents the results of the long-term experiment. Both HDPE T and PP appear bleached out after eight months of service. Nevertheless, the reddish color could be seen even after that long service. The pigment was not completely washed out even after several months of continuous operation. The PP material appeared slightly less faded than HDPE T. This clearly indicated that the CO_2 impregnation process could achieve a long-lasting coating effect.

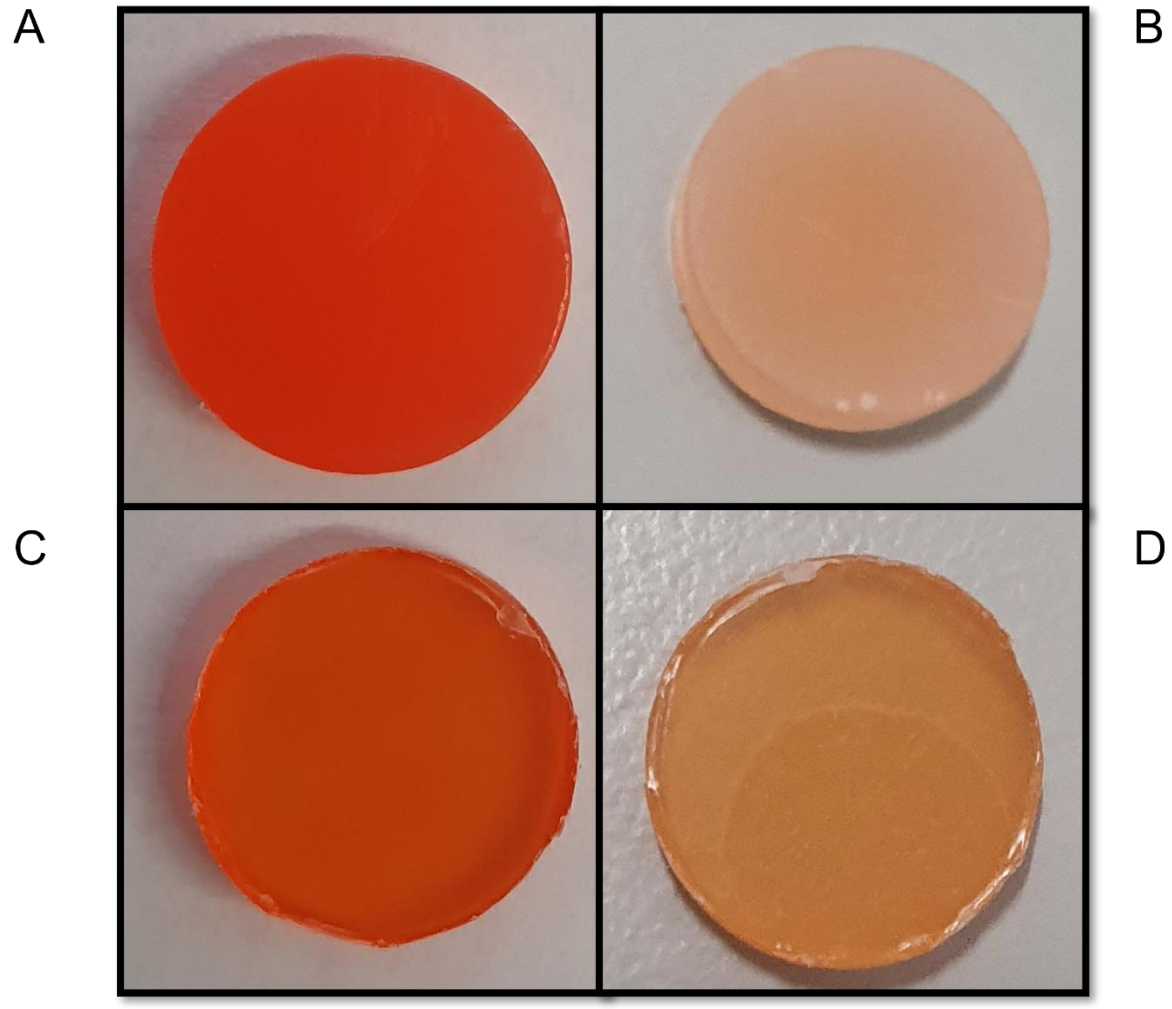

Fig 3.4.9 The effect of continuous operation for the impregnated materials. (A) The HDPE T material was impregnated with Solvaperm Red before the long-term experiment. (B) The impregnated HDPE T material after eight months under constant flow in the *Panta Rhei* system. (C) The PP material was impregnated with Solvaperm Red before the long-term experiment. (D) The impregnated PP material after eight months under constant flow in the *Panta Rhei* system. The flow rate applied for the measurements was 10 ml/h.

As the effect of the impregnation on biofilm formation was observed to be significant and visible after extended use, the challenge was to simulate the application by testing the impregnated surfaces under realistic conditions. An especially constructed simulation center from Kebos Group was utilized for this process (Fig. 3.4.10A). The simulation center was run with drinking water from the supply line and therefore simulated the drinking water distribution of a household. However, the operation itself was carried out separately without any coupling to the potable water system of the building. Furthermore, specially designed reactors, which could accommodate a disk adapter for holding up to 80 plastic plates, were created so that, with the assistance of

two valves, the connection and disconnection to the simulation center occurred trouble-free.

Since it was noticed that with HDPE T, the effects on the biofilm appeared to be slightly stronger, this material was used for the real-life simulation. In addition, it was also decided to use impregnated platelets, which were not treated with EtOH during production. This was done for logistical purposes. Initially, the platelet adapters were loaded with blank samples and HDPE T samples impregnated with phenylethylamides/tryptamides in equal quantities. The disk adapter was then coiled as shown in Fig. 3.4.10A and inserted into the reactor. The reactor was then connected to the simulation center. The complete system was filled with 60 L of water. The intended run time was 3 weeks. To ensure that there were indeed bacteria in the sample water, a total of 10^7 bacterial cells were added. The bacterial mixture consisted of equal numbers of cells from *P. aeruginosa*, *S. adhaesiva*, *M. mesophilicum*, and *B. nasdae*. Once the simulation was complete, the pressure was removed from the simulation center, and the reactors were detached from the system. The platelet adapters were then removed from the reactor, and the plates inside were stained with crystal violet. The biofilm analysis was then performed at 575 nm.

The results of the realistic simulation can be seen in Fig. 3.4.10B. It was noticed that the blank samples exhibited substantially increased biofilm adhesion. On the other hand, the samples coated with phenylethylamides/tryptamides displayed less biofilm attachment. Furthermore, after photometric analysis, a reduction in the biofilm formation of up to 70% was obtained compared to the control. Consequently, it was demonstrated on an applicative level that impregnated plastics with secondary metabolites from entomopathogenic bacteria remarkably decreased biofilm formation by drinking water bacteria.

A

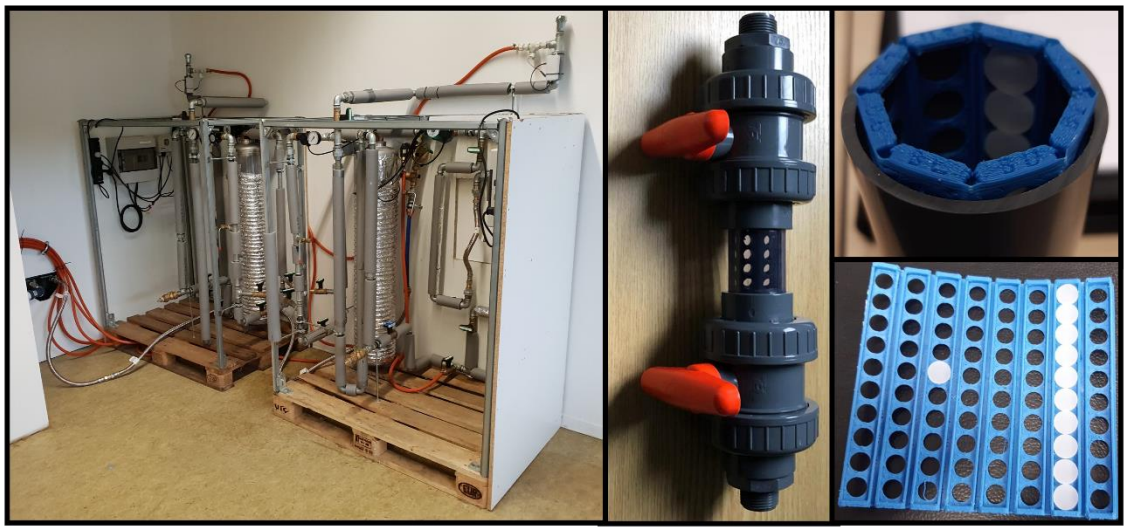

B

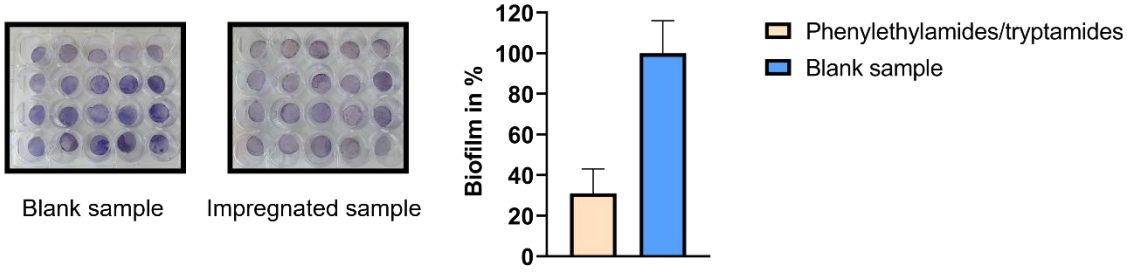

Fig. 3.4.10 Realistic simulation setup for sampling impregnated surfaces and the effect on drinking water bacteria by secondary metabolite-impregnated materials. (A) The simulation center was designed to be supplied with 60 L of water from the existing facility's drinking water distribution system. A special reactor was designed to hold a platelet adapter and be easily installed and removed into the simulation center by two valves. The platelet adapter was designed to hold up to 80 discs and could be enrolled. (B) The effects on the biofilm formation of drinking water bacteria after 3 weeks of continuous operation. The standard deviation of three biologically independently performed experiments is represented by the error bars. The images of the simulation setup were provided by the Kebos Group.

The results in this chapter indicate that secondary metabolites from entomopathogenic bacteria of the genera *Photorhabdus* and *Xenorhabdus* not only exhibit antibiotic effects as previously described but also have antibiofilm properties based on putative quorum quenching mechanisms as a mode of action. It was shown that biofilm formation in marine and drinking water bacteria is significantly reduced by secondary metabolites produced during the life cycle of *Photorhabdus* and *Xenorhabdus*. Furthermore, several secondary metabolites such as phenylethylamides/tryptamides, xenofuranones, or PAX peptides were observed to reduce biofilm in several bacteria without minimizing the planktonic cell count. Although xenocoumacin showed an antibiotic effect on most bacteria, this was not the case for *P. aeruginosa* and *B. nasdae*. In addition, a biofilm inhibitory effect was observed. Moreover, it could be shown that dilutions of the substances still displayed an effect. The phenylethylamides/tryptamides were also able to reduce the biofilm when used in the *Panta Rhei* microfluidic system. Additionally, the phenylethylamides/tryptamides were able to strongly reduce pyocyanin production. Plastic platelets were successfully coated with the secondary metabolites. The CO_2 impregnation method could stand out from its long-lasting function. Furthermore, a simulation with realistic conditions confirmed that the biofilm formation of drinking water bacteria decreased noticeably on the impregnated surfaces.

These secondary metabolites, therefore, provide an alternative to toxic and antibiotic biofilm control solutions used today. Accordingly, an application for a patent for the secondary metabolites xenocoumacin, phenylethylamides, tryptamides, xenofuranones, and PAX peptides has been deposited at the patent attorney.

3.5 The use of nanoparticles as potential approach to combat bacterial biofilms

The increasing antibiotic resistance of bacteria and the enhanced tolerance of bacterial biofilms to chemicals and antimicrobial drugs nowadays require the search for new antimicrobial strategies. So-called nanoparticles represent one option to tackle microorganisms and biofilms, which are becoming widely accepted due to their properties (Shkodenko et al., 2020). Furthermore, it is known that certain nanoparticles exhibit anti-bacterial properties (Lange et al., 2021; Muzammil et al., 2020). However, it is still unexplored to what extent nanoparticles can inhibit bacterial biofilm or even interfere with bacterial cell-cell communication.

One main part of this thesis was investigating the biofilm inhibiting properties of different nanoparticles such as tungsten oxides and cerium oxides. Additionally, for tungsten oxides, it was intended to test whether the antimicrobial properties could be enhanced by infrared exposure. Furthermore, biosensors were to be used to examine whether the bacterial QS system is influenced by tungsten oxides and cerium oxides. Moreover, it was to be studied whether cerium oxides incorporated on different surfaces displayed antibiofilm activity.

3.5.1 Tungsten oxides provide inhibition of bacterial biofilm and additionally demonstrate enhanced antimicrobial activity upon infrared irradiation

Specific tungsten oxides were already identified as possessing a function like that of haloperoxidase ((Dören, 2022; Dören et al., 2021a) ([redacted], Universität Mainz, personal communication)). Thus, the issue emerged as to whether this characteristic could be used for biofilm control. To explore the possibility, *P. aeruginosa* was utilized, whose biofilm formation is under the control of well-studied QS mechanisms (de Kievit, 2009).

Initially, an overnight *P. aeruginosa* culture was adjusted to a starting OD_{600} of 0.5. After that, tungsten oxides WO_{3-x} and c-$Cs_{0.6}WO_3$ were added to the bacteria at a final concentration of 0.1 mg/ml. To test the haloperoxidase-like function, 32 mM KBr and 0.8 mM H_2O_2 were also supplemented. $Na_2WO_4 * 2H_2O$ was the internal control, known already for haloperoxidase function. No addition of tungsten oxides served as a further control. Following incubation at 30 °C for 72 h in LB medium, a 600 nm measurement

was taken to determine the relative planktonic cell number. After the planktonic cells were removed, the attached bacterial cells were stained with crystal violet. Biofilm intensity was quantified at 575 nm.

The effect of the different tungsten oxides on *P. aeruginosa* can be seen in Fig. 3.5.1. A reduction in planktonic cell number of about 30% was observed with WO_{3-x}. For the nanoparticles, c-$Cs_{0.6}WO_3$ and the internal control Na_2WO_4 * $2H_2O$, a decrease of approximately 8% and 12%, respectively, occurred compared to the control without the addition of tungsten oxides. Surprisingly, however, a drastic reduction in *P. aeruginosa* biofilm of about 40% was also observed with c-$Cs_{0.6}WO_3$. For WO_{3-x}, a 45% reduction in biofilm was noted, however, antibiotic activity also contributed strongly in this case. The internal control Na_2WO_4 * $2H_2O$ diminished the biofilm by 20%.

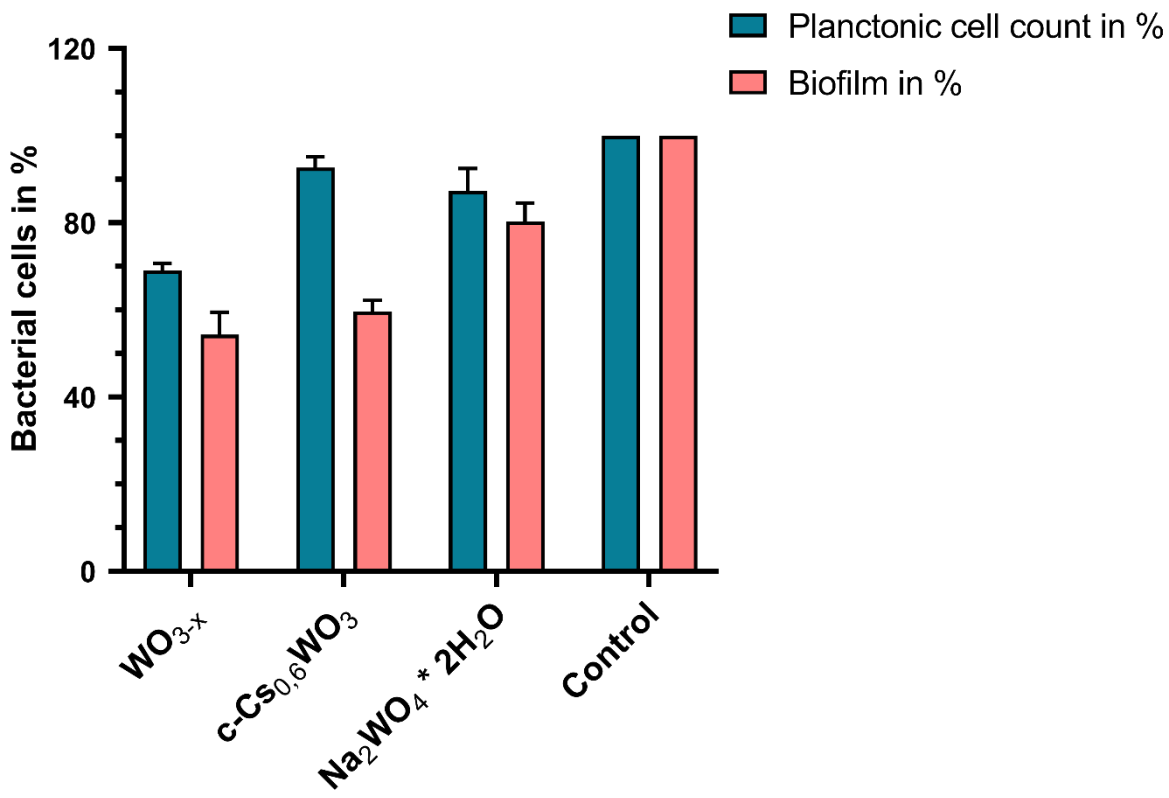

Fig. 3.5.1 The impact of tungsten oxides on the planktonic cells and biofilm formation of *P. aeruginosa*. The bacteria were cultured with and without the addition of the tungsten oxides for 72 h at 30 °C in LB medium. Subsequently, the planktonic cell count was quantified at 600 nm. After removing the planktonic cells, the biofilm was stained with crystal violet. The effect on the biofilm was determined at 575 nm. The standard deviation of three biologically independently performed experiments is represented by the error bars. Modified from (Dören, 2022).

Since the tungsten oxides were shown to influence bacterial biofilm formation, the intention was to examine whether the nanoparticles interfered with the QS system. *Agrobacterium tumefaciens* A136, a biosensor capable of sensing long-chain AHL, was selected for this task (Tang et al., 2013). *P. aeruginosa* utilizes the long-chain AHL 3-oxo-C_{12}-AHL as a signal molecule in one of its QS systems (J. Zhang et al., 2014). Based on the above, that AHL was externally spiked with a final concentration of 0.1 mg/ml of tungsten oxides. Additionally, H_2O_2 and KBr were mixed to determine a possible modification of the signal molecule by the haloperoxidase-like function. After 12 h incubation of the signal molecule, it was then added to *A. tumefaciens* A136 along with X-Gal. *A. tumefaciens* A136 is engineered to produce β-galactosidase upon the perception of long-chain AHL, which is capable of cleaving X-Gal. *A. tumefaciens* A136 carries the two plasmids pCF218 and pCF372. The plasmid pCF218 encodes for *traR* so that the receptor TraR is synthesized. Once the receptor TraR subsequently binds a long-chain AHL, it binds to the promoter *traI::lacZ* on the plasmid pCF372. After the expression of *lacZ*, the β-galactosidase formed can cleave X-Gal. Thus, a blue cleavage product is formed, which can be analyzed photometrically (Tang et al., 2013). Subsequently, further incubation of 8 h at 30 °C was carried out. This was followed by quantification at 630 nm.

As can be seen in Fig. 3.5.2, an effect of the QS system could be achieved with the application of the tungsten oxides. WO_{3-x} obtained a 17% reduction of the cleavage product. With c-$Cs_{0.6}WO_3$, a 27% decrease could be detected. The internal control Na_2WO_4 * $2H_2O$ resulted in a slight 10% drop in the production of the split compound. This was indicative that tungsten oxides potentially affect the QS system of bacteria.

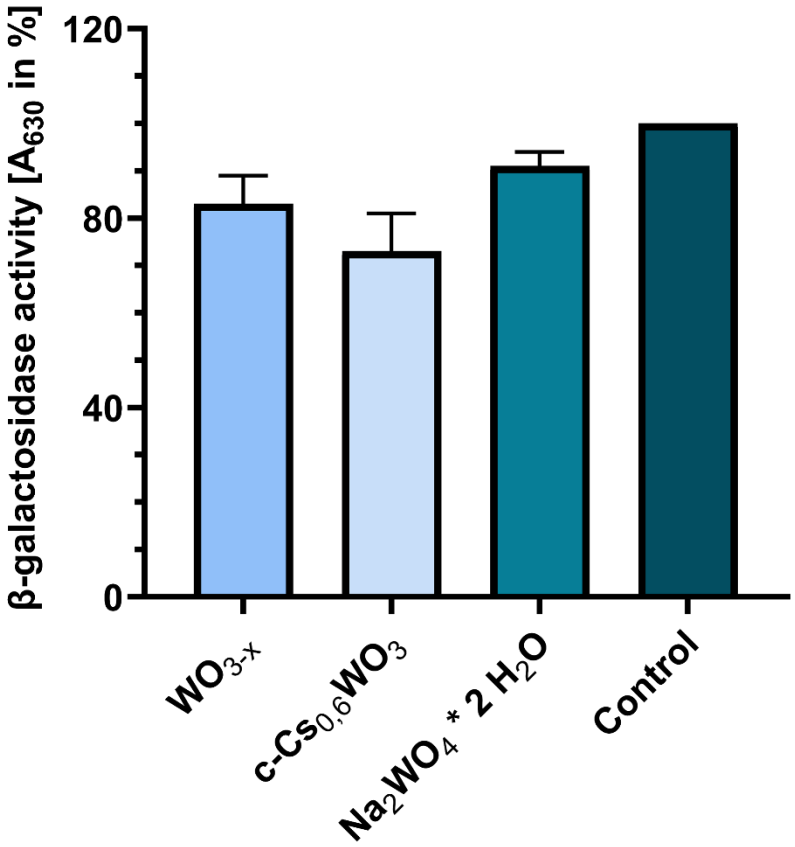

Fig. 3.5.2 Determination of the effect of tungsten oxides on AHL-mediated QS by quantification of β-galactosidase. The 3-oxo-C_{12}-AHL was incubated in the presence and absence of the tungsten oxides for 12 at room temperature. After the incubation was complete, the AHLs were then added to reporter strain *A. tumefaciens* A136, where the *lacZ* gene is under the control of the P_{tral} promoter, which is activated by long-chain AHLs. The bacteria were further incubated for another 8 h at 30° C in LB medium supplemented with X-Gal. The standard deviation of three biologically independently performed experiments is represented by the error bars. Modified from (Dören, 2022).

Moreover, it was further noticed that tungsten oxides are chromatic metallic solids exhibiting optical properties which can be ascribed to localized surface plasmon resonances (LSPR) in the visible to near-infrared range of the optical spectrum ((Dören, 2022; Wu et al., 2019) ([redacted], Universität Mainz, personal communication)). The strong LSPR absorption of WO_{3-x} suggested the concept of screening the effect of these properties on bacteria. *P. aeruginosa* and *S. aureus* were chosen for this investigation. *S. aureus* is a Gram-positive pathogenic bacterium that exhibits resistance to antibiotics and can cause significant damage to health (Chambers and DeLeo, 2009; Lowy, 2003). Besides WO_{3-x}, the tungsten oxides h-$(NH_4)_{0.2}WO_3$ and m-$Cs_{0.3}WO_3$ were also used since they displayed different

absorptions in the visible to near-infrared range (Dören, 2022) ([redacted], [redacted], personal communication). In addition, $Na_2WO_4 * 2H_2O$ was included as an internal control. Bacteria were incubated in LB medium at 30 °C for 72 h after either addition or no addition of the tungsten oxides. During incubation, infrared beam irradiation at 950 nm was performed every 30 min.

Fig 3.5.3 illustrates the effect of infrared irradiation on the bacteria. Surprisingly, it was observed that the tungsten oxides had similar effects for both bacterial species. The m-$Cs_{0.3}WO_3$ nanoparticles were able to decrease the planktonic cells of *P. aeruginosa* and *S. aureus* by approximately 30% by using infrared irradiation. The internal control $Na_2WO_4 * 2H_2O$ hardly achieved any effect using infrared exposure. The h-$(NH_4)_{0.2}WO_3$ induced a reduction of about 10% in *P. aeruginosa* and *S. aureus*, respectively, with infrared. For WO_{3-x}, a roughly 7% overall reduction was obtained with irradiation. However, as seen before (Fig. 3.5.1), an antibiotic effect could already be observed for WO_{3-x} without infrared.

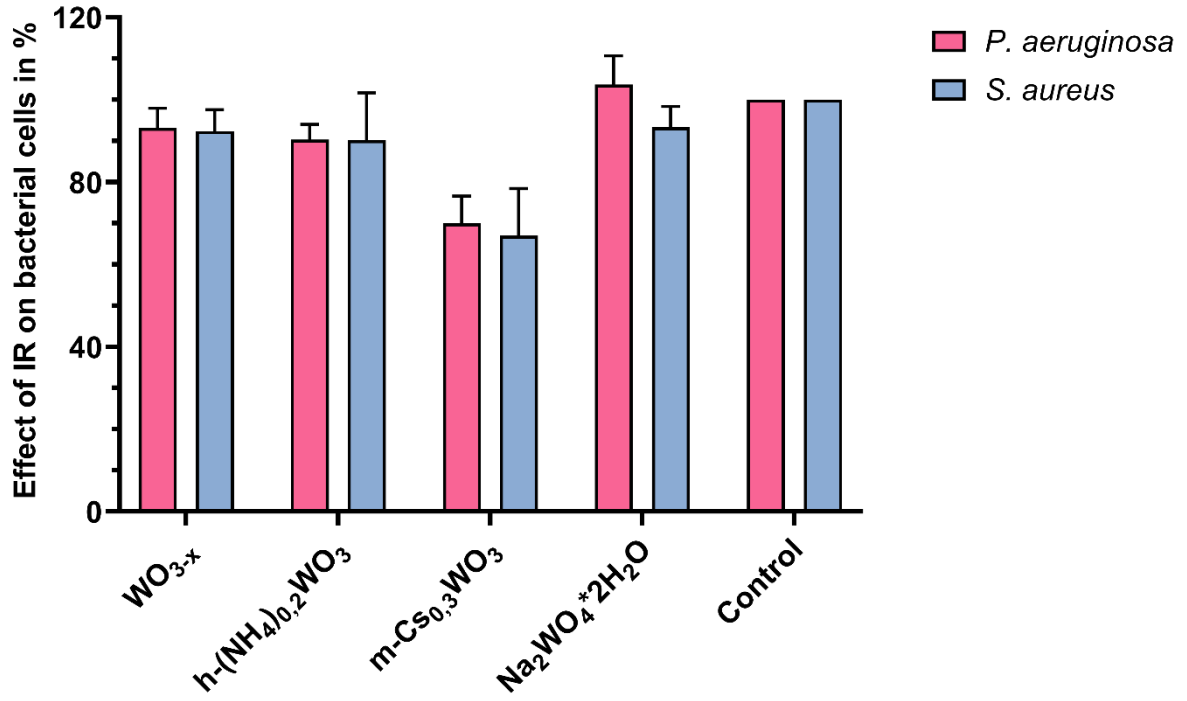

Fig. 3.5.3 Effect of infrared irradiation on *P. aeruginosa* and *S. aureus*. Bacteria were incubated at 30 °C in LB medium for 72 h with and without the addition of the tungsten oxides. Irradiation with 950 nm infrared was performed every 30 min. After 72 h, quantification of the relative cell number of planktonic cells was determined at 600 nm. The standard deviation of three biologically independently performed experiments is represented by the error bars. Modified from (Dören, 2022).

3.5.2 Bacterial biofilm prevention by cerium oxide nanoparticles

As another nanoparticle class besides tungsten oxides, cerium oxides have demonstrated even much stronger haloperoxidase-like function (Frerichs, 2020; Pfitzner, 2021; Pütz, 2022) ([redacted], [redacted], [redacted]; Universität Mainz; personal communication) it should be investigated additionally whether cerium oxides might be used further as another nanoparticle class representing a new antibiofilm strategy. Cerium oxide nanoparticles synthesized in different ways ([redacted]; Universität Mainz), as referred to in the methods part, were utilized for this task. To test a broader spectrum of biofilm-forming bacteria, two bacteria belonging to the OPPPs, *P. aeruginosa* and *M. mesophilicum* (Szwetkowski and Falkinham, 2020), were chosen. A marine bacterium, *P. gallaeciensis*, capable of colonizing biotic and abiotic surfaces initially in the marine sector (de Carvalho, 2018; Zhao et al., 2016),

was used. *K. pneumoniae* was included in this study to complement the medical sector as a Gram-negative, human pathogenic bacterium that often colonizes catheters and infects the urinary tract (X. Liu et al., 2020; Stahlhut et al., 2012; Wang et al., 2020). In addition, *S. aureus* was considered as a representative of the Gram-positive bacteria (Chambers and DeLeo, 2009; Lowy, 2003).

Initially, the individual bacteria were cultured in the presence and absence of the various cerium oxide nanoparticles. *P. aeruginosa*, *K. pneumoniae*, and *S. aureus* were cultivated in LB medium. *P. gallaeciensis* and *M. mesophilicum* were grown in 2216 medium and M1 medium, respectively. Incubation was carried out for 72 h at 30 °C. All runs were supplemented with KBr and H_2O_2. No addition of any ceria nanoparticles served as a control.

The impact of the cerium oxides on the different bacteria is shown in Fig. 3.5.4. Surprisingly, none of the cerium oxide nanoparticle classes showed a biofilm inhibitory effect on *S. aureus*. In addition, EP60A and CeO_2-SG were detected as cerium oxide nanoparticle classes that demonstrated no effect on biofilm in any of the five bacteria that were tested. For *P. aeruginosa*, *K. pneumoniae*, and *M. mesophilicum*, the classes EP157 and EP151 exhibited the strongest effects on the respective biofilm. EP157 was able to reduce the biofilm of e.g., *P. aeruginosa* by up to 60%. In turn, with EP151, a 55% reduction could be reached for *P. aeruginosa*. The nanoparticles CeO_2-HT, $BiCeO_2$-HT, EP128-a, and EP132-400 resulted in a reduction of the biofilm in *P. aeruginosa* between 30% and 50%. In the case of the marine bacterium *P. gallaeciensis*, the EP128-a class displayed the strongest effect on biofilm formation, as only about 60% of the biofilm could be detected compared to the control without the addition of nanoparticles.

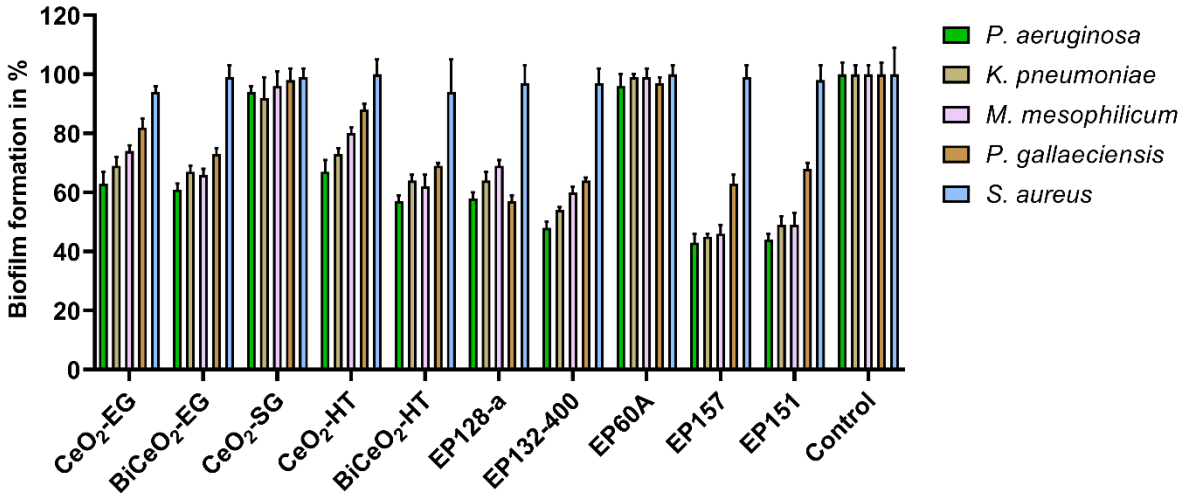

Fig. 3.5.4 The effects of different cerium oxides on the biofilm formation of various species of biofilm-forming bacteria. The microorganisms *P. aeruginosa*, *K. pneumoniae*, and *S. aureus* were cultured in LB medium. *P. gallaeciensis* was cultivated in 2216 medium. *M. mesophilicum* was grown in TSY medium. Additional KBr and H_2O_2 were supplemented to each CeO_2 nanoparticle class. After 72 h incubation at 30 °C in the presence and absence of the various ceroxides, bacterial biofilm was determined by crystal violet staining. The standard deviation of three biologically independently performed experiments is represented by the error bars. Modified from (Frerichs, 2020; Jegel, 2022; Pütz, 2022).

Following the results obtained with cerium oxides in relation to biofilm formation, the question arose as to whether cerium oxides influence the QS of bacteria. To investigate this, it was intended to perform experiments with the QS reporter strain *A. tumefaciens* A136, which can detect long-chain AHLs but cannot synthesize AHLs. Upon addition of substrates such as 5-bromo-4-chloro-3-indoxyl-β-D-galactopyranoside (X-Gal) or o-nitrophenyl-β-D-galactopyranoside (ONPG), for example, such substrates can then be cleaved by the formation of β-galactosidase. The generation of β-galactosidase depends on the concentration of AHL detected (Tang et al., 2013). For logistical reasons and since the effect on the biofilm was one of the strongest observed, further investigations were carried out with the EP151 nanoparticle class. Considering that *P. aeruginosa* has a very well-studied QS mechanism and that biofilm formation in this bacterium is regulated by QS, *P. aeruginosa* was used for further analyses.

To investigate an impact on the QS system, external 3-oxo-C_{12}-AHL was incubated in the presence and absence of the ceria nanoparticles. This was supplemented with KBr and H_2O_2. After incubating for 8 h at RT, the AHL treated with and without ceria nanoparticles were provided to *A. tumefaciens* A136. At this point, supplemental X-Gal was subsequently added. After another 8 h of cultivation at 30 °C, the cells were

centrifuged, and the culture fluid was measured at 630 nm. Furthermore, ONPG was also used as a substrate. In this case, after the addition of the AHL to *A. tumefaciens* A136, no substrate was initially added. The bacteria were incubated for 8 h at 30 °C. Next, 1 ml was separated by centrifugation, and the bacteria were resuspended in buffer Z. ONPG was then added after treatment with chloroform and SDS for 30 min at 30 °C. Finally, the time was stopped, necessary until the solution turned yellow. After stopping the reaction and centrifuging the cells, a measurement was performed at 420 nm and 550 nm for analysis.

The results of the reporter assay can be observed in Fig. 3.5.5. Obviously, the addition of the cerium oxide nanoparticles resulted in lower AHL detection by *A. tumefaciens* A136. A decrease of approximately 40% was observed with the addition of X-Gal in Fig. 3.5.5A compared to the control, which was not treated with ceroxides. The calculation of Miller Units in Fig. 3.5.5B confirmed the results, as only 2940 units could be determined with the addition of cerium oxide, compared to 4700 for the control. This was the equivalent of about 62%. Therefore, the decrease with this substrate represented approximately 40% as well. These results provided a first indication that the QS system of *P. aeruginosa* could be affected by the cerium oxides.

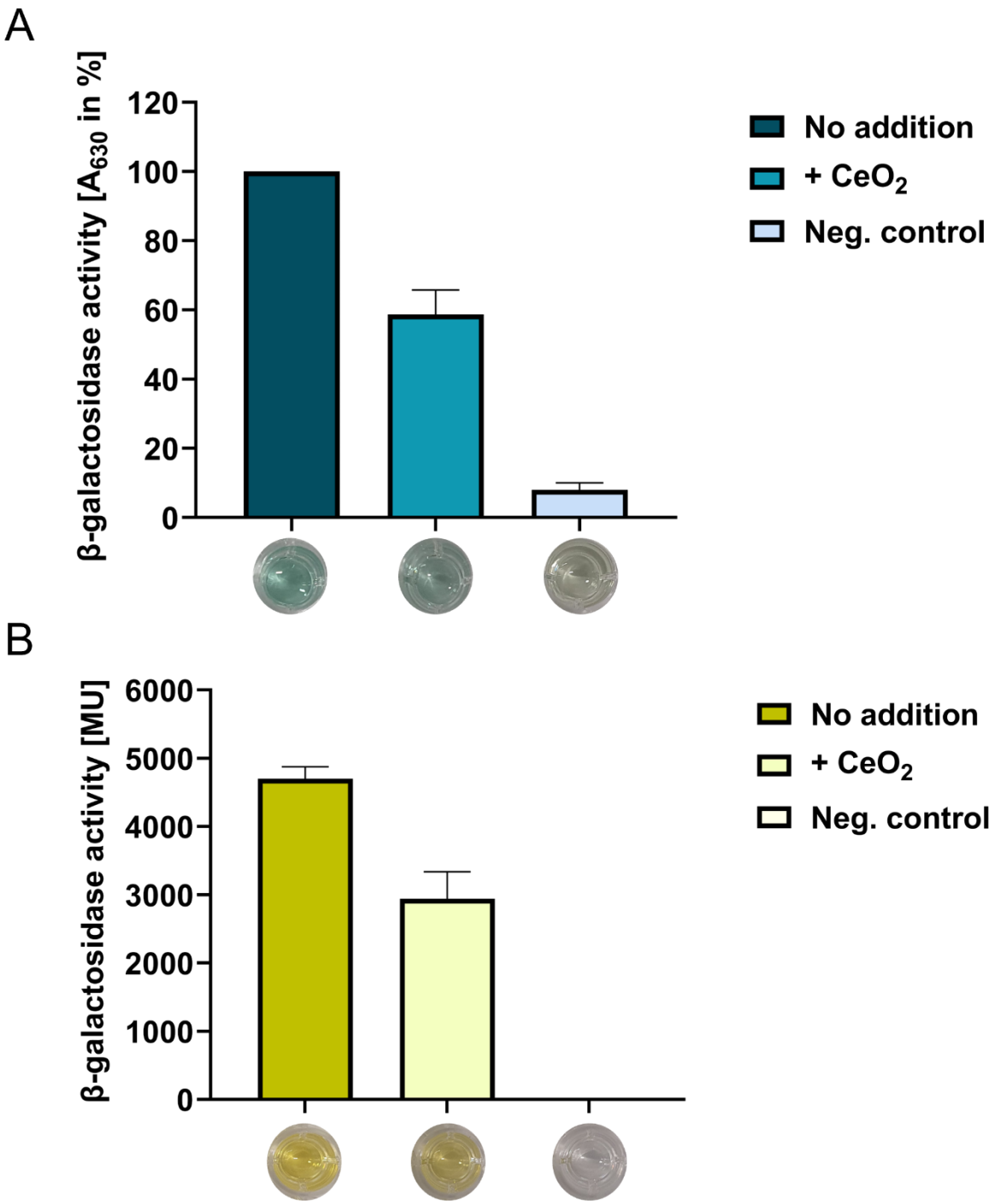

Fig. 3.5.5 Effect of cerium oxides on long-chain AHL using the biosensor *A. tumefaciens* A136. Two different substrates were used for this study. (A) For quantification with X-Gal, the 3-oxo-C_{12}-AHL was incubated in the presence and absence of the cerium oxide nanoparticles and H_2O_2 and KBr for 8 h. Subsequently, the AHLs were added to *A. tumefaciens* A136 along with the substrate X-Gal. After another 8 h of incubation at 30 °C, the cells were separated by centrifugation. The culture fluid was measured at 630 nm. LB medium served as a negative control. (B) After incubation was performed with and without ceroxides, AHL were added to *A. tumefaciens* A136 and incubated for 8 h at 30 °C. Then, 1 ml was collected and centrifuged. The cells were resuspended in buffer Z. After the addition of chloroform and SDS and incubation at 30 °C for 30 min, ONPG was supplemented. The time was recorded until the

samples turned yellow. After halting the reaction and centrifugation of the cells, the culture fluid was measured at 420 nm and 550 nm. Buffer Z served as a negative control. The standard deviation of three biologically independently performed experiments is represented by the error bars. Modified from (Pütz, 2022; Pütz et al., 2022).

Based on the biosensor experiments showing that the ceria nanoparticles affected the amount of AHL, the level of 3-oxo-C_{12}-AHL and C_4-AHL in *P. aeruginosa* should be determined with and without the addition of the ceria nanoparticles. In this context, the bacteria were incubated in the presence and absence of the cerium oxide nanoparticles for 24 h at 30 °C upon the supplementation of KBr and H_2O_2. Subsequently, the bacteria were centrifuged, and the culture fluid was then extracted by ethyl acetate. Analysis was performed by LC-MS.

Fig. 3.5.6A illustrates the different AHL levels of *P. aeruginosa* in the presence and absence of the cerium oxides. The reduction of both AHL was detected. For 3-oxo-C_{12}-AHL, only about 45% of the actual concentration was detectable. For C_4-AHL, about 50% was still present. A drastic reduction of AHL concentrations in *P. aeruginosa* could therefore be identified upon the addition of ceroxides.

In the following, it was intended to investigate whether the haloperoxidase-like function of the cerium oxides was involved in the decrease of the AHL concentrations. Therefore, IC-CD was used to examine whether a fixed bromide concentration could be affected by the addition of cerium oxide. Briefly, the bacteria were incubated with the addition of 30 µM NaBr and in the presence and absence of the nanoparticles.

It can be clearly seen in Fig. 3.5.6B that the bromide concentration decreased by about 20% when CeO_2 was added. Thus, it could be observed that externally added bromide could no longer be detected completely in the culture fluid, and therefore the non-detectable bromide may be integrated into molecules.

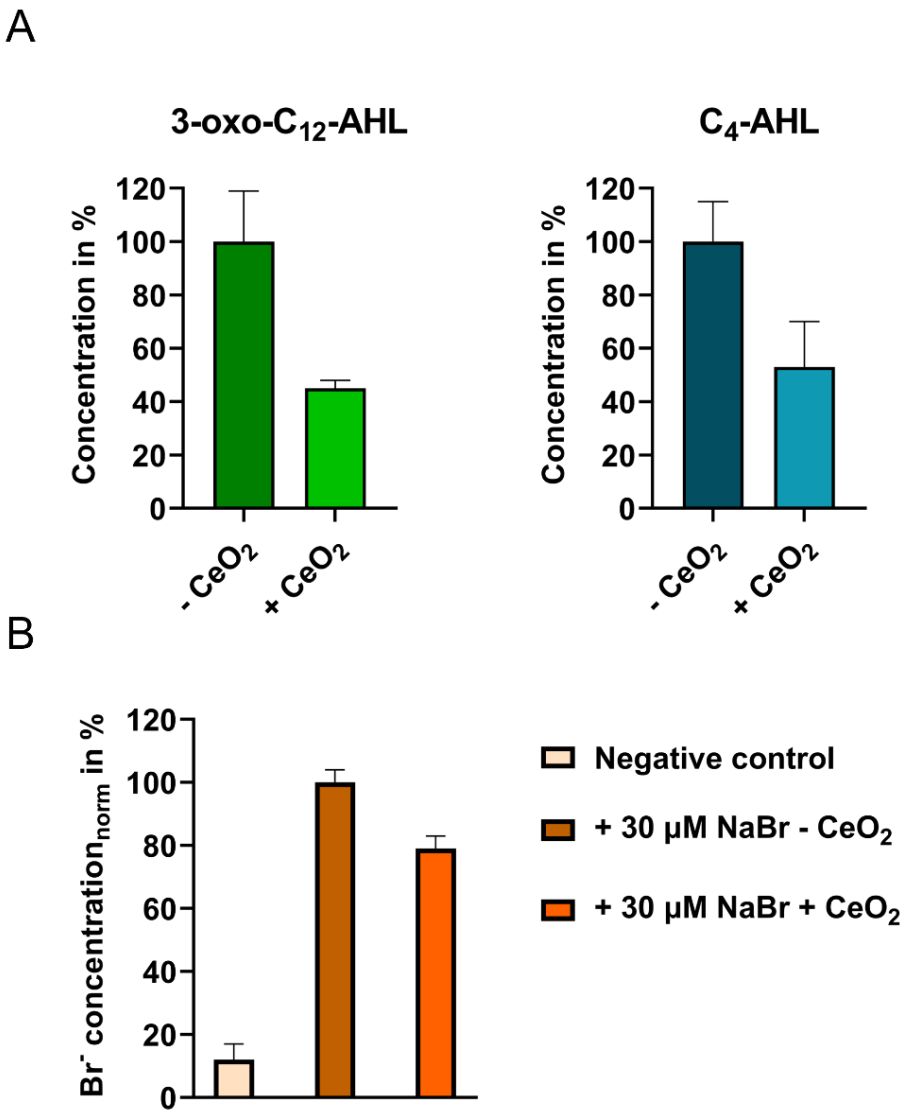

Fig. 3.5.6 Detection of the influence of cerium oxides on AHL concentration and bromide levels in the culture fluid. (A) *P. aeruginosa* was incubated in LB medium, H_2O_2, and KBr at 30 °C for 24 h in the presence and absence of ceroxides. The cells were then centrifuged, and the culture fluid was extracted with ethyl acetate after filtration. Analysis of AHL C_4 and 3-oxo-C_{12} was carried out by LC-MS. (B) *P. aeruginosa* was incubated in LB medium and H_2O_2 together with 30 µM NaBr and in the presence and absence of cerium oxides for 24 h at 30 °C. Cells were then centrifuged, and bromide concentration was measured by IC-CD. The bromide concentration in the LB medium served as a negative control. The standard deviation of three biologically independently performed experiments is represented by the error bars. Modified from (Pütz, 2022; Pütz et al., 2022).

To support this assumption, degradation studies of external 3-oxo-C_{12}-AHL were performed using LC-HRMS. The AHL was incubated in the presence and absence of CeO_2 nanoparticles together with H_2O_2 and NaBr in water.

Fig. 3.5.7A clearly demonstrates that the AHL is degraded by adding CeO_2. Surprisingly, however, two additional degradation products, DAHSL and DAHS, were found (Fig. 3.5.7B), which increased with time in the presence of the nanoparticles.

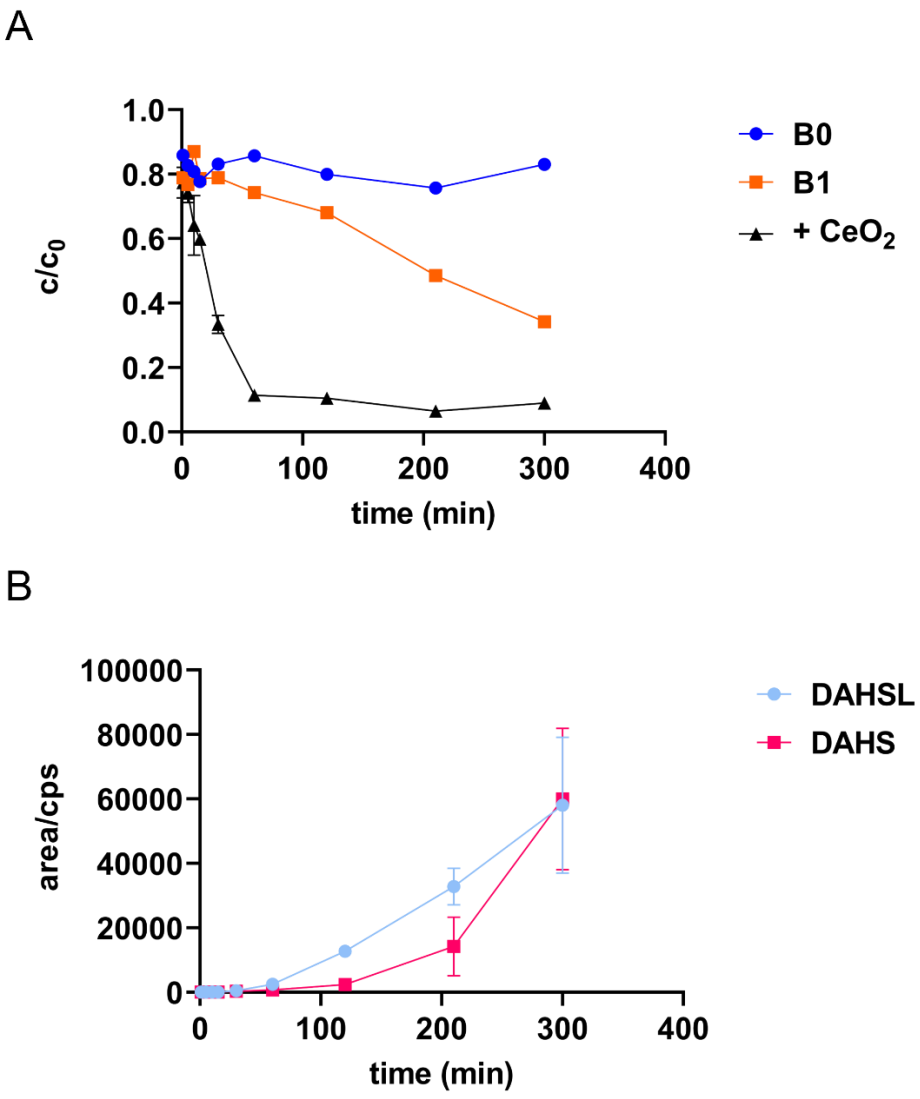

Fig. 3.5.7 Degradation studies of 3-oxo-C_{12}-AHL and detection of two intermediates. With the supplementation of ceria nanoparticles, NaBr, and H_2O_2 in MilliQ water, the decomposition of AHL (A) and the gain of two intermediates, DAHSL and DAHS, (B) were quantified by LC-HRMS. No addition of CeO_2 served as a control. The standard deviation of three biologically independently performed experiments is represented by the error bars. Modified from (Pütz, 2022; Pütz et al., 2022).

The next step included the examination of the effect of the DAHSL degradation product on *P. aeruginosa*. Different concentrations were applied for this aim. Moreover, 3-oxo-C_{12}-AHL and C_4-AHL were also applied to *P. aeruginosa* at different concentrations and cultivated for 72 h at 30 °C in LB medium. Measurement at 600 nm was then performed to determine the relative planktonic cells. After removing the planktonic cells, the biofilm was stained using crystal violet. Finally, the biofilm formation was analyzed by measuring the absorption at 575 nm.

The results of the molecule addition on the planktonic cells and the biofilm are graphically described in Fig. 3.5.8. Neither the signal molecules 3-oxo-C_{12}-AHL and C_4-AHL nor the degradation product DAHSL had an influence on the planktonic cells (Fig. 3.5.8A). The picture was different, however, for the biofilm formation of *P. aeruginosa* (Fig. 3.5.8B) since the addition of the signal molecules 3-oxo-C_{12}-AHL and C_4-AHL promoted biofilm formation, and a reduction in biofilm formation was observed with the addition of DAHSL.

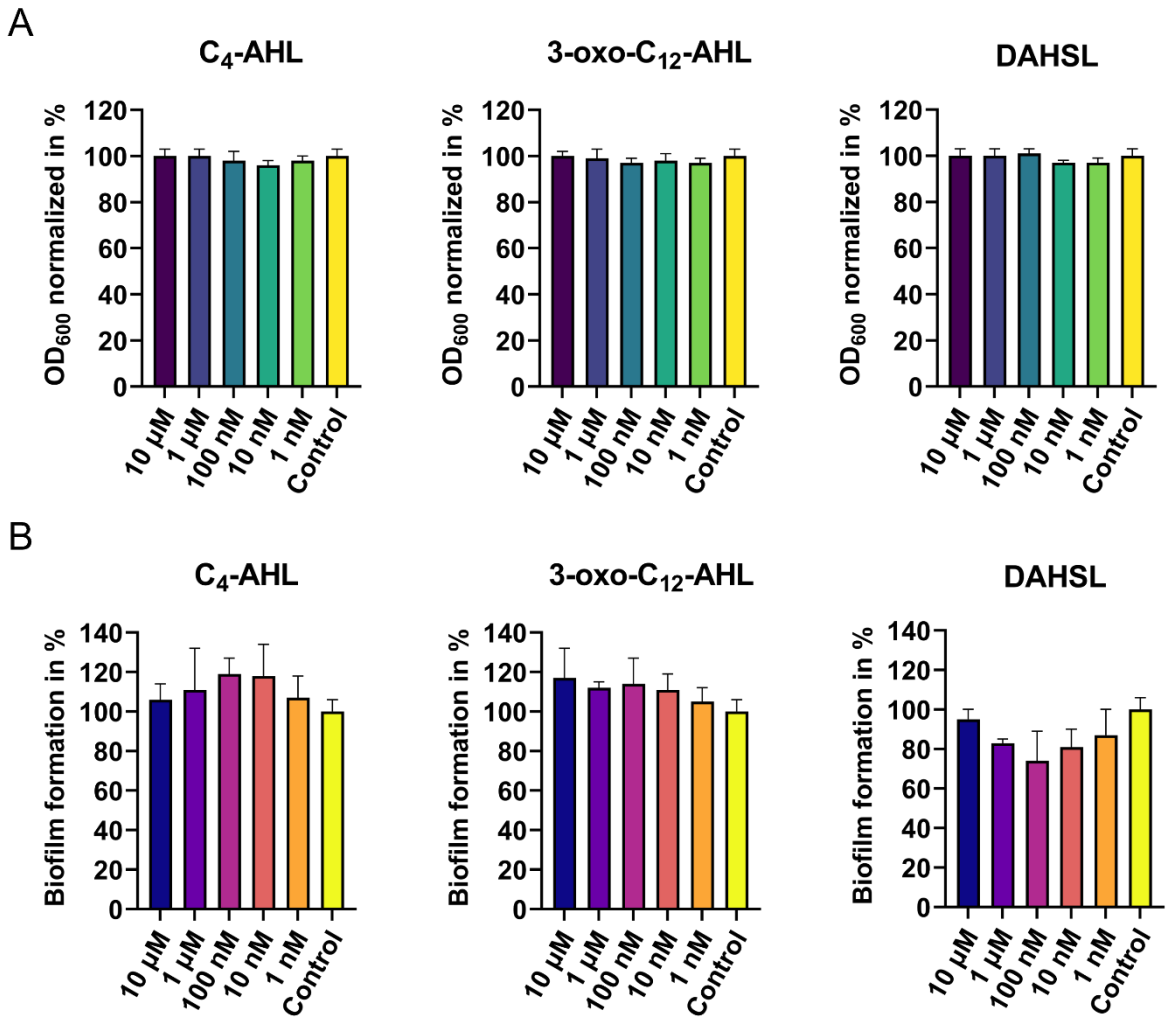

Fig. 3.5.8 Influence of C_4-AHL, 3-oxo-C_{12}-AHL and DAHSL on the planktonic cells and biofilm formation of *P. aeruginosa*. The bacteria were incubated after the addition of the different concentrations (1 nM – 10 µM) of C_4-AHL, 3-oxo-C_{12}-AHL, and DAHSL in LB medium for 72 h at 30 °C. No addition served as a positive control. (A) After incubation, absorption was measured at 600 nm to determine the effect on planktonic cell count. (B) This was followed by crystal violet staining to quantify the effect on biofilm. The biofilm analysis was conducted by measuring absorbance at 575 nm. The standard deviation of three biologically independently performed experiments is represented by the error bars. Modified from (Pütz, 2022; Pütz et al., 2022).

Nevertheless, since the degradation product DAHSL could not be detected when *P. aeruginosa* and CeO_2 were cultivated together, the issue became whether this degradation product is not only formed *in vitro* but also in the biological system or whether it is subsequently degraded or becomes unstable if it is generated. Therefore, DAHSL was synthesized and then added to *P. aeruginosa* in two different concentrations. The bacteria were then incubated for 24 h at 30 °C in LB medium.

Surprisingly, DAHSL that was externally added to the bacteria could not be detected at all at 10 nM and could be found in minimal amounts at 100 nM (Fig. 3.5.9). However, since the *in vitro* experiments revealed that DAHSL seemed not to be unstable, it was possible that the DAHSL was degraded by the bacteria.

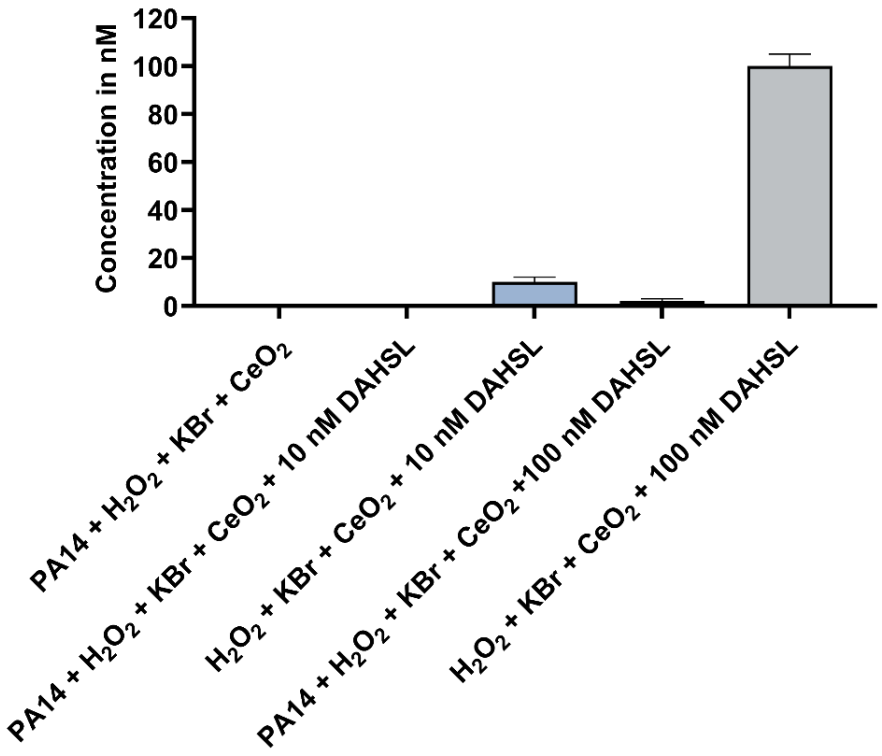

Fig. 3.5.9 Detection of the presence of DAHSL after addition to *P. aeruginosa*. 10 nM and 100 nM DAHSL were respectively dosed to the bacteria. Incubation at 30 °C for 24 h in LB medium was then carried out. No addition of the bacteria or the breakdown product DAHSL respectively were used as controls. The standard deviation of three biologically independently performed experiments is represented by the error bars. Modified from (Pütz, 2022; Pütz et al., 2022).

However, these observed results could not elucidate the decline in bromide concentration (Fig. 3.5.6B) and the fate of the remaining bromide. Therefore, LC-ESI-QToF was used to search for additional brominated molecules. A list of potential products could thus be generated. The most abundant product showed quinolone-specific fragments and the corresponding halogenated analogs like 2-heptyl-1-hydroxyquinolin-4-one (HQNO). HQNO is regulated by the *Pseudomonas* quinolone

signaling system and acts as a cytochrome inhibitor in prokaryotic and eukaryotic cells (Liu et al., 2018).

To confirm the obtained results, HQNO was incubated externally with the addition of CeO_2, NaBr and H_2O_2 in water. Fig. 3.5.10A depicts the result of the degradation study of HQNO. Thus, the CeO_2 nanoparticles were able to brominate the HQNO and consequently generate the reaction product Br-HQNO (Fig. 3.5.10B). Consequently, it was confirmed that the cerium oxide nanoparticles were able to brominate molecules in *P. aeruginosa* with the help of the haloperoxidase-like function, thereby affecting the formation of the biofilm.

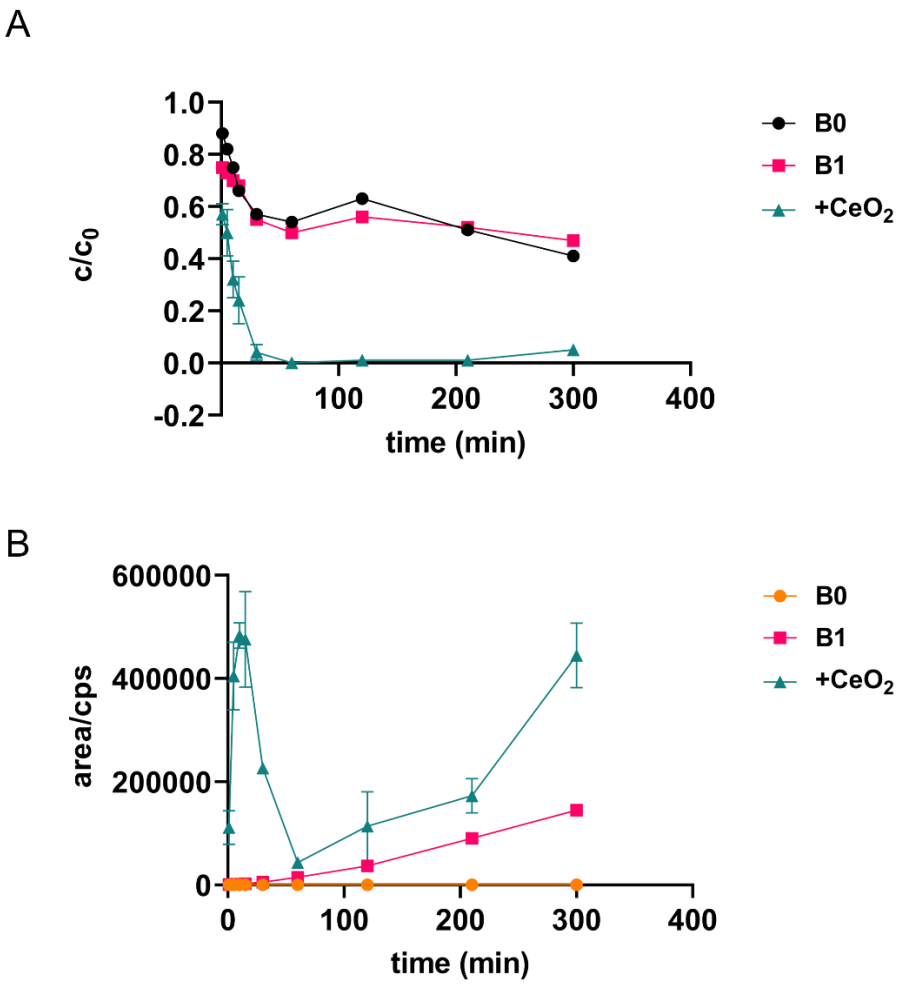

Fig. 3.5.10 Degradation of HQNO and respective formation of Br-HQNO. With the supplementation of ceria nanoparticles, NaBr and H_2O_2 in MilliQ water, the decomposition of HQNO (A) and the gain of the reaction product Br-HQNO (B) were quantified by LC-HRMS. No addition of CeO_2 served as a control. The standard deviation of three biologically independently performed experiments is represented by the error bars. Modified from (Pütz, 2022; Pütz et al., 2022).

3.5.3 A variety of surfaces coated with cerium oxides as preventive measure for biofilm control

Considering that the results obtained with cerium oxide nanoparticles revealed a significant inhibition of biofilm formation by Gram-negative bacteria, the next goal was to deposit the nanoparticles on different surfaces and thus demonstrate an application utilization. Since the application areas that are affected by undesirable biofilms are various (Allion et al., 2011; Bereschenko et al., 2010; Donlan, 2002; Muhammad et al., 2020; Procópio, 2019; Vaksmaa et al., 2021), different materials were used for the surface evaluation experiments: membranes, different polymer materials, and steel.

At baseline, polyethersulfone (PES) membranes were coated with CeO_2-HT and $BiCeO_2$-HT. An uncoated variant served as a positive control. Following this, *P. aeruginosa* was added to the different membranes, supplemented with KBr and H_2O_2, and incubated at 30 °C for 72 h in LB medium. The membranes were then rinsed so that planktonic cells were removed. Following, the attached bacteria were treated with SYTO9/propidium iodide, so that all cells attached, alive or dead, were visualized in the biofilm.

The influence of the coated surfaces on the biofilm of *P. aeruginosa* is depicted in Fig. 3.5.11. The non-coated surface (Fig. 3.5.11A) was entirely overgrown by biofilm (green fluorescence), so that no uncolonized area was detectable. However, the surfaces coated with CeO_2-HT (Fig. 3.5.11B) and $BiCeO_2$-HT (Fig. 3.5.11B) showed a different pattern. It was obvious here that not the entire surface was colonized with biofilm and that vacant areas (white in the figure) were present. In summary, it was shown that a membrane could be produced with reduced *P. aeruginosa* biofilm susceptibility and is thus suitable for a broad range of applications.

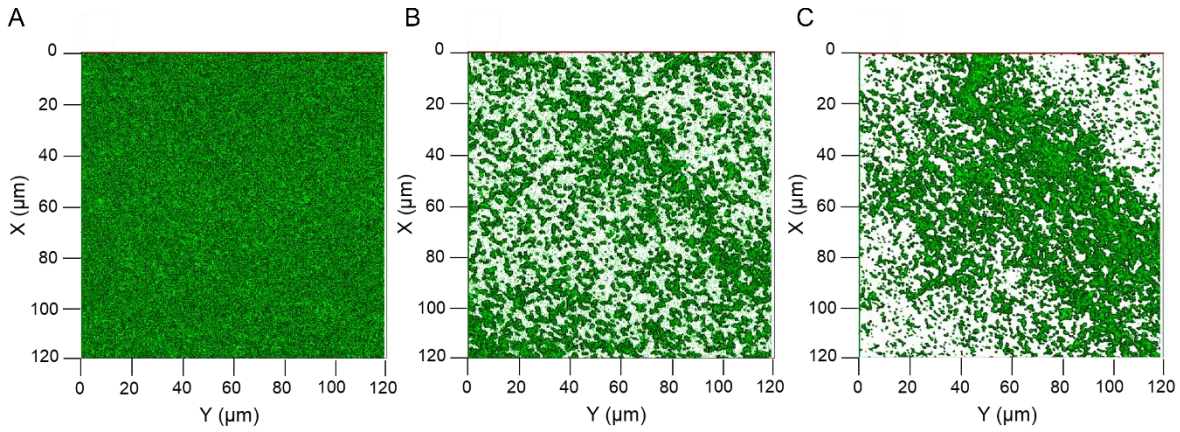

Fig. 3.5.11 Effect of cerium oxide nanoparticles embedded in polyethersulfone membranes on *P. aeruginosa*. CLSM images of *P. aeruginosa* on non-coated (A), with CeO_2-HT (B) and $BiCeO_2$-HT (C) coated PES membranes. Bacteria were cultured for 72 h at 30 °C in LB medium on the surfaces, supplemented with H_2O_2 and KBr. Subsequently, after removing the planktonic cells, the attached cells were stained with SYTO9/propidium iodide. The effect of the nanoparticles was then analyzed visually using CLSM. The uncoated surface was utilized as a positive control. Modified from (Frerichs, 2020; Frerichs et al., 2020).

Moreover, different polymeric materials were coated with CeO_2-FPEG to cover a wide range of possible applications (Klein, 2011). *P. aeruginosa* was cultivated for this purpose on uncoated or coated plastics for 72 h at 30 °C in LB medium. This was followed by biofilm analysis using crystal violet staining and measuring absorption at 575 nm.

As shown in Fig. 3.5.12, the coated surfaces were less susceptible to *P. aeruginosa* biofilm formation. The most pronounced effect was observed with the PS filament. The biofilm was decreased by approximately 75%. However, coated PETG and PLA were also able to achieve approximately 70-75% reduction in biofilm formation. PMMA had the weakest effect among the tested materials, with a reduction of about 50%. Nevertheless, biofilm could still be minimized by approximately 50%. Thus, it could be shown that an application of cerium oxide nanoparticles on different plastic polymers could inhibit *P. aeruginosa* biofilm formation.

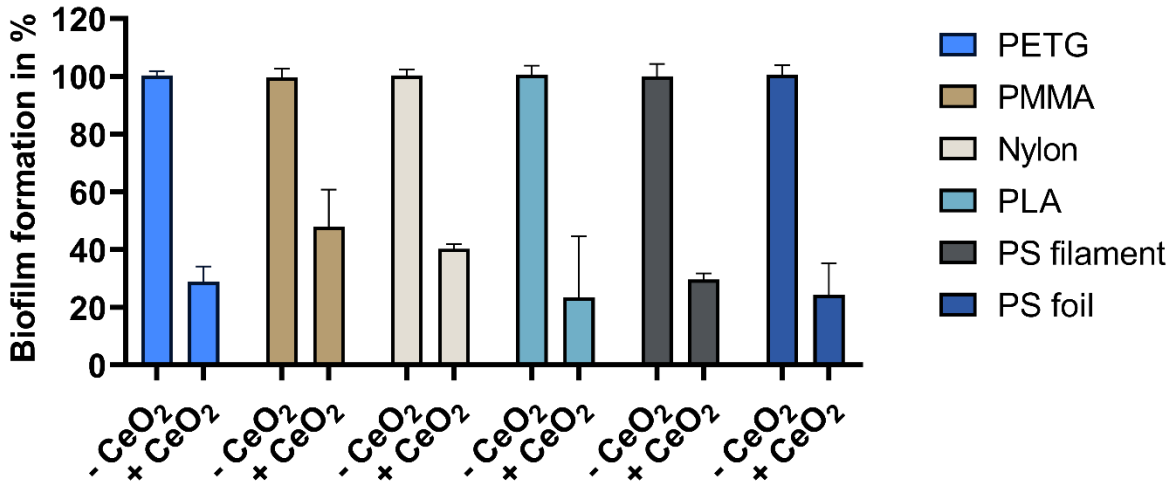

Fig. 3.5.12 Influence of various cerium oxide-covered polymers on the biofilm development of *P. aeruginosa*. The bacteria were cultured together with CeO_2-FPEG-coated and uncoated plastic materials for 72 h at 30 °C in LB medium supplemented with KBr and H_2O_2. Subsequently, the planktonic cells were washed off the materials and the attached bacteria were stained with crystal violet. The biofilm analysis was performed at 575 nm. The standard deviation of three biologically independently performed experiments is represented by the error bars. Modified from (Pfitzner, 2021).

As the results with PETG were promising in terms of biofilm inhibition and the specific material has applications in different fields, the next step was to incorporate the CeO_2-FPEG nanoparticles into PETG filaments, which could be used for 3D printing. This was intended to increase the flexibility of the potential applications (Behrens et al., 2020, p. 3; Kováčová et al., 2020; O'Grady et al., 2021; Tümer and Erbil, 2021; T. Zhang et al., 2014). One might assume that cost efficiency could probably be improved enormously by the fact that products could be manufactured directly from CeO_2-coated material and did not have to be subsequently coated after production.

Small platelets were prepared for bacterial assays after the production of CeO_2-coated PETG filament. No coating of PETG served as a positive control. In addition, commercially available copper-coated material was used as a negative control due to the copper.

Following the addition of *P. aeruginosa* to the platelets, the discs were incubated in LB medium at 30 °C for 72 h, supplemented with H_2O_2 and KBr to determine the biofilm formation. After the removal of the planktonic bacteria, the attached cells were stained with crystal violet. Analysis was then performed by measuring absorption at 575 nm. Pyocyanin production by *P. aeruginosa* was also investigated. Previously, it was

shown that the addition of CeO_2 decreases the AHL concentrations, therefore, these results should be confirmed with the coated surfaces. Briefly, the bacteria were incubated at 37 °C and the analysis was performed at 695 nm.

The effects of the coated materials on biofilm formation and pyocyanin production in *P. aeruginosa* are presented in Fig. 3.5.13. As shown graphically in Fig. 3.5.13A, a minimization of biofilm by approximately 62% occurred for the CeO_2-coated surface compared to the uncoated control. Approximately 86% reduction was achieved for the copper-coated variant. However, since copper has an antibiotic effect on bacteria, the negative control could be validated. Furthermore, pyocyanin production could also be influenced, as can be clearly observed in Fig. 3.5.13B. In the case of the CeO_2-coated materials, a reduction of 40% could be observed. For the copper variant, even a reduction of 80% could be noticed, however, this was due to the antibiotic effect of copper. The flexible use of CeO_2-coated PETG thus assured the production of a range of products for application in different industries.

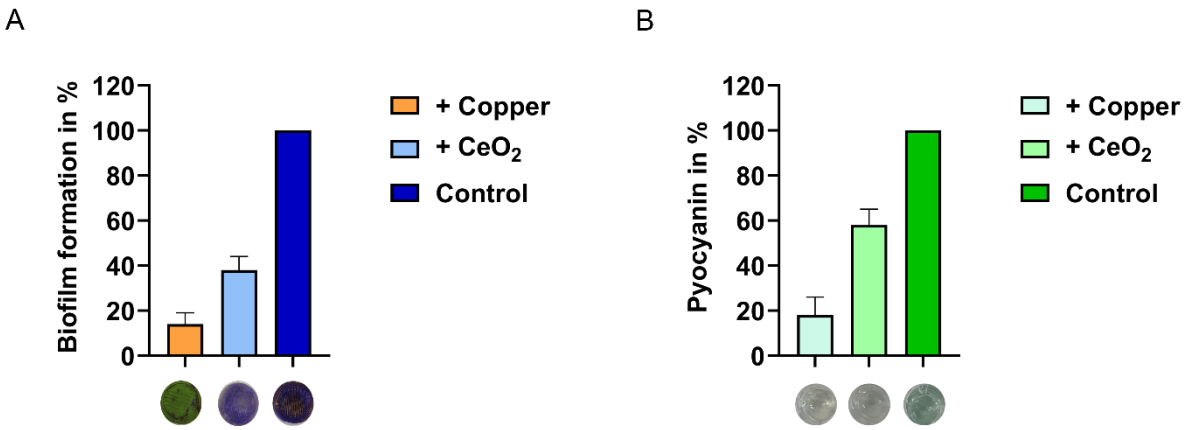

Fig. 3.5.13 Impact of CeO_2 and copper-coated 3D printed material on the biofilm formation and pyocyanin production of *P. aeruginosa*. The cerium oxide was incorporated into PETG and produced as filament for 3D printing. In addition, commercial copper coated PLA material was used as a negative control. No coating served as a positive control. The bacteria were cultured for 72 h at 30 °C in LB medium along with the 3D printing materials to determine biofilm formation. This was followed by analysis of the biofilm using crystal violet. For the determination of pyocyanin production, the cultivation was performed at 37 °C for 72 h in LB medium. The culture fluid was then removed and measured at 695 nm after centrifugation. The standard deviation of three biologically independently performed experiments is represented by the error bars. Modified from (Pfitzner, 2021).

Since among the various types of polymers, PC also has a wide range of applications and is installed in many sectors that are affected by biofilm (Batté et al., 2003; Dhandapani et al., 2022; Park and Kim, 2017; Sharafimasooleh et al., 2016), the next task was to apply cerium oxide nanoparticles to this material to investigate its possible effect on biofilm. Specific CeO_2-NTA nanoparticles were used to accomplish this task. The cerium oxides in this case were synthesized using nitrilotriacetic acid (NTA) as a capping agent.

Following fabrication of the CeO_2-coated PC platelets, *P. aeruginosa* was added to the surfaces, supplemented with KBr and H_2O_2 and incubated for 72 h at 30 °C in LB medium. Uncoated slides were used as a control. To determine the biofilm, crystal violet was applied after removing the planktonic cells. The measurement was performed at 575 nm. Additionally, a potential impact on the QS system was also examined by measuring the pyocyanin formation in *P. aeruginosa*. Therefore, the cells were incubated on the surfaces for 72 h at 37 °C in LB medium. The culture fluid was then centrifuged and measured at 695 nm.

The results of the CeO_2-coated PC platelets are graphically summarized in Fig. 3.5.14. Biofilm was observed to be reduced by 75% on the coated platelets (Fig. 3.5.14A). The coated samples stained with crystal violet were barely covered by biofilm in contrast to the uncoated control. Regarding pyocyanin production, a decrease of approximately 45% was also detected. The culture fluid associated with the CeO_2-coated sample appeared significantly less colored green than the control.

To visually confirm the results obtained, CLSM images were taken of the bacteria on the surfaces. Following incubation, the planktonic cells were rinsed away, and the attached bacteria were stained with the fluorescent dyes SYTO9/propidium iodide. The biofilm thickness was then determined using CLSM.

As shown in Fig. 3.5.14C, the biofilm layer on the CeO_2-coated platelets was significantly reduced compared to the control. Although sporadic areas of biofilm were detected, the surface of the control was completely overgrown with a biofilm depth of approximately 50 µm. Hence, it could be concluded that PC was suitable to be covered with CeO_2 nanoparticles which showed a significant effect against bacterial biofilm.

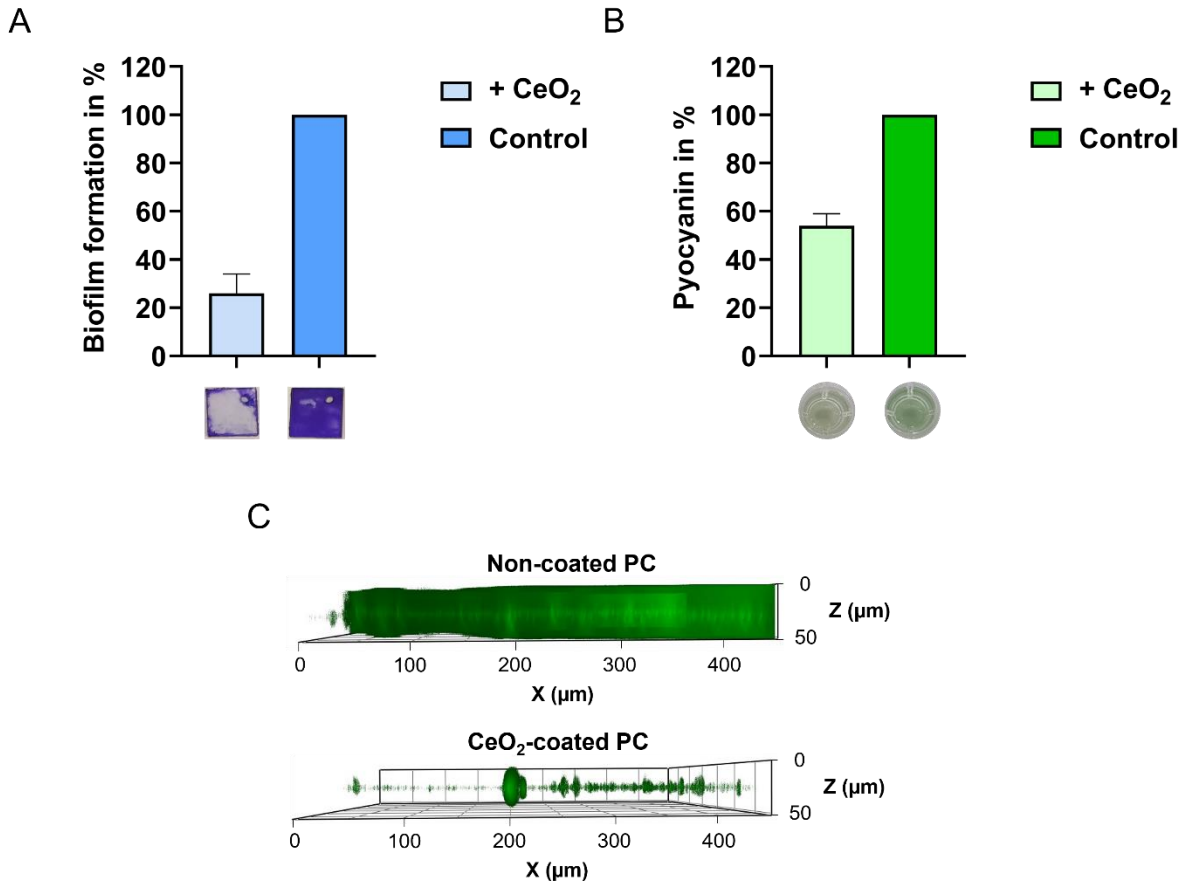

Fig. 3.5.14 Effect of CeO_2-NTA coated PC on biofilm formation and pyocyanin production by *P. aeruginosa*. The CeO_2-NTA nanoparticles were deposited on the PC substrate and the bacteria were then incubated on the surfaces for 72 h at 30 °C in LB medium, supplemented with KBr and H_2O_2. This was followed by analysis of the effect on the biofilm using crystal violet (A). To determine the impact on pyocyanin production, the bacteria were further incubated on the surfaces at 37 °C for 72 h in LB medium. Analysis was performed at 695 nm (B). The samples with the bacterial biofilm on the surfaces were analyzed by CLSM for visual confirmation (C). The standard deviation of three biologically independently performed experiments is represented by the error bars. Modified from (Jegel, 2022; Jegel et al., 2022).

As it was successfully demonstrated that PC coated with ceria nanoparticles could significantly inhibit biofilm formation in *P. aeruginosa*, the synthesis of CeO_2 nanoparticles was modified to such an extent that a higher throughput could be achieved at the same time, and thus more of the PC coatings could be produced faster (Sarif et al., 2022). CeO_2-OLA nanoparticles were utilized for this project. During the synthesis of these nanoparticles, oleylamine (OLA) was applied as a capping agent.

Additionally, a segmented flow method was adopted, which ensured a much faster and higher production of cerium oxides.

Once the cerium oxides were produced, one part was incorporated into the PC material without annealing, while the other part was first annealed at 185 °C and was then integrated into the coating.

To investigate whether the cerium oxides prepared by the segmented flow method were indeed effective and the PC coatings continued to demonstrate an effect on biofilm formation, the surfaces were cultured together with *P. aeruginosa* at 30 °C for 72 h in LB medium with the addition of H_2O_2 and KBr. Subsequently, the adherent cells were stained with SYTO9/propidium iodide and visual analysis was performed using CLSM.

The effect of CeO_2-OLA generated by the segmented flow method on the biofilm of *P. aeruginosa* can be seen in Fig. 3.5.15. Without coating (A), the biofilm was able to cover the entire surface, so no clear area could be detected. However, this looked different when using the coated surfaces. In the case of CeO_2 that were not annealed (B), the surface was colonized by the bacteria, but uninhabited spots on the surface were also detected. Surprisingly, a much stronger effect was observed with the CeO_2 which were heated at 185 °C before embedding (C). In these samples, the surface was largely uncolonized and the bacteria only attached themselves sporadically to the surface.

Confirmation of the obtained results by quantification was achieved by staining with crystal violet and subsequent measurement of absorption at 575 nm. As illustrated in Fig. 3.5.15D, the results reported previously by CLSM were validated. A reduction in biofilm of about 27% was observed for the coatings with CeO_2, which were not heated. The purple stained plate also showed a few uncolonized areas in contrast to the control. As previously in the CLSM, the CeO_2 which were baked at 185 °C beforehand achieved the strongest effect in terms of biofilm. The platelet was only slightly overgrown and in comparison, to the control, the biofilm was reduced by about 65%.

Furthermore, pyocyanin production was also evaluated to investigate whether the QS system was affected by these coatings. Fig. 3.5.15E depicts the results of these trials. Both coatings were able to minimize pyocyanin production compared to the control. The CeO_2 heated at 185 °C achieved the highest reduction of about 43%. This

demonstrated that ceria nanoparticles produced in a segmented flow method could be used to control bacterial biofilm formation in coatings.

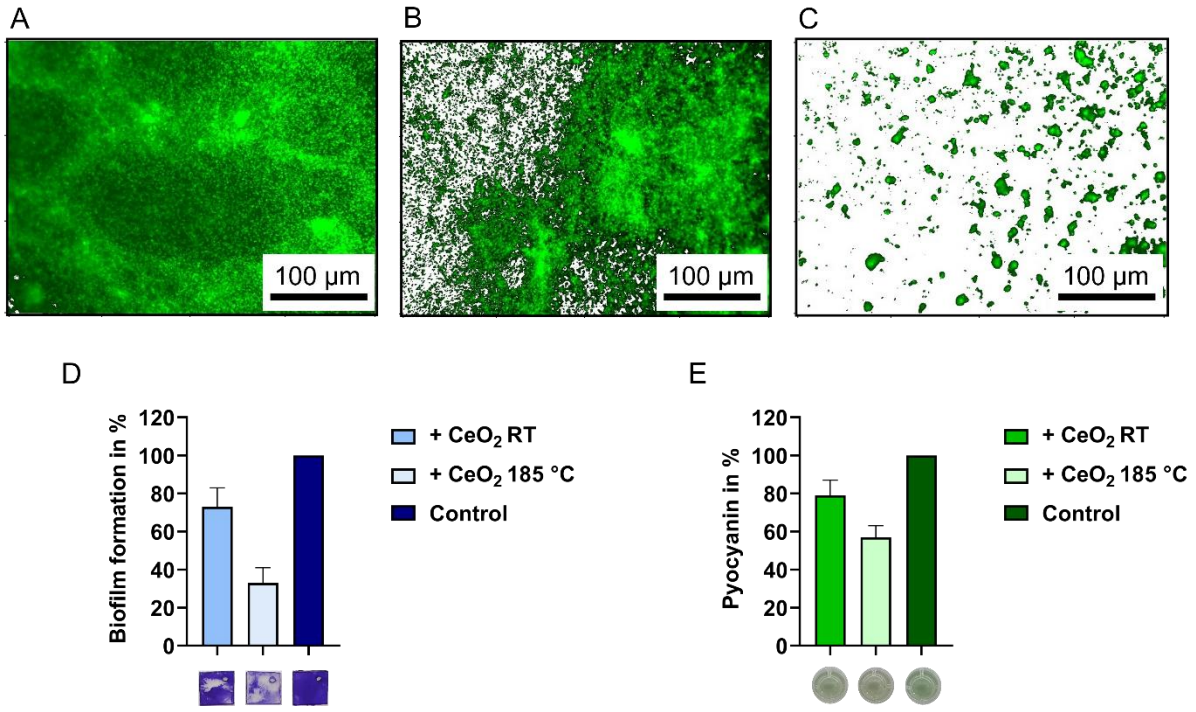

Fig. 3.5.15 Impact of CeO_2-OLA coated PC plates on biofilm formation and pyocyanin production of *P. aeruginosa*. Bacteria were cultured on the different surfaces for 72 h at 30 °C in LB medium supplemented with KBr and H_2O_2 for biofilm formation. Subsequently, for CLSM analysis, staining of adherent cells was performed on the uncoated (A), CeO_2 without annealing (B), and CeO_2 annealed at 185 °C (C) coated variant with SYTO9/propidium iodide after removal of planktonic cells. To quantify the biofilm, the bacteria on the different surfaces were stained with crystal violet (D). The measurement was made at 575 nm. To determine the effect on pyocyanin generation (E), the bacteria on the surfaces were cultured at 37 °C for 72 h in LB medium supplemented with KBr and H_2O_2. The culture fluid was then measured at 695 nm after centrifugation. The standard deviation of three biologically independently performed experiments is represented by the error bars. Modified from (Sarif, 2021; Sarif et al., 2022).

Based on the results of coatings on membranes and plastics, showing a strong inhibition of biofilm formation, it was further investigated to what degree steel could be coated with CeO_2 nanoparticles. Steel is applied in various industrial applications as well as forming an integral part of many structural elements, particularly in the marine sector, and is therefore susceptible to biofilm and biofouling (de Messano et al., 2009;

Moynihan and Allwood, 2014; Tuck et al., 2022). As the coating of steel often requires a varnish, a special polyurethane lacquer should be used (Wang et al., 2021). Cerium oxide nanoparticles EP151 were applied in this case, which should be embedded in the varnish. Painted steel plates without embedded nanoparticles were used as a control.

Considering that *P. aeruginosa* was used for the previously coated surfaces and, moreover, the cerium oxides showed a clear effect on its biofilm formation, *P. aeruginosa* was applied to the steel platelets. In addition, KBr and H_2O_2 were added. The bacteria were cultured on the surfaces at 30 °C for 72 h in LB medium. Then, the planktonic cells were washed off and the remaining bacteria on the surfaces were stained with SYTO9/propidium iodide. This was followed by analysis using CLSM.

The results of the microscopy can be seen in Fig. 3.5.16. The surface without embedded CeO_2 (A) was completely colonized by the biofilm. The biofilm thickness was measured at approximately 60 µm. In contrast, bacteria could only partially colonize the CeO_2-coated surface (B). Although spots were detected which were colonized by bacteria, uncolonized spots predominated.

With steel being used very frequently in the marine sector (Procópio, 2019), the CeO_2 coating also had to be examined for biofilm formation by marine bacteria. Therefore, the primary colonizer, *P. gallaeciensis* (de Carvalho, 2018; Gram et al., 2015), was chosen. The bacteria were added to the surfaces and incubated in 2216 medium together with KBr and H_2O_2 for 72 h at 30 °C. Subsequently, the attached bacteria were stained using crystal violet. Quantification was performed at 575 nm.

As shown clearly in Fig. 3.5.16C, the CeO_2 coated steel surface was able to reduce the biofilm by up to 80%. The purple platelets displayed many uncolonized areas on the surface compared to the control without CeO_2. The entire surface was overgrown in the control. Cerium oxide nanoparticles therefore demonstrated the biofilm inhibitory function even when embedded in a lacquer.

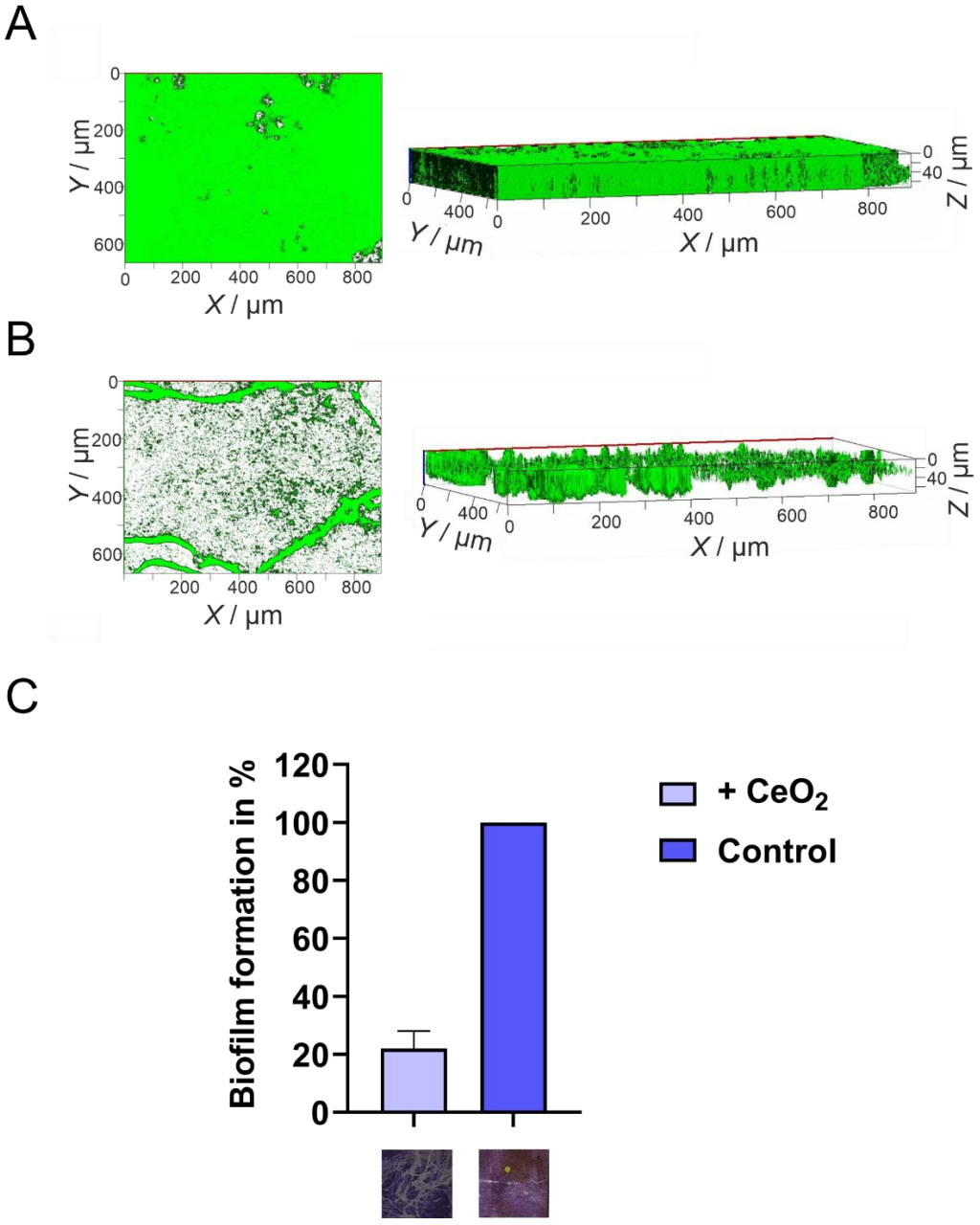

Fig 3.5.16 Effect of CeO_2 coated steel platelets on biofilm formation of *P. aeruginosa* and *P. gallaeciensis*. *P. aeruginosa* was incubated on the coated and non-coated steel plates at 30 °C for 72 h in LB medium together with KBr and H_2O_2. Then, the adherent cells on the uncoated control (A) and CeO_2-coated platelets (B) were stained with SYTO9/propidium iodide and analyzed using CLSM. *P. gallaeciensis* was cultured on the steel platelets for 72 h at 30 °C in 2216 medium together with KBr and H_2O_2. After removal of planktonic cells, the biofilm was stained with crystal violet (C). Quantification was performed at 575 nm. Error bars symbolize standard deviation of three biologically independently performed experiments. Modified from (Pütz, 2022; Pütz et al., 2022).

Overall, the results in this chapter indicate that nanoparticles can be used as alternative strategy to combat bacterial biofilms. Tungsten oxides were found to inhibit biofilm formation in *P. aeruginosa*. Furthermore, using the reporter strain *A. tumefaciens* A136, it was discovered that the tungsten oxides WO_{3-x} and c-$Cs_{0.6}WO_3$ affect the 3-oxo-C_{12}-AHL, resulting in the biosensor detecting less AHL. Additionally, infrared irradiation of the tungsten oxides was observed to significantly enhance antibiotic activity. Planktonic cells of *P. aeruginosa* and *S. aureus* were reduced by up to 30%. This feature opens opportunities in various fields of applied technology.

Furthermore, cerium oxide nanoparticles were identified that reduced the biofilm formation of Gram-negative bacteria. Moreover, it was discovered that AHL molecules were brominated due to the haloperoxidase-like function of cerium oxides. In the case of *P. aeruginosa*, bromination of HQNO was demonstrated, which had a significant effect on biofilm formation. A putative novel mechanism was thereby identified.

Further, different CeO_2 nanoparticles were applied to different surfaces. It was demonstrated that several coated materials were applicable for biofilm control. Moreover, the efficacy of CeO_2/PETG filament enabled the manufacturing process for various products to be accelerated, as subsequent coating might no longer to be required. Additionally, using a segmented flow method, the production of biofilm inhibiting CeO_2 and thus coated PC could be significantly enhanced. The embedding of cerium oxide nanoparticles in PUR lacquer and the effective reduction of biofilm launches many promising future applications, among others possibly in the marine sector.

4 Discussion

The growing number of resistant bacteria is a matter of great concern and demands urgent action. Bacterial biofilms not only affect the environment and human health but also inflict heavy financial losses on the industries (Cámara et al., 2022; Chambers and DeLeo, 2009; de Carvalho, 2018; Flemming, 2020; Muhammad et al., 2020; Rossiter et al., 2017). In this thesis, a significant contribution towards the analysis and battle of bacterial biofilms has been made. By developing the *Panta Rhei* microfluidic system, a platform was established to analyze biofilms both microscopically and macroscopically. Furthermore, external conditions affecting the formation of biofilms in marine and drinking water bacteria could be revealed. Regarding alternatives to antibiotics, secondary metabolites from entomopathogenic bacteria *Photorhabdus* and *Xenorhabdus* could be identified as promising compounds inhibiting biofilm formation. Moreover, bacteria from marine and drinking water environments capable of either inhibiting bacterial biofilm or contributing to its dispersal could eventually be identified. Lastly, tungsten oxide and ceroxides nanoparticles as alternatives for biofilm suppression were discovered.

4.1 A green all-in-one device for biofilm analysis in the future?

An initial objective of this work was to design and construct a microfluidic solution for the analysis of bacterial biofilms. Microfluidics is a field that has been increasingly used in microbiology over recent time (Pérez-Rodríguez et al., 2022). Between 2007 and 2016, the number of publications containing microfluidic research regarding biofilm formation increased at a rapid pace (Pousti et al., 2019). Previously performed experiments using conventional approaches can be reproduced with microfluidics, leading to an increased reliance on this technique (Pérez-Rodríguez et al., 2022). It was demonstrated that chemotaxis studies in *E. coli* carried out with a capillary (Adler, 1973) could be reproduced utilizing a microfluidic flow cell (Roggo et al., 2018). While with the traditional approach, an ideal aspartate concentration of 10 mM could be determined (Adler, 1973), it was possible to detect effects even at lower concentrations between 0.1 mM and 1 mM by applying microfluidics (Roggo et al., 2018). Besides chemotaxis, the microfluidic method supports the examination on other stimuli such as

thermotaxis, magnetotaxis or rheotaxis and also bacterial biofilm formation (Pérez-Rodríguez et al., 2022). Moreover, compared to traditional tools such as cultivation in well plates or flasks (Halldorsson et al., 2015), it seems that more realistic conditions might be simulated with microfluidics (Pérez-Rodríguez et al., 2022). Previous studies have shown that *Pantoea* spec. cultivated on a surface with various pores and under a constant flow of a rainwater simulation exhibited growth alongside the availability of nutrients in the continuous flow (Aufrecht et al., 2019). In contrast, cultivating *Pantoea* spec. on an agar plate displayed distribution homogeneity without preferential movement of growth (Bible et al., 2016). Additionally, the microfluidic approach provides a solution for the cultivation of bacteria that are challenging to be cultured, such as oligotrophic organisms (Overmann et al., 2017), by application of a high-throughput microfluidic cultivation platform (Grünberger et al., 2015).

Multiple variants of microfluidic flow cells have been reported (Pérez-Rodríguez et al., 2022), featuring, for example, linear (Jeong et al., 2014) and mixed channels (Englert et al., 2009; Kim et al., 2012), consisting of multiple layers (Demir and Salman, 2012; Salman et al., 2006), or even equipped with pores (Aufrecht et al., 2019). Such microfluidic solutions typically operate with volumes in the microliter range (Pérez-Rodríguez et al., 2022). Furthermore, microscopic, electrochemical, and spectroscopic methods appear frequently for the analysis of biofilms in microfluidic systems (Pousti et al., 2019). Conversely, the *Panta Rhei* flow cells, designed in this work, are adaptable and suitable for operation in the microliter as well as up to 5 ml range, providing ultimate flexibility. Additionally, microscopic analysis by light microscope, fluorescence microscope, or CLSM, as well as macroscopic analysis of external samples inside the *Panta Rhei* flow cells, are supported (Fig. 4.1).

As mentioned in the literature, most microfluidic flow cells are constructed from polydimethylsiloxane (PDMS) (Friend and Yeo, 2010; Pérez-Rodríguez et al., 2022). This material has the advantage of being transparent and permeable to gases, biocompatible, and cost effective (Weibel et al., 2007; Niculescu et al., 2021; Pérez-Rodríguez et al., 2022). Nevertheless, PDMS also entails disadvantages (Mukhopadhyay, 2007; Ren et al., 2013), such as the absorption of molecules, since it is a porous material (Wang et al., 2018; Niculescu et al., 2021). Therefore, organic solvents are not suitable, as they are absorbed by the material (Ren et al., 2013). Furthermore, evaporation of water may occur, altering the concentration of aqueous

solutions inside (Shim et al., 2007; Niculescu et al., 2021). Due to the character of PDMS, any small hydrophobic compound would permeate into the material, distorting potential new drug screening results (Wang et al., 2018). Therefore, the materials PE or PP were selected for the *Panta Rhei* flow cells. These materials belong to the category of thermoplastics (Graziano et al., 2019). Previous reports have already shown that thermoplastics find use in microfluidics (Ren et al., 2013; Sackmann et al., 2014; Pérez-Rodríguez et al., 2022). The big advantage, however, lies in the fact that thermoplastics can be recycled to a certain extent. Shredding machines can be used to grind the materials, which can then be remelted and further extruded (Grigore, 2017; Kazemi et al., 2021). It is therefore conceivable that after several cycles of use, the *Panta Rhei* flow cells could be shredded and then remelted to produce new flow cells made from the used ones by injection molding. This would provide a sustainable green alternative to the world's current plastic consumption.

However, due to the complexity of the application of microfluidic techniques and the lack of sufficient expertise in most cases, utilization of the microfluidic approach is quite restricted (Azeredo et al., 2017). Consequently, it is essential that future work is required to create a device for microfluidics that combines all the necessary components within one tool, thus alleviating the complexity of the method. In reviewing the literature, it was found that all-in-one solutions have already been developed that include microfluidic components for the diagnosis of pathogens in one device using a CF-PCR chip (Li et al., 2019). Furthermore, the development of an all-in-one automated microfluidic control system, capable of running autonomously while requiring external control by a computer, has already been realized (Watson and Senyo, 2019). Moreover, an all-in-one system controlled by an external smartphone has been developed (Li et al., 2014). Besides, a standalone device with a 3D printed microfluidic chip based on low cost could be showcased (Zhang et al., 2021).

In the wake of automatization and digitalization, keeping up and advancing the technology of microfluidics is a necessity. Eventually, in the future, a *Panta Rhei* device containing all the *Panta Rhei* characteristics in one unit could be invented. This remains a topic of further investigation.

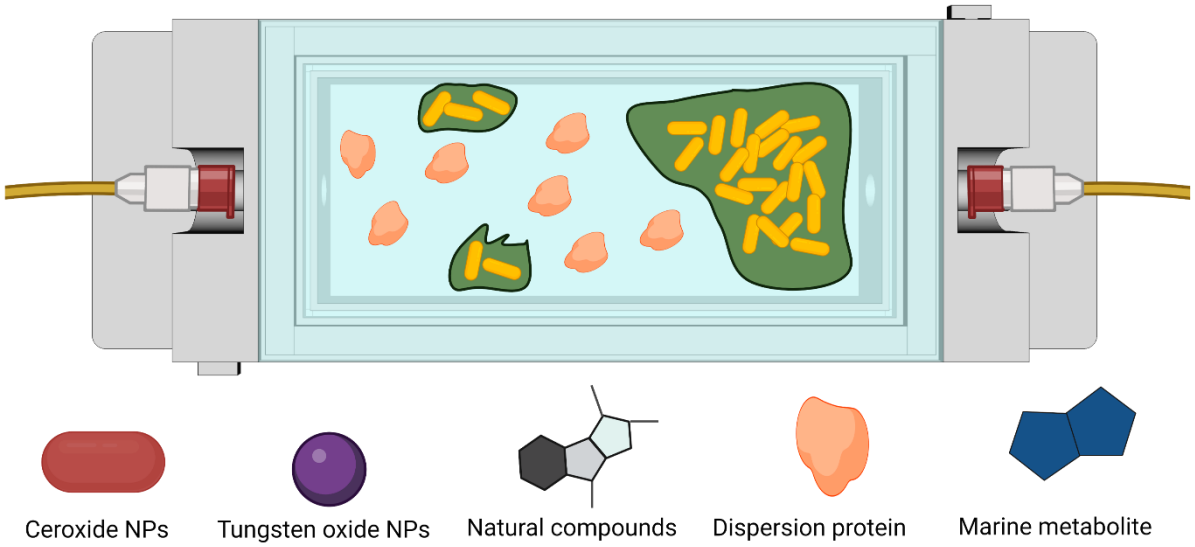

Fig. 4.1 The *Panta Rhei* D2 flow cell with potential applications in future studies. Depicted is the *Panta Rhei* D2 cell, which contains a biofilm that has been cultivated and undergoes an exemplary solution containing enzymes (dispersion protein) that dissolve the matrix of the biofilm. Alternatively, the use of natural products from entomopathogenic bacteria of the genus *Photorhabdus* and *Xenorhabdus* is conceivable, as well as metabolites isolated from marine bacteria. The *Panta Rhei* system can also be used to analyze the effect of nanoparticles on biofilms. In addition, microscopic as well as macroscopic analyses are possible. Created with BioRender.com

4.2 External factors affecting biofilm formation in marine and drinking water bacteria

4.2.1 Glucose, peptides and the salt variety affect biofilm formation

Furthermore, this work set out with the aim to identify external factors that affect biofilm formation in bacteria from the marine and drinking water sectors. Prior studies have noted the importance of environmental factors in biofilm formation, such as the composition of the media (Y. Liu et al., 2020). In the field of drinking water bacteria, *S. adhaesiva* developed the strongest biofilm in the HD medium. Beyond that, a high degree of biofilm formation was also achieved in the TSY and M1 media. The cultivation medium HD is notable for its glucose content. It is therefore conceivable that glucose has an influence on biofilm formation. This finding is consistent with previously reported research in *S. aureus* and *S. epidermidis*, where glucose was shown to increase biofilm formation due to the *agr* pathway (Waldrop et al., 2014). This result is also in accordance with a previously reported study in *E. faecalis*, as glucose was

shown to have a biofilm-enhancing effect (Seneviratne et al., 2013). A remarkable element in the composition of the media TSY and M1 is the amount of peptones. An assumption might therefore suggest that peptones could play a role in the formation of biofilms. Increased biofilm formation by tryptone was indeed observed in *Pseudomonas putida* (Puhm et al., 2022), supporting the results of this work. It was proposed that *P. putida* utilizes the peptides to strengthen the biofilm structure (Puhm et al., 2022). TSY medium also resulted in the most severe biofilm development in *M. mesophilicum*. *Sphingomonas* spec. can be located on membranes serving for clean drinking water supply production (de Vries et al., 2019). Based on the biofilm formation on the surface of the membranes, it leads to biofouling (Flemming et al., 1997). It seems possible that sugars, such as glucose and other nutrients found in wastewater (Scherhag and Ackermann, 2021; Shahid et al., 2021) enhance bacterial biofilms on cleaning membranes, contributing to and accelerating biofouling.

In the case of *B. nasdae*, biofilm formed second strongest when cultivated with TSY. The most pronounced biofilm was obtained when culturing in RS medium. This medium is supplemented with trace elements. Therefore, the assumption could be made that these trace elements might contribute towards high biofilm levels. Prior research has demonstrated that Zn^{2+} (Geoghegan et al., 2010), a trace element (Suryawati, 2018), intensifies the biofilm formation of *S. aureus*. This is due to the surface protein SasG in *S. aureus*, a protein involved in the biofilm assembly phase. During this step, Zn^{2+} is a required component (Geoghegan et al., 2010). Consequently, it is probable that a comparable procedure triggering the formation of biofilms also occurs in drinking water bacteria since trace elements can be found in drinking water (Thygesen et al., 2021).

On the question of the influence of nutrient composition on biofilm formation in marine bacteria, it was found that the biofilm of *P. gallaeciensis* and that of *H. aquamarina* appeared most abundant upon cultivation in medium 2216. High salinity with a wide range of salts can be found in this medium, along with elevated nutrient content. A strong relationship between salts and nutrients in promoting biofilm formation has been reported in the marine bacterium *Vibrio fischeri* (Marsden et al., 2017). Surprisingly, the medium MM, also containing high levels of nutrients and NaCl, caused less biofilm accumulation in *P. gallaeciensis* and *H. aquamarina*. However, in this cultivation medium, the range of salts was restricted to NaCl. A possible explanation for this might be the missing variety of different salts. Prior research in *Vibrio vulnificus* has demonstrated that biofilm formation is mediated by calcium. CabA, a protein located in

the biofilm matrix, is capable of binding calcium resulting in a conformational change and initiating a much more solid biofilm structure (Park et al., 2015). Therefore, the possibility that different salts impact biofilm formation in *P. gallaeciensis* and *H. aquamarina* suggests a reasonable assumption. *H. alkalilenta* formed a dense biofilm in all media used. Despite this, a slightly weaker biofilm was detected in the low-nutrient medium M9. Although it was shown in a previous study with *L. monocytogenes* that the concentration of nutrients had an impact on biofilm structure (Cherifi et al., 2017), a differentiation of salts as can be found in the M9 medium could conceivably boost biofilm production under these conditions. A note of caution is due here since no conclusion could be drawn about the distribution of live and dead bacteria in the biofilm. A more accurate method to unambiguously identify the living and dead bacteria would be a specific fluorescent staining method, as already presented in a previous report (Kadam et al., 2013).

4.2.2 Nutrient limitation as inducer for biofilm dispersion

One further question regarding the impact of external factors on biofilm formation was the effect of incubation time. Regarding the drinking water bacteria, *S. adhaesiva* and *M. mesophilicum* developed the most intense biofilm after 120 h, while in *M. mesophilicum*, the biofilm grew continuously over the course of the experiment. These findings corroborate previous observations, as it was demonstrated that *Methylobacterium* spec. developed a continuously growing biofilm during the experiment length of 72 h (Simões et al., 2010). A similar observation was obtained in the marine setting, as *H. aquamarina* appeared to reach the highest level of biofilm after 120 h, increasing gradually by day. In *H. alkalilenta*, a very strong biofilm was achieved already after 48 h. Prior research has demonstrated that the build-up of a microbial biofilm may take as long as 10 days to acquire a completed structure, varying by bacterial species (Guzmán-Soto et al., 2021). Significant findings to emerge from this analysis are the dynamics of the biofilms of *B. nasdae* and *P. gallaeciensis*. While the biofilm of *B. nasdae* increased for up to 48 h, a decrease in the amount of biofilm could be noticed after 72 h. The biofilm of *P. gallaeciensis* reached maturity after 24 h and declined steadily afterwards during the length of the experiment. There are several possible explanations for these results. As it is already mentioned in the literature, a biofilm experiences a partial decrease after a certain period of time, caused either by

detachment or dispersion (Guzmán-Soto et al., 2021). However, since these experiments were performed under static conditions, it is highly unlikely that the biofilm was detached by mechanical action or shear forces, as is usually the case with detachment by abrasion, erosion, or sloughing (Petrova and Sauer, 2016). Furthermore, the possibility of grazing can be ruled out since no external additives were applied to the biofilm. This would require, for example, protozoa to be introduced to the microbial biofilm to allow bacterial consumption (Seiler et al., 2017; Guzmán-Soto et al., 2021). The observed decline of the biofilms could most plausibly be attributed to the dispersion. Dispersion can be triggered by environmental factors or specific signals (Rumbaugh and Sauer, 2020). However, dispersion due to nutrient shortage could also be considered, as previously reported for *P. aeruginosa* (Nair et al., 2021). Alternatively, it is quite reasonable to assume that the existing biofilm is not actually dispersed, but rather new biofilm is prevented from accumulating. Such an effect could be achieved, for instance, by suitable suppressors of the QS system (Paluch et al., 2020). Another conceivable possibility would be the production of matrix-degrading enzymes (Kaplan, 2014; Saggu et al., 2019; Torelli et al., 2017). In addition, it would also be possible that, for example, fatty acids are produced, which might serve as a signal for biofilm dispersion (Davies and Marques, 2009; Rumbaugh and Sauer, 2020).

4.2.3 The Fe^{2+} and Mn^{2+} in steel promote biofilm formation of marine bacteria

The third question regarding the influence of external factors on biofilms in marine and drinking water sectors sought to determine the impact of different surfaces. It could be obtained that the biofilm formation of *M. mesophilicum* on steel was fewer in comparison to PS. These results are in accord with recent studies, as it could be shown to be significantly fewer cells attached to steel than to PVC in *Methylobacterium* spec. such as *M. hispanicum* and *M. extorquens* (Szwetkowski and Falkinham, 2020). Besides, it could be shown that *Methylobacterium* spec. are able to develop an intense biofilm on PS (Simões et al., 2010). Both PVC and PS belong to the class of vinyl polymers (Behr et al., 2016). Unfortunately, since these materials are incorporated in several aspects of drinking water systems (Orlov et al., 2016; Schöntag and Sens, 2015; Xu et al., 2019), addressing biofilm suppression has proven to be a difficult task. Therefore, future research is required to evaluate alternatives. Swapping the polymers

for steel elements could be a promising first step. The results regarding the different polymeric surfaces and the effect on the biofilm of the marine bacterium *P. gallaeciensis* indicate among the tested plastics, the strongest biofilm formation with PS. These results seem to be in agreement with prior findings, reporting the biofilm formation of marine bacteria on PS (Michels et al., 2018). However, it is somewhat surprising that steel exceeded biofilm formation on PS by approximately 280%. As mentioned in the literature, iron-oxidizing and iron-reducing bacteria occur on metals in the marine environment since steel is a source of iron. Furthermore, unlike polymer-based surfaces, an iron oxide layer is generated quite fast on steel surfaces, which might impact biofilm formation (Tuck et al., 2022). The results of the external addition of metal cations to *P. gallaeciensis* provided greater insights. Apart from Fe^{2+}, Mn^{2+} was also able to enhance the formation of the biofilm. Contrary to this, biofilm production was diminished after the addition of Cu^{2+}. It was previously found that copper as an alloying component can negatively impact the attachment of *Desulfovibrio vulgaris* (Tran et al., 2021; Tuck et al., 2022). Nevertheless, it has been demonstrated that Cu^{2+} has an adverse effect on the growth of *Desulfovibrio desulfuricans* (Sani et al., 2001). Consequently, it is highly likely that this might also be the case for *P. gallaeciensis*. Referring to iron, it was demonstrated an ability of the extracellular matrix in binding the Fe^{2+} (Beech and Cheung, 1995). In addition, EPS of *Pseudomonas fluorescens* and *D. desulfuricans* were reported to have a major contribution to the initial adherence to unalloyed steel (Javed et al., 2015). Furthermore, it could be shown that lipopolysaccharides located on the outer membrane of *Desulfovibrio* are capable of specifically binding Fe^{2+} (Bradley and Gaylarde, 1988; Javed et al., 2015). Besides, *P. inhibens* is known to contain siderophores (Srinivas et al., 2022). Considering that *Phaeobacter* belongs to the *Roseobacter* group (Sonnenschein et al., 2021) and that *Roseobacter* are already known to be primary colonizers of marine surfaces and have proteins located on the outer membrane that are essential for biofilm formation (Ma et al., 2020), it would be reasonable to assume that the Fe^{2+} specific mode of action in *Phaeobacter* is possible related to the EPS and molecules on the outer membrane (Fig. 4.2). Moreover, *Phaeobacter* would be able to seize Fe^{2+} from the steel surfaces due to siderophore production. A further study with more focus on the mechanism of Fe^{2+} in *P. gallaeciensis* is therefore suggested. Very little was found in the literature regarding a biofilm enhancing effect of Mn^{2+} in Gram-negative bacteria. Regardless, prior research

revealed a biofilm-promoting impact of Mn^{2+} in the Gram-positive bacterium *B. subtilis*. Furthermore, it was observed that in the absence of Mn^{2+}, genes encoding for biofilm formation and sporulation were downregulated. Moreover, the production of surfactin was also reduced (Mhatre et al., 2016). The synthesis of surfactin and the generation of the biofilm matrix in *B. subtilis* are indirectly regulated by the QS system (Kalamara et al., 2018). Although the QS systems in Gram-positive and Gram-negative bacteria differ (Haque et al., 2019), there is still a possibility that manganese might be involved in QS in *P. gallaeciensis* (Fig. 4.2) since biofilm formation in *P. inhibens* is regulated by QS (Beyersmann et al., 2017; Srinivas et al., 2022). There are still unanswered questions regarding the Mn^{2+} mechanism in *P. gallaeciensis*, and therefore this topic requires future work to develop a full picture.

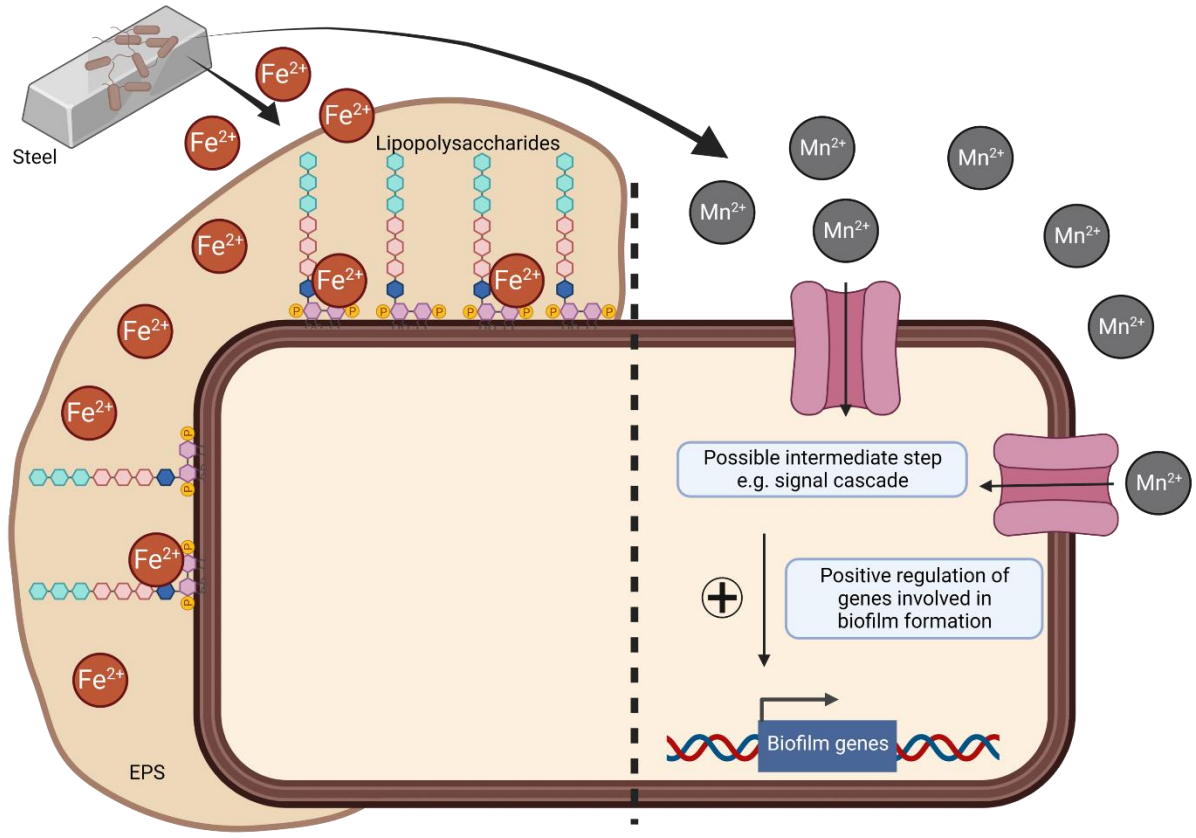

Fig. 4.2 Possible modes of action of Fe^{2+} and Mn^{2+} on biofilm formation in *P. gallaeciensis*. The Fe^{2+} struck out of the steel by the bacteria possibly binds to the lipopolysaccharides or EPS of *P. gallaeciensis*, thereby strengthening the structure perchance on the left. In addition, the Mn^{2+} chipped out of the steel may correlate with the QS of *P. gallaeciensis*, thus potentially regulating directly or indirectly biofilm-related genes on the right. Created with BioRender.com.

4.2.4 Synergism and antagonism in multi-species biofilms

Bacterial biofilms frequently appear in nature composed of multiple species (Elias and Banin, 2012). With respect to the question of whether a biofilm in the drinking water sector as well as in the marine environment turns out to be stronger when consisting of several bacterial species rather than of a single species, it could be shown that in both, the drinking water sector as well as in the marine field, the biofilm formed by multiple species produced higher levels than the biofilm from the respective single species. The biofilm consisting of a consortium of *S. adhaesiva*, *B. nasdae*, and *M. mesophilicum* achieved the strongest level compared to the biofilms composed of the individual species when exposed to the same conditions. Similar outcomes resulted among the marine bacteria *P. gallaeciensis*, *H. alkalilenta*, and *H. aquamarina*. The findings in this work regarding the drinking water consortium and, in particular, *M. mesophilicum* differ from previous research, demonstrating no higher biofilm formation in a dual-species biofilm of *Methylobacterium* spec., and *Mycobacterium mucogenicum* or *Methylobacterium* spec. and *Acinetobacter calcoaceticus* than the single-species counterparts, respectively (Simões et al., 2007). However, there seem to be some similarities with the results of another study demonstrating that a dual-species biofilm consisting of *Methylobacterium* species developed significantly stronger structures than a biofilm composed of only one *Methylobacterium* species (Xu et al., 2014). Furthermore, it has been shown in earlier investigations that *Methylobacterium*, together with *Sphingomonas*, could be encountered in a biofilm (Kelley et al., 2004; Xu et al., 2014). The discrepancy with the prior investigation could be explained by the fact that three different bacterial species were used in this work as opposed to two in the prior study (Simões et al., 2007). In addition, it is most likely that different bacteria species in a consortium will not consistently result in a stronger biofilm. There is already known antagonism within a biofilm alongside synergistic effects (Elias and Banin, 2012). Regarding marine multi-species biofilms, a previous study showed that a biofilm consisting of four marine bacteria could achieve a greater settlement rate in the larva *Leptastrea purpurea* than monospecies equivalents (Petersen et al., 2021). Additionally, in terms of consortium properties, it was previously shown that multi-species biofilms could trigger significantly worse infections than biofilms consisting of one species (Rao et al., 2020). Moreover, *Ralstonia insidiosa* represents an example of a so-called bridging bacterium in biofilms involving several foodborne pathogenic bacteria such as, e.g., *L. monocytogenes*, since dual-species biofilms containing

different species were stronger as soon as *R. insidiosa* was involved (Liu et al., 2016). The results contained in this work regarding the effect of multi-species consortia raise intriguing questions concerning the purpose in drinking water and marine environments. Although a stronger biofilm formation in the consortium was found in this study, these findings have to be taken with caution, as competition is also likely to depend on the composition of a multi-species biofilm (Joshi et al., 2021).

4.2.5 Priority effects in dual biofilm of marine and drinking water bacteria?

Another significant aspect of multi-species biofilms is the initial colonization of the surface. Based on this question, dual-biofilm analyses were performed for marine and drinking water areas to determine whether an effect occurred depending on which bacterium within the dual-biofilm first colonized the surface. As a point of observation, it could be shown that it makes an actual difference which bacterium can colonize the surface first. In dual-biofilm simulations of the marine sector and drinking water, variations of up to 30% and 45%, respectively, could be achieved. While exploring the scientific literature, a theory from the field of ecology suggested that the development of a community is often affected by the succession of organisms that have joined the ecosystem. These effects are then referred to as priority effects (Fukami, 2015; Sprockett et al., 2018). A previous study investigated how a multi-species biofilm consisting of 4 species differs when one species colonizes the surface first, and the other organisms are subsequently added. It was demonstrated that no significant influence was evident, and the respective biofilm composition did not differ despite the earlier colonization with the varying primary colonizer (Olsen et al., 2019). Nevertheless, it could also be observed from a study with the bacteria *S. aureus* and *Citrobacter freundii* and the fungus *Candida albicans* that a priority effect can be observed, depending on which organism from the consortium colonizes the surface first. In addition to the species composition, the growth interactions could also be influenced (Cheong et al., 2021). It is fundamental to consider that the observed priority effects in this work also might be related to the surface properties, which is why further investigations should be carried out in future experiments with the aim of obtaining a more definite statement. Despite this, initial findings could be gathered in this work, indicating that in biofilm formation, the primary colonizer has a prominent role to play

in terms of subsequent biofilm accumulation (Fig. 4.3), and hence, ideas for combating biofilm should considerate prevention of the primary colonizer.

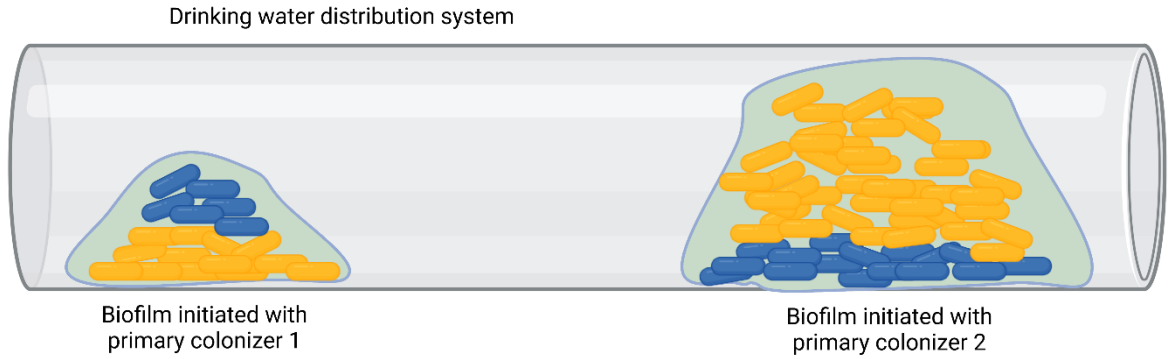

Fig. 4.3 A conceivable scheme of the influence of the primary colonizer on overall biofilm formation. Using a drinking water pipe as an example for this scheme, priority effects might eventually play a role in biofilm formation. Depending on which primary colonizer adheres to the surface first, this may later affect the development of the overall biofilm. Consequently, the biofilm formed with primary colonizer 2 on the right might possibly achieve a thicker biofilm than if primary colonizer 1 on the left first adhered to the surface. Created with BioRender.com.

4.3 Marine bacterial symbionts as QQ compound producers?

An intriguing observation in this work was that the marine bacterium *P. gallaeciensis* might produce a compound capable of not only inhibiting the own biofilm formation and that of *P. inhibens* but also that of human pathogen (Tuon et al., 2022) *P. aeruginosa*. Furthermore, first results could be obtained, indicating that the QS system seems somehow affected in *P. aeruginosa* due to the generation of less pyocyanin. Pyocyanin production is indirectly controlled by QS (Lee and Zhang, 2015), which leads to the assumption that the unknown compounds could be a QQ substance. Literature review revealed that it has already been demonstrated that marine bacteria from the Red Sea prevent the QS of *P. aeruginosa*. These bacteria belong to the families *Erythrobacter*, *Labrenzia*, and *Bacterioplanes*. In addition, lactonases and acylases were identified that could degrade 3-oxo-C_{12}-AHL, a signaling molecule used by *P. aeruginosa* for QS (J. Zhang et al., 2014). Acylases and lactonases were also identified by genomic analysis in *Deinococcus* spec., *Hyphomonas* spec. and *Ralstonia* spec. (Chandra

Kalia, 2011). Moreover, the lactonase RmmL from *Ruegeria mobilis*, a marine bacterium which, like *Phaeobacter* spec. belongs to the *Roseobacter* group, was identified (Cai et al., 2018; Sonnenschein et al., 2021). Lactonases and acylases inhibit QS by either hydrolyzing the lactone ring of AHLs or clipping the side chain, respectively (Sikdar and Elias, 2020; Zhang and Li, 2016). These are QS-inhibiting enzymes, which can be inactivated by heat or the addition of proteinase K (Torabi Delshad et al., 2018). The QQ features of *R. mobilis* could be prohibited by treatment with proteinase K and heat (Cai et al., 2018). Therefore, it can be assumed that the candidate compound produced by *P. gallaeciensis* is likely not a QQ enzyme. Additionally, it is known that pH fluctuations lead to degradations in polymers with labile acid or base links (Ofridam et al., 2021). Well-known acid labile bonds include, for example, the hydrazone, ketal, and acetal ester. These acid-labile compounds are often used to deliver anti-cancer therapeutics close to the target site (Dutta et al., 2016; Ofridam et al., 2021; Wei et al., 2013). Further, there are known polymers in the literature that alter their structure depending on the pH (Kocak et al., 2017). Since it was not observed in this thesis that pH variations affected anti-biofilm activity, it can be considered that the possible molecule is unlikely a polymer with pH labile bonds. Following HPLC fractionation, a fraction was detected that inhibited the biofilm in *P. aeruginosa*, suggesting that the candidate molecule might be a secondary metabolite. Previously, it was demonstrated that the Gram-positive bacterium *S. aureus* produces compounds that affect the QS system of several Gram-negative bacteria and additionally could inhibit pyocyanin production in *P. aeruginosa* (Chu et al., 2013). Furthermore, a previous study revealed that the culture fluid of the marine bacterium *Vibrio alginolyticus*, living in symbiosis with the coral *Pocillopora damicornis*, could inhibit biofilm formation in *P. aeruginosa*. In addition, the activity of elastase and the production of rhamnolipids could be reduced (Song et al., 2018). These, together with pyocyanin, are virulence factors regulated by the QS system (Malgaonkar and Nair, 2019). The detailed analysis could show that the substance might be rhodamine isothiocyanate (Song et al., 2018). Since it is already known from prior studies that *P. gallaeciensis* lives in symbiosis with the microalga *Emiliania huxleyi*, it might be possible that a similar compound is the cause of the observed anti-biofilm activity and reduced pyocyanin formation in *P. aeruginosa* (Fig. 4.4). Despite these very promising findings in this work, there are still unanswered questions regarding the nature of the compound that need to be focused on in future studies.

The results regarding the biofilm-dispersing ability of the culture fluid of *B. nasdae* indicated that most likely an enzyme is involved, as both the heat and the use of proteinase K nullified the biofilm-dispersing effect. Proteases such as proteinase K act as catalysator of peptide bond hydrolysis and, therefore, can degrade proteins (Skowron et al., 2020). Moreover, denaturation occurs at higher temperatures in proteins that are not heat stable (Bischof and He, 2005). Although it is well-established that heat-stable proteins can be encountered in bacteria (H. Li et al., 2020), it is doubtful that the sought-after molecule is heat-stable and tolerant to treatment with protease. Potential enzymes that initiate biofilm dispersion are, e.g., dispersin B, proteases, and DNases, as known from the literature (Wille and Coenye, 2020). Previous research, therefore, has shown that a marine strain of *B. licheniformis* produces the DNase NucB, which induces dispersion in *B. subtilis* as well as in *Micrococcus luteus* and in several *Pseudomonas* species (Nijland et al., 2010). Consequently, it might be the case that a similar enzyme is also produced in *B. nasdae*. While preliminary, the findings in this work suggest that bacteria found in drinking water might be a good repertoire for biofilm degrading enzymes. Nevertheless, further studies will need to be undertaken in the future.

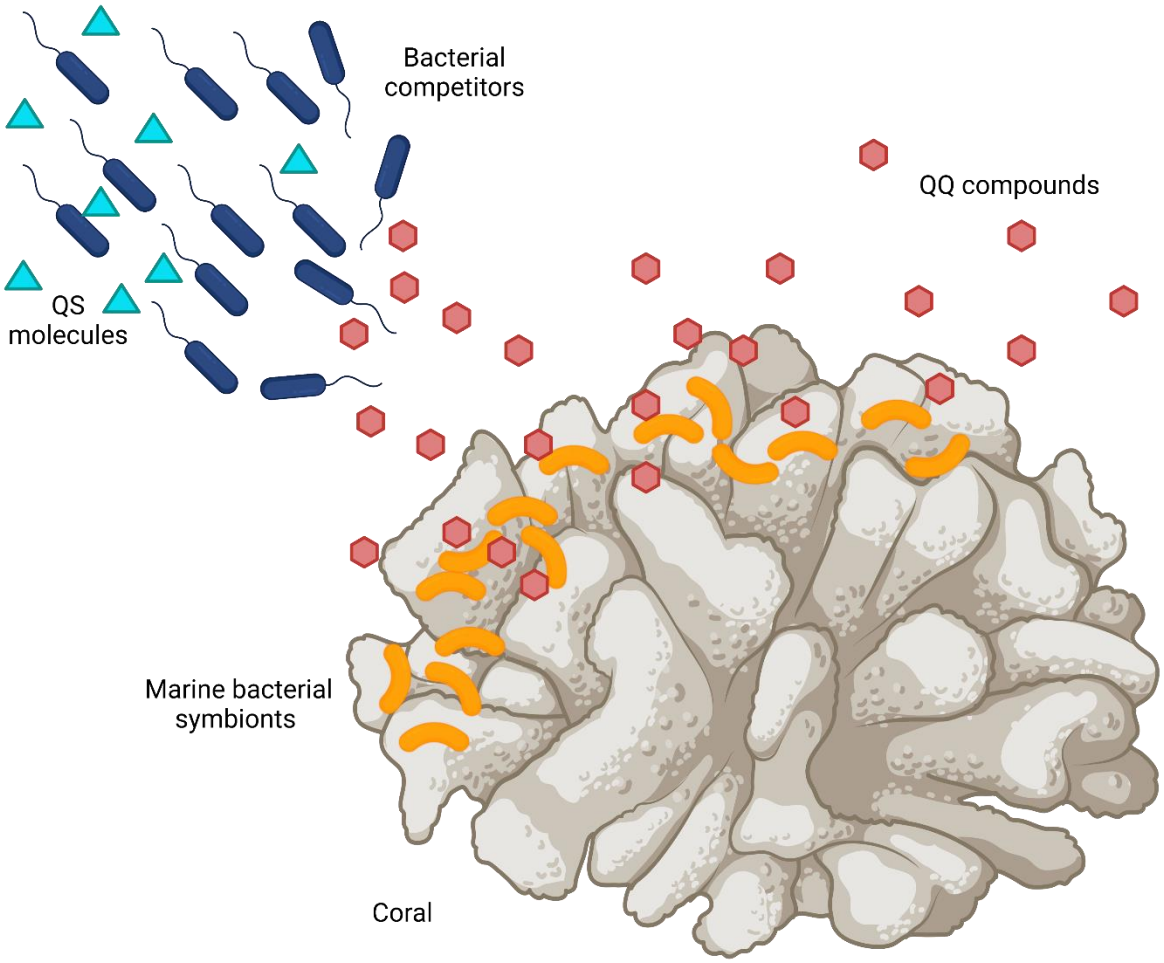

Fig. 4.4 A possible demonstration of the potential use of QQ compounds from marine bacterial symbionts. It is conceivable that marine symbionts may potentially use the QQ compounds produced for defense against competing bacteria. Thus, the marine bacterial symbionts may eventually protect the bacterial population and the respective symbiont (in this scheme, e.g., a coral). It is conceivable to identify such QQ compounds-producing bacteria and eventually use the QQ compounds biotechnologically in the future. Created with BioRender.com.

4.4 *Photorhabdus* and *Xenorhabdus* – an unlimited repertoire for QQ drugs?

Photorhabdus spec. and *Xenorhabdus* spec. are entomopathogenic bacteria producing an extensive repertoire of natural products and secondary metabolites due to their complex life cycle (Bode, 2009; Tobias et al., 2018, 2016). It was hypothesized that several natural products might interfere with bacterial biofilm formation. Screening the varying secondary metabolites of *Photorhabdus* and *Xenorhabdus* on biofilm formation of a range of marine and drinking water bacteria provided a large set of

promising results. Secondary metabolites were identified that hindered the biofilm and negatively affected the number of planktonic cells, presumably causing an antimicrobial effect. An example thereof included the natural compound rhabduscin (No. 52), which is used by entomopathogenic bacteria to shut down the immune system of insect larvae in order to kill them (Crawford et al., 2012). Nevertheless, it could also be imaginable that an antibiotic activity would also be possible in addition to the insecticidal effect. Previous research has shown that substances do exist that have an antimicrobial effect in addition to their insecticidal effect (Rehman et al., 2015). It could be cautiously argued that the substances might have a similar site of action if they are compared (Parihar et al., 2022; Rehman et al., 2015). Again, however, caution must be applied, and further studies must be completed to develop a full picture of the potential antimicrobial effect of rhabduscin.

The surprising aspect is that xenocoumacin (No. 33) (Park et al., 2009) inhibited the biofilm formation of most bacteria and the number of planktonic cells. Thus, one can most likely assume an antibiotic effect. However, in *P. aeruginosa*, only the biofilm was inhibited, not the number of planktonic cells. It has previously been shown that xenocoumacin exhibits very high bioactivity against several organisms, including Gram-positive and Gram-negative bacteria, oomycetes, and higher eukaryotes (Bode et al., 2019). In addition, recent research has also shown an effect of xenocoumacin on human cell lines, which suggests a possible application as cancer therapeutics (Brehm, 2021). However, no bioactivity was shown against *P. aeruginosa* (Bode et al., 2019). Nevertheless, compounds with comparable structures to xenocoumacin could be identified (Soukarieh et al., 2018). For example, naringenin, which belongs to the flavanones, could be detected as a QQ compound in *P. aeruginosa* (Vandeputte et al., 2011). Coumarin is another example of a QQ molecule in *P. aeruginosa*. Besides biofilm formation, phenazine production was also reduced (Gutiérrez-Barranquero et al., 2015). Consequently, it would be conceivable that xenocoumacin influences the QS system in *P. aeruginosa*. Another possibility is that *P. aeruginosa* cleaves xenocoumacin into secondary products or modifies the compound, thereby influencing the QS system. However, multiple studies need to be conducted in the future before a definitive statement can be made.

Other classes of natural compounds that affected biofilm formation in several bacteria without impacting planktonic cell numbers are the phenylethylamides/tryptamides (No. 28). Furthermore, dilutions of the extract were able to obtain a significant effect on

biofilm formation, suggesting that low concentrations are sufficient for activity. Moreover, pyocyanin formation in *P. aeruginosa* could be reduced. Previous studies have reported that phenylethylamides exhibit a possible QQ effect, like the compound from *Halobacillus salinus*, which demonstrated QQ activity against Gram-negative bacteria (Teasdale et al., 2009). Furthermore, amides with different chain lengths from *X. doucetiae* displayed an effect on violacein production of *Chromobacterium* as well as *Janthinobacterium* (Bode et al., 2017). The tryptamides were also able to demonstrate a QQ effect on *Chromobacterium violaceum* (Bode et al., 2017). Moreover, in prior screening research, phenylethylamides were observed to have a negative effect on the PpyS/PluR system of *P. luminescens* ([redacted], [redacted], [redacted], [redacted], 2015, unpublished data). The PpyS/PluR system of *P. luminescens* regulates cell clumping and utilizes photopyrones as signaling molecules (Tobias et al., 2020). The findings in this work raise intriguing questions regarding the mode of action of phenylethylamides/tryptamides. It is strongly suspected that a QQ mechanism (Fig. 4.5) is operating herein, which will need to be clarified in future studies.

Another significant result was the extract containing xenofuranones (No. 55) which likewise exhibited a strong biofilm inhibitory effect on nearly all bacteria tested. Moreover, when diluted, the extracts still had a powerful impact on reducing the biofilm of *P. gallaeciensis*. The QS system regulates biofilm formation in *P. gallaeciensis* (Berger et al., 2011; Beyersmann et al., 2017; Cude and Buchan, 2013), suggesting that a QQ mechanism may be involved in these results. As reported in the literature, several furanones, both naturally occurring and synthetic, appear to exhibit a QQ effect (Proctor et al., 2020). Additionally, a recent study demonstrated that 2(5H)-furanone inhibited biofilm formation in the marine bacterium *Pseudoalteromonas marina* (Y.-F. Li et al., 2020). This finding has important implications for combating marine biofilms, as it could possibly slow down biofouling (de Carvalho, 2018). However, additional investigations must be performed in order to confirm a possible involved QQ mechanism.

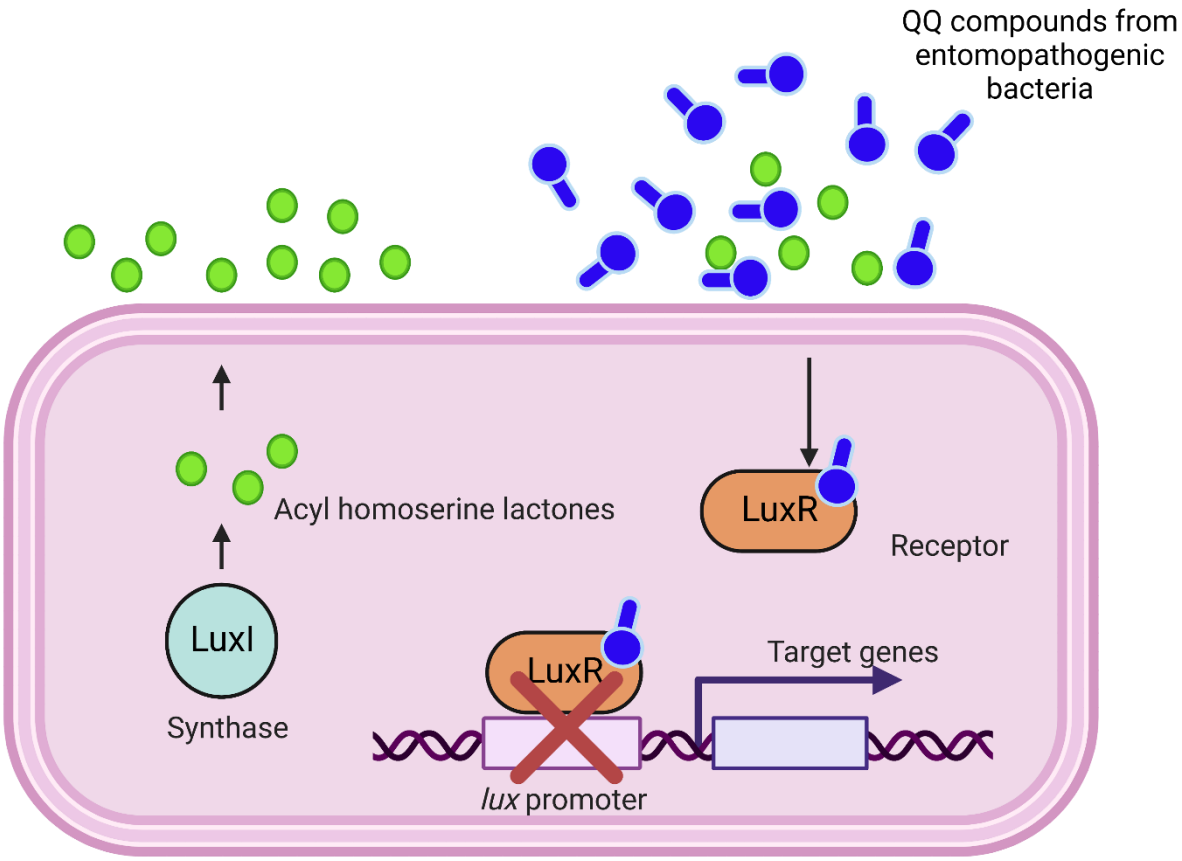

Fig. 4.5 A possible QQ mechanism of compounds from the entomopathogenic bacteria *Photorhabdus* and *Xenorhabdus*. It is conceivable that the compounds from entomopathogenic bacteria may inhibit the QS system due to the antagonistic mode of action towards the QS signaling molecules. Furthermore, the compounds from the entomopathogenic bacteria might eventually bind to the receptors, thus blocking the QS system, resulting in QQ. Created with BioRender.com.

4.5 Nanoparticles as an alternative to biofilm control

4.5.1 Tungsten oxide nanoparticles proficient in multitasking

Nanoparticles are receiving increasing attention as an antibiotic alternative and are being used more frequently to combat bacterial biofilms (Shkodenko et al., 2020). Surprisingly, in this study, tungsten oxide nanoparticles exhibited two modes of action. Whereas specific tungsten oxide nanoparticles like c-$Cs_{0,6}WO_3$ showed a haloperoxidase-like function and thus could affect the AHLs of bacteria, others like m-$Cs_{0,3}WO_3$ were able to use infrared to minimize the planktonic cells of the bacteria tested. Nanoparticles resembling a peroxidase function are already known from previous studies (Ragg et al., 2016). Peroxidases comprise enzymes that can oxidize various substrates such as H_2O_2 (Khan et al., 2014). Previous research demonstrated that Fe_3O_4 nanoparticles exhibited more stable activity than naturally occurring peroxidases, tolerating greater temperature and pH fluctuations (Ragg et al., 2016). Haloperoxidases belong to the class of peroxidases and can catalyze the oxidation of halides by H_2O_2, enabling the halogenation of organic molecules (Wang et al., 2019). Besides the previously known anti-biofilm V_2O_5 (Natalio et al., 2012) and anti-biofouling CeO_{2-x} nanoparticles (Herget et al., 2017), CuO nanoparticles were identified to exhibit a haloperoxidase-like function (Wang et al., 2019). Furthermore, it was shown that a mixture of a metal-organic framework and Ce likewise exhibited a haloperoxidase-like function (Cheng et al., 2021). In addition, previous research has revealed that WO_{3-x} exhibits a unique oxidase-like function (Dören et al., 2021a). One point that emerges from these findings is that tungsten oxide nanoparticles might be an advanced option to combat bacterial biofilm through haloperoxidase activity to inhibit QS by modification of organic compounds such as AHLs (Fig. 4.6). Therefore, it is essential to explore alternatives in nanotechnology, as antibiotic resistance is on the rise. Nevertheless, further studies in terms of quality and stability have to be undertaken in future investigations of tungsten oxides as potential QQ agents.

Another important finding in this work was the ability of tungsten oxides to reduce planktonic cells of the bacteria *P. aeruginosa* and *S. aureus* under infrared irradiation. After a literature review, it was found that nanoparticles are used for the application of so-called photothermal killing (Kaur et al., 2021; Yougbaré et al., 2020). In this process, photothermally active particles convert the absorbed photon energy into antimicrobial

heat energy (Borzenkov et al., 2020). Suitable materials are, e.g., gold, graphene oxide, molybdenum disulfide nanosheets, zinc-based and copper-based nanoparticles (Gharatape et al., 2016; Jia et al., 2017; Kaur et al., 2021; X. Li et al., 2020; Yougbaré et al., 2020). Applications of such photothermal active nanoparticles include cancer treatment and photodynamic therapies (Hu et al., 2018; Yang et al., 2019). It was also demonstrated that nanoparticles efficiently eliminate bacteria when treated with visible light (Xu et al., 2021). The point of action of these photothermally active nanoparticles is the bacterial membrane since it results in the reduction of cell permeability and the development of reactive oxygen species (ROS) (Agnihotri et al., 2020; Kaur et al., 2021). Subsequently, the generated radicals can lead to lipid peroxidation, ultimately damaging the lipids in the cell membrane and destroying the microorganisms (Kaur et al., 2021). It has been previously demonstrated that tungsten oxides exhibit strong photoabsorption properties at infrared wavelengths due to their structure (Wu et al., 2019). The obtained outcome in this work implicates further alternatives against antibiotic-resistant bacteria. In addition, the initial results indicate that further research is needed to optimize the activity. However, it is conceivable that the tungsten oxides from this work could be used to create coated surfaces that could be efficiently thermally sterilized using infrared treatment (Fig. 4.6).

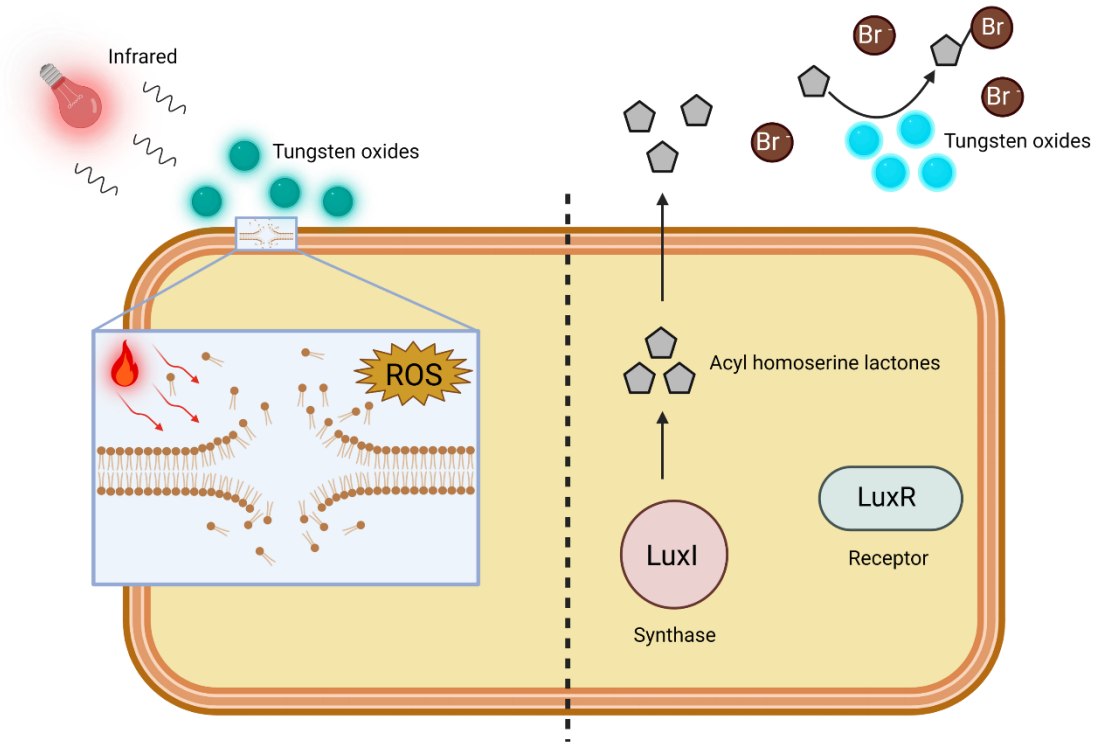

Fig. 4.6 Possible fields of action of tungsten oxide nanoparticles. Potential applications for tungsten oxides might include using infrared on the left to potentially induce the photothermal activity of tungsten oxides to disrupt bacterial membranes by generating heat and ROS eventually. Another possible application might be using tungsten oxides eventually as QQ nanoparticles on the right by modifying bacterial signaling molecules with the haloperoxidase-like function, thereby eventually shutting down the QS system and bacterial communication. Created with BioRender.com.

4.5.2 Ceroxide nanoparticles as a treatment against cystic fibrosis?

The other promising finding concerns the effect of cerium oxide nanoparticles on the bacterial QS system in Gram-negative bacteria. It has already been shown that cerium oxide nanoparticles have a haloperoxidase-like function (Herget et al., 2017; Jegel et al., 2022; Sarif et al., 2022). Haloperoxidase enzymes are frequently used to modify QS signaling molecules (Baumgartner and McKinnie, 2021; Frerichs et al., 2020). It was shown in this work by using biosensors that cerium oxide nanoparticles affect the AHLs of Gram-negative bacteria. Previous studies have already described nanoparticles that exhibit a QQ function. Silver nanoparticles were coated with an amino cellulose layer. Subsequently, acylases were topped up on the coating. Thus, the nanoparticles degraded the AHLs and inhibited the violacein production of *C. violaceum* (Ivanova et al., 2020). Another study demonstrated that silver and titanium dioxide nanoparticles prevented the synthesis of AHLs in *C. violaceum*. Additionally, it was shown that zinc oxide nanoparticles prohibited the binding of AHLs to the receptor (Gómez-Gómez et al., 2019). This work also demonstrated *in vitro* that adding ceroxide nanoparticles leads to a decrease in AHLs, and halogenated byproducts are formed. Surprisingly, these halogenated byproducts could not be detected in *P. aeruginosa*, although it was seen that the concentration of externally added bromide decreased. One unexpected result was that the chemically synthesized byproduct DAHSL was also barely detected after external addition. However, it could be shown that biofilm formation in *P. aeruginosa* decreased slightly after adding DAHSL. A possible explanation might be that *P. aeruginosa* degrades DAHSL, making it undetectable. However, it is already known that *P. aeruginosa* contains acylases such as PvdQ, an AHL acylase specialized for long-chain AHLs (Utari et al., 2018). Another acylase present in *P. aeruginosa* is QuiP (Huang et al., 2006). The reduction in biofilm may be accounted for by the fact that DAHSL can still bind to the LasR receptor until final degradation by the acylases. As is known, the LasR receptor may have a larger binding pocket than, e.g., TraR (Ng and Bassler, 2009). A binding of DAHSL would thus be quite a possibility. A connection of DAHSL to QscR would also be highly conceivable. This LuxR solo is known to have a more permissive ligand specificity (Papenfort and Bassler, 2016). However, the brominated Br-HQNO was identified in *P. aeruginosa*, while HQNO was reduced. HQNO belongs to the 2-alkyl-4(1H) -quinolones, which include the signaling molecule PQS, also responsible for QS in *P. aeruginosa*.

However, HQNO is not participating in the QS system but impairs respiratory electron transport and thus blocks the cytochrome bc_1 complex and the pyrimidine synthesis (Thierbach et al., 2019). However, previous findings have shown that HQNO contributes to a programmed cell killing system via self-intoxication. In addition, as a result of the lysed cells, DNA is leaked, which subsequently increases biofilm formation and antibiotic tolerance to beta-lactams (Hazan et al., 2016). In addition, HQNO was shown to provide stimulation of *S. aureus* biofilm formation (Fugère et al., 2014). Moreover, previous studies have demonstrated that HQNO can trigger small colony variants (SCV) in *S. aureus*. These variants exhibit resistance to aminoglycosides and are persistent in chronic infections (Hoffman et al., 2006). Besides, these SCV can be overlooked easily on agar plates (Proctor et al., 2006). Both *P. aeruginosa* and *S. aureus* predominantly colonize the cystic fibrosis lung, which can cause death for these patients (Camus et al., 2021; Villaverde-Hueso et al., 2019). Thus, it is hypothesized that the bromination of HQNO by the ceria nanoparticles triggers the biofilm reduction of *P. aeruginosa* observed in this work. These results may shed light on a new mechanism of action of ceria nanoparticles in *P. aeruginosa*. In addition, this could be a foundation for future studies and applications (Fig. 4.7), considering the use of ceria nanoparticles in medicine. Bromination of HQNO could conceivably reduce the biofilm formation of *P. aeruginosa* and *S. aureus*. Moreover, this might not trigger SCV, resulting in problematic therapy. In co-culturing a lung of a cystic fibrosis patient by these two organisms, bromination of HQNO could facilitate detection of typical formed *S. aureus* colonies. The results of this work raise many questions that need to be investigated in the future.

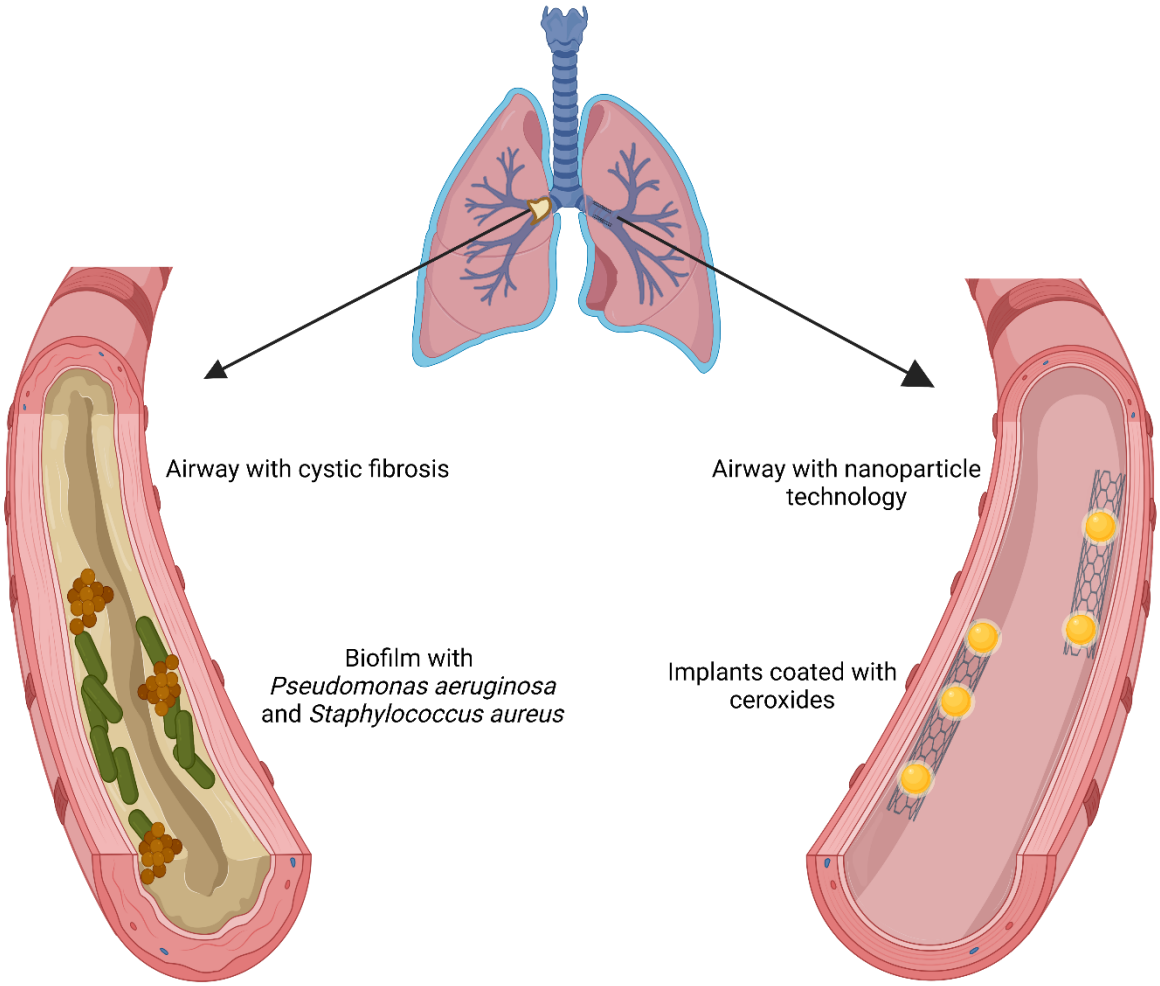

Fig. 4.7 A potential application of cerium oxide nanoparticles for putative cystic fibrosis treatment. It might be possible to eventually use implants coated with ceroxides to reduce or inhibit biofilm formation in lungs affected by cystic fibrosis. In contrast to the mucus- and biofilm-clogged airway on the left, a clearer airway might be likely by using nanoparticles, as shown on the right. However, this scheme represents only a simplified idea that must be investigated and validated in future studies to identify the chances, risks, and limitations. Created with BioRender.com

4.6 QQ natural products and QQ nanoparticles as anti-biofouling agents

Another aspect of this work was to examine whether biofilm inhibiting substances and nanoparticles can be applied to surfaces and maintain their activity. Due to biofilm and biofouling in different areas, such as the marine sector or drinking water systems, problems in health and financial damages occur in all industrial sectors (de Carvalho, 2018; Flemming, 2020; Masaka et al., 2021). Therefore, it is crucial to prevent these biofilms and the subsequent formation of biofouling. Various approaches are available for this purpose, which can be divided into physical or mechanical, chemical, and biological options. However, these solutions are often very difficult or impossible to implement (Flemming, 2020). The most widely applied mechanical method for cleaning an affected area is hydraulic flushing (Flemming, 2020). According to the literature, research has shown that cleaning aims to remove the biofilm, which is why a combination of air-water flushing has been used (Bucs et al., 2018). In order to successfully implement measures, three steps are required, which include the detection of biofouling, followed by the remediation of the affected area, whereby cleaning instead of killing is more important, and the last step includes the subsequent preventive measures (Flemming, 2002). The results obtained in this work were encouraging for the platelets coated with natural compounds from entomopathogenic bacteria and the many different surfaces tested, which were coated with cerium oxide nanoparticles. Based on the findings, the compounds and nanoparticles identified in this work as anti-biofilm agents might apply in industry and other sectors. Additionally, it has been shown in previous research that cerium oxide nanoparticles have the potential to be used against biofouling (Herget et al., 2017). Further studies are essential in the future for an answer to this issue, such as cytotoxic research, as several natural products from entomopathogenic bacteria showed bioactivity on different organisms (Bode et al., 2019) and, e.g., xenocoumacin demonstrated activity on human cell lines (Brehm, 2021). Regarding the nanoparticles, it is imaginable that different compositions might cause a harmful reaction. Furthermore, antibiotic effects were partially observed in this work regarding the tungsten oxides. However, in recent studies, no effect on human cells could be identified for the cerium oxide nanoparticles (Jegel et al., 2022). In conclusion, the results suggest that biofilm formation could be significantly diminished, although not the entire biofilm in many cases. Therefore, combining two or more strategies, such as natural products and nanoparticles, could

conceivably be used for future applications such as anti-fouling paints (Fig. 4.8) to achieve optimal biofilm inhibition.

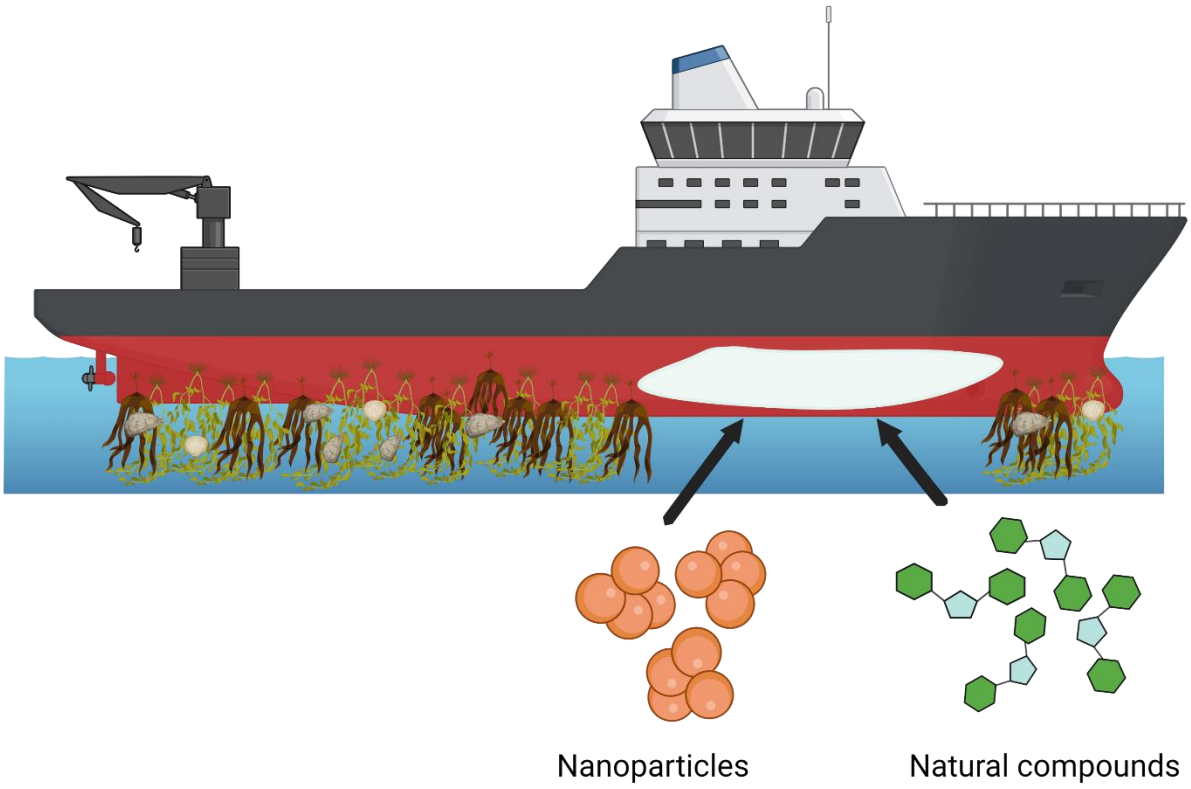

Fig. 4.8 A possible anti-biofouling application of the natural products and nanoparticles identified in this work. One possible future application of the natural substances or nanoparticles would be to incorporate them into paint and thus act as an anti-fouling coating on ships. It would also be highly likely that a combination of natural substances and nanoparticles would be applied, as a more potent biofilm inhibition would most likely be the result. Created with BioRender.com

5 Conclusion

In this thesis, the main objective was to analyze bacterial biofilms under realistic conditions both microscopically and macroscopically and identify possible new drug candidates and strategies for combating biofilms. As bacterial biofilms cause economic damage in addition to human health(Cámara et al., 2022; Muhammad et al., 2020), it is essential to suppress or tackle these. Furthermore, by developing optimized flow cells, this work provided an excellent basis for analyzing the effect of various biofilm-inhibiting compounds in the future.

In addition, it was possible to identify factors that influence the biofilm in marine and drinking water bacteria. By determining the biofilm-enhancing effect of steel on *P. gallaeciensis* and the reduced biofilm growth on plastic polymers, it is possible to conclude that part of the biofilm problem might be self-inflicted by the choice of material. Similar conclusions were drawn from investigating different commercially available pipe materials for biofilm susceptibility. Thus, in the future, a steel coating could be considered, for example, which would significantly slow down fouling since it has been shown in this work that Fe^{2+} and Mn^{2+} have a biofilm-inducing effect in *P. gallaeciensis*. However, coating with plastic polymers would entail other limitations, such as accumulating further microplastics. Therefore, further research in this area is needed to provide a suitable satisfactory alternative. One conceivable option would be an alloy with no effect on the biofilm.

Furthermore, by investigating the influence of nutrient composition on biofilm formation, an exciting behavior was observed in *B. nasdae* and *P. gallaeciensis*, respectively. Consequently, an analysis of possible initiating factors led to the discovery of potential compounds that were able to inhibit or disperse the biofilm. This leads to the question of whether the solid biofilm-forming bacteria might offer a pool of solutions and whether further investigations should focus on bacteria capable of forming a biofilm.

In addition, this work also identified potentially QQ-acting compounds from entomopathogenic bacteria that could inhibit the biofilms even at lower concentrations. The effect on pyocyanin formation in *P. aeruginosa* strongly suggests that bacterial communication is most likely inhibited, but further studies are necessary to confirm these results. Nevertheless, these findings imply that natural products from

entomopathogenic bacteria of the genera *Photorhabdus* and *Xenorhabdus* could be included among the future anti-biofilm agents.

Finally, this work demonstrated that different classes of nanoparticles constitute potential alternatives for combating bacterial biofilm. Moreover, for the tungsten oxide nanoparticles, photothermal activity was observed in addition to haloperoxidase activity, and thus a bactericidal effect was described in addition to the biofilm inhibiting effect. This flexible activity opens possibilities for using the same nanoparticle class in different fields. Furthermore, the research on cerium oxide nanoparticles showed that a QQ effect could be assumed. Thus, this class of nanoparticles can be categorized as one the potent anti-biofilm agents. In addition, a new mechanism of action in *P. aeruginosa* could be identified by the bromination of HQNO, which could be a crucial element in improving the treatment of cystic fibrosis.

6 Outlook

Bacterial biofilms continue to cause a significant threat to the environment, human health, and the economy in a wide variety of sectors (Cámara et al., 2022; Muhammad et al., 2020). Due to the protected environment within the biofilm, bacterial infections continue to increase (Muhammad et al., 2020; Yin et al., 2019). In addition, the rising incidence of antibiotic resistance requires immediate alternatives (Kumar et al., 2021). Therefore, it is still common nowadays to use biocides or to apply mechanical cleaning to a surface affected by biofilm (Flemming, 2020).

It was shown in this thesis that a microfluidic system could be developed that is suitable for both microscopic and macroscopic applications. However, to perform high-throughput screening and thus identify potential new compounds, an upgrade of the *Panta Rhei* system is essential. It is therefore the future goal to take the system developed in this thesis to the next level and translate the development of the all-in-one device into reality, as the theoretical basics have already been accomplished in this thesis. Furthermore, a university spin-off is envisioned. In this context, the start-up company should position itself on the market with its own microfluidic device. However, further innovations in the field of microfluidics should also be created in the future to be able to remain on the market. The dedication and future direction in this regard is already reflected in the found company name. The name BIAttiva is composed of the claim of wanting to counter biofilm analyses by means of microfluidic innovation combined with the wording “active” compounds [**B**iofilm **I**nhibition **A**nalysis, **attiva** (active)]. In addition, the flow cells should be manufactured from sustainable plastics such as laboratory discards or food packaging. Hereby, the young company should be directly grown up with ecological values and also be connected to them. Furthermore, equipment is planned to be designed to simplify the handling of bacterial biofilms in laboratories, especially with crystal violet. In addition, developments of new flow cells are intended, not only for biofilm analysis, but also for biotechnological use and drug generation.

The results obtained regarding the various factors for biofilm formation of marine and drinking water bacteria in this work are revealing. However, other steel surfaces with different alloy content could be investigated in the future, especially for *P. gallaeciensis*. In addition, mutants of *P. gallaeciensis* could be created that do not

possess individual components of the QS, allowing a more unambiguous indication of whether metal ions may interfere with the QS system. Furthermore, mutants without the specific ABC transporter should also be created to exclude a direct or indirect involvement in biofilm formation. Moreover, other metal ions present in steel could also be examined.

First, insights could be gained concerning the observed variations in the primary colonization of surfaces. A more precise picture can probably be obtained with a microfluidic analysis, as previously described (Monmeyran et al., 2021). Furthermore, different surfaces and additional species combinations containing different organisms could be conducted. Finally, the observed priority effect might be connected to the surfaces.

In this work, natural compounds from entomopathogenic bacteria were identified, showing an influence on biofilm formation but not affecting planktonic growth. Furthermore, first insights could be made about a potential QQ effect. To obtain a more detailed picture, reporter strains that function by bioluminescence or fluorescence may be suitable as readouts. Studies of hundreds of compounds would also be conceivable using such a readout. Previous research has revealed different options for high-throughput screening using a biosensor (Kaczmarek and Prather, 2021). However, it should not be overlooked that all possible components of the QS system of *P. aeruginosa*, for example, must be subjected to testing. If the readout confirms a QQ effect, surface plasmon resonance spectroscopy can be used to confirm potential binding. The application of surface plasmon resonance spectroscopy has been previously reported for the detection of binding (Wiechert et al., 2020). In addition, toxicological studies, as prior described (Brehm, 2021), are indispensable in the future, as certain natural substances have shown negative bioactivity.

Additionally, a biofilm dispersing effect was detected in the culture fluid of *B. nasdae*. Most likely, this effect is due to an enzyme that possibly degrades the biofilm matrix. Future experiments may include protein purification followed by concentrating so that crystallization can be used to provide information about the structure. A comprehensive step-by-step guide for that purpose has already been published (Chayen and Saridakis, 2008).

A molecule was identified in the culture fluid of *P. gallaeciensis*, which is highly unlikely a protein. However, mass spectrometry and NMR analysis might help identify a more

precise nature of the unknown substance since these techniques were already used for the identification of a secondary metabolite in *V. alginolyticus* (Song et al., 2018).

Different classes of nanoparticles were successfully investigated in this thesis, demonstrating QQ activity and photothermal efficiency. Investigations could be made in the future to increase the effectiveness. Furthermore, application to other organisms such as fungi would also be conceivable. Especially concerning cystic fibrosis, further research is necessary, as it is quite possible that nanoparticles might be applied as a therapeutic agent.

As this work revealed natural products from entomopathogenic bacteria and nanoparticles with a high probability of influencing the QS system of bacteria, new active substances should be sought across organisms. Furthermore, given that fungi also live in soil and produce a broad repertoire of metabolites (Karlovsky, 2008; Pusztahelyi et al., 2015), the Institute of Biotechnology and Drug research (IBWF) natural compound library should be screened for QQ functions soon.

7 References

Abbot, E.L., Smith, W.D., Siou, G.P.S., Chiriboga, C., Smith, R.J., Wilson, J.A., Hirst, B.H., Kehoe, M.A., 2007. Pili mediate specific adhesion of *Streptococcus pyogenes* to human tonsil and skin. Cell. Microbiol. 9, 1822–1833. https://doi.org/10.1111/j.1462-5822.2007.00918.x

Abd El Aleem, F.A., Al-Sugair, K.A., Alahmad, M.I., 1998. Biofouling problems in membrane processes for water desalination and reuse in Saudi Arabia. Int. Biodeterior. Biodegrad. 41, 19–23. https://doi.org/10.1016/S0964-8305(98)80004-8

Abraham, W.-R., 2016. Going beyond the control of quorum-sensing to combat biofilm infections. Antibiotics 5, 3. https://doi.org/10.3390/antibiotics5010003

Acosta-Jurado, S., Fuentes-Romero, F., Ruiz-Sainz, J.-E., Janczarek, M., Vinardell, J.-M., 2021. Rhizobial exopolysaccharides: genetic regulation of their synthesis and relevance in symbiosis with legumes. Int. J. Mol. Sci. 22, 6233. https://doi.org/10.3390/ijms22126233

Adler, J., 1973. A method for measuring chemotaxis and use of the method to determine optimum conditions for chemotaxis by *Escherichia coli*. J. Gen. Microbiol. 74, 77–91. https://doi.org/10.1099/00221287-74-1-77

Agnihotri, S., Mohan, T., Jha, D., Gautam, H.K., Roy, I., 2020. Dual modality FeS nanoparticles with reactive oxygen species-induced and photothermal toxicity toward pathogenic bacteria. ACS Omega 5, 597–602. https://doi.org/10.1021/acsomega.9b03177

Agostini, V.O., Macedo, A.J., Muxagata, E., Pinho, G.L.L., 2019. Surface coatings select their micro and macrofouling communities differently on steel. Environ. Pollut. 254, 113086. https://doi.org/10.1016/j.envpol.2019.113086

Ahimou, F., Semmens, M.J., Haugstad, G., Novak, P.J., 2007. Effect of protein, polysaccharide, and oxygen concentration profiles on biofilm cohesiveness. Appl. Environ. Microbiol. 73, 2905–2910. https://doi.org/10.1128/AEM.02420-06

Akyıldız, İ., Take, G., Uygur, K., Kızıl, Y., Aydil, U., 2013. Bacterial biofilm formation in the middle-ear mucosa of chronic otitis media patients. Indian J. Otolaryngol. Head Neck Surg. 65, 557–561. https://doi.org/10.1007/s12070-012-0513-x

Al-Abri, M., Al-Ghafri, B., Bora, T., Dobretsov, S., Dutta, J., Castelletto, S., Rosa, L., Boretti, A., 2019. Chlorination disadvantages and alternative routes for biofouling control in reverse osmosis desalination. Npj Clean Water 2, 2. https://doi.org/10.1038/s41545-018-0024-8

Alavi, M., Rai, M., 2019. Recent advances in antibacterial applications of metal nanoparticles (MNPs) and metal nanocomposites (MNCs) against multidrug-resistant (MDR) bacteria. Expert Rev. Anti Infect. Ther. 17, 419–428. https://doi.org/10.1080/14787210.2019.1614914

Alexander, D.E., 2017. Fluid biomechanics, in: Nature's Machines. Elsevier, pp. 51–97. https://doi.org/10.1016/B978-0-12-804404-9.00003-7

Ali, I.A.A., Cheung, B.P.K., Yau, J.Y.Y., Matinlinna, J.P., Lévesque, C.M., Belibasakis, G.N., Neelakantan, P., 2020. The influence of substrate surface conditioning and biofilm age on the composition of *Enterococcus faecalis* biofilms. Int. Endod. J. 53, 53–61. https://doi.org/10.1111/iej.13202

Ali, I.A.A., Lévesque, C.M., Neelakantan, P., 2022. Fsr quorum sensing system modulates the temporal development of *Enterococcus faecalis* biofilm matrix. Mol. Oral Microbiol. 37, 22–30. https://doi.org/10.1111/omi.12357
Ali, L., Goraya, M., Arafat, Y., Ajmal, M., Chen, J.-L., Yu, D., 2017. Molecular mechanism of quorum-sensing in *Enterococcus faecalis*: Its role in virulence and therapeutic approaches. Int. J. Mol. Sci. 18, 960. https://doi.org/10.3390/ijms18050960
Allegretta, G., Maurer, C.K., Eberhard, J., Maura, D., Hartmann, R.W., Rahme, L., Empting, M., 2017. In-depth profiling of MvfR-regulated small molecules in *Pseudomonas aeruginosa* after quorum sensing inhibitor treatment. Front. Microbiol. 8, 924. https://doi.org/10.3389/fmicb.2017.00924
Allion, A., Lassiaz, S., Peguet, L., Boillot, P., Jacques, S., Peultier, J., Bonnet, M.-C., 2011. A long term study on biofilm development in drinking water distribution system: comparison of stainless steel grades with commonly used materials. Rev. Métallurgie 108, 259–268. https://doi.org/10.1051/metal/2011063
Aloni, Y., Delmer, D.P., Benziman, M., 1982. Achievement of high rates of in vitro synthesis of 1,4-beta-D-glucan: activation by cooperative interaction of the *Acetobacter xylinum* enzyme system with GTP, polyethylene glycol, and a protein factor. Proc. Natl. Acad. Sci. 79, 6448–6452. https://doi.org/10.1073/pnas.79.21.6448
Alotaibi, G.F., Bukhari, M.A., 2021. Factors influencing bacterial biofilm formation and development. Am. J. Biomed. Sci. Res. 12, 617–626. https://doi.org/10.34297/AJBSR.2021.12.001820
Altaf, M., Zeyad, M.T., Hashmi, M.A., Manoharadas, S., Hussain, S.A., Ali Abuhasil, M.S., Almuzaini, M.A.M., 2021. Effective inhibition and eradication of pathogenic biofilms by titanium dioxide nanoparticles synthesized using *Carum copticum* extract. RSC Adv. 11, 19248–19257. https://doi.org/10.1039/D1RA02876F
Amaning Danquah, C., Osei-Djarbeng, S., Appiah, T., Duah Boakye, Y., Adu, F., 2020. Combating biofilm and quorum sensing: a new strategy to fight infections, in: Dincer, S., Sümengen Özdenefe, M., Arkut, A. (Eds.), Bacterial Biofilms. IntechOpen. https://doi.org/10.5772/intechopen.89227
Apaza-Bedoya, K., Tarce, M., Benfatti, C.A.M., Henriques, B., Mathew, M.T., Teughels, W., Souza, J.C.M., 2017. Synergistic interactions between corrosion and wear at titanium-based dental implant connections: A scoping review. J. Periodontal Res. 52, 946–954. https://doi.org/10.1111/jre.12469
Aqeel, H., Liss, S.N., 2022. Fate of sloughed biomass in integrated fixed-film systems. PLOS ONE 17, e0262603. https://doi.org/10.1371/journal.pone.0262603
Arciola, C.R., Campoccia, D., Ehrlich, G.D., Montanaro, L., 2015. Biofilm-based implant infections in orthopaedics, in: Donelli, G. (Ed.), Biofilm-Based Healthcare-Associated Infections, Advances in Experimental Medicine and Biology. Springer International Publishing, Cham, pp. 29–46. https://doi.org/10.1007/978-3-319-11038-7_2
Arnold, J.W., 2008. Colorimetric assay for biofilms in wet processing conditions. J. Ind. Microbiol. Biotechnol. 35, 1475–1480. https://doi.org/10.1007/s10295-008-0449-z
Asghar, M., Habib, S., Zaman, W., Hussain, S., Ali, H., Saqib, S., 2020. Synthesis and characterization of microbial mediated cadmium oxide nanoparticles. Microsc. Res. Tech. 83, 1574–1584. https://doi.org/10.1002/jemt.23553

Aufrecht, J.A., Fowlkes, J.D., Bible, A.N., Morrell-Falvey, J., Doktycz, M.J., Retterer, S.T., 2019. Pore-scale hydrodynamics influence the spatial evolution of bacterial biofilms in a microfluidic porous network. PLOS ONE 14, e0218316. https://doi.org/10.1371/journal.pone.0218316
Azeredo, J., Azevedo, N.F., Briandet, R., Cerca, N., Coenye, T., Costa, A.R., Desvaux, M., Di Bonaventura, G., Hébraud, M., Jaglic, Z., Kačániová, M., Knøchel, S., Lourenço, A., Mergulhão, F., Meyer, R.L., Nychas, G., Simões, M., Tresse, O., Sternberg, C., 2017. Critical review on biofilm methods. Crit. Rev. Microbiol. 43, 313–351. https://doi.org/10.1080/1040841X.2016.1208146
Bai, X., Nakatsu, C.H., Bhunia, A.K., 2021. Bacterial biofilms and their implications in pathogenesis and food safety. Foods 10, 2117. https://doi.org/10.3390/foods10092117
Bakker, D.P., Busscher, H.J., van Zanten, J., de Vries, J., Klijnstra, J.W., van der Mei, H.C., 2004. Multiple linear regression analysis of bacterial deposition to polyurethane coatings after conditioning film formation in the marine environment. Microbiology 150, 1779–1784. https://doi.org/10.1099/mic.0.26983-0
Baraquet, C., Harwood, C.S., 2013. Cyclic diguanosine monophosphate represses bacterial flagella synthesis by interacting with the Walker A motif of the enhancer-binding protein FleQ. Proc. Natl. Acad. Sci. 110, 18478–18483. https://doi.org/10.1073/pnas.1318972110
Barnard, A.M.L., Bowden, S.D., Burr, T., Coulthurst, S.J., Monson, R.E., Salmond, G.P.C., 2007. Quorum sensing, virulence and secondary metabolite production in plant soft-rotting bacteria. Philos. Trans. R. Soc. B Biol. Sci. 362, 1165–1183. https://doi.org/10.1098/rstb.2007.2042
Baron, S. (Ed.), 1996. Medical microbiology, 4th ed. ed. University of Texas Medical Branch at Galveston, Galveston, Tex.
Barth, E., Myrvik, Q., Wagner, W., Gristina, A., 1989. In vitro and in vivo comparative colonization of *Staphylococcus aureus* and *Staphylococcus epidermidis* on orthopaedic implant materials. Biomaterials 10, 325–328. https://doi.org/10.1016/0142-9612(89)90073-2
Bassler, B.L., Losick, R., 2006. Bacterially speaking. Cell 125, 237–246. https://doi.org/10.1016/j.cell.2006.04.001
Bassler, B.L., Wright, M., Showalter, R.E., Silverman, M.R., 1993. Intercellular signalling in *Vibrio harveyi*: sequence and function of genes regulating expression of luminescence. Mol. Microbiol. 9, 773–786. https://doi.org/10.1111/j.1365-2958.1993.tb01737.x
Bassler, B.L., Wright, M., Silverman, M.R., 1994. Multiple signalling systems controlling expression of luminescence in *Vibrio harveyi* : sequence and function of genes encoding a second sensory pathway. Mol. Microbiol. 13, 273–286. https://doi.org/10.1111/j.1365-2958.1994.tb00422.x
Basu Roy, A., Sauer, K., 2014. Diguanylate cyclase NicD-based signalling mechanism of nutrient-induced dispersion by *Pseudomonas aeruginosa*: NicD and dispersion. Mol. Microbiol. 94, 771–793. https://doi.org/10.1111/mmi.12802
Batté, M., Appenzeller, B.M.R., Grandjean, D., Fass, S., Gauthier, V., Jorand, F., Mathieu, L., Boualam, M., Saby, S., Block, J.C., 2003. Biofilms in drinking water distribution systems. Rev. Environ. Sci. Biotechnol. 2, 147–168. https://doi.org/10.1023/B:RESB.0000040456.71537.29
Baumgartner, J.T., McKinnie, S.M.K., 2021. Investigating the role of vanadium-dependent haloperoxidase enzymology in microbial secondary metabolism

and chemical ecology. mSystems 6, e00780-21. https://doi.org/10.1128/mSystems.00780-21
Beckmann, B.E., Knoester, D.B., Connelly, B.D., Waters, C.M., McKinley, P.K., 2012. Evolution of resistance to quorum quenching in digital organisms. Artif. Life 18, 291–310. https://doi.org/10.1162/artl_a_00066
Beech, I.B., Cheung, C.W.S., 1995. Interactions of exopolymers produced by sulphate-reducing bacteria with metal ions. Int. Biodeterior. Biodegrad. 35, 59–72. https://doi.org/10.1016/0964-8305(95)00082-G
Behr, A., Agar, D.W., Jörissen, J., Vorholt, A.J., 2016. Organische Endprodukte, in: Einführung in die Technische Chemie. Springer Berlin Heidelberg, Berlin, Heidelberg, pp. 213–223. https://doi.org/10.1007/978-3-662-52856-3_16
Behrens, M.R., Fuller, H.C., Swist, E.R., Wu, J., Islam, Md.M., Long, Z., Ruder, W.C., Steward, R., 2020. Open-source, 3D-printed peristaltic pumps for small volume point-of-care liquid handling. Sci. Rep. 10, 1543. https://doi.org/10.1038/s41598-020-58246-6
Beitelshees, M., Hill, A., Jones, C., Pfeifer, B., 2018. Phenotypic variation during biofilm formation: implications for anti-biofilm therapeutic design. Materials 11, 1086. https://doi.org/10.3390/ma11071086
Beloin, C., Fernández-Hidalgo, N., Lebeaux, D., 2017. Understanding biofilm formation in intravascular device-related infections. Intensive Care Med. 43, 443–446. https://doi.org/10.1007/s00134-016-4480-7
Bereschenko, L.A., Stams, A.J.M., Euverink, G.J.W., van Loosdrecht, M.C.M., 2010. Biofilm formation on reverse osmosis membranes is initiated and dominated by *Sphingomonas* spp. Appl. Environ. Microbiol. 76, 2623–2632. https://doi.org/10.1128/AEM.01998-09
Berger, M., Neumann, A., Schulz, S., Simon, M., Brinkhoff, T., 2011. Tropodithietic acid production in *Phaeobacter gallaeciensis* is regulated by N-acyl homoserine lactone-mediated quorum sensing. J. Bacteriol. 193, 6576–6585. https://doi.org/10.1128/JB.05818-11
Berlanga, M., Guerrero, R., 2016. Living together in biofilms: the microbial cell factory and its biotechnological implications. Microb. Cell Factories 15, 165. https://doi.org/10.1186/s12934-016-0569-5
Berman, T., Passow, U., 2007. Transparent exopolymer particles (TEP): an overlooked factor in the process of biofilm formation in aquatic environments. Nat. Preced. https://doi.org/10.1038/npre.2007.1182.1
Berne, C., Ducret, A., Hardy, G.G., Brun, Y.V., 2015. Adhesins involved in attachment to abiotic surfaces by Gram-negative bacteria. Microbiol. Spectr. 3, 3.4.15. https://doi.org/10.1128/microbiolspec.MB-0018-2015
Bester, E., Wolfaardt, G., Joubert, L., Garny, K., Saftic, S., 2005. Planktonic-cell yield of a *Pseudomonad* biofilm. Appl. Environ. Microbiol. 71, 7792–7798. https://doi.org/10.1128/AEM.71.12.7792-7798.2005
Beyersmann, P.G., Tomasch, J., Son, K., Stocker, R., Göker, M., Wagner-Döbler, I., Simon, M., Brinkhoff, T., 2017. Dual function of tropodithietic acid as antibiotic and signaling molecule in global gene regulation of the probiotic bacterium *Phaeobacter inhibens*. Sci. Rep. 7, 730. https://doi.org/10.1038/s41598-017-00784-7
Bhagirath, A.Y., Li, Y., Somayajula, D., Dadashi, M., Badr, S., Duan, K., 2016. Cystic fibrosis lung environment and *Pseudomonas aeruginosa* infection. BMC Pulm. Med. 16, 174. https://doi.org/10.1186/s12890-016-0339-5

Bhagwat, G., O'Connor, W., Grainge, I., Palanisami, T., 2021. Understanding the fundamental basis for biofilm formation on plastic surfaces: role of conditioning films. Front. Microbiol. 12, 687118. https://doi.org/10.3389/fmicb.2021.687118
Bhardwaj, V., Kaushik, A., 2017. Biomedical applications of nanotechnology and nanomaterials. Micromachines 8, 298. https://doi.org/10.3390/mi8100298
Bible, A.N., Fletcher, S.J., Pelletier, D.A., Schadt, C.W., Jawdy, S.S., Weston, D.J., Engle, N.L., Tschaplinski, T., Masyuko, R., Polisetti, S., Bohn, P.W., Coutinho, T.A., Doktycz, M.J., Morrell-Falvey, J.L., 2016. A carotenoid-deficient mutant in *Pantoea* sp. YR343, a bacteria isolated from the rhizosphere of *Populus deltoides*, is defective in root colonization. Front. Microbiol. 7. https://doi.org/10.3389/fmicb.2016.00491
Bischof, J.C., He, X., 2005. Thermal stability of proteins. Ann. N. Y. Acad. Sci. 1066, 12–33. https://doi.org/10.1196/annals.1363.003
Bode, E., Brachmann, A.O., Kegler, C., Simsek, R., Dauth, C., Zhou, Q., Kaiser, M., Klemmt, P., Bode, H.B., 2015. Simple "on-demand" production of bioactive natural products. ChemBioChem 16, 1115–1119. https://doi.org/10.1002/cbic.201500094
Bode, E., He, Y., Vo, T.D., Schultz, R., Kaiser, M., Bode, H.B., 2017. Biosynthesis and function of simple amides in *Xenorhabdus doucetiae*. Environ. Microbiol. 19, 4564–4575. https://doi.org/10.1111/1462-2920.13919
Bode, E., Heinrich, A.K., Hirschmann, M., Abebew, D., Shi, Yan-Ni, Vo, T.D., Wesche, F., Shi, Yi-Ming, Grün, P., Simonyi, S., Keller, N., Engel, Y., Wenski, S., Bennet, R., Beyer, S., Bischoff, I., Buaya, A., Brandt, S., Cakmak, I., Çimen, H., Eckstein, S., Frank, D., Fürst, R., Gand, M., Geisslinger, G., Hazir, S., Henke, M., Heermann, R., Lecaudey, V., Schäfer, W., Schiffmann, S., Schüffler, A., Schwenk, R., Skaljac, M., Thines, E., Thines, M., Ulshöfer, T., Vilcinskas, A., Wichelhaus, T.A., Bode, H.B., 2019. Promoter activation in Δ*hfq* mutants as an efficient tool for specialized metabolite production enabling direct bioactivity testing. Angew. Chem. Int. Ed. 58, 18957–18963. https://doi.org/10.1002/anie.201910563
Bode, H.B., 2009. Entomopathogenic bacteria as a source of secondary metabolites. Curr. Opin. Chem. Biol. 13, 224–230. https://doi.org/10.1016/j.cbpa.2009.02.037
Bogino, P., Oliva, M., Sorroche, F., Giordano, W., 2013. The role of bacterial biofilms and surface components in plant-bacterial associations. Int. J. Mol. Sci. 14, 15838–15859. https://doi.org/10.3390/ijms140815838
Boles, B.R., Thoendel, M., Singh, P.K., 2004. Self-generated diversity produces "insurance effects" in biofilm communities. Proc. Natl. Acad. Sci. 101, 16630–16635. https://doi.org/10.1073/pnas.0407460101
Booysen, E., Dicks, L.M.T., 2020. Does the future of antibiotics lie in secondary metabolites produced by *Xenorhabdus* spp.? A review. Probiotics Antimicrob. Proteins 12, 1310–1320. https://doi.org/10.1007/s12602-020-09688-x
Borzenkov, M., Pallavicini, P., Taglietti, A., D'Alfonso, L., Collini, M., Chirico, G., 2020. Photothermally active nanoparticles as a promising tool for eliminating bacteria and biofilms. Beilstein J. Nanotechnol. 11, 1134–1146. https://doi.org/10.3762/bjnano.11.98
Bott, T.R., 1998. Techniques for reducing the amount of biocide necessary to counteract the effects of biofilm growth in cooling water systems. Appl. Therm. Eng. 18, 1059–1066. https://doi.org/10.1016/S1359-4311(98)00017-9
Bouillaut, L., Perchat, S., Arold, S., Zorrilla, S., Slamti, L., Henry, C., Gohar, M., Declerck, N., Lereclus, D., 2008. Molecular basis for group-specific activation

of the virulence regulator PlcR by PapR heptapeptides. Nucleic Acids Res. 36, 3791–3801. https://doi.org/10.1093/nar/gkn149
Bowler, P., Murphy, C., Wolcott, R., 2020. Biofilm exacerbates antibiotic resistance: Is this a current oversight in antimicrobial stewardship? Antimicrob. Resist. Infect. Control 9, 162. https://doi.org/10.1186/s13756-020-00830-6
Brachmann, A.O., Forst, S., Furgani, G.M., Fodor, A., Bode, H.B., 2006. Xenofuranones A and B: phenylpyruvate dimers from *Xenorhabdus szentirmaii*. J. Nat. Prod. 69, 1830–1832. https://doi.org/10.1021/np060409n
Bradley, G., Gaylarde, C.C., 1988. Iron uptake by *Desulfovibrio vulgaris* outer membrane components in artificial vesicles. Curr. Microbiol. 17, 189–192. https://doi.org/10.1007/BF01589450
Brameyer, S., 2015. Cell-cell communication via LuxR solos in *Photorhabdus* species (Dissertation). Ludwig-Maximilians-Universität München.
Brameyer, S., Heermann, R., 2016. Quorum sensing and LuxR solos in *Photorhabdus*, in: ffrench-Constant, R.H. (Ed.), The Molecular Biology of Photorhabdus Bacteria, Current Topics in Microbiology and Immunology. Springer International Publishing, Cham, pp. 103–119. https://doi.org/10.1007/82_2016_28
Brameyer, S., Kresovic, D., Bode, H.B., Heermann, R., 2014. LuxR solos in *Photorhabdus* species. Front. Cell. Infect. Microbiol. 4. https://doi.org/10.3389/fcimb.2014.00166
Brehm, J., 2021. The pathogenic part of the *Photorhabdus* and *Xenorhabdus* lifecycle with regard to the development of novel drugs (Dissertation). Ludwig-Maximilians-Universität München.
Bridges, A.A., Fei, C., Bassler, B.L., 2020. Identification of signaling pathways, matrix-digestion enzymes, and motility components controlling *Vibrio cholerae* biofilm dispersal. Proc. Natl. Acad. Sci. 117, 32639–32647. https://doi.org/10.1073/pnas.2021166117
Bronesky, D., Wu, Z., Marzi, S., Walter, P., Geissmann, T., Moreau, K., Vandenesch, F., Caldelari, I., Romby, P., 2016. *Staphylococcus aureus* RNAIII and its regulon link quorum sensing, stress responses, metabolic adaptation, and regulation of virulence gene expression. Annu. Rev. Microbiol. 70, 299–316. https://doi.org/10.1146/annurev-micro-102215-095708
Bucs, S.S., Farhat, N., Kruithof, J.C., Picioreanu, C., van Loosdrecht, M.C.M., Vrouwenvelder, J.S., 2018. Review on strategies for biofouling mitigation in spiral wound membrane systems. Desalination 434, 189–197. https://doi.org/10.1016/j.desal.2018.01.023
Buddruhs, N., Pradella, S., Göker, M., Päuker, O., Pukall, R., Spröer, C., Schumann, P., Petersen, J., Brinkhoff, T., 2013. Molecular and phenotypic analyses reveal the non-identity of the *Phaeobacter gallaeciensis* type strain deposits CIP 105210T and DSM 17395. Int. J. Syst. Evol. Microbiol. 63, 4340–4349. https://doi.org/10.1099/ijs.0.053900-0
Busscher, H.J., Der Mei, R.B.H.C., 1995. Initial microbial adhesion is a determinant for the strength of biofilm adhesion. FEMS Microbiol. Lett. 128, 229–234. https://doi.org/10.1111/j.1574-6968.1995.tb07529.x
But, A., 2019. Design for manufacturing using TEBIS CAM software for milling processing. IOP Conf. Ser. Mater. Sci. Eng. 564, 012056. https://doi.org/10.1088/1757-899X/564/1/012056
Bzdrenga, J., Daudé, D., Rémy, B., Jacquet, P., Plener, L., Elias, M., Chabrière, E., 2017. Biotechnological applications of quorum quenching enzymes. Chem. Biol. Interact. 267, 104–115. https://doi.org/10.1016/j.cbi.2016.05.028

Cai, X., Challinor, V.L., Zhao, L., Reimer, D., Adihou, H., Grün, P., Kaiser, M., Bode, H.B., 2017. Biosynthesis of the antibiotic nematophin and its elongated derivatives in entomopathogenic bacteria. Org. Lett. 19, 806–809. https://doi.org/10.1021/acs.orglett.6b03796

Cai, X., Yu, M., Shan, H., Tian, X., Zheng, Y., Xue, C., Zhang, X.-H., 2018. Characterization of a Novel N-Acylhomoserine Lactonase RmmL from Ruegeria mobilis YJ3. Mar. Drugs 16, 370. https://doi.org/10.3390/md16100370

Callow, J.A., Callow, M.E., 2011. Trends in the development of environmentally friendly fouling-resistant marine coatings. Nat. Commun. 2, 244. https://doi.org/10.1038/ncomms1251

Cámara, M., Green, W., MacPhee, C.E., Rakowska, P.D., Raval, R., Richardson, M.C., Slater-Jefferies, J., Steventon, K., Webb, J.S., 2022. Economic significance of biofilms: a multidisciplinary and cross-sectoral challenge. Npj Biofilms Microbiomes 8, 42. https://doi.org/10.1038/s41522-022-00306-y

Camargo, A.C., Woodward, J.J., Call, D.R., Nero, L.A., 2017. *Listeria monocytogenes* in food-processing facilities, food contamination, and human listeriosis: the brazilian scenario. Foodborne Pathog. Dis. 14, 623–636. https://doi.org/10.1089/fpd.2016.2274

Camus, L., Briaud, P., Vandenesch, F., Moreau, K., 2021. How bacterial adaptation to cystic fibrosis environment shapes interactions between *Pseudomonas aeruginosa* and *Staphylococcus aureus*. Front. Microbiol. 12, 617784. https://doi.org/10.3389/fmicb.2021.617784

Cao, H., Krishnan, G., Goumnerov, B., Tsongalis, J., Tompkins, R., Rahme, L.G., 2001. A quorum sensing-associated virulence gene of *Pseudomonas aeruginosa* encodes a LysR-like transcription regulator with a unique self-regulatory mechanism. Proc. Natl. Acad. Sci. 98, 14613–14618. https://doi.org/10.1073/pnas.251465298

Cao, S., Wang, J., Chen, H., Chen, D., 2011. Progress of marine biofouling and antifouling technologies. Chin. Sci. Bull. 56, 598–612. https://doi.org/10.1007/s11434-010-4158-4

Carette, J., Nachtergael, A., Duez, P., El Jaziri, M., Rasamiravaka, T., 2020. Natural compounds inhibiting *Pseudomonas aeruginosa* biofilm formation by targeting quorum sensing circuitry, in: Dincer, S., Sümengen Özdenefe, M., Arkut, A. (Eds.), Bacterial Biofilms. IntechOpen. https://doi.org/10.5772/intechopen.90833

Carniello, V., Peterson, B.W., van der Mei, H.C., Busscher, H.J., 2018. Physico-chemistry from initial bacterial adhesion to surface-programmed biofilm growth. Adv. Colloid Interface Sci. 261, 1–14. https://doi.org/10.1016/j.cis.2018.10.005

Carrascosa, C., Raheem, D., Ramos, F., Saraiva, A., Raposo, A., 2021. Microbial biofilms in the food industry—a comprehensive review. Int. J. Environ. Res. Public. Health 18, 2014. https://doi.org/10.3390/ijerph18042014

Case, R.J., Labbate, M., Kjelleberg, S., 2008. AHL-driven quorum-sensing circuits: their frequency and function among the *Proteobacteria*. ISME J. 2, 345–349. https://doi.org/10.1038/ismej.2008.13

Chacón-Orozco, J.G., Bueno, C., Shapiro-Ilan, D.I., Hazir, S., Leite, L.G., Harakava, R., 2020. Antifungal activity of *Xenorhabdus* spp. and *Photorhabdus* spp. against the soybean pathogenic *Sclerotinia sclerotiorum*. Sci. Rep. 10, 20649. https://doi.org/10.1038/s41598-020-77472-6

Chagnot, C., Zorgani, M.A., Astruc, T., Desvaux, M., 2013. Proteinaceous determinants of surface colonization in bacteria: bacterial adhesion and biofilm formation from a protein secretion perspective. Front. Microbiol. 4. https://doi.org/10.3389/fmicb.2013.00303

Chambers, H.F., DeLeo, F.R., 2009. Waves of resistance: *Staphylococcus aureus* in the antibiotic era. Nat. Rev. Microbiol. 7, 629–641. https://doi.org/10.1038/nrmicro2200

Chan, S., Pullerits, K., Keucken, A., Persson, K.M., Paul, C.J., Rådström, P., 2019. Bacterial release from pipe biofilm in a full-scale drinking water distribution system. Npj Biofilms Microbiomes 5, 9. https://doi.org/10.1038/s41522-019-0082-9

Chandra Kalia, V., 2011. Genomic analysis reveals versatile organisms for quorum quenching enzymes: acyl-homoserine lactone-acylase and -lactonase. Open Microbiol. J. 3, 1–11. https://doi.org/10.2174/1874285801105010001

Chaston, J.M., Suen, G., Tucker, S.L., Andersen, A.W., Bhasin, A., Bode, E., Bode, H.B., Brachmann, A.O., Cowles, C.E., Cowles, K.N., Darby, C., de Léon, L., Drace, K., Du, Z., Givaudan, A., Herbert Tran, E.E., Jewell, K.A., Knack, J.J., Krasomil-Osterfeld, K.C., Kukor, R., Lanois, A., Latreille, P., Leimgruber, N.K., Lipke, C.M., Liu, R., Lu, X., Martens, E.C., Marri, P.R., Médigue, C., Menard, M.L., Miller, N.M., Morales-Soto, N., Norton, S., Ogier, J.-C., Orchard, S.S., Park, D., Park, Y., Qurollo, B.A., Sugar, D.R., Richards, G.R., Rouy, Z., Slominski, B., Slominski, K., Snyder, H., Tjaden, B.C., van der Hoeven, R., Welch, R.D., Wheeler, C., Xiang, B., Barbazuk, B., Gaudriault, S., Goodner, B., Slater, S.C., Forst, S., Goldman, B.S., Goodrich-Blair, H., 2011. The entomopathogenic bacterial endosymbionts *Xenorhabdus* and *Photorhabdus*: convergent lifestyles from divergent genomes. PLoS ONE 6, e27909. https://doi.org/10.1371/journal.pone.0027909

Chatterjee, S.N., Chaudhuri, K., 2006. Lipopolysaccharides of *Vibrio cholerae*: III. Biological functions. Biochim. Biophys. Acta BBA - Mol. Basis Dis. 1762, 1–16. https://doi.org/10.1016/j.bbadis.2005.08.005

Chattopadhyay, S., Perkins, S.D., Shaw, M., Nichols, T.L., 2017. Evaluation of exposure to *Brevundimonas diminuta* and *Pseudomonas aeruginosa* during showering. J. Aerosol Sci. 114, 77–93. https://doi.org/10.1016/j.jaerosci.2017.08.008

Chaudhari, B., Panda, B., Šavija, B., Chandra Paul, S., 2022. Microbiologically induced concrete corrosion: a concise review of assessment methods, effects, and corrosion-resistant coating materials. Materials 15, 4279. https://doi.org/10.3390/ma15124279

Chavant, P., Martinie, B., Meylheuc, T., Bellon-Fontaine, M.-N., Hebraud, M., 2002. *Listeria monocytogenes* LO28: surface physicochemical properties and ability to form biofilms at different temperatures and growth phases. Appl. Environ. Microbiol. 68, 728–737. https://doi.org/10.1128/AEM.68.2.728-737.2002

Chaves Simões, L., Simões, M., 2013. Biofilms in drinking water: problems and solutions. RSC Adv 3, 2520–2533. https://doi.org/10.1039/C2RA22243D

Chayen, N.E., Saridakis, E., 2008. Protein crystallization: from purified protein to diffraction-quality crystal. Nat. Methods 5, 147–153. https://doi.org/10.1038/nmeth.f.203

Chen, F., Gao, Y., Chen, X., Yu, Z., Li, X., 2013. Quorum quenching enzymes and their application in degrading signal molecules to block quorum sensing-dependent infection. Int. J. Mol. Sci. 14, 17477–17500. https://doi.org/10.3390/ijms140917477

Chen, M., Yu, Q., Sun, H., 2013. Novel strategies for the prevention and treatment of biofilm related infections. Int. J. Mol. Sci. 14, 18488–18501. https://doi.org/10.3390/ijms140918488
Cheng, Y., Liang, L., Ye, F., Zhao, S., 2021. Ce-MOF with intrinsic haloperoxidase-like activity for ratiometric colorimetric detection of hydrogen peroxide. Biosensors 11, 204. https://doi.org/10.3390/bios11070204
Cheong, J.Z.A., Johnson, C.J., Wan, H., Liu, A., Kernien, J.F., Gibson, A.L.F., Nett, J.E., Kalan, L.R., 2021. Priority effects dictate community structure and alter virulence of fungal-bacterial biofilms. ISME J. 15, 2012–2027. https://doi.org/10.1038/s41396-021-00901-5
Cherifi, T., Jacques, M., Quessy, S., Fravalo, P., 2017. Impact of nutrient restriction on the structure of *Listeria monocytogenes* biofilm grown in a microfluidic system. Front. Microbiol. 8, 864. https://doi.org/10.3389/fmicb.2017.00864
Chessa, D., Ganau, G., Mazzarello, V., 2015. An overview of *Staphylococcus epidermidis* and *Staphylococcus aureus* with a focus on developing countries. J. Infect. Dev. Ctries. 9, 547–550. https://doi.org/10.3855/jidc.6923
Choi, Y.C., Morgenroth, E., 2003. Monitoring biofilm detachment under dynamic changes in shear stress using laser-based particle size analysis and mass fractionation. Water Sci. Technol. 47, 69–76. https://doi.org/10.2166/wst.2003.0284
Chu, Y.-Y., Nega, M., Wölfle, M., Plener, L., Grond, S., Jung, K., Götz, F., 2013. A new class of quorum quenching molecules from *Staphylococcus* species affects communication and growth of Gram-negative bacteria. PLoS Pathog. 9, e1003654. https://doi.org/10.1371/journal.ppat.1003654
Chua, S.L., Liu, Y., Yam, J.K.H., Chen, Y., Vejborg, R.M., Tan, B.G.C., Kjelleberg, S., Tolker-Nielsen, T., Givskov, M., Yang, L., 2014. Dispersed cells represent a distinct stage in the transition from bacterial biofilm to planktonic lifestyles. Nat. Commun. 5, 4462. https://doi.org/10.1038/ncomms5462
Chugani, S., Greenberg, E.P., 2010. LuxR homolog-independent gene regulation by acyl-homoserine lactones in *Pseudomonas aeruginosa*. Proc. Natl. Acad. Sci. 107, 10673–10678. https://doi.org/10.1073/pnas.1005909107
Collins, M.D., Lund, B.M., Farrow, J.A.E., Schleifer, K.H., 1983. Chemotaxonomic study of an alkalophilic bacterium, *Exiguobacterium aurantiacum* gen. nov., sp. nov. Microbiology 129, 2037–2042. https://doi.org/10.1099/00221287-129-7-2037
Colvin, K.M., Irie, Y., Tart, C.S., Urbano, R., Whitney, J.C., Ryder, C., Howell, P.L., Wozniak, D.J., Parsek, M.R., 2012. The Pel and Psl polysaccharides provide *Pseudomonas aeruginosa* structural redundancy within the biofilm matrix. Environ. Microbiol. 14, 1913–1928. https://doi.org/10.1111/j.1462-2920.2011.02657.x
Compère, C., Bellon-Fontaine, M., Bertrand, P., Costa, D., Marcus, P., Poleunis, C., Pradier, C., Rondot, B., Walls, M.G., 2001. Kinetics of conditioning layer formation on stainless steel immersed in seawater. Biofouling 17, 129–145. https://doi.org/10.1080/08927010109378472
Conley, S., Franco, G., Faloona, I., Blake, D.R., Peischl, J., Ryerson, T.B., 2016. Methane emissions from the 2015 Aliso Canyon blowout in Los Angeles, CA. Science 351, 1317–1320. https://doi.org/10.1126/science.aaf2348
Cooke, A.C., Florez, C., Dunshee, E.B., Lieber, A.D., Terry, M.L., Light, C.J., Schertzer, J.W., 2020. *Pseudomonas* quinolone signal-induced outer membrane vesicles enhance biofilm dispersion in *Pseudomonas aeruginosa*. mSphere 5, e01109-20. https://doi.org/10.1128/mSphere.01109-20

Cooksey, K., Wigglesworth-Cooksey, B., 1995. Adhesion of bacteria and diatoms to surfaces in the sea: a review. Aquat. Microb. Ecol. 9, 87–96. https://doi.org/10.3354/ame009087
Coquant, G., Grill, J.-P., Seksik, P., 2020. Impact of N-acyl-homoserine lactones, quorum sensing molecules, on gut immunity. Front. Immunol. 11, 1827. https://doi.org/10.3389/fimmu.2020.01827
Cornforth, J.W., James, A.T., 1956. Structure of a naturally occurring antagonist of dihydrostreptomycin. Biochem. J. 63, 124–130. https://doi.org/10.1042/bj0630124
Costa, O.Y.A., Raaijmakers, J.M., Kuramae, E.E., 2018. Microbial extracellular polymeric substances: ecological function and impact on soil aggregation. Front. Microbiol. 9, 1636. https://doi.org/10.3389/fmicb.2018.01636
Costa-Orlandi, C., Sardi, J., Pitangui, N., de Oliveira, H., Scorzoni, L., Galeane, M., Medina-Alarcón, K., Melo, W., Marcelino, M., Braz, J., Fusco-Almeida, A., Mendes-Giannini, M., 2017. Fungal biofilms and polymicrobial diseases. J. Fungi 3, 22. https://doi.org/10.3390/jof3020022
Costerton, J.W., Cheng, K.J., Geesey, G.G., Ladd, T.I., Nickel, J.C., Dasgupta, M., Marrie, T.J., 1987. Bacterial biofilms in nature and disease. Annu. Rev. Microbiol. 41, 435–464. https://doi.org/10.1146/annurev.mi.41.100187.002251
Costerton, J.W., Lewandowski, Z., Caldwell, D.E., Korber, D.R., Lappin-Scott, H.M., 1995. Microbial biofilms. Annu. Rev. Microbiol. 49, 711–745. https://doi.org/10.1146/annurev.mi.49.100195.003431
Cotter, P.A., Stibitz, S., 2007. c-di-GMP-mediated regulation of virulence and biofilm formation. Curr. Opin. Microbiol. 10, 17–23. https://doi.org/10.1016/j.mib.2006.12.006
Crawford, J.M., Portmann, C., Zhang, X., Roeffaers, M.B.J., Clardy, J., 2012. Small molecule perimeter defense in entomopathogenic bacteria. Proc. Natl. Acad. Sci. 109, 10821–10826. https://doi.org/10.1073/pnas.1201160109
Crusz, S.A., Popat, R., Rybtke, M.T., Cámara, M., Givskov, M., Tolker-Nielsen, T., Diggle, S.P., Williams, P., 2012. Bursting the bubble on bacterial biofilms: a flow cell methodology. Biofouling 28, 835–842. https://doi.org/10.1080/08927014.2012.716044
Cude, W.N., Buchan, A., 2013. Acyl-homoserine lactone-based quorum sensing in the *Roseobacter* clade: complex cell-to-cell communication controls multiple physiologies. Front. Microbiol. 4. https://doi.org/10.3389/fmicb.2013.00336
Dai, T., Wen, D., Bates, C.T., Wu, L., Guo, X., Liu, S., Su, Y., Lei, J., Zhou, J., Yang, Y., 2022. Nutrient supply controls the linkage between species abundance and ecological interactions in marine bacterial communities. Nat. Commun. 13, 175. https://doi.org/10.1038/s41467-021-27857-6
Dang, H., Li, T., Chen, M., Huang, G., 2008. Cross-ocean distribution of *Rhodobacterales* bacteria as primary surface colonizers in temperate coastal marine waters. Appl. Environ. Microbiol. 74, 52–60. https://doi.org/10.1128/AEM.01400-07
Dang, H., Lovell, C.R., 2016. Microbial surface colonization and biofilm development in marine environments. Microbiol. Mol. Biol. Rev. 80, 91–138. https://doi.org/10.1128/MMBR.00037-15
Darouiche, R.O., 2001. Device-associated infections: a macroproblem that starts with microadherence. Clin. Infect. Dis. 33, 1567–1572. https://doi.org/10.1086/323130
Das, K., Rajawat, M.V.S., Saxena, A.K., Prasanna, R., 2017. Development of *Mesorhizobium ciceri*-based biofilms and analyses of their antifungal and plant

growth promoting activity in chickpea challenged by *Fusarium* wilt. Indian J. Microbiol. 57, 48–59. https://doi.org/10.1007/s12088-016-0610-8
Dassanayake, R.P., Falkenberg, S.M., Stasko, J.A., Shircliff, A.L., Lippolis, J.D., Briggs, R.E., 2020. Identification of a reliable fixative solution to preserve the complex architecture of bacterial biofilms for scanning electron microscopy evaluation. PLOS ONE 15, e0233973. https://doi.org/10.1371/journal.pone.0233973
Davies, D.G., Marques, C.N.H., 2009. A fatty acid messenger is responsible for inducing dispersion in microbial biofilms. J. Bacteriol. 191, 1393–1403. https://doi.org/10.1128/JB.01214-08
de Carvalho, C.C.C.R., 2018. Marine biofilms: a successful microbial strategy with economic implications. Front. Mar. Sci. 5, 126. https://doi.org/10.3389/fmars.2018.00126
de Carvalho, C.C.C.R., 2017. Biofilms: microbial strategies for surviving UV exposure, in: Ahmad, S.I. (Ed.), Ultraviolet Light in Human Health, Diseases and Environment, Advances in Experimental Medicine and Biology. Springer International Publishing, Cham, pp. 233–239. https://doi.org/10.1007/978-3-319-56017-5_19
de Kievit, T.R., 2009. Quorum sensing in *Pseudomonas aeruginosa* biofilms. Environ. Microbiol. 11, 279–288. https://doi.org/10.1111/j.1462-2920.2008.01792.x
de Kievit, T.R., Iglewski, B.H., 2000. Bacterial quorum sensing in pathogenic relationships. Infect. Immun. 68, 4839–4849. https://doi.org/10.1128/IAI.68.9.4839-4849.2000
de Kievit, T.R., Kakai, Y., Register, J.K., Pesci, E.C., Iglewski, B.H., 2002. Role of the *Pseudomonas aeruginosa las* and *rhl* quorum-sensing systems in *rhlI* regulation. FEMS Microbiol. Lett. 212, 101–106. https://doi.org/10.1111/j.1574-6968.2002.tb11251.x
de la Haba, R.R., Arahal, D.R., Sánchez-Porro, C., Ventosa, A., 2014. The family *Halomonadaceae*, in: Rosenberg, E., DeLong, E.F., Lory, S., Stackebrandt, E., Thompson, F. (Eds.), The Prokaryotes. Springer Berlin Heidelberg, Berlin, Heidelberg, pp. 325–360. https://doi.org/10.1007/978-3-642-38922-1_235
de Messano, L.V.R., Sathler, L., Reznik, L.Y., Coutinho, R., 2009. The effect of biofouling on localized corrosion of the stainless steels N08904 and UNS S32760. Int. Biodeterior. Biodegrad. 63, 607–614. https://doi.org/10.1016/j.ibiod.2009.04.006
de Vries, H.J., Beyer, F., Jarzembowska, M., Lipińska, J., van den Brink, P., Zwijnenburg, A., Timmers, P.H.A., Stams, A.J.M., Plugge, C.M., 2019. Isolation and characterization of *Sphingomonadaceae* from fouled membranes. Npj Biofilms Microbiomes 5, 6. https://doi.org/10.1038/s41522-018-0074-1
Dean, S.N., Chung, M.-C., van Hoek, M.L., 2015. *Burkholderia* diffusible signal factor signals to *Francisella novicida* to disperse biofilm and increase siderophore production. Appl. Environ. Microbiol. 81, 7057–7066. https://doi.org/10.1128/AEM.02165-15
Delago, A., Mandabi, A., Meijler, M.M., 2016. Natural quorum sensing inhibitors - small molecules, big messages. Isr. J. Chem. 56, 310–320. https://doi.org/10.1002/ijch.201500052
Demir, M., Salman, H., 2012. Bacterial thermotaxis by speed modulation. Biophys. J. 103, 1683–1690. https://doi.org/10.1016/j.bpj.2012.09.005

Demirel, Y.K., Uzun, D., Zhang, Y., Fang, H.-C., Day, A.H., Turan, O., 2017. Effect of barnacle fouling on ship resistance and powering. Biofouling 33, 819–834. https://doi.org/10.1080/08927014.2017.1373279
Deng, Y., Wang, L., Chen, Y., Long, Y., 2020. Optimization of staining with SYTO 9/propidium iodide: interplay, kinetics and impact on *Brevibacillus brevis*. BioTechniques 69, 88–98. https://doi.org/10.2144/btn-2020-0036
Denner, E.B., Paukner, S., Kämpfer, P., Moore, E.R., Abraham, W.R., Busse, H.J., Wanner, G., Lubitz, W., 2001. *Sphingomonas pituitosa* sp. nov., an exopolysaccharide-producing bacterium that secretes an unusual type of sphingan. Int. J. Syst. Evol. Microbiol. 51, 827–841. https://doi.org/10.1099/00207713-51-3-827
Deschaine, B.M., Heysel, A.R., Lenhart, B.A., Murphy, H.A., 2018. Biofilm formation and toxin production provide a fitness advantage in mixed colonies of environmental yeast isolates. Ecol. Evol. 8, 5541–5550. https://doi.org/10.1002/ece3.4082
Déziel, E., Lépine, F., Milot, S., He, J., Mindrinos, M.N., Tompkins, R.G., Rahme, L.G., 2004. Analysis of *Pseudomonas aeruginosa* 4-hydroxy-2-alkylquinolines (HAQs) reveals a role for 4-hydroxy-2-heptylquinoline in cell-to-cell communication. Proc. Natl. Acad. Sci. 101, 1339–1344. https://doi.org/10.1073/pnas.0307694100
Dhandapani, A., Krishnasamy, S., Muthukumar, C., Thiagamani, S.M.K., Nagarajan, R., Siengchin, S., 2022. Plastics in marine engineering, in: Encyclopedia of Materials: Plastics and Polymers. Elsevier, pp. 225–236. https://doi.org/10.1016/B978-0-12-820352-1.00058-4
Ding, F., Oinuma, K.-I., Smalley, N.E., Schaefer, A.L., Hamwy, O., Greenberg, E.P., Dandekar, A.A., 2018. The *Pseudomonas aeruginosa* orphan quorum sensing signal receptor QscR regulates global quorum sensing gene expression by activating a single linked operon. mBio 9, e01274-18. https://doi.org/10.1128/mBio.01274-18
Dogs, M., Voget, S., Teshima, H., Petersen, J., Davenport, K., Dalingault, H., Chen, A., Pati, A., Ivanova, N., Goodwin, L.A., Chain, P., Detter, J.C., Standfest, S., Rohde, M., Gronow, S., Kyrpides, N.C., Woyke, T., Simon, M., Klenk, H.-P., Göker, M., Brinkhoff, T., 2013. Genome sequence of *Phaeobacter inhibens* type strain (T5T), a secondary metabolite producing representative of the marine *Roseobacter* clade, and emendation of the species description of *Phaeobacter inhibens*. Stand. Genomic Sci. 9, 334–350. https://doi.org/10.4056/sigs.4448212
Dong, Y.-H., Wang, L.-H., Zhang, L.-H., 2007. Quorum-quenching microbial infections: mechanisms and implications. Philos. Trans. R. Soc. B Biol. Sci. 362, 1201–1211. https://doi.org/10.1098/rstb.2007.2045
Dongari-Bagtzoglou, A., 2008. Pathogenesis of mucosal biofilm infections: challenges and progress. Expert Rev. Anti Infect. Ther. 6, 201–208. https://doi.org/10.1586/14787210.6.2.201
Donlan, R., 2001. Biofilms and device-associated infections. Emerg. Infect. Dis. 7, 277–281. https://doi.org/10.3201/eid0702.010226
Donlan, R.M., 2002. Biofilms: microbial life on surfaces. Emerg. Infect. Dis. 8, 881–890. https://doi.org/10.3201/eid0809.020063
Dören, R., 2022. Syntheses and applications of tungsten oxide-based nanocrystals (Dissertation). Johannes Gutenberg-Universität Mainz.
Dören, R., Hartmann, J., Leibauer, B., Panthöfer, M., Mondeshki, M., Tremel, W., 2021a. Magneli-type tungsten oxide nanorods as catalysts for the selective

oxidation of organic sulfides. Dalton Trans. 50, 14027–14037. https://doi.org/10.1039/D1DT02243A
Dören, R., Leibauer, B., Lange, M.A., Schechtel, E., Prädel, L., Panthöfer, M., Mondeshki, M., Tremel, W., 2021b. Gram-scale selective synthesis of WO_{3-x} nanorods and $(NH_4)_x WO_3$ ammonium tungsten bronzes with tunable plasmonic properties. Nanoscale 13, 8146–8162. https://doi.org/10.1039/D0NR09055G
Dou, W., Xu, D., Gu, T., 2021. Biocorrosion caused by microbial biofilms is ubiquitous around us. Microb. Biotechnol. 14, 803–805. https://doi.org/10.1111/1751-7915.13690
Douterelo, I., Husband, S., Loza, V., Boxall, J., 2016. Dynamics of biofilm regrowth in drinking water distribution systems. Appl. Environ. Microbiol. 82, 4155–4168. https://doi.org/10.1128/AEM.00109-16
Dow, J.M., Crossman, L., Findlay, K., He, Y.-Q., Feng, J.-X., Tang, J.-L., 2003. Biofilm dispersal in *Xanthomonas campestris* is controlled by cell–cell signaling and is required for full virulence to plants. Proc. Natl. Acad. Sci. 100, 10995–11000. https://doi.org/10.1073/pnas.1833360100
Dragoš, A., Kiesewalter, H., Martin, M., Hsu, C.-Y., Hartmann, R., Wechsler, T., Eriksen, C., Brix, S., Drescher, K., Stanley-Wall, N., Kümmerli, R., Kovács, Á.T., 2018. Division of labor during biofilm matrix production. Curr. Biol. 28, 1903-1913.e5. https://doi.org/10.1016/j.cub.2018.04.046
Dunne, W.M., 2002. Bacterial adhesion: seen any good biofilms lately? Clin. Microbiol. Rev. 15, 155–166. https://doi.org/10.1128/CMR.15.2.155-166.2002
Dutta, S., Samanta, P., Dhara, D., 2016. Temperature, pH and redox responsive cellulose based hydrogels for protein delivery. Int. J. Biol. Macromol. 87, 92–100. https://doi.org/10.1016/j.ijbiomac.2016.02.042
Egbuna, C., 2019. An unusual color change in tetracycline HCl powder – from drug to poison. Med. J. Dr Patil Vidyapeeth 12, 152. https://doi.org/10.4103/mjdrdypu.mjdrdypu_97_18
Eickhoff, M.J., Bassler, B.L., 2018. SnapShot: bacterial quorum sensing. Cell 174, 1328-1328.e1. https://doi.org/10.1016/j.cell.2018.08.003
El-Ganiny, A.M., Shaker, G.H., Aboelazm, A.A., El-Dash, H.A., 2017. Prevention of bacterial biofilm formation on soft contact lenses using natural compounds. J. Ophthalmic Inflamm. Infect. 7, 11. https://doi.org/10.1186/s12348-017-0129-0
Elias, S., Banin, E., 2012. Multi-species biofilms: living with friendly neighbors. FEMS Microbiol. Rev. 36, 990–1004. https://doi.org/10.1111/j.1574-6976.2012.00325.x
El-Liethy, M.A., Hemdan, B.A., El-Taweel, G.E., 2018. Phenotyping using semi-automated BIOLOG and conventional PCR for identification of *Bacillus* isolated from biofilm of sink drainage pipes. Acta Ecol. Sin. 38, 334–338. https://doi.org/10.1016/j.chnaes.2018.01.011
Elshaer, S.L., Shaaban, M.I., 2021. Inhibition of quorum sensing and virulence factors of *Pseudomonas aeruginosa* by biologically synthesized gold and selenium nanoparticles. Antibiotics 10, 1461. https://doi.org/10.3390/antibiotics10121461
Engebrecht, J., Nealson, K., Silverman, M., 1983. Bacterial bioluminescence: isolation and genetic analysis of functions from *Vibrio fischeri*. Cell 32, 773–781. https://doi.org/10.1016/0092-8674(83)90063-6
Engebrecht, J., Silverman, M., 1984. Identification of genes and gene products necessary for bacterial bioluminescence. Proc. Natl. Acad. Sci. 81, 4154–4158. https://doi.org/10.1073/pnas.81.13.4154

Englert, D.L., Manson, M.D., Jayaraman, A., 2009. Flow-based microfluidic device for quantifying bacterial chemotaxis in stable, competing gradients. Appl. Environ. Microbiol. 75, 4557–4564. https://doi.org/10.1128/AEM.02952-08
Ercan, D., Demirci, A., 2015. Current and future trends for biofilm reactors for fermentation processes. Crit. Rev. Biotechnol. 35, 1–14. https://doi.org/10.3109/07388551.2013.793170
Fabra, M., Williams, L., Watts, J.E.M., Hale, M.S., Couceiro, F., Preston, J., 2021. The plastic Trojan horse: biofilms increase microplastic uptake in marine filter feeders impacting microbial transfer and organism health. Sci. Total Environ. 797, 149217. https://doi.org/10.1016/j.scitotenv.2021.149217
Falkinham, J., 2015. Common features of opportunistic premise plumbing pathogens. Int. J. Environ. Res. Public. Health 12, 4533–4545. https://doi.org/10.3390/ijerph120504533
Falkinham, J., Pruden, A., Edwards, M., 2015. Opportunistic premise plumbing pathogens: increasingly important pathogens in drinking water. Pathogens 4, 373–386. https://doi.org/10.3390/pathogens4020373
Fang, H., Toyofuku, M., Kiyokawa, T., Ichihashi, A., Tateda, K., Nomura, N., 2013. The impact of anaerobiosis on strain-dependent phenotypic variations in *Pseudomonas aeruginosa*. Biosci. Biotechnol. Biochem. 77, 1747–1752. https://doi.org/10.1271/bbb.130309
Farkas, A., Song, S., Degiuli, N., Martić, I., Demirel, Y.K., 2020. Impact of biofilm on the ship propulsion characteristics and the speed reduction. Ocean Eng. 199, 107033. https://doi.org/10.1016/j.oceaneng.2020.107033
Feng, G.-D., Yang, S.-Z., Zhu, H.-H., Li, H.-P., 2018. Emended descriptions of the species *Sphingomonas adhaesiva* Yabuuchi et al. 1990 and *Sphingomonas ginsenosidimutans* Choi et al. 2011. Int. J. Syst. Evol. Microbiol. 68, 970–973. https://doi.org/10.1099/ijsem.0.002557
Filardo, S., Di Pietro, M., Tranquilli, G., Sessa, R., 2019. Biofilm in genital ecosystem: a potential risk factor for *Chlamydia trachomatis* infection. Can. J. Infect. Dis. Med. Microbiol. 2019, 1–6. https://doi.org/10.1155/2019/1672109
Fischer-Le Saux, M., Viallard, V., Brunel, B., Normand, P., Boemare, N.E., 1999. Polyphasic classification of the genus *Photorhabdus* and proposal of new taxa: *P. luminescens* subsp. *luminescens* subsp. nov., *P. luminescens* subsp. *akhurstii* subsp. nov., *P. luminescens* subsp. *laumondii* subsp. nov., *P. temperata* sp. nov., *P. temperata* subsp. *temperata* subsp. nov. and *P. asymbiotica* sp. nov. Int. J. Syst. Evol. Microbiol. 49, 1645–1656. https://doi.org/10.1099/00207713-49-4-1645
Fish, K.E., Boxall, J.B., 2018. Biofilm microbiome (re)growth dynamics in drinking water distribution systems are impacted by chlorine concentration. Front. Microbiol. 9, 2519. https://doi.org/10.3389/fmicb.2018.02519
Fish, K.E., Osborn, A.M., Boxall, J., 2016. Characterising and understanding the impact of microbial biofilms and the extracellular polymeric substance (EPS) matrix in drinking water distribution systems. Environ. Sci. Water Res. Technol. 2, 614–630. https://doi.org/10.1039/C6EW00039H
Fitridge, I., Dempster, T., Guenther, J., de Nys, R., 2012. The impact and control of biofouling in marine aquaculture: a review. Biofouling 28, 649–669. https://doi.org/10.1080/08927014.2012.700478
Fleming, D., Rumbaugh, K., 2018. The consequences of biofilm dispersal on the host. Sci. Rep. 8, 10738. https://doi.org/10.1038/s41598-018-29121-2
Fleming, D., Rumbaugh, K., 2017. Approaches to dispersing medical biofilms. Microorganisms 5, 15. https://doi.org/10.3390/microorganisms5020015

Flemming, H.-C., 2020. Biofouling and me: my Stockholm syndrome with biofilms. Water Res. 173, 115576. https://doi.org/10.1016/j.watres.2020.115576
Flemming, H.-C., 2002. Biofouling in water systems – cases, causes and countermeasures. Appl. Microbiol. Biotechnol. 59, 629–640. https://doi.org/10.1007/s00253-002-1066-9
Flemming, H.-C., Neu, T.R., Wozniak, D.J., 2007. The EPS matrix: the "house of biofilm cells." J. Bacteriol. 189, 7945–7947. https://doi.org/10.1128/JB.00858-07
Flemming, H.-C., Schaule, G., Griebe, T., Schmitt, J., Tamachkiarowa, A., 1997. Biofouling—the Achilles heel of membrane processes. Desalination 113, 215–225. https://doi.org/10.1016/S0011-9164(97)00132-X
Flemming, H.-C., Wingender, J., 2010. The biofilm matrix. Nat. Rev. Microbiol. 8, 623–633. https://doi.org/10.1038/nrmicro2415
Flemming, H.-C., Wingender, J., Szewzyk, U., Steinberg, P., Rice, S.A., Kjelleberg, S., 2016. Biofilms: an emergent form of bacterial life. Nat. Rev. Microbiol. 14, 563–575. https://doi.org/10.1038/nrmicro.2016.94
Flemming, H.-C., Wuertz, S., 2019. Bacteria and archaea on Earth and their abundance in biofilms. Nat. Rev. Microbiol. 17, 247–260. https://doi.org/10.1038/s41579-019-0158-9
Fletcher, M., 1994. Bacterial biofilms and biofouling. Curr. Opin. Biotechnol. 5, 302–306. https://doi.org/10.1016/0958-1669(94)90033-7
Forst, S., Dowds, B., Boemare, N., Stackebrandt, E., 1997. *Xenorhabdus* and *Photorhabdus* spp.: bugs that kill bugs. Annu. Rev. Microbiol. 51, 47–72. https://doi.org/10.1146/annurev.micro.51.1.47
Francius, G., El Zein, R., Mathieu, L., Gosselin, F., Maul, A., Block, J.-C., 2017. Nano-exploration of organic conditioning film formed on polymeric surfaces exposed to drinking water. Water Res. 109, 155–163. https://doi.org/10.1016/j.watres.2016.11.038
Fredrickson, J.K., 2015. Ecological communities by design. Science 348, 1425–1427. https://doi.org/10.1126/science.aab0946
Frerichs, H., 2020. Nano-Ceroxid und Komposite: Bismut substituiertes Ceroxid als Katalysator zur oxidativen Bromierung (Dissertation). Johannes Gutenberg-Universität Mainz.
Frerichs, H., Pütz, E., Pfitzner, F., Reich, T., Gazanis, A., Panthöfer, M., Hartmann, J., Jegel, O., Heermann, R., Tremel, W., 2020. Nanocomposite antimicrobials prevent bacterial growth through the enzyme-like activity of Bi-doped cerium dioxide ($Ce_{1-x}Bi_xO_{2-\delta}$). Nanoscale 12, 21344–21358. https://doi.org/10.1039/D0NR06165D
Friend, J., Yeo, L., 2010. Fabrication of microfluidic devices using polydimethylsiloxane. Biomicrofluidics 4, 026502. https://doi.org/10.1063/1.3259624
Fuchs, S.W., Proschak, A., Jaskolla, T.W., Karas, M., Bode, H.B., 2011. Structure elucidation and biosynthesis of lysine-rich cyclic peptides in *Xenorhabdus nematophila*. Org. Biomol. Chem. 9, 3130. https://doi.org/10.1039/c1ob05097d
Fugère, A., Lalonde Séguin, D., Mitchell, G., Déziel, E., Dekimpe, V., Cantin, A.M., Frost, E., Malouin, F., 2014. Interspecific small molecule interactions between clinical isolates of *Pseudomonas aeruginosa* and *Staphylococcus aureus* from adult cystic fibrosis patients. PLoS ONE 9, e86705. https://doi.org/10.1371/journal.pone.0086705

Fukami, T., 2015. Historical contingency in community assembly: integrating niches, species pools, and priority effects. Annu. Rev. Ecol. Evol. Syst. 46, 1–23. https://doi.org/10.1146/annurev-ecolsys-110411-160340
Fuqua, C., 2006. The QscR quorum-sensing regulon of *Pseudomonas aeruginosa* : an orphan claims its identity. J. Bacteriol. 188, 3169–3171. https://doi.org/10.1128/JB.188.9.3169-3171.2006
Galié, S., García-Gutiérrez, C., Miguélez, E.M., Villar, C.J., Lombó, F., 2018. Biofilms in the food industry: health aspects and control methods. Front. Microbiol. 9, 898. https://doi.org/10.3389/fmicb.2018.00898
Galloway, W.R.J.D., Hodgkinson, J.T., Bowden, S.D., Welch, M., Spring, D.R., 2011. Quorum sensing in Gram-negative bacteria: small-molecule modulation of AHL and AI-2 quorum sensing pathways. Chem. Rev. 111, 28–67. https://doi.org/10.1021/cr100109t
Garrett, T.R., Bhakoo, M., Zhang, Z., 2008. Bacterial adhesion and biofilms on surfaces. Prog. Nat. Sci. 18, 1049–1056. https://doi.org/10.1016/j.pnsc.2008.04.001
Garrity, G.M., Bell, J.A., Lilburn, T., 2015. *Rhodobacteraceae fam. nov.*, in: Whitman, W.B., Rainey, F., Kämpfer, P., Trujillo, M., Chun, J., DeVos, P., Hedlund, B., Dedysh, S. (Eds.), Bergey's Manual of Systematics of Archaea and Bacteria. Wiley, pp. 1–2. https://doi.org/10.1002/9781118960608.fbm00173
Geisinger, E., Muir, T.W., Novick, R.P., 2009. *agr* receptor mutants reveal distinct modes of inhibition by staphylococcal autoinducing peptides. Proc. Natl. Acad. Sci. 106, 1216–1221. https://doi.org/10.1073/pnas.0807760106
Geoghegan, J.A., Corrigan, R.M., Gruszka, D.T., Speziale, P., O'Gara, J.P., Potts, J.R., Foster, T.J., 2010. Role of surface protein SasG in biofilm formation by *Staphylococcus aureus*. J. Bacteriol. 192, 5663–5673. https://doi.org/10.1128/JB.00628-10
Gerlach, R., Hensel, M., 2007. Protein secretion systems and adhesins: The molecular armory of Gram-negative pathogens. Int. J. Med. Microbiol. 297, 401–415. https://doi.org/10.1016/j.ijmm.2007.03.017
Gharatape, A., Davaran, S., Salehi, R., Hamishehkar, H., 2016. Engineered gold nanoparticles for photothermal cancer therapy and bacteria killing. RSC Adv. 6, 111482–111516. https://doi.org/10.1039/C6RA18760A
Gibson, T., 1944. 306. A study of *Bacillus subtilis* and related organisms. J. Dairy Res. 13, 248–260. https://doi.org/10.1017/S0022029900003848
Gjermansen, M., Nilsson, M., Yang, L., Tolker-Nielsen, T., 2010. Characterization of starvation-induced dispersion in *Pseudomonas putida* biofilms: genetic elements and molecular mechanisms. Mol. Microbiol. 75, 815–826. https://doi.org/10.1111/j.1365-2958.2009.06793.x
Gjermansen, M., Ragas, P., Sternberg, C., Molin, S., Tolker-Nielsen, T., 2005. Characterization of starvation-induced dispersion in *Pseudomonas putida* biofilms: programmed dispersal of *P. putida* biofilms. Environ. Microbiol. 7, 894–904. https://doi.org/10.1111/j.1462-2920.2005.00775.x
Glaeser, S.P., Tobias, N.J., Thanwisai, A., Chantratita, N., Bode, H.B., Kämpfer, P., 2017. *Photorhabdus luminescens* subsp. *namnaonensis* subsp. nov., isolated from *Heterorhabditis baujardi* nematodes. Int. J. Syst. Evol. Microbiol. 67, 1046–1051. https://doi.org/10.1099/ijsem.0.001761
Glick, R., Gilmour, C., Tremblay, J., Satanower, S., Avidan, O., Déziel, E., Greenberg, E.P., Poole, K., Banin, E., 2010. Increase in rhamnolipid synthesis under iron-limiting conditions influences surface motility and biofilm formation

in *Pseudomonas aeruginosa*. J. Bacteriol. 192, 2973–2980. https://doi.org/10.1128/JB.01601-09
Goller, C.C., Romeo, T., 2008. Environmental influences on biofilm development, in: Romeo, T. (Ed.), Bacterial Biofilms, Current Topics in Microbiology and Immunology. Springer Berlin Heidelberg, Berlin, Heidelberg, pp. 37–66. https://doi.org/10.1007/978-3-540-75418-3_3
Gómez-Gómez, B., Arregui, L., Serrano, S., Santos, A., Pérez-Corona, T., Madrid, Y., 2019. Unravelling mechanisms of bacterial quorum sensing disruption by metal-based nanoparticles. Sci. Total Environ. 696, 133869. https://doi.org/10.1016/j.scitotenv.2019.133869
Gómez-Suárez, C., Busscher, H.J., van der Mei, H.C., 2001. Analysis of bacterial detachment from substratum surfaces by the passage of air-liquid Interfaces. Appl. Environ. Microbiol. 67, 2531–2537. https://doi.org/10.1128/AEM.67.6.2531-2537.2001
Gorbushina, A.A., Broughton, W.J., 2009. Microbiology of the atmosphere-rock interface: how biological interactions and physical stresses modulate a sophisticated microbial ecosystem. Annu. Rev. Microbiol. 63, 431–450. https://doi.org/10.1146/annurev.micro.091208.073349
Gram, L., Rasmussen, B.B., Wemheuer, B., Bernbom, N., Ng, Y.Y., Porsby, C.H., Breider, S., Brinkhoff, T., 2015. *Phaeobacter inhibens* from the *Roseobacter* clade has an environmental niche as a surface colonizer in harbors. Syst. Appl. Microbiol. 38, 483–493. https://doi.org/10.1016/j.syapm.2015.07.006
Grandclément, C., Tannières, M., Moréra, S., Dessaux, Y., Faure, D., 2016. Quorum quenching: role in nature and applied developments. FEMS Microbiol. Rev. 40, 86–116. https://doi.org/10.1093/femsre/fuv038
Graziano, A., Jaffer, S., Sain, M., 2019. Review on modification strategies of polyethylene/polypropylene immiscible thermoplastic polymer blends for enhancing their mechanical behavior. J. Elastomers Plast. 51, 291–336. https://doi.org/10.1177/0095244318783806
Green, P.N., Bousfield, I.J., 1982. A taxonomic study of some Gram-negative facultatively methylotrophic bacteria. Microbiology 128, 623–638. https://doi.org/10.1099/00221287-128-3-623
Grigore, M., 2017. Methods of recycling, properties and applications of recycled thermoplastic polymers. Recycling 2, 24. https://doi.org/10.3390/recycling2040024
Groleau, M.-C., de Oliveira Pereira, T., Dekimpe, V., Déziel, E., 2020. PqsE is essential for RhlR-dependent quorum sensing regulation in *Pseudomonas aeruginosa*. mSystems 5, e00194-20. https://doi.org/10.1128/mSystems.00194-20
Grünberger, A., Probst, C., Helfrich, S., Nanda, A., Stute, B., Wiechert, W., von Lieres, E., Nöh, K., Frunzke, J., Kohlheyer, D., 2015. Spatiotemporal microbial single-cell analysis using a high-throughput microfluidics cultivation platform: single-cell analysis in microfluidics. Cytometry A 87, 1101–1115. https://doi.org/10.1002/cyto.a.22779
Guan, P., Terigele, Schmidt, F., Riemann, M., Fischer, J., Thines, E., Nick, P., 2020. Hunting modulators of plant defence: the grapevine trunk disease fungus *Eutypa lata* secretes an amplifier for plant basal immunity. J. Exp. Bot. 71, 3710–3724. https://doi.org/10.1093/jxb/eraa152
Guilhen, C., Charbonnel, N., Parisot, N., Gueguen, N., Iltis, A., Forestier, C., Balestrino, D., 2016. Transcriptional profiling of *Klebsiella pneumoniae* defines

signatures for planktonic, sessile and biofilm-dispersed cells. BMC Genomics 17, 237. https://doi.org/10.1186/s12864-016-2557-x
Guilhen, C., Forestier, C., Balestrino, D., 2017. Biofilm dispersal: multiple elaborate strategies for dissemination of bacteria with unique properties. Mol. Microbiol. 105, 188–210. https://doi.org/10.1111/mmi.13698
Guillonneau, R., Baraquet, C., Bazire, A., Molmeret, M., 2018. Multispecies biofilm development of marine bacteria implies complex relationships through competition and synergy and modification of matrix components. Front. Microbiol. 9, 1960. https://doi.org/10.3389/fmicb.2018.01960
Guo, H., Yi, W., Song, J., Wang, P., 2008. Current understanding on biosynthesis of microbial polysaccharides. Curr. Top. Med. Chem. 8, 141–151. https://doi.org/10.2174/156802608783378873
Gutiérrez-Barranquero, J.A., Reen, F.J., McCarthy, R.R., O'Gara, F., 2015. Deciphering the role of coumarin as a novel quorum sensing inhibitor suppressing virulence phenotypes in bacterial pathogens. Appl. Microbiol. Biotechnol. 99, 3303–3316. https://doi.org/10.1007/s00253-015-6436-1
Guzmán-Soto, I., McTiernan, C., Gonzalez-Gomez, M., Ross, A., Gupta, K., Suuronen, E.J., Mah, T.-F., Griffith, M., Alarcon, E.I., 2021. Mimicking biofilm formation and development: recent progress in *in vitro* and *in vivo* biofilm models. iScience 24, 102443. https://doi.org/10.1016/j.isci.2021.102443
Ha, D.-G., O'Toole, G.A., 2015. c-di-GMP and its effects on biofilm formation and dispersion: a *Pseudomonas aeruginosa* review. Microbiol. Spectr. 3, 3.2.27. https://doi.org/10.1128/microbiolspec.MB-0003-2014
Hakim, M.L., Nugroho, B., Nurrohman, M.N., Suastika, I.K., Utama, I.K.A.P., 2019. Investigation of fuel consumption on an operating ship due to biofouling growth and quality of anti-fouling coating. IOP Conf. Ser. Earth Environ. Sci. 339, 012037. https://doi.org/10.1088/1755-1315/339/1/012037
Halabi, M., Wiesholzer-Pittl, M., Schöberl, J., Mittermayer, H., 2001. Non-touch fittings in hospitals: a possible source of *Pseudomonas aeruginosa* and *Legionella* spp. J. Hosp. Infect. 49, 117–121. https://doi.org/10.1053/jhin.2001.1060
Halldorsson, S., Lucumi, E., Gómez-Sjöberg, R., Fleming, R.M.T., 2015. Advantages and challenges of microfluidic cell culture in polydimethylsiloxane devices. Biosens. Bioelectron. 63, 218–231. https://doi.org/10.1016/j.bios.2014.07.029
Hall-Stoodley, L., Costerton, J.W., Stoodley, P., 2004. Bacterial biofilms: from the natural environment to infectious diseases. Nat. Rev. Microbiol. 2, 95–108. https://doi.org/10.1038/nrmicro821
Hamilos, D.L., 2019. Biofilm formations in pediatric respiratory tract infection: Part 1: biofilm structure, role of innate immunity in protection against and response to biofilm, methods of biofilm detection, pediatric respiratory tract diseases associated with mucosal biofilm formation. Curr. Infect. Dis. Rep. 21, 6. https://doi.org/10.1007/s11908-019-0658-9
Han, R., Ehlers, R.-U., 2000. Pathogenicity, development, and reproduction of *Heterorhabditis bacteriophora* and *Steinernema carpocapsae* under axenic *in vivo* conditions. J. Invertebr. Pathol. 75, 55–58. https://doi.org/10.1006/jipa.1999.4900
Haque, S., Yadav, D.K., Bisht, S.C., Yadav, N., Singh, V., Dubey, K.K., Jawed, A., Wahid, M., Dar, S.A., 2019. Quorum sensing pathways in Gram-positive and -negative bacteria: potential of their interruption in abating drug resistance. J. Chemother. 31, 161–187. https://doi.org/10.1080/1120009X.2019.1599175

Harrison, J.J., Ceri, H., Turner, R.J., 2007. Multimetal resistance and tolerance in microbial biofilms. Nat. Rev. Microbiol. 5, 928–938. https://doi.org/10.1038/nrmicro1774
Hathroubi, S., Mekni, M.A., Domenico, P., Nguyen, D., Jacques, M., 2017. Biofilms: microbial shelters against antibiotics. Microb. Drug Resist. 23, 147–156. https://doi.org/10.1089/mdr.2016.0087
Hayat, S., Muzammil, S., Shabana, Aslam, B., Siddique, M.H., Saqalein, M., Nisar, M.A., 2019. Quorum quenching: role of nanoparticles as signal jammers in Gram-negative bacteria. Future Microbiol. 14, 61–72. https://doi.org/10.2217/fmb-2018-0257
Hayward, C., Ross, K.E., Brown, M.H., Bentham, R., Whiley, H., 2022. The presence of opportunistic premise plumbing pathogens in residential buildings: a literature review. Water 14, 1129. https://doi.org/10.3390/w14071129
Hazan, R., Que, Y.A., Maura, D., Strobel, B., Majcherczyk, P.A., Hopper, L.R., Wilbur, D.J., Hreha, T.N., Barquera, B., Rahme, L.G., 2016. Auto poisoning of the respiratory chain by a quorum-sensing-regulated molecule favors biofilm formation and antibiotic tolerance. Curr. Biol. 26, 195–206. https://doi.org/10.1016/j.cub.2015.11.056
He, J., Baldini, R.L., Déziel, E., Saucier, M., Zhang, Q., Liberati, N.T., Lee, D., Urbach, J., Goodman, H.M., Rahme, L.G., 2004. The broad host range pathogen *Pseudomonas aeruginosa* strain PA14 carries two pathogenicity islands harboring plant and animal virulence genes. Proc. Natl. Acad. Sci. 101, 2530–2535. https://doi.org/10.1073/pnas.0304622101
Heeb, S., Fletcher, M.P., Chhabra, S.R., Diggle, S.P., Williams, P., Cámara, M., 2011. Quinolones: from antibiotics to autoinducers. FEMS Microbiol. Rev. 35, 247–274. https://doi.org/10.1111/j.1574-6976.2010.00247.x
Hengge, R., 2009. Principles of c-di-GMP signalling in bacteria. Nat. Rev. Microbiol. 7, 263–273. https://doi.org/10.1038/nrmicro2109
Herget, K., Hubach, P., Pusch, S., Deglmann, P., Götz, H., Gorelik, T.E., Gural'skiy, I.A., Pfitzner, F., Link, T., Schenk, S., Panthöfer, M., Ksenofontov, V., Kolb, U., Opatz, T., André, R., Tremel, W., 2017. Haloperoxidase mimicry by CeO_{2-x} nanorods combats biofouling. Adv. Mater. 29, 1603823. https://doi.org/10.1002/adma.201603823
Hofer, U., 2022. The cost of biofilms. Nat. Rev. Microbiol. https://doi.org/10.1038/s41579-022-00758-1
Hoffman, L.R., Déziel, E., D'Argenio, D.A., Lépine, F., Emerson, J., McNamara, S., Gibson, R.L., Ramsey, B.W., Miller, S.I., 2006. Selection for *Staphylococcus aureus* small-colony variants due to growth in the presence of *Pseudomonas aeruginosa*. Proc. Natl. Acad. Sci. 103, 19890–19895. https://doi.org/10.1073/pnas.0606756104
Hoffman, M.D., Zucker, L.I., Brown, P.J.B., Kysela, D.T., Brun, Y.V., Jacobson, S.C., 2015. Timescales and frequencies of reversible and irreversible adhesion events of single bacterial cells. Anal. Chem. 87, 12032–12039. https://doi.org/10.1021/acs.analchem.5b02087
Hogt, A.H., Dankert, J., Feijen, J., 1985. Adhesion of *Staphylococcus epidermidis* and *Staphylococcus saprophyticus* to a hydrophobic biomaterial. Microbiology 131, 2485–2491. https://doi.org/10.1099/00221287-131-9-2485
Hornby, J.M., Jensen, E.C., Lisec, A.D., Tasto, J.J., Jahnke, B., Shoemaker, R., Dussault, P., Nickerson, K.W., 2001. Quorum sensing in the dimorphic fungus *Candida albicans* is mediated by farnesol. Appl. Environ. Microbiol. 67, 2982–2992. https://doi.org/10.1128/AEM.67.7.2982-2992.2001

Hoštacká, A., Čižnár, I., Štefkovičová, M., 2010. Temperature and pH affect the production of bacterial biofilm. Folia Microbiol. (Praha) 55, 75–78. https://doi.org/10.1007/s12223-010-0012-y
Hou, J., Veeregowda, D.H., van de Belt-Gritter, B., Busscher, H.J., van der Mei, H.C., 2018. Extracellular polymeric matrix production and relaxation under fluid shear and mechanical pressure in *Staphylococcus aureus* biofilms. Appl. Environ. Microbiol. 84, e01516-17. https://doi.org/10.1128/AEM.01516-17
Hu, J.-J., Cheng, Y.-J., Zhang, X.-Z., 2018. Recent advances in nanomaterials for enhanced photothermal therapy of tumors. Nanoscale 10, 22657–22672. https://doi.org/10.1039/C8NR07627H
Hu, X., Kang, F., Yang, B., Zhang, W., Qin, C., Gao, Y., 2019. Extracellular polymeric substances acting as a permeable barrier hinder the lateral transfer of antibiotic resistance genes. Front. Microbiol. 10, 736. https://doi.org/10.3389/fmicb.2019.00736
Huang, J.J., Petersen, A., Whiteley, M., Leadbetter, J.R., 2006. Identification of QuiP, the product of gene *PA1032*, as the second acyl-homoserine lactone acylase of *Pseudomonas aeruginosa* PAO1. Appl. Environ. Microbiol. 72, 1190–1197. https://doi.org/10.1128/AEM.72.2.1190-1197.2006
Hudaiberdiev, S., Choudhary, K.S., Vera Alvarez, R., Gelencsér, Z., Ligeti, B., Lamba, D., Pongor, S., 2015. Census of solo LuxR genes in prokaryotic genomes. Front. Cell. Infect. Microbiol. 5. https://doi.org/10.3389/fcimb.2015.00020
Inbakandan, D., Sriyutha Murthy, P., Venkatesan, R., Ajmal Khan, S., 2010. 16S rDNA sequence analysis of culturable marine biofilm forming bacteria from a ship's hull. Biofouling 26, 893–899. https://doi.org/10.1080/08927014.2010.530347
Ivanova, A., Ivanova, K., Tied, A., Heinze, T., Tzanov, T., 2020. Layer-by-layer coating of aminocellulose and quorum quenching acylase on silver nanoparticles synergistically eradicate bacteria and their biofilms. Adv. Funct. Mater. 30, 2001284. https://doi.org/10.1002/adfm.202001284
Jain, A., Bhosle, N.B., 2009. Biochemical composition of the marine conditioning film: implications for bacterial adhesion. Biofouling 25, 13–19. https://doi.org/10.1080/08927010802411969
Jamal, M., Ahmad, W., Andleeb, S., Jalil, F., Imran, M., Nawaz, M.A., Hussain, T., Ali, M., Rafiq, M., Kamil, M.A., 2018. Bacterial biofilm and associated infections. J. Chin. Med. Assoc. 81, 7–11. https://doi.org/10.1016/j.jcma.2017.07.012
Javed, M.A., Stoddart, P.R., Wade, S.A., 2015. Corrosion of carbon steel by sulphate reducing bacteria: initial attachment and the role of ferrous ions. Corros. Sci. 93, 48–57. https://doi.org/10.1016/j.corsci.2015.01.006
Jegel, O., 2022. Synthesis and application of CeO_2 nanoparticles as catalyst for oxidative bromination (Dissertation). Johannes Gutenberg-Universität Mainz.
Jegel, O., Pfitzner, F., Gazanis, A., Oberländer, J., Pütz, E., Lange, M., von der Au, M., Meermann, B., Mailänder, V., Klasen, A., Heermann, R., Tremel, W., 2022. Transparent polycarbonate coated with CeO_2 nanozymes repel *Pseudomonas aeruginosa* PA14 biofilms. Nanoscale 14, 86–98. https://doi.org/10.1039/D1NR03320D
Jeong, H.-H., Jeong, S.-G., Park, A., Jang, S.-C., Hong, S.G., Lee, C.-S., 2014. Effect of temperature on biofilm formation by Antarctic marine bacteria in a microfluidic device. Anal. Biochem. 446, 90–95. https://doi.org/10.1016/j.ab.2013.10.027

Ji, G., Beavis, R.C., Novick, R.P., 1995. Cell density control of staphylococcal virulence mediated by an octapeptide pheromone. Proc. Natl. Acad. Sci. 92, 12055–12059. https://doi.org/10.1073/pnas.92.26.12055
Jia, X., Ahmad, I., Yang, R., Wang, C., 2017. Versatile graphene-based photothermal nanocomposites for effectively capturing and killing bacteria, and for destroying bacterial biofilms. J. Mater. Chem. B 5, 2459–2467. https://doi.org/10.1039/C6TB03084J
Joshi, R.V., Gunawan, C., Mann, R., 2021. We are one: multispecies metabolism of a biofilm consortium and their treatment strategies. Front. Microbiol. 12, 635432. https://doi.org/10.3389/fmicb.2021.635432
Kaczmarek, J.A., Prather, K.L.J., 2021. Effective use of biosensors for high-throughput library screening for metabolite production. J. Ind. Microbiol. Biotechnol. 48, kuab049. https://doi.org/10.1093/jimb/kuab049
Kadam, S.R., den Besten, H.M.W., van der Veen, S., Zwietering, M.H., Moezelaar, R., Abee, T., 2013. Diversity assessment of *Listeria monocytogenes* biofilm formation: impact of growth condition, serotype and strain origin. Int. J. Food Microbiol. 165, 259–264. https://doi.org/10.1016/j.ijfoodmicro.2013.05.025
Kaiser, D., Kowalski, N., Waniek, J.J., 2017. Effects of biofouling on the sinking behavior of microplastics. Environ. Res. Lett. 12, 124003. https://doi.org/10.1088/1748-9326/aa8e8b
Kalamara, M., Spacapan, M., Mandic-Mulec, I., Stanley-Wall, N.R., 2018. Social behaviours by *Bacillus subtilis* : quorum sensing, kin discrimination and beyond. Mol. Microbiol. 110, 863–878. https://doi.org/10.1111/mmi.14127
Kanamori, H., Weber, D.J., Rutala, W.A., 2016. Healthcare outbreaks associated with a water reservoir and infection prevention strategies. Clin. Infect. Dis. 62, 1423–1435. https://doi.org/10.1093/cid/ciw122
Kanehisa, M., 2000. KEGG: Kyoto encyclopedia of genes and genomes. Nucleic Acids Res. 28, 27–30. https://doi.org/10.1093/nar/28.1.27
Kanematsu, H., Barry, D.M., 2020. A sequence between microfouling and macrofouling in marine biofouling, in: Marine Ecology: Current and Future Developments. Bentham Science Publishers, pp. 67–80. https://doi.org/10.2174/9789811437250120020009
Kaplan, J.B., 2014. Biofilm matrix-degrading enzymes, in: Donelli, G. (Ed.), Microbial Biofilms, Methods in Molecular Biology. Springer New York, New York, NY, pp. 203–213. https://doi.org/10.1007/978-1-4939-0467-9_14
Kaplan, J.B., 2010. Biofilm dispersal: mechanisms, clinical implications, and potential therapeutic uses. J. Dent. Res. 89, 205–218. https://doi.org/10.1177/0022034509359403
Karigar, C.S., Rao, S.S., 2011. Role of microbial enzymes in the bioremediation of pollutants: a review. Enzyme Res. 2011, 1–11. https://doi.org/10.4061/2011/805187
Karlovsky, P. (Ed.), 2008. Secondary metabolites in soil ecology, Soil biology. Springer, Berlin.
Karygianni, L., Ren, Z., Koo, H., Thurnheer, T., 2020. Biofilm matrixome: extracellular components in structured microbial communities. Trends Microbiol. 28, 668–681. https://doi.org/10.1016/j.tim.2020.03.016
Katsikogianni, M., Missirlis, Y., 2004. Concise review of mechanisms of bacterial adhesion to biomaterials and of techniques used in estimating bacteria-material interactions. Eur. Cell. Mater. 8, 37–57. https://doi.org/10.22203/eCM.v008a05

Kaur, K., Reddy, S., Barathe, P., Shriram, V., Anand, U., Proćków, J., Kumar, V., 2021. Combating drug-resistant bacteria using photothermally active nanomaterials: a perspective review. Front. Microbiol. 12, 747019. https://doi.org/10.3389/fmicb.2021.747019
Kazemi, M., Faisal Kabir, S., Fini, E.H., 2021. State of the art in recycling waste thermoplastics and thermosets and their applications in construction. Resour. Conserv. Recycl. 174, 105776. https://doi.org/10.1016/j.resconrec.2021.105776
Kelleher, Brian.P., Simpson, Andre.J., 2006. Humic substances in soils: are they really chemically distinct? Environ. Sci. Technol. 40, 4605–4611. https://doi.org/10.1021/es0608085
Kelley, S.T., Theisen, U., Angenent, L.T., St. Amand, A., Pace, N.R., 2004. Molecular analysis of shower curtain biofilm microbes. Appl. Environ. Microbiol. 70, 4187–4192. https://doi.org/10.1128/AEM.70.7.4187-4192.2004
Khan, A.A., Rahmani, A.H., Aldebasi, Y.H., Aly, S.M., 2014. Biochemical and pathological studies on peroxidases – an updated review. Glob. J. Health Sci. 6, p87. https://doi.org/10.5539/gjhs.v6n5p87
Khatoon, Z., McTiernan, C.D., Suuronen, E.J., Mah, T.-F., Alarcon, E.I., 2018. Bacterial biofilm formation on implantable devices and approaches to its treatment and prevention. Heliyon 4, e01067. https://doi.org/10.1016/j.heliyon.2018.e01067
Killer, H.E., Hou, R., Wostyn, P., Meyer, P., Pircher, A., 2019. Pressure and velocity in intraocular and subarachnoid space fluid chambers: an inseparable couple. Eye 33, 343–346. https://doi.org/10.1038/s41433-018-0231-z
Kim, J., Hegde, M., Kim, S.H., Wood, T.K., Jayaraman, A., 2012. A microfluidic device for high throughput bacterial biofilm studies. Lab. Chip 12, 1157. https://doi.org/10.1039/c2lc20800h
Kim, J.S., Kuk, E., Yu, K.N., Kim, J.-H., Park, S.J., Lee, H.J., Kim, S.H., Park, Y.K., Park, Y.H., Hwang, C.-Y., Kim, Y.-K., Lee, Y.-S., Jeong, D.H., Cho, M.-H., 2007. Antimicrobial effects of silver nanoparticles. Nanomedicine Nanotechnol. Biol. Med. 3, 95–101. https://doi.org/10.1016/j.nano.2006.12.001
Kim, L.H., Chong, T.H., 2017. Physiological responses of salinity-stressed *Vibrio* sp. and the effect on the biofilm formation on a nanofiltration membrane. Environ. Sci. Technol. 51, 1249–1258. https://doi.org/10.1021/acs.est.6b02904
Klein, R., 2011. Laser welding of plastics: materials, processes and industrial applications, 1st ed. Wiley. https://doi.org/10.1002/9783527636969
Kobayashi, K., Ikemoto, Y., 2019. Biofilm-associated toxin and extracellular protease cooperatively suppress competitors in *Bacillus subtilis* biofilms. PLOS Genet. 15, e1008232. https://doi.org/10.1371/journal.pgen.1008232
Kocak, G., Tuncer, C., Bütün, V., 2017. pH-responsive polymers. Polym. Chem. 8, 144–176. https://doi.org/10.1039/C6PY01872F
Koo, H., Allan, R.N., Howlin, R.P., Stoodley, P., Hall-Stoodley, L., 2017. Targeting microbial biofilms: current and prospective therapeutic strategies. Nat. Rev. Microbiol. 15, 740–755. https://doi.org/10.1038/nrmicro.2017.99
Kostakioti, M., Hadjifrangiskou, M., Hultgren, S.J., 2013. Bacterial biofilms: development, dispersal, and therapeutic strategies in the dawn of the postantibiotic era. Cold Spring Harb. Perspect. Med. 3, a010306–a010306. https://doi.org/10.1101/cshperspect.a010306
Kostylev, M., Kim, D.Y., Smalley, N.E., Salukhe, I., Greenberg, E.P., Dandekar, A.A., 2019. Evolution of the *Pseudomonas aeruginosa* quorum-sensing hierarchy.

Proc. Natl. Acad. Sci. 116, 7027–7032. https://doi.org/10.1073/pnas.1819796116
Kováčová, M., Kozakovičová, J., Procházka, M., Janigová, I., Vysopal, M., Černičková, I., Krajčovič, J., Špitalský, Z., 2020. Novel hybrid PETG composites for 3D printing. Appl. Sci. 10, 3062. https://doi.org/10.3390/app10093062
Kragh, K.N., Hutchison, J.B., Melaugh, G., Rodesney, C., Roberts, A.E.L., Irie, Y., Jensen, P.Ø., Diggle, S.P., Allen, R.J., Gordon, V., Bjarnsholt, T., 2016. Role of multicellular aggregates in biofilm formation. mBio 7, e00237-16. https://doi.org/10.1128/mBio.00237-16
Kumar, C.G., Anand, S.K., 1998. Significance of microbial biofilms in food industry: a review. Int. J. Food Microbiol. 42, 9–27. https://doi.org/10.1016/S0168-1605(98)00060-9
Kumar, M., Sarma, D.K., Shubham, S., Kumawat, M., Verma, V., Nina, P.B., Jp, D., Kumar, S., Singh, B., Tiwari, R.R., 2021. Futuristic non-antibiotic therapies to combat antibiotic resistance: a review. Front. Microbiol. 12, 609459. https://doi.org/10.3389/fmicb.2021.609459
Lade, H., Paul, D., Kweon, J.H., 2014. Quorum quenching mediated approaches for control of membrane biofouling. Int. J. Biol. Sci. 10, 550–565. https://doi.org/10.7150/ijbs.9028
Lan, X., Zhai, W., Zheng, W., 2013. Critical effects of polyethylene addition on the autoclave foaming behavior of polypropylene and the melting behavior of polypropylene foams blown with *n*-Pentane and CO_2. Ind. Eng. Chem. Res. 52, 5655–5665. https://doi.org/10.1021/ie302899m
Lange, A., Grzenia, A., Wierzbicki, M., Strojny-Cieslak, B., Kalińska, A., Gołębiewski, M., Radzikowski, D., Sawosz, E., Jaworski, S., 2021. Silver and copper nanoparticles inhibit biofilm formation by mastitis pathogens. Animals 11, 1884. https://doi.org/10.3390/ani11071884
Lanter, B.B., Sauer, K., Davies, D.G., 2014. Bacteria present in carotid arterial plaques are found as biofilm deposits which may contribute to enhanced risk of plaque rupture. mBio 5, e01206-14. https://doi.org/10.1128/mBio.01206-14
Lau, G.W., Hassett, D.J., Ran, H., Kong, F., 2004. The role of pyocyanin in *Pseudomonas aeruginosa* infection. Trends Mol. Med. 10, 599–606. https://doi.org/10.1016/j.molmed.2004.10.002
Lawrence, J.R., Neu, T.R., Paule, A., Korber, D.R., Wolfaardt, G.M., 2015. Aquatic biofilms: development, cultivation, analyses, and applications, in: Yates, M.V., Nakatsu, C.H., Miller, R.V., Pillai, S.D. (Eds.), Manual of Environmental Microbiology. ASM Press, Washington, DC, USA, p. 4.2.3-1-4.2.3-33. https://doi.org/10.1128/9781555818821.ch4.2.3
Le, K.Y., Otto, M., 2015. Quorum-sensing regulation in *staphylococci* — an overview. Front. Microbiol. 6. https://doi.org/10.3389/fmicb.2015.01174
Lear, G., Kingsbury, J.M., Franchini, S., Gambarini, V., Maday, S.D.M., Wallbank, J.A., Weaver, L., Pantos, O., 2021. Plastics and the microbiome: impacts and solutions. Environ. Microbiome 16, 2. https://doi.org/10.1186/s40793-020-00371-w
Lebeaux, D., Ghigo, J.-M., Beloin, C., 2014. Biofilm-related infections: bridging the gap between clinical management and fundamental aspects of recalcitrance toward antibiotics. Microbiol. Mol. Biol. Rev. 78, 510–543. https://doi.org/10.1128/MMBR.00013-14
Lee, J., Wu, J., Deng, Y., Wang, Jing, Wang, C., Wang, Jianhe, Chang, C., Dong, Y., Williams, P., Zhang, L.-H., 2013. A cell-cell communication signal integrates

quorum sensing and stress response. Nat. Chem. Biol. 9, 339–343. https://doi.org/10.1038/nchembio.1225
Lee, J., Zhang, L., 2015. The hierarchy quorum sensing network in *Pseudomonas aeruginosa*. Protein Cell 6, 26–41. https://doi.org/10.1007/s13238-014-0100-x
Lee, J.-H., Lequette, Y., Greenberg, E.P., 2006. Activity of purified QscR, a *Pseudomonas aeruginosa* orphan quorum-sensing transcription factor: *Pseudomonas aeruginosa* QscR activity. Mol. Microbiol. 59, 602–609. https://doi.org/10.1111/j.1365-2958.2005.04960.x
Lee, K., Yoon, S.S., 2017. *Pseudomonas aeruginosa* biofilm, a programmed bacterial life for fitness. J. Microbiol. Biotechnol. 27, 1053–1064. https://doi.org/10.4014/jmb.1611.11056
Lee, K.-J., Kim, J.-A., Hwang, W., Park, S.-J., Lee, K.-H., 2013. Role of capsular polysaccharide (CPS) in biofilm formation and regulation of CPS production by quorum-sensing in *Vibrio vulnificus*. Mol. Microbiol. 90, 841–857. https://doi.org/10.1111/mmi.12401
Lengyel, K., Lang, E., Fodor, A., Szállás, E., Schumann, P., Stackebrandt, E., 2005. Description of four novel species of *Xenorhabdus*, family *Enterobacteriaceae*: *Xenorhabdus budapestensis* sp. nov., *Xenorhabdus ehlersii* sp. nov., *Xenorhabdus innexi* sp. nov., and *Xenorhabdus szentirmaii* sp. nov. Syst. Appl. Microbiol. 28, 115–122. https://doi.org/10.1016/j.syapm.2004.10.004
Levering, V., Cao, C., Shivapooja, P., Levinson, H., Zhao, X., López, G.P., 2016. Urinary catheter capable of repeated on-demand removal of infectious biofilms via active deformation. Biomaterials 77, 77–86. https://doi.org/10.1016/j.biomaterials.2015.10.070
Lewis, K., 2001. Riddle of biofilm resistance. Antimicrob. Agents Chemother. 45, 999–1007. https://doi.org/10.1128/AAC.45.4.999-1007.2001
Li, B., Li, L., Guan, A., Dong, Q., Ruan, K., Hu, R., Li, Z., 2014. A smartphone controlled handheld microfluidic liquid handling system. Lab Chip 14, 4085–4092. https://doi.org/10.1039/C4LC00227J
Li, G., Tang, J.X., 2009. Accumulation of microswimmers near a surface mediated by collision and rotational Brownian motion. Phys. Rev. Lett. 103, 078101. https://doi.org/10.1103/PhysRevLett.103.078101
Li, H., Mercer, R., Behr, J., Heinzlmeir, S., McMullen, L.M., Vogel, R.F., Gänzle, M.G., 2020. Heat and pressure resistance in *Escherichia coli* relates to protein folding and aggregation. Front. Microbiol. 11, 111. https://doi.org/10.3389/fmicb.2020.00111
Li, X., Li, S., Bai, Q., Sui, N., Zhu, Z., 2020. Gold nanoclusters decorated amine-functionalized graphene oxide nanosheets for capture, oxidative stress, and photothermal destruction of bacteria. Colloids Surf. B Biointerfaces 196, 111313. https://doi.org/10.1016/j.colsurfb.2020.111313
Li, Y., Kawamura, Y., Fujiwara, N., Naka, T., Liu, H., Huang, X., Kobayashi, K., Ezaki, T., 2004. *Sphingomonas yabuuchiae* sp. nov. and *Brevundimonas nasdae* sp. nov., isolated from the Russian space laboratory Mir. Int. J. Syst. Evol. Microbiol. 54, 819–825. https://doi.org/10.1099/ijs.0.02829-0
Li, Y.-F., Zhu, X., Cheng, Z.-Y., Liang, X., Zhu, Y.-T., Feng, D.-D., Dobretsov, S., Yang, J.-L., 2020. 2(5H)-furanone disrupts bacterial biofilm formation and indirectly reduces the settlement of plantigrades of the mussel *Mytilus coruscus*. Front. Mar. Sci. 7, 564075. https://doi.org/10.3389/fmars.2020.564075
Li, Z., Ju, R., Sekine, S., Zhang, D., Zhuang, S., Yamaguchi, Y., 2019. All-in-one microfluidic device for on-site diagnosis of pathogens based on an integrated

continuous flow PCR and electrophoresis biochip. Lab. Chip 19, 2663–2668. https://doi.org/10.1039/C9LC00305C
Liang, Y., Hilal, N., Langston, P., Starov, V., 2007. Interaction forces between colloidal particles in liquid: theory and experiment. Adv. Colloid Interface Sci. 134–135, 151–166. https://doi.org/10.1016/j.cis.2007.04.003
Liaqat, I., Sumbal, F., Sabri, A.N., 2009. Tetracycline and chloramphenicol efficiency against selected biofilm forming bacteria. Curr. Microbiol. 59, 212–220. https://doi.org/10.1007/s00284-009-9424-9
Lightbown, J.W., Jackson, F.L., 1956. Inhibition of cytochrome systems of heart muscle and certain bacteria by the antagonists of dihydrostreptomycin: 2-alkyl-4-hydroxyquinoline *N* -oxides. Biochem. J. 63, 130–137. https://doi.org/10.1042/bj0630130
Limoli, D.H., Jones, C.J., Wozniak, D.J., 2015. Bacterial extracellular polysaccharides in biofilm formation and function. Microbiol. Spectr. 3, 3.3.29. https://doi.org/10.1128/microbiolspec.MB-0011-2014
Lin, J., Cheng, J., Wang, Y., Shen, X., 2018. The *Pseudomonas* quinolone signal (PQS): not just for quorum sensing anymore. Front. Cell. Infect. Microbiol. 8, 230. https://doi.org/10.3389/fcimb.2018.00230
Little, B.J., Blackwood, D.J., Hinks, J., Lauro, F.M., Marsili, E., Okamoto, A., Rice, S.A., Wade, S.A., Flemming, H.-C., 2020. Microbially influenced corrosion — any progress? Corros. Sci. 170, 108641. https://doi.org/10.1016/j.corsci.2020.108641
Liu, N.T., Bauchan, G.R., Francoeur, C.B., Shelton, D.R., Lo, Y.M., Nou, X., 2016. *Ralstonia insidiosa* serves as bridges in biofilm formation by foodborne pathogens *Listeria monocytogenes*, *Salmonella enterica*, and enterohemorrhagic *Escherichia coli*. Food Control 65, 14–20. https://doi.org/10.1016/j.foodcont.2016.01.004
Liu, X., Bimerew, M., Ma, Y., MÃ¼ller, H., Ovadis, M., Eberl, L., Berg, G., Chernin, L., 2007. Quorum-sensing signaling is required for production of the antibiotic pyrrolnitrin in a rhizospheric biocontrol strain of *Serratia plymuthica*. FEMS Microbiol. Lett. 270, 299–305. https://doi.org/10.1111/j.1574-6968.2007.00681.x
Liu, X., Sai, F., Li, L., Zhu, C., Huang, H., 2020. Clinical characteristics and risk factors of catheter-associated urinary tract infections caused by *Klebsiella pneumoniae*. Ann. Palliat. Med. 9, 2668–2677. https://doi.org/10.21037/apm-20-1052
Liu, Y., Zhang, J., Ji, Y., 2020. Environmental factors modulate biofilm formation by *Staphylococcus aureus*. Sci. Prog. 103, 003685041989865. https://doi.org/10.1177/0036850419898659
Liu, Y.-C., Hussain, F., Negm, O., Paiva, A.C., Halliday, N., Dubern, J.-F., Singh, S., Muntaka, S., Wheldon, L., Luckett, J., Tighe, P., Bosquillon, C., Williams, P., Cámara, M., Martínez-Pomares, L., 2018. Contribution of the alkylquinolone quorum-sensing system to the interaction of *Pseudomonas aeruginosa* with bronchial epithelial cells. Front. Microbiol. 9, 3018. https://doi.org/10.3389/fmicb.2018.03018
Lobelle, D., Cunliffe, M., 2011. Early microbial biofilm formation on marine plastic debris. Mar. Pollut. Bull. 62, 197–200. https://doi.org/10.1016/j.marpolbul.2010.10.013
Loeb, G., Neihof, R. (Eds.), 1975. Marine conditioning films, Advances in chemistry. American Chemical Society, Washington, D. C. https://doi.org/10.1021/ba-1975-0145

Loosdrecht, M.C.M., Picioreanu, C., Heijnen, J.J., 1997. A more unifying hypothesis for biofilm structures. FEMS Microbiol. Ecol. 24, 181–183. https://doi.org/10.1111/j.1574-6941.1997.tb00434.x
Lopez, D., Vlamakis, H., Kolter, R., 2010. Biofilms. Cold Spring Harb. Perspect. Biol. 2, a000398–a000398. https://doi.org/10.1101/cshperspect.a000398
Loustau, E., Leflaive, J., Boscus, C., Amalric, Q., Ferriol, J., Oleinikova, O., Pokrovsky, O.S., Girbal-Neuhauser, E., Rols, J.-L., 2021. The response of extracellular polymeric substances production by phototrophic biofilms to a sequential disturbance strongly depends on environmental conditions. Front. Microbiol. 12, 742027. https://doi.org/10.3389/fmicb.2021.742027
Loveday, H.P., Wilson, J.A., Kerr, K., Pitchers, R., Walker, J.T., Browne, J., 2014. Association between healthcare water systems and *Pseudomonas aeruginosa* infections: a rapid systematic review. J. Hosp. Infect. 86, 7–15. https://doi.org/10.1016/j.jhin.2013.09.010
Lowy, F.D., 2003. Antimicrobial resistance: the example of *Staphylococcus aureus*. J. Clin. Invest. 111, 1265–1273. https://doi.org/10.1172/JCI18535
Lyon, G.J., Wright, J.S., Muir, T.W., Novick, R.P., 2002. Key determinants of receptor activation in the *agr* autoinducing peptides of *Staphylococcus aureus*. Biochemistry 41, 10095–10104. https://doi.org/10.1021/bi026049u
Ma, Y., Zhang, Y., Zhang, R., Guan, F., Hou, B., Duan, J., 2020. Microbiologically influenced corrosion of marine steels within the interaction between steel and biofilms: a brief view. Appl. Microbiol. Biotechnol. 104, 515–525. https://doi.org/10.1007/s00253-019-10184-8
Machado, F., Malpica, N., Borromeo, S., 2019. Parametric CAD modeling for open source scientific hardware: comparing OpenSCAD and FreeCAD Python scripts. PLOS ONE 14, e0225795. https://doi.org/10.1371/journal.pone.0225795
Machado, R.A.R., Wüthrich, D., Kuhnert, P., Arce, C.C.M., Thönen, L., Ruiz, C., Zhang, X., Robert, C.A.M., Karimi, J., Kamali, S., Ma, J., Bruggmann, R., Erb, M., 2018. Whole-genome-based revisit of *Photorhabdus* phylogeny: proposal for the elevation of most *Photorhabdus* subspecies to the species level and description of one novel species *Photorhabdus bodei* sp. nov., and one novel subspecies *Photorhabdus laumondii* subsp. *clarkei* subsp. nov. Int. J. Syst. Evol. Microbiol. 68, 2664–2681. https://doi.org/10.1099/ijsem.0.002820
Maddah, H., Chogle, A., 2017. Biofouling in reverse osmosis: phenomena, monitoring, controlling and remediation. Appl. Water Sci. 7, 2637–2651. https://doi.org/10.1007/s13201-016-0493-1
Maeda, T., García-Contreras, R., Pu, M., Sheng, L., Garcia, L.R., Tomás, M., Wood, T.K., 2012. Quorum quenching quandary: resistance to antivirulence compounds. ISME J. 6, 493–501. https://doi.org/10.1038/ismej.2011.122
Makhlouf, A.S.H., Botello, M.A., 2018. Failure of the metallic structures due to microbiologically induced corrosion and the techniques for protection, in: Handbook of Materials Failure Analysis. Elsevier, pp. 1–18. https://doi.org/10.1016/B978-0-08-101928-3.00001-X
Maki, D.G., Kluger, D.M., Crnich, C.J., 2006. The risk of bloodstream infection in adults with different intravascular devices: a systematic review of 200 published prospective studies. Mayo Clin. Proc. 81, 1159–1171. https://doi.org/10.4065/81.9.1159
Maksimova, Yu.G., 2014. Microbial biofilms in biotechnological processes. Appl. Biochem. Microbiol. 50, 750–760. https://doi.org/10.1134/S0003683814080043

Malgaonkar, A., Nair, M., 2019. Quorum sensing in *Pseudomonas aeruginosa* mediated by RhlR is regulated by a small RNA PhrD. Sci. Rep. 9, 432. https://doi.org/10.1038/s41598-018-36488-9
Malhotra, S., Hayes, D., Wozniak, D.J., 2019. Cystic fibrosis and *Pseudomonas aeruginosa*: the host-microbe interface. Clin. Microbiol. Rev. 32, e00138-18. https://doi.org/10.1128/CMR.00138-18
Marks, L.R., Davidson, B.A., Knight, P.R., Hakansson, A.P., 2013. Interkingdom signaling induces *Streptococcus pneumoniae* biofilm dispersion and transition from asymptomatic colonization to disease. mBio 4, e00438-13. https://doi.org/10.1128/mBio.00438-13
Marques, C., Davies, D., Sauer, K., 2015. Control of biofilms with the fatty acid signaling molecule cis-2-decenoic acid. Pharmaceuticals 8, 816–835. https://doi.org/10.3390/ph8040816
Marsden, A.E., Grudzinski, K., Ondrey, J.M., DeLoney-Marino, C.R., Visick, K.L., 2017. Impact of salt and nutrient content on biofilm formation by *Vibrio fischeri*. PLOS ONE 12, e0169521. https://doi.org/10.1371/journal.pone.0169521
Martens, T., Heidorn, T., Pukall, R., Simon, M., Tindall, B.J., Brinkhoff, T., 2006. Reclassification of *Roseobacter gallaeciensis* Ruiz-Ponte et al. 1998 as *Phaeobacter gallaeciensis* gen. nov., comb. nov., description of *Phaeobacter inhibens* sp. nov., reclassification of *Ruegeria algicola* (Lafay et al. 1995) Uchino et al. 1999 as *Marinovum algicola* gen. nov., comb. nov., and emended descriptions of the genera *Roseobacter*, *Ruegeria* and *Leisingera*. Int. J. Syst. Evol. Microbiol. 56, 1293–1304. https://doi.org/10.1099/ijs.0.63724-0
Masaka, E., Reed, S., Davidson, M., Oosthuizen, J., 2021. Opportunistic premise plumbing pathogens. A potential health risk in water mist systems used as a cooling intervention. Pathogens 10, 462. https://doi.org/10.3390/pathogens10040462
Masters, E.A., Trombetta, R.P., de Mesy Bentley, K.L., Boyce, B.F., Gill, A.L., Gill, S.R., Nishitani, K., Ishikawa, M., Morita, Y., Ito, H., Bello-Irizarry, S.N., Ninomiya, M., Brodell, J.D., Lee, C.C., Hao, S.P., Oh, I., Xie, C., Awad, H.A., Daiss, J.L., Owen, J.R., Kates, S.L., Schwarz, E.M., Muthukrishnan, G., 2019. Evolving concepts in bone infection: redefining “biofilm”, “acute vs. chronic osteomyelitis”, “the immune proteome” and “local antibiotic therapy.” Bone Res. 7, 20. https://doi.org/10.1038/s41413-019-0061-z
Masurkar, S.A., Chaudhari, P.R., Shidore, V.B., Kamble, S.P., 2012. Effect of biologically synthesised silver nanoparticles on *Staphylococcus aureus* biofilm quenching and prevention of biofilm formation. IET Nanobiotechnol. 6, 110. https://doi.org/10.1049/iet-nbt.2011.0061
Matin, A., Khan, Z., Zaidi, S.M.J., Boyce, M.C., 2011. Biofouling in reverse osmosis membranes for seawater desalination: phenomena and prevention. Desalination 281, 1–16. https://doi.org/10.1016/j.desal.2011.06.063
Matz, C., Kjelleberg, S., 2005. Off the hook – how bacteria survive protozoan grazing. Trends Microbiol. 13, 302–307. https://doi.org/10.1016/j.tim.2005.05.009
McCaig, A.E., Grayston, S.J., Prosser, J.I., Glover, L.A., 2001. Impact of cultivation on characterisation of species composition of soil bacterial communities. FEMS Microbiol. Ecol. 35, 37–48. https://doi.org/10.1111/j.1574-6941.2001.tb00786.x
McDougald, D., Klebensberger, J., Tolker-Nielsen, T., Webb, J.S., Conibear, T., Rice, S.A., Kirov, S.M., Matz, C., Kjelleberg, S., 2008. *Pseudomonas aeruginosa*: a model for biofilm formation, in: Rehm, B.H.A. (Ed.), Pseudomonas. Wiley-VCH

Verlag GmbH & Co. KGaA, Weinheim, Germany, pp. 215–253. https://doi.org/10.1002/9783527622009.ch9
McDougald, D., Rice, S.A., Barraud, N., Steinberg, P.D., Kjelleberg, S., 2012. Should we stay or should we go: mechanisms and ecological consequences for biofilm dispersal. Nat. Rev. Microbiol. 10, 39–50. https://doi.org/10.1038/nrmicro2695
McInnis, C.E., Blackwell, H.E., 2011. Thiolactone modulators of quorum sensing revealed through library design and screening. Bioorg. Med. Chem. 19, 4820–4828. https://doi.org/10.1016/j.bmc.2011.06.071
McKnight, S.L., Iglewski, B.H., Pesci, E.C., 2000. The *Pseudomonas* quinolone signal regulates *rhl* quorum sensing in *Pseudomonas aeruginosa*. J. Bacteriol. 182, 2702–2708. https://doi.org/10.1128/JB.182.10.2702-2708.2000
Mena, K.D., Gerba, C.P., 2009. Risk assessment of *Pseudomonas aeruginosa* in water, in: Whitacre, D.M. (Ed.), Reviews of Environmental Contamination and Toxicology Vol 201, Reviews of Environmental Contamination and Toxicology. Springer US, Boston, MA, pp. 71–115. https://doi.org/10.1007/978-1-4419-0032-6_3
Meschwitz, S.M., Teasdale, M.E., Mozzer, A., Martin, N., Liu, J., Forschner-Dancause, S., Rowley, D.C., 2019. Antagonism of quorum sensing phenotypes by analogs of the marine bacterial secondary metabolite 3-methyl-N-(2′-phenylethyl)-butyramide. Mar. Drugs 17, 389. https://doi.org/10.3390/md17070389
Mhatre, E., Troszok, A., Gallegos-Monterrosa, R., Lindstädt, S., Hölscher, T., Kuipers, O.P., Kovács, Á.T., 2016. The impact of manganese on biofilm development of *Bacillus subtilis*. Microbiology 162, 1468–1478. https://doi.org/10.1099/mic.0.000320
Michels, J., Stippkugel, A., Lenz, M., Wirtz, K., Engel, A., 2018. Rapid aggregation of biofilm-covered microplastics with marine biogenic particles. Proc. R. Soc. B Biol. Sci. 285, 20181203. https://doi.org/10.1098/rspb.2018.1203
Michiels, J., Dirix, G., Vanderleyden, J., Xi, C., 2001. Processing and export of peptide pheromones and bacteriocins in Gram-negative bacteria. Trends Microbiol. 9, 164–168. https://doi.org/10.1016/S0966-842X(01)01979-5
Miller, J.H., 1972. Experiments in molecular genetics. Cold Spring Harbor Laboratory, Cold Spring Harbor, N.Y.
Miller, M.B., Bassler, B.L., 2001. Quorum sensing in bacteria. Annu. Rev. Microbiol. 55, 165–199. https://doi.org/10.1146/annurev.micro.55.1.165
Minchin, D., Gollasch, S., 2003. Fouling and ships' hulls: how changing circumstances and spawning events may result in the spread of exotic species. Biofouling 19, 111–122. https://doi.org/10.1080/0892701021000057891
Mirzaei, M., Furxhi, I., Murphy, F., Mullins, M., 2021. A machine learning tool to predict the antibacterial capacity of nanoparticles. Nanomaterials 11, 1774. https://doi.org/10.3390/nano11071774
Mizan, Md.F.R., Jahid, I.K., Ha, S.-D., 2015. Microbial biofilms in seafood: a food-hygiene challenge. Food Microbiol. 49, 41–55. https://doi.org/10.1016/j.fm.2015.01.009
Mölders, N., Renner, M., Errenst, C., Weidner, E., 2018. Incorporation of antibacterial active additives inside polycarbonate surfaces by using compressed carbon dioxide as transport aid. J. Supercrit. Fluids 132, 83–90. https://doi.org/10.1016/j.supflu.2017.02.009

Mombelli, A., Hashim, D., Cionca, N., 2018. What is the impact of titanium particles and biocorrosion on implant survival and complications? A critical review. Clin. Oral Implants Res. 29, 37–53. https://doi.org/10.1111/clr.13305
Monmeyran, A., Benyoussef, W., Thomen, P., Dahmane, N., Baliarda, A., Jules, M., Aymerich, S., Henry, N., 2021. Four species of bacteria deterministically assemble to form a stable biofilm in a millifluidic channel. Npj Biofilms Microbiomes 7, 64. https://doi.org/10.1038/s41522-021-00233-4
Monnet, V., Gardan, R., 2015. Quorum-sensing regulators in Gram-positive bacteria: 'cherchez le peptide.' Mol. Microbiol. 97, 181–184. https://doi.org/10.1111/mmi.13060
Morikawa, M., 2006. Beneficial biofilm formation by industrial bacteria *Bacillus subtilis* and related species. J. Biosci. Bioeng. 101, 1–8. https://doi.org/10.1263/jbb.101.1
Moscoso, M., García, E., Lopez, R., 2009. Pneumococcal biofilms. Int. Microbiol. 77–85. https://doi.org/10.2436/20.1501.01.84
Mouchka, M.E., Hewson, I., Harvell, C.D., 2010. Coral-associated bacterial assemblages: current knowledge and the potential for climate-driven impacts. Integr. Comp. Biol. 50, 662–674. https://doi.org/10.1093/icb/icq061
Moynihan, M.C., Allwood, J.M., 2014. Utilization of structural steel in buildings. Proc. R. Soc. Math. Phys. Eng. Sci. 470, 20140170. https://doi.org/10.1098/rspa.2014.0170
Muhammad, M.H., Idris, A.L., Fan, X., Guo, Y., Yu, Y., Jin, X., Qiu, J., Guan, X., Huang, T., 2020. Beyond risk: bacterial biofilms and their regulating approaches. Front. Microbiol. 11, 928. https://doi.org/10.3389/fmicb.2020.00928
Mukherjee, S., Bassler, B.L., 2019. Bacterial quorum sensing in complex and dynamically changing environments. Nat. Rev. Microbiol. 17, 371–382. https://doi.org/10.1038/s41579-019-0186-5
Mukherjee, S., Moustafa, D., Smith, C.D., Goldberg, J.B., Bassler, B.L., 2017. The RhlR quorum-sensing receptor controls *Pseudomonas aeruginosa* pathogenesis and biofilm development independently of its canonical homoserine lactone autoinducer. PLOS Pathog. 13, e1006504. https://doi.org/10.1371/journal.ppat.1006504
Mukhi, M., Vishwanathan, A.S., 2022. Beneficial biofilms: a minireview of strategies to enhance biofilm formation for biotechnological applications. Appl. Environ. Microbiol. 88, e01994-21. https://doi.org/10.1128/AEM.01994-21
Mukhopadhyay, R., 2007. When PDMS isn't the best. Anal. Chem. 79, 3248–3253. https://doi.org/10.1021/ac071903e
Mulcahy, L.R., Isabella, V.M., Lewis, K., 2014. *Pseudomonas aeruginosa* biofilms in disease. Microb. Ecol. 68, 1–12. https://doi.org/10.1007/s00248-013-0297-x
Murugan, K., Selvanayaki, K., Al-Sohaibani, S., 2016. Urinary catheter indwelling clinical pathogen biofilm formation, exopolysaccharide characterization and their growth influencing parameters. Saudi J. Biol. Sci. 23, 150–159. https://doi.org/10.1016/j.sjbs.2015.04.016
Muzammil, S., Khurshid, M., Nawaz, I., Siddique, M.H., Zubair, M., Nisar, M.A., Imran, M., Hayat, S., 2020. Aluminium oxide nanoparticles inhibit EPS production, adhesion and biofilm formation by multidrug resistant *Acinetobacter baumannii*. Biofouling 36, 492–504. https://doi.org/10.1080/08927014.2020.1776856

Nadell, C.D., Drescher, K., Foster, K.R., 2016. Spatial structure, cooperation and competition in biofilms. Nat. Rev. Microbiol. 14, 589–600. https://doi.org/10.1038/nrmicro.2016.84
Naidoo, S., Olaniran, A., 2013. Treated wastewater effluent as a source of microbial pollution of surface water resources. Int. J. Environ. Res. Public. Health 11, 249–270. https://doi.org/10.3390/ijerph110100249
Nair, H.A.S., Periasamy, S., Yang, L., Kjelleberg, S., Rice, S.A., 2017. Real time, spatial, and temporal mapping of the distribution of c-di-GMP during biofilm development. J. Biol. Chem. 292, 477–487. https://doi.org/10.1074/jbc.M116.746743
Nair, H.A.S., Subramoni, S., Poh, W.H., Hasnuddin, N.T.B., Tay, M., Givskov, M., Tolker-Nielsen, T., Kjelleberg, S., McDougald, D., Rice, S.A., 2021. Carbon starvation of *Pseudomonas aeruginosa* biofilms selects for dispersal insensitive mutants. BMC Microbiol. 21, 255. https://doi.org/10.1186/s12866-021-02318-8
Nakamura, Y., Yamamoto, Nao, Kino, Y., Yamamoto, Nozomi, Kamei, S., Mori, H., Kurokawa, K., Nakashima, N., 2016. Establishment of a multi-species biofilm model and metatranscriptomic analysis of biofilm and planktonic cell communities. Appl. Microbiol. Biotechnol. 100, 7263–7279. https://doi.org/10.1007/s00253-016-7532-6
Natalio, F., André, R., Hartog, A.F., Stoll, B., Jochum, K.P., Wever, R., Tremel, W., 2012. Vanadium pentoxide nanoparticles mimic vanadium haloperoxidases and thwart biofilm formation. Nat. Nanotechnol. 7, 530–535. https://doi.org/10.1038/nnano.2012.91
Nealson, K.H., Platt, T., Hastings, J.W., 1970. Cellular control of the synthesis and activity of the bacterial luminescent system. J. Bacteriol. 104, 313–322. https://doi.org/10.1128/jb.104.1.313-322.1970
Nemati, M., Jenneman, G.E., Voordouw, G., 2001. Mechanistic study of microbial control of hydrogen sulfide production in oil reservoirs. Biotechnol. Bioeng. 74, 424–434. https://doi.org/10.1002/bit.1133
Ng, W.-L., Bassler, B.L., 2009. Bacterial quorum-sensing network architectures. Annu. Rev. Genet. 43, 197–222. https://doi.org/10.1146/annurev-genet-102108-134304
Nguyen, T.-K., Duong, H.T.T., Selvanayagam, R., Boyer, C., Barraud, N., 2015. Iron oxide nanoparticle-mediated hyperthermia stimulates dispersal in bacterial biofilms and enhances antibiotic efficacy. Sci. Rep. 5, 18385. https://doi.org/10.1038/srep18385
Ni, N., Li, M., Wang, J., Wang, B., 2009. Inhibitors and antagonists of bacterial quorum sensing. Med. Res. Rev. 29, 65–124. https://doi.org/10.1002/med.20145
Niculescu, A.-G., Chircov, C., Bîrcă, A.C., Grumezescu, A.M., 2021. Fabrication and applications of microfluidic devices: a review. Int. J. Mol. Sci. 22, 2011. https://doi.org/10.3390/ijms22042011
Nijland, R., Hall, M.J., Burgess, J.G., 2010. Dispersal of biofilms by secreted, matrix degrading, bacterial DNase. PLoS ONE 5, e15668. https://doi.org/10.1371/journal.pone.0015668
Nikitin, L.N., Gallyamov, M.O., Vinokur, R.A., Nikolaec, A.Y., Said-Galiyev, E.E., Khokhlov, A.R., Jespersen, H.T., Schaumburg, K., 2003. Swelling and impregnation of polystyrene using supercritical carbon dioxide. J. Supercrit. Fluids 26, 263–273. https://doi.org/10.1016/S0896-8446(02)00183-3

Noronha Oliveira, M., Schunemann, W.V.H., Mathew, M.T., Henriques, B., Magini, R.S., Teughels, W., Souza, J.C.M., 2018. Can degradation products released from dental implants affect peri-implant tissues? J. Periodontal Res. 53, 1–11. https://doi.org/10.1111/jre.12479

Norwood, D.E., Gilmour, A., 2001. The differential adherence capabilities of two *Listeria monocytogenes* strains in monoculture and multispecies biofilms as a function of temperature. Lett. Appl. Microbiol. 33, 320–324. https://doi.org/10.1046/j.1472-765X.2001.01004.x

Novick, R.P., Geisinger, E., 2008. Quorum sensing in *Staphylococci*. Annu. Rev. Genet. 42, 541–564. https://doi.org/10.1146/annurev.genet.42.110807.091640

Ntougias, S., Zervakis, G.I., Fasseas, C., 2007. *Halotalea alkalilenta* gen. nov., sp. nov., a novel osmotolerant and alkalitolerant bacterium from alkaline olive mill wastes, and emended description of the family *Halomonadaceae* Franzmann et al. 1989, emend. Dobson and Franzmann 1996. Int. J. Syst. Evol. Microbiol. 57, 1975–1983. https://doi.org/10.1099/ijs.0.65078-0

Nürenberg, G., Schulz, M., Kunkel, U., Ternes, T.A., 2015. Development and validation of a generic nontarget method based on liquid chromatography – high resolution mass spectrometry analysis for the evaluation of different wastewater treatment options. J. Chromatogr. A 1426, 77–90. https://doi.org/10.1016/j.chroma.2015.11.014

Ofridam, F., Tarhini, M., Lebaz, N., Gagnière, É., Mangin, D., Elaissari, A., 2021. pH-sensitive polymers: classification and some fine potential applications. Polym. Adv. Technol. 32, 1455–1484. https://doi.org/10.1002/pat.5230

Oga, M., Sugioka, Y., Hobgood, C.D., Gristina, A.G., Myrvik, Q.N., 1988. Surgical biomaterials and differential colonization by *Staphylococcus epidermidis*. Biomaterials 9, 285–289. https://doi.org/10.1016/0142-9612(88)90100-7

O'Grady, B.J., Geuy, M.D., Kim, H., Balotin, K.M., Allchin, E.R., Florian, D.C., Bute, N.N., Scott, T.E., Lowen, G.B., Fricker, C.M., Fitzgerald, M.L., Guelcher, S.A., Wikswo, J.P., Bellan, L.M., Lippmann, E.S., 2021. Rapid prototyping of cell culture microdevices using parylene-coated 3D prints. Lab. Chip 21, 4814–4822. https://doi.org/10.1039/D1LC00744K

Okada, M., Sato, I., Cho, S.J., Iwata, H., Nishio, T., Dubnau, D., Sakagami, Y., 2005. Structure of the *Bacillus subtilis* quorum-sensing peptide pheromone ComX. Nat. Chem. Biol. 1, 23–24. https://doi.org/10.1038/nchembio709

Okada, M., Sugita, T., Abe, I., 2017. Posttranslational isoprenylation of tryptophan in bacteria. Beilstein J. Org. Chem. 13, 338–346. https://doi.org/10.3762/bjoc.13.37

Oliveira, W.F., Silva, P.M.S., Silva, R.C.S., Silva, G.M.M., Machado, G., Coelho, L.C.B.B., Correia, M.T.S., 2018. *Staphylococcus aureus* and *Staphylococcus epidermidis* infections on implants. J. Hosp. Infect. 98, 111–117. https://doi.org/10.1016/j.jhin.2017.11.008

O'Loughlin, C.T., Miller, L.C., Siryaporn, A., Drescher, K., Semmelhack, M.F., Bassler, B.L., 2013. A quorum-sensing inhibitor blocks *Pseudomonas aeruginosa* virulence and biofilm formation. Proc. Natl. Acad. Sci. 110, 17981–17986. https://doi.org/10.1073/pnas.1316981110

Olsen, N.M.C., Røder, H.L., Russel, J., Madsen, J.S., Sørensen, S.J., Burmølle, M., 2019. Priority of early colonizers but no effect on cohabitants in a synergistic biofilm community. Front. Microbiol. 10, 1949. https://doi.org/10.3389/fmicb.2019.01949

Oluniyi Solomon, O., Palanisami, T., 2016. Microplastics in the marine environment: current status, assessment methodologies, impacts and solutions. J. Pollut. Eff. Control 04. https://doi.org/10.4172/2375-4397.1000161
Ono, K., Oka, R., Toyofuku, M., Sakaguchi, A., Hamada, M., Yoshida, S., Nomura, N., 2014. cAMP signaling affects irreversible attachment during biofilm formation by *Pseudomonas aeruginosa* PAO1. Microbes Environ. 29, 104–106. https://doi.org/10.1264/jsme2.ME13151
Opitz, P., Jegel, O., Nasir, J., Rios-Studer, T., Gazanis, A., Pham, D.-H., Domke, K., Heermann, R., Schmedt auf der Günne, J., Tremel, W., 2022. Defect-controlled halogenating properties of lanthanide-doped ceria nanozymes. Nanoscale 14, 4740–4752. https://doi.org/10.1039/D2NR00501H
Orlov, V., Martynov, S., Kunytskiy, S., 2016. Energy saving in water treatment technologies with polystyrene foam filters. J. Water Land Dev. 31, 119–122. https://doi.org/10.1515/jwld-2016-0042
O'Toole, G., Kaplan, H.B., Kolter, R., 2000. Biofilm formation as microbial development. Annu. Rev. Microbiol. 54, 49–79. https://doi.org/10.1146/annurev.micro.54.1.49
O'Toole, G.A., 2011. Microtiter dish biofilm formation assay. J. Vis. Exp. 2437. https://doi.org/10.3791/2437
O'Toole, G.A., Kolter, R., 1998. Initiation of biofilm formation in *Pseudomonas fluorescens* WCS365 proceeds via multiple, convergent signalling pathways: a genetic analysis. Mol. Microbiol. 28, 449–461. https://doi.org/10.1046/j.1365-2958.1998.00797.x
Overmann, J., Abt, B., Sikorski, J., 2017. Present and future of culturing bacteria. Annu. Rev. Microbiol. 71, 711–730. https://doi.org/10.1146/annurev-micro-090816-093449
Paddle-Ledinek, J.E., Nasa, Z., Cleland, H.J., 2006. Effect of different wound dressings on cell viability and proliferation. Plast. Reconstr. Surg. 117, 110S-118S. https://doi.org/10.1097/01.prs.0000225439.39352.ce
Palmer, J., Flint, S., Brooks, J., 2007. Bacterial cell attachment, the beginning of a biofilm. J. Ind. Microbiol. Biotechnol. 34, 577–588. https://doi.org/10.1007/s10295-007-0234-4
Paluch, E., Rewak-Soroczyńska, J., Jędrusik, I., Mazurkiewicz, E., Jermakow, K., 2020. Prevention of biofilm formation by quorum quenching. Appl. Microbiol. Biotechnol. 104, 1871–1881. https://doi.org/10.1007/s00253-020-10349-w
Pandit, A., Adholeya, A., Cahill, D., Brau, L., Kochar, M., 2020. Microbial biofilms in nature: unlocking their potential for agricultural applications. J. Appl. Microbiol. 129, 199–211. https://doi.org/10.1111/jam.14609
Papenfort, K., Bassler, B.L., 2016. Quorum sensing signal–response systems in Gram-negative bacteria. Nat. Rev. Microbiol. 14, 576–588. https://doi.org/10.1038/nrmicro.2016.89
Parihar, R.D., Dhiman, U., Bhushan, A., Gupta, P.K., Gupta, P., 2022. *Heterorhabditis* and *Photorhabdus* symbiosis: a natural mine of bioactive compounds. Front. Microbiol. 13, 790339. https://doi.org/10.3389/fmicb.2022.790339
Park, D., Ciezki, K., van der Hoeven, R., Singh, S., Reimer, D., Bode, H.B., Forst, S., 2009. Genetic analysis of xenocoumacin antibiotic production in the mutualistic bacterium *Xenorhabdus nematophila*. Mol. Microbiol. 73, 938–949. https://doi.org/10.1111/j.1365-2958.2009.06817.x
Park, J.-A., Kim, S.-B., 2017. Anti-biofouling enhancement of a polycarbonate membrane with functionalized poly(vinyl alcohol) electrospun nanofibers:

Permeation flux, biofilm formation, contact, and regeneration tests. J. Membr. Sci. 540, 192–199. https://doi.org/10.1016/j.memsci.2017.06.071
Park, J.H., Jo, Y., Jang, S.Y., Kwon, H., Irie, Y., Parsek, M.R., Kim, M.H., Choi, S.H., 2015. The *cabABC* operon essential for biofilm and rugose colony development in *Vibrio vulnificus*. PLOS Pathog. 11, e1005192. https://doi.org/10.1371/journal.ppat.1005192
Parsek, M.R., Val, D.L., Hanzelka, B.L., Cronan, J.E., Greenberg, E.P., 1999. Acyl homoserine-lactone quorum-sensing signal generation. Proc. Natl. Acad. Sci. 96, 4360–4365. https://doi.org/10.1073/pnas.96.8.4360
Patankar, A.V., González, J.E., 2009. Orphan LuxR regulators of quorum sensing. FEMS Microbiol. Rev. 33, 739–756. https://doi.org/10.1111/j.1574-6976.2009.00163.x
Pena, R.T., Blasco, L., Ambroa, A., González-Pedrajo, B., Fernández-García, L., López, M., Bleriot, I., Bou, G., García-Contreras, R., Wood, T.K., Tomás, M., 2019. Relationship between quorum sensing and secretion systems. Front. Microbiol. 10, 1100. https://doi.org/10.3389/fmicb.2019.01100
Penesyan, A., Paulsen, I.T., Gillings, M.R., Kjelleberg, S., Manefield, M.J., 2020. Secondary effects of antibiotics on microbial biofilms. Front. Microbiol. 11, 2109. https://doi.org/10.3389/fmicb.2020.02109
Penesyan, A., Paulsen, I.T., Kjelleberg, S., Gillings, M.R., 2021. Three faces of biofilms: a microbial lifestyle, a nascent multicellular organism, and an incubator for diversity. Npj Biofilms Microbiomes 7, 80. https://doi.org/10.1038/s41522-021-00251-2
Peng, J.-S., Tsai, W.-C., Chou, C.-C., 2002. Inactivation and removal of *Bacillus cereus* by sanitizer and detergent. Int. J. Food Microbiol. 77, 11–18. https://doi.org/10.1016/S0168-1605(02)00060-0
Pérez-Rodríguez, S., García-Aznar, J.M., Gonzalo-Asensio, J., 2022. Microfluidic devices for studying bacterial taxis, drug testing and biofilm formation. Microb. Biotechnol. 15, 395–414. https://doi.org/10.1111/1751-7915.13775
Pesci, E.C., Milbank, J.B.J., Pearson, J.P., McKnight, S., Kende, A.S., Greenberg, E.P., Iglewski, B.H., 1999. Quinolone signaling in the cell-to-cell communication system of *Pseudomonas aeruginosa*. Proc. Natl. Acad. Sci. 96, 11229–11234. https://doi.org/10.1073/pnas.96.20.11229
Petersen, L.-E., Moeller, M., Versluis, D., Nietzer, S., Kellermann, M.Y., Schupp, P.J., 2021. Mono- and multispecies biofilms from a crustose coralline alga induce settlement in the scleractinian coral *Leptastrea purpurea*. Coral Reefs 40, 381–394. https://doi.org/10.1007/s00338-021-02062-5
Petrachi, T., Resca, E., Piccinno, M., Biagi, F., Strusi, V., Dominici, M., Veronesi, E., 2017. An alternative approach to investigate biofilm in medical devices: a feasibility study. Int. J. Environ. Res. Public. Health 14, 1587. https://doi.org/10.3390/ijerph14121587
Petrova, O.E., Sauer, K., 2016. Escaping the biofilm in more than one way: desorption, detachment or dispersion. Curr. Opin. Microbiol. 30, 67–78. https://doi.org/10.1016/j.mib.2016.01.004
Petrova, O.E., Sauer, K., 2012. Sticky situations: key components that control bacterial surface attachment. J. Bacteriol. 194, 2413–2425. https://doi.org/10.1128/JB.00003-12
Pettigrew, M.M., Marks, L.R., Kong, Y., Gent, J.F., Roche-Hakansson, H., Hakansson, A.P., 2014. Dynamic changes in the *Streptococcus pneumoniae* transcriptome during transition from biofilm formation to invasive disease upon

Influenza A virus infection. Infect. Immun. 82, 4607–4619. https://doi.org/10.1128/IAI.02225-14
Pezzoni, M., Meichtry, M., Pizarro, R.A., Costa, C.S., 2015. Role of the *Pseudomonas* quinolone signal (PQS) in sensitising *Pseudomonas aeruginosa* to UVA radiation. J. Photochem. Photobiol. B 142, 129–140. https://doi.org/10.1016/j.jphotobiol.2014.11.014
Pfeiffer, T., Schuster, S., Bonhoeffer, S., 2001. Cooperation and competition in the evolution of ATP-producing pathways. Science 292, 504–507. https://doi.org/10.1126/science.1058079
Pfitzner, F., 2021. Biofilminhibition durch Nano-Ceroxid-Komposite (Dissertation). Johannes Gutenberg-Universität Mainz.
Pier, G.B., Grout, M., Zaidi, T.S., 1997. Cystic fibrosis transmembrane conductance regulator is an epithelial cell receptor for clearance of *Pseudomonas aeruginosa* from the lung. Proc. Natl. Acad. Sci. 94, 12088–12093. https://doi.org/10.1073/pnas.94.22.12088
Pinkston, K.L., Gao, P., Diaz-Garcia, D., Sillanpää, J., Nallapareddy, S.R., Murray, B.E., Harvey, B.R., 2011. The Fsr quorum-sensing system of *Enterococcus faecalis* modulates surface display of the collagen-binding MSCRAMM ace through regulation of *gelE*. J. Bacteriol. 193, 4317–4325. https://doi.org/10.1128/JB.05026-11
Pomerantsev, A.P., Pomerantseva, O.M., Camp, A.S., Mukkamala, R., Goldman, S., Leppla, S.H., 2009. PapR peptide maturation: role of the NprB protease in *Bacillus cereus* 569 PlcR/PapR global gene regulation. FEMS Immunol. Med. Microbiol. 55, 361–377. https://doi.org/10.1111/j.1574-695X.2008.00521.x
Porter, S.L., Wadhams, G.H., Armitage, J.P., 2011. Signal processing in complex chemotaxis pathways. Nat. Rev. Microbiol. 9, 153–165. https://doi.org/10.1038/nrmicro2505
Poulin, M.B., Kuperman, L.L., 2021. Regulation of biofilm exopolysaccharide production by cyclic di-guanosine monophosphate. Front. Microbiol. 12, 730980. https://doi.org/10.3389/fmicb.2021.730980
Pousti, M., Zarabadi, M.P., Abbaszadeh Amirdehi, M., Paquet-Mercier, F., Greener, J., 2019. Microfluidic bioanalytical flow cells for biofilm studies: a review. The Analyst 144, 68–86. https://doi.org/10.1039/C8AN01526K
Premarathna, M., Rathnathilaka, T., Seneviratne, G., Madawala, S., 2022. Engineering microbial biofilms for improved productivity of biochemicals important in restoration of degraded ecosystems. Adv. Biosci. Biotechnol. 13, 145–158. https://doi.org/10.4236/abb.2022.133007
Prescott, R.D., Decho, A.W., 2020. Flexibility and adaptability of quorum sensing in nature. Trends Microbiol. 28, 436–444. https://doi.org/10.1016/j.tim.2019.12.004
Procópio, L., 2019. The role of biofilms in the corrosion of steel in marine environments. World J. Microbiol. Biotechnol. 35, 73. https://doi.org/10.1007/s11274-019-2647-4
Proctor, C.R., McCarron, P.A., Ternan, N.G., 2020. Furanone quorum-sensing inhibitors with potential as novel therapeutics against *Pseudomonas aeruginosa*. J. Med. Microbiol. 69, 195–206. https://doi.org/10.1099/jmm.0.001144
Proctor, R.A., von Eiff, C., Kahl, B.C., Becker, K., McNamara, P., Herrmann, M., Peters, G., 2006. Small colony variants: a pathogenic form of bacteria that facilitates persistent and recurrent infections. Nat. Rev. Microbiol. 4, 295–305. https://doi.org/10.1038/nrmicro1384

Prokein, M., Dyes, T., Renner, M., Weidner, E., 2021. Waterless leather dyeing with dense carbon dioxide as solvent for dyes. J. Supercrit. Fluids 178, 105377. https://doi.org/10.1016/j.supflu.2021.105377
Puhm, M., Ainelo, H., Kivisaar, M., Teras, R., 2022. Tryptone in growth media enhances *Pseudomonas putida* biofilm. Microorganisms 10, 618. https://doi.org/10.3390/microorganisms10030618
Pusztahelyi, T., Holb, I.J., PÃ³csi, I., 2015. Secondary metabolites in fungus-plant interactions. Front. Plant Sci. 6. https://doi.org/10.3389/fpls.2015.00573
Pütz, E., 2022. Cerium oxide nanoparticles as nanozymes and for antifouling applications (Dissertation). Johannes Gutenberg-Universität Mainz.
Pütz, E., Gazanis, A., Keltsch, N., Jegel, O., Pfitzner, F., Heermann, R., Ternes, T., Tremel, W., 2022. Communication breakdown: into the molecular mechanism of biofilm inhibition by CeO_2 nanocrystal enzyme mimics and how it can be exploited (Submitted manuscript in ACS Nano).
Qais, F.A., Khan, M.S., Ahmad, I., 2018. Nanoparticles as quorum sensing inhibitor: prospects and limitations, in: Kalia, V.C. (Ed.), Biotechnological Applications of Quorum Sensing Inhibitors. Springer Singapore, Singapore, pp. 227–244. https://doi.org/10.1007/978-981-10-9026-4_11
Qian, P.-Y., Cheng, A., Wang, R., Zhang, R., 2022. Marine biofilms: diversity, interactions and biofouling. Nat. Rev. Microbiol. https://doi.org/10.1038/s41579-022-00744-7
Qin, R., Duan, C., 2017. The principle and applications of Bernoulli equation. J. Phys. Conf. Ser. 916, 012038. https://doi.org/10.1088/1742-6596/916/1/012038
Qureshi, N., Annous, B.A., Ezeji, T.C., Karcher, P., Maddox, I.S., 2005. Biofilm reactors for industrial bioconversion processes: employing potential of enhanced reaction rates. Microb. Cell Factories 4, 24. https://doi.org/10.1186/1475-2859-4-24
Rabus, R., 2014. Fifteen years of physiological proteo(geno)mics with (marine) environmental bacteria. Arch. Physiol. Biochem. 120, 173–187. https://doi.org/10.3109/13813455.2014.951658
Ragg, R., Tahir, M.N., Tremel, W., 2016. Solids go bio: inorganic nanoparticles as enzyme mimics. Eur. J. Inorg. Chem. 2016, 1906–1915. https://doi.org/10.1002/ejic.201501237
Raghupathi, P.K., Liu, W., Sabbe, K., Houf, K., Burmølle, M., Sørensen, S.J., 2018. Synergistic interactions within a multispecies biofilm enhance individual species protection against grazing by a pelagic protozoan. Front. Microbiol. 8, 2649. https://doi.org/10.3389/fmicb.2017.02649
Railkin, A.I., 2003. Marine biofouling: colonization processes and defenses, 0 ed. CRC Press. https://doi.org/10.1201/9780203503232
Rampioni, G., Leoni, L., Williams, P., 2014. The art of antibacterial warfare: deception through interference with quorum sensing–mediated communication. Bioorganic Chem. 55, 60–68. https://doi.org/10.1016/j.bioorg.2014.04.005
Rao, Y., Shang, W., Yang, Y., Zhou, R., Rao, X., 2020. Fighting mixed-species microbial biofilms with cold atmospheric plasma. Front. Microbiol. 11, 1000. https://doi.org/10.3389/fmicb.2020.01000
Rau, J.V., De Santis, R., Ciofani, G., 2017. Exploring challenges ahead of nanotechnology for biomedicine. Bioact. Mater. 2, 119–120. https://doi.org/10.1016/j.bioactmat.2017.09.004
Reddinger, R.M., Luke-Marshall, N.R., Hakansson, A.P., Campagnari, A.A., 2016. Host physiologic changes induced by Influenza A virus lead to *Staphylococcus*

aureus biofilm dispersion and transition from asymptomatic colonization to invasive disease. mBio 7, e01235-16. https://doi.org/10.1128/mBio.01235-16
Rehman, Azizur, Rehman, Ali, Ahmad, I., 2015. Antibacterial, antifungal, and insecticidal potentials of *Oxalis corniculata* and its isolated compounds. Int. J. Anal. Chem. 2015, 1–5. https://doi.org/10.1155/2015/842468
Rehman, Z.U., Leiknes, T., 2018. Quorum-quenching bacteria isolated from Red Sea sediments reduce biofilm formation by *Pseudomonas aeruginosa*. Front. Microbiol. 9, 1354. https://doi.org/10.3389/fmicb.2018.01354
Ren, K., Zhou, J., Wu, H., 2013. Materials for microfluidic chip fabrication. Acc. Chem. Res. 46, 2396–2406. https://doi.org/10.1021/ar300314s
Rendueles, O., Ghigo, J.-M., 2015. Mechanisms of competition in biofilm communities. Microbiol. Spectr. 3, 3.3.28. https://doi.org/10.1128/microbiolspec.MB-0009-2014
Rieger, U.M., Mesina, J., Kalbermatten, D.F., Haug, M., Frey, H.P., Pico, R., Frei, R., Pierer, G., Lüscher, N.J., Trampuz, A., 2013. Bacterial biofilms and capsular contracture in patients with breast implants. Br. J. Surg. 100, 768–774. https://doi.org/10.1002/bjs.9084
Riley, M.A., Wertz, J.E., 2002. Bacteriocins: evolution, ecology, and application. Annu. Rev. Microbiol. 56, 117–137. https://doi.org/10.1146/annurev.micro.56.012302.161024
Rittle, K.H., Helmstetter, C.E., Meyer, A.E., Baier, R.E., 1990. *Escherichia coli* retention on solid surfaces as functions of substratum surface energy and cell growth phase. Biofouling 2, 121–130. https://doi.org/10.1080/08927019009378138
Roche, E.D., Renick, P.J., Tetens, S.P., Ramsay, S.J., Daniels, E.Q., Carson, D.L., 2012. Increasing the presence of biofilm and healing delay in a porcine model of MRSA-infected wounds. Wound Repair Regen. n/a-n/a. https://doi.org/10.1111/j.1524-475X.2012.00808.x
Rochex, A., Massé, A., Escudié, R., Godon, J.-J., Bernet, N., 2009. Influence of abrasion on biofilm detachment: evidence for stratification of the biofilm. J. Ind. Microbiol. Biotechnol. 36, 467–470. https://doi.org/10.1007/s10295-009-0543-x
Roggo, C., Picioreanu, C., Richard, X., Mazza, C., van Lintel, H., van der Meer, J.R., 2018. Quantitative chemical biosensing by bacterial chemotaxis in microfluidic chips. Environ. Microbiol. 20, 241–258. https://doi.org/10.1111/1462-2920.13982
Romero, M., Martin-Cuadrado, A.-B., Roca-Rivada, A., Cabello, A.M., Otero, A., 2011. Quorum quenching in cultivable bacteria from dense marine coastal microbial communities. FEMS Microbiol. Ecol. 75, 205–217. https://doi.org/10.1111/j.1574-6941.2010.01011.x
Römling, U., Kjelleberg, S., Normark, S., Nyman, L., Uhlin, B.E., Åkerlund, B., 2014. Microbial biofilm formation: a need to act. J. Intern. Med. 276, 98–110. https://doi.org/10.1111/joim.12242
Ross, P., Weinhouse, H., Aloni, Y., Michaeli, D., Weinberger-Ohana, P., Mayer, R., Braun, S., de Vroom, E., van der Marel, G.A., van Boom, J.H., Benziman, M., 1987. Regulation of cellulose synthesis in *Acetobacter xylinum* by cyclic diguanylic acid. Nature 325, 279–281. https://doi.org/10.1038/325279a0
Rossi, C.C., Pereira, M.F., Giambiagi-deMarval, M., 2020. Underrated *Staphylococcus* species and their role in antimicrobial resistance spreading. Genet. Mol. Biol. 43, e20190065. https://doi.org/10.1590/1678-4685-gmb-2019-0065

Rossiter, S.E., Fletcher, M.H., Wuest, W.M., 2017. Natural products as platforms to overcome antibiotic resistance. Chem. Rev. 117, 12415–12474. https://doi.org/10.1021/acs.chemrev.7b00283
Roy, A.B., Petrova, O.E., Sauer, K., 2012. The phosphodiesterase DipA (*PA5017*) is essential for *Pseudomonas aeruginosa* biofilm dispersion. J. Bacteriol. 194, 2904–2915. https://doi.org/10.1128/JB.05346-11
Roy, R., Tiwari, M., Donelli, G., Tiwari, V., 2018. Strategies for combating bacterial biofilms: a focus on anti-biofilm agents and their mechanisms of action. Virulence 9, 522–554. https://doi.org/10.1080/21505594.2017.1313372
Roy, V., Fernandes, R., Tsao, C.-Y., Bentley, W.E., 2010. Cross species quorum quenching using a native AI-2 processing enzyme. ACS Chem. Biol. 5, 223–232. https://doi.org/10.1021/cb9002738
Ruiz-Ponte, C., Cilia, V., Lambert, C., Nicolas, J.L., 1998. *Roseobacter gallaeciensis* sp. nov., a new marine bacterium isolated from rearings and collectors of the scallop *Pecten maximus*. Int. J. Syst. Bacteriol. 48, 537–542. https://doi.org/10.1099/00207713-48-2-537
Rumbaugh, K.P., Sauer, K., 2020. Biofilm dispersion. Nat. Rev. Microbiol. 18, 571–586. https://doi.org/10.1038/s41579-020-0385-0
Rumbo-Feal, S., Gómez, M.J., Gayoso, C., Álvarez-Fraga, L., Cabral, M.P., Aransay, A.M., Rodríguez-Ezpeleta, N., Fullaondo, A., Valle, J., Tomás, M., Bou, G., Poza, M., 2013. Whole transcriptome analysis of *Acinetobacter baumannii* assessed by RNA-sequencing reveals different mRNA expression profiles in biofilm compared to planktonic cells. PLoS ONE 8, e72968. https://doi.org/10.1371/journal.pone.0072968
Rupp, M.E., 2014. Clinical characteristics of infections in humans due to *Staphylococcus epidermidis*, in: Fey, P.D. (Ed.), *Staphylococcus Epidermidis*, Methods in Molecular Biology. Humana Press, Totowa, NJ, pp. 1–16. https://doi.org/10.1007/978-1-62703-736-5_1
Rutherford, S.T., Bassler, B.L., 2012. Bacterial quorum sensing: its role in virulence and possibilities for its control. Cold Spring Harb. Perspect. Med. 2, a012427–a012427. https://doi.org/10.1101/cshperspect.a012427
Ryan, M.P., Pembroke, J.T., 2018. *Brevundimonas* spp: emerging global opportunistic pathogens. Virulence 9, 480–493. https://doi.org/10.1080/21505594.2017.1419116
Sackmann, E.K., Fulton, A.L., Beebe, D.J., 2014. The present and future role of microfluidics in biomedical research. Nature 507, 181–189. https://doi.org/10.1038/nature13118
Saggu, S.K., Jha, G., Mishra, P.C., 2019. Enzymatic Degradation of biofilm by metalloprotease from *Microbacterium* sp. SKS10. Front. Bioeng. Biotechnol. 7, 192. https://doi.org/10.3389/fbioe.2019.00192
Sakuragi, Y., Kolter, R., 2007. Quorum-sensing regulation of the biofilm matrix genes (*pel*) of *Pseudomonas aeruginosa*. J. Bacteriol. 189, 5383–5386. https://doi.org/10.1128/JB.00137-07
Salama, Y., Chennaoui, M., Sylla, A., Mountadar, M., Rihani, M., Assobhei, O., 2016. Characterization, structure, and function of extracellular polymeric substances (EPS) of microbial biofilm in biological wastewater treatment systems: a review. Desalination Water Treat. 57, 16220–16237. https://doi.org/10.1080/19443994.2015.1077739
Salgar-Chaparro, S.J., Lepkova, K., Pojtanabuntoeng, T., Darwin, A., Machuca, L.L., 2020. Nutrient level determines biofilm characteristics and subsequent impact

on microbial corrosion and biocide effectiveness. Appl. Environ. Microbiol. 86, e02885-19. https://doi.org/10.1128/AEM.02885-19
Salman, H., Zilman, A., Loverdo, C., Jeffroy, M., Libchaber, A., 2006. Solitary modes of bacterial culture in a temperature gradient. Phys. Rev. Lett. 97, 118101. https://doi.org/10.1103/PhysRevLett.97.118101
Samuel, U., Guggenbichler, J.P., 2004. Prevention of catheter-related infections: the potential of a new nano-silver impregnated catheter. Int. J. Antimicrob. Agents 23, 75–78. https://doi.org/10.1016/j.ijantimicag.2003.12.004
Sánchez, M.C., Romero-Lastra, P., Ribeiro-Vidal, H., Llama-Palacios, A., Figuero, E., Herrera, D., Sanz, M., 2019. Comparative gene expression analysis of planktonic *Porphyromonas gingivalis* ATCC 33277 in the presence of a growing biofilm versus planktonic cells. BMC Microbiol. 19, 58. https://doi.org/10.1186/s12866-019-1423-9
Sanford, E., Faulkner, A., 2018. Lucidchart for easy workflow mapping. Ser. Rev. 44, 157–162. https://doi.org/10.1080/00987913.2018.1472468
Sani, R.K., Peyton, B.M., Brown, L.T., 2001. Copper-induced inhibition of growth of *Desulfovibrio desulfuricans* G20: assessment of its toxicity and correlation with those of zinc and lead. Appl. Environ. Microbiol. 67, 4765–4772. https://doi.org/10.1128/AEM.67.10.4765-4772.2001
Sankar Ganesh, P., Ravishankar Rai, V., 2018. Alternative strategies to regulate quorum sensing and biofilm formation of pathogenic *Pseudomonas* by quorum sensing inhibitors of diverse origins, in: Kalia, V.C. (Ed.), Biotechnological Applications of Quorum Sensing Inhibitors. Springer Singapore, Singapore, pp. 33–61. https://doi.org/10.1007/978-981-10-9026-4_3
Santhakumari, S., Ravi, A.V., 2019. Targeting quorum sensing mechanism: An alternative anti-virulent strategy for the treatment of bacterial infections. South Afr. J. Bot. 120, 81–86. https://doi.org/10.1016/j.sajb.2018.09.028
Santos, A.P.A., Watanabe, E., Andrade, D. de, 2011. Biofilm on artificial pacemaker: fiction or reality? Arq. Bras. Cardiol. 97, e113–e120. https://doi.org/10.1590/S0066-782X2011001400018
Santos, A.L.S. dos, Galdino, A.C.M., Mello, T.P. de, Ramos, L. de S., Branquinha, M.H., Bolognese, A.M., Columbano Neto, J., Roudbary, M., 2018. What are the advantages of living in a community? A microbial biofilm perspective! Mem. Inst. Oswaldo Cruz 113. https://doi.org/10.1590/0074-02760180212
Sarif, M., 2021. Synthesis of various metal oxides by different synthetic methods (Dissertation). Johannes Gutenberg-Universität Mainz.
Sarif, M., Jegel, O., Gazanis, A., Hartmann, J., Plana-Ruiz, S., Hilgert, J., Frerichs, H., Viel, M., Panthöfer, M., Kolb, U., Tahir, M.N., Schemberg, J., Kappl, M., Heermann, R., Tremel, W., 2022. High-throughput synthesis of CeO_2 nanoparticles for transparent nanocomposites repelling *Pseudomonas aeruginosa* biofilms. Sci. Rep. 12, 3935. https://doi.org/10.1038/s41598-022-07833-w
Sauer, K., Camper, A.K., Ehrlich, G.D., Costerton, J.W., Davies, D.G., 2002. *Pseudomonas aeruginosa* displays multiple phenotypes during development as a biofilm. J. Bacteriol. 184, 1140–1154. https://doi.org/10.1128/jb.184.4.1140-1154.2002
Sauer, K., Cullen, M.C., Rickard, A.H., Zeef, L.A.H., Davies, D.G., Gilbert, P., 2004. Characterization of nutrient-induced dispersion in *Pseudomonas aeruginosa* PAO1 biofilm. J. Bacteriol. 186, 7312–7326. https://doi.org/10.1128/JB.186.21.7312-7326.2004

Schäfer, H., Küpper, K., Wollschläger, J., Kashaev, N., Hardege, J., Walder, L., Mohsen Beladi-Mousavi, S., Hartmann-Azanza, B., Steinhart, M., Sadaf, S., Dorn, F., 2015. Oxidized Mild Steel S235: An Efficient Anode for Electrocatalytically Initiated Water Splitting. ChemSusChem 8, 3099–3110. https://doi.org/10.1002/cssc.201500666
Scherhag, P., Ackermann, J., 2021. Removal of sugars in wastewater from food production through heterotrophic growth of *Galdieria sulphuraria*. Eng. Life Sci. 21, 233–241. https://doi.org/10.1002/elsc.202000075
Schleifer, K.H., Kocur, M., 1973. Classification of *staphylococci* based on chemical and biochemical properties. Arch. Für Mikrobiol. 93, 65–85. https://doi.org/10.1007/BF00666081
Schluter, J., Nadell, C.D., Bassler, B.L., Foster, K.R., 2015. Adhesion as a weapon in microbial competition. ISME J. 9, 139–149. https://doi.org/10.1038/ismej.2014.174
Schmitt, M.J., Breinig, F., 2006. Yeast viral killer toxins: lethality and self-protection. Nat. Rev. Microbiol. 4, 212–221. https://doi.org/10.1038/nrmicro1347
Schneider, C.A., Rasband, W.S., Eliceiri, K.W., 2012. NIH Image to ImageJ: 25 years of image analysis. Nat. Methods 9, 671–675. https://doi.org/10.1038/nmeth.2089
Schniederberend, M., Williams, J.F., Shine, E., Shen, C., Jain, R., Emonet, T., Kazmierczak, B.I., 2019. Modulation of flagellar rotation in surface-attached bacteria: a pathway for rapid surface-sensing after flagellar attachment. PLOS Pathog. 15, e1008149. https://doi.org/10.1371/journal.ppat.1008149
Schoenmakers, J.W.A., Heuker, M., López-Álvarez, M., Nagengast, W.B., van Dam, G.M., van Dijl, J.M., Jutte, P.C., van Oosten, M., 2021. Image-guided in situ detection of bacterial biofilms in a human prosthetic knee infection model: a feasibility study for clinical diagnosis of prosthetic joint infections. Eur. J. Nucl. Med. Mol. Imaging 48, 757–767. https://doi.org/10.1007/s00259-020-04982-w
Schöntag, J.M., Sens, M.L., 2015. Effective production of rapid filters with polystyrene granules as a media filter. Water Supply 15, 1088–1098. https://doi.org/10.2166/ws.2015.072
Schroll, C., Barken, K.B., Krogfelt, K.A., Struve, C., 2010. Role of type 1 and type 3 fimbriae in *Klebsiella pneumoniae* biofilm formation. BMC Microbiol. 10, 179. https://doi.org/10.1186/1471-2180-10-179
Schultz, M.P., 2007. Effects of coating roughness and biofouling on ship resistance and powering. Biofouling 23, 331–341. https://doi.org/10.1080/08927010701461974
Schultz, M.P., Bendick, J.A., Holm, E.R., Hertel, W.M., 2011. Economic impact of biofouling on a naval surface ship. Biofouling 27, 87–98. https://doi.org/10.1080/08927014.2010.542809
Schwering, M., Song, J., Louie, M., Turner, R.J., Ceri, H., 2013. Multi-species biofilms defined from drinking water microorganisms provide increased protection against chlorine disinfection. Biofouling 29, 917–928. https://doi.org/10.1080/08927014.2013.816298
Secchi, E., Savorana, G., Vitale, A., Eberl, L., Stocker, R., Rusconi, R., 2022. The structural role of bacterial eDNA in the formation of biofilm streamers. Proc. Natl. Acad. Sci. 119, e2113723119. https://doi.org/10.1073/pnas.2113723119
Seed, P.C., Passador, L., Iglewski, B.H., 1995. Activation of the *Pseudomonas aeruginosa lasI* gene by LasR and the *Pseudomonas* autoinducer PAI: an autoinduction regulatory hierarchy. J. Bacteriol. 177, 654–659. https://doi.org/10.1128/jb.177.3.654-659.1995

Segers, P., Vancanneyt, M., Pot, B., Torck, U., Hoste, B., Dewettinck, D., Falsen, E., Kersters, K., De Vos, P., 1994. Classification of *Pseudomonas diminuta* Leifson and Hugh 1954 and *Pseudomonas vesicularis* Busing, Doll, and Freytag 1953 in *Brevundimonas* gen. nov. as *Brevundimonas diminuta* comb. nov. and *Brevundimonas vesicularis* comb. nov., respectively. Int. J. Syst. Bacteriol. 44, 499–510. https://doi.org/10.1099/00207713-44-3-499

Seghal Kiran, G., Hassan, S., Sajayan, A., Selvin, J., 2017. Quorum quenching compounds from natural sources, in: Sugathan, S., Pradeep, N.S., Abdulhameed, S. (Eds.), Bioresources and Bioprocess in Biotechnology. Springer Singapore, Singapore, pp. 351–364. https://doi.org/10.1007/978-981-10-4284-3_14

Seiler, C., van Velzen, E., Neu, T.R., Gaedke, U., Berendonk, T.U., Weitere, M., 2017. Grazing resistance of bacterial biofilms: a matter of predators' feeding trait. FEMS Microbiol. Ecol. 93. https://doi.org/10.1093/femsec/fix112

Seneviratne, C.J., Yip, J.W.Y., Chang, J.W.W., Zhang, C.F., Samaranayake, L.P., 2013. Effect of culture media and nutrients on biofilm growth kinetics of laboratory and clinical strains of *Enterococcus faecalis*. Arch. Oral Biol. 58, 1327–1334. https://doi.org/10.1016/j.archoralbio.2013.06.017

Serra, D.O., Hengge, R., 2014. Stress responses go three dimensional – the spatial order of physiological differentiation in bacterial macrocolony biofilms. Environ. Microbiol. 16, 1455–1471. https://doi.org/10.1111/1462-2920.12483

Shahid, K., Srivastava, V., Sillanpää, M., 2021. Protein recovery as a resource from waste specifically via membrane technology—from waste to wonder. Environ. Sci. Pollut. Res. 28, 10262–10282. https://doi.org/10.1007/s11356-020-12290-x

Shallcross, L.J., Howard, S.J., Fowler, T., Davies, S.C., 2015. Tackling the threat of antimicrobial resistance: from policy to sustainable action. Philos. Trans. R. Soc. B Biol. Sci. 370, 20140082. https://doi.org/10.1098/rstb.2014.0082

Sharafimasooleh, M., Rand, J.L., Walsh, M.E., 2016. Effect of high chloride concentrations on microbial regrowth in drinking water distribution systems. J. Environ. Eng. 142, 04015061. https://doi.org/10.1061/(ASCE)EE.1943-7870.0001027

Sharma, D., Misba, L., Khan, A.U., 2019. Antibiotics versus biofilm: an emerging battleground in microbial communities. Antimicrob. Resist. Infect. Control 8, 76. https://doi.org/10.1186/s13756-019-0533-3

Shim, J., Cristobal, G., Link, D.R., Thorsen, T., Jia, Y., Piattelli, K., Fraden, S., 2007. Control and measurement of the phase behavior of aqueous solutions using microfluidics. J. Am. Chem. Soc. 129, 8825–8835. https://doi.org/10.1021/ja071820f

Shkodenko, L., Kassirov, I., Koshel, E., 2020. Metal oxide nanoparticles against bacterial biofilms: perspectives and limitations. Microorganisms 8, 1545. https://doi.org/10.3390/microorganisms8101545

Sifri, C.D., 2008. Quorum sensing: bacteria talk sense. Clin. Infect. Dis. 47, 1070–1076. https://doi.org/10.1086/592072

Sikdar, R., Elias, M., 2020. Quorum quenching enzymes and their effects on virulence, biofilm, and microbiomes: a review of recent advances. Expert Rev. Anti Infect. Ther. 18, 1221–1233. https://doi.org/10.1080/14787210.2020.1794815

Silva, V.O., Soares, L.O., Silva Júnior, A., Mantovani, H.C., Chang, Y.-F., Moreira, M.A.S., 2014. Biofilm formation on biotic and abiotic surfaces in the presence of antimicrobials by *Escherichia coli* isolates from cases of bovine mastitis.

Appl. Environ. Microbiol. 80, 6136–6145. https://doi.org/10.1128/AEM.01953-14
Simões, L.C., Simões, M., Vieira, M.J., 2010. Adhesion and biofilm formation on polystyrene by drinking water-isolated bacteria. Antonie Van Leeuwenhoek 98, 317–329. https://doi.org/10.1007/s10482-010-9444-2
Simões, L.C., Simões, M., Vieira, M.J., 2007. Biofilm interactions between distinct bacterial genera isolated from drinking water. Appl. Environ. Microbiol. 73, 6192–6200. https://doi.org/10.1128/AEM.00837-07
Simon, M.I., Crane, B.R., Crane, A. (Eds.), 2007. Two-component signaling systems, Methods in enzymology. Academic Press, San Diego, Calif.
Singh, P.K., Bartalomej, S., Hartmann, R., Jeckel, H., Vidakovic, L., Nadell, C.D., Drescher, K., 2017. *Vibrio cholerae* combines individual and collective sensing to trigger biofilm dispersal. Curr. Biol. 27, 3359-3366.e7. https://doi.org/10.1016/j.cub.2017.09.041
Skovhus, T.L., Enning, D., Lee, J.S. (Eds.), 2017. Microbiologically influenced corrosion in the upstream oil and gas industry, 1st ed. CRC Press, Boca Raton : Taylor & Francis, CRC Press, 2017. https://doi.org/10.1201/9781315157818
Skowron, P.M., Krefft, D., Brodzik, R., Kasperkiewicz, P., Drag, M., Koller, K.-P., 2020. An alternative for proteinase K-heat-sensitive protease from fungus *Onygena corvina* for biotechnology: cloning, engineering, expression, characterization and special application for protein sequencing. Microb. Cell Factories 19, 135. https://doi.org/10.1186/s12934-020-01392-3
Soberón-Chávez, G., González-Valdez, A., Soto-Aceves, M.P., Cocotl-Yañez, M., 2021. Rhamnolipids produced by *Pseudomonas* : from molecular genetics to the market. Microb. Biotechnol. 14, 136–146. https://doi.org/10.1111/1751-7915.13700
Song, J., Beule, L., Jongmans-Hochschulz, E., Wichels, A., Gerdts, G., 2022. The travelling particles: community dynamics of biofilms on microplastics transferred along a salinity gradient. ISME Commun. 2, 35. https://doi.org/10.1038/s43705-022-00117-4
Song, Y., Cai, Z.-H., Lao, Y.-M., Jin, H., Ying, K.-Z., Lin, G.-H., Zhou, J., 2018. Antibiofilm activity substances derived from coral symbiotic bacterial extract inhibit biofouling by the model strain *Pseudomonas aeruginosa* PAO1. Microb. Biotechnol. 11, 1090–1105. https://doi.org/10.1111/1751-7915.13312
Sonnenschein, E.C., Jimenez, G., Castex, M., Gram, L., 2021. The *Roseobacter* -group bacterium *Phaeobacter* as a safe probiotic solution for aquaculture. Appl. Environ. Microbiol. 87, e02581-20. https://doi.org/10.1128/AEM.02581-20
Soukarieh, F., Williams, P., Stocks, M.J., Cámara, M., 2018. *Pseudomonas aeruginosa* quorum sensing systems as drug discovery targets: current position and future perspectives. J. Med. Chem. 61, 10385–10402. https://doi.org/10.1021/acs.jmedchem.8b00540
Southey-Pillig, C.J., Davies, D.G., Sauer, K., 2005. Characterization of temporal protein production in *Pseudomonas aeruginosa* biofilms. J. Bacteriol. 187, 8114–8126. https://doi.org/10.1128/JB.187.23.8114-8126.2005
Sprockett, D., Fukami, T., Relman, D.A., 2018. Role of priority effects in the early-life assembly of the gut microbiota. Nat. Rev. Gastroenterol. Hepatol. 15, 197–205. https://doi.org/10.1038/nrgastro.2017.173
Spröer, C., Mendrock, U., Swiderski, J., Lang, E., Stackebrandt, E., 1999. The phylogenetic position of *Serratia*, *Buttiauxella* and some other genera of the

family *Enterobacteriaceae*. Int. J. Syst. Evol. Microbiol. 49, 1433–1438. https://doi.org/10.1099/00207713-49-4-1433
Srinivas, S., Berger, M., Brinkhoff, T., Niggemann, J., 2022. Impact of quorum sensing and tropodithietic acid production on the exometabolome of *Phaeobacter inhibens*. Front. Microbiol. 13, 917969. https://doi.org/10.3389/fmicb.2022.917969
Srivastava, D., Waters, C.M., 2012. A tangled web: regulatory connections between quorum sensing and cyclic di-GMP. J. Bacteriol. 194, 4485–4493. https://doi.org/10.1128/JB.00379-12
Stahlhut, S.G., Struve, C., Krogfelt, K.A., Reisner, A., 2012. Biofilm formation of *Klebsiella pneumoniae* on urethral catheters requires either type 1 or type 3 fimbriae. FEMS Immunol. Med. Microbiol. 65, 350–359. https://doi.org/10.1111/j.1574-695X.2012.00965.x
Stewart, P.S., 1993. A model of biofilm detachment. Biotechnol. Bioeng. 41, 111–117. https://doi.org/10.1002/bit.260410115
Stewart, P.S., Franklin, M.J., 2008. Physiological heterogeneity in biofilms. Nat. Rev. Microbiol. 6, 199–210. https://doi.org/10.1038/nrmicro1838
Stickler, D.J., 2008. Bacterial biofilms in patients with indwelling urinary catheters. Nat. Clin. Pract. Urol. 5, 598–608. https://doi.org/10.1038/ncpuro1231
Stoodley, P., Sauer, K., Davies, D.G., Costerton, J.W., 2002. Biofilms as complex differentiated communities. Annu. Rev. Microbiol. 56, 187–209. https://doi.org/10.1146/annurev.micro.56.012302.160705
Sturme, M.H.J., Kleerebezem, M., Nakayama, J., Akkermans, A.D.L., Vaughan, E.E., de Vos, W.M., 2002. Cell to cell communication by autoinducing peptides in Gram-positive bacteria. Antonie Van Leeuwenhoek 81, 233–243. https://doi.org/10.1023/A:1020522919555
Subramani, R., Jayaprakashvel, M., 2019. Bacterial quorum sensing: biofilm formation, survival behaviour and antibiotic resistance, in: Bramhachari, P.V. (Ed.), Implication of Quorum Sensing and Biofilm Formation in Medicine, Agriculture and Food Industry. Springer Singapore, Singapore, pp. 21–37. https://doi.org/10.1007/978-981-32-9409-7_3
Subramoni, S., Venturi, V., 2009. LuxR-family 'solos': bachelor sensors/regulators of signalling molecules. Microbiology 155, 1377–1385. https://doi.org/10.1099/mic.0.026849-0
Suryawati, B., 2018. Zinc homeostasis mechanism and its role in bacterial virulence capacity. Presented at the THE 8TH ANNUAL BASIC SCIENCE INTERNATIONAL CONFERENCE: Coverage of Basic Sciences toward the World's Sustainability Challanges, East Java, Indonesia, p. 070021. https://doi.org/10.1063/1.5062819
Sweet, M.J., Croquer, A., Bythell, J.C., 2011. Development of bacterial biofilms on artificial corals in comparison to surface-associated microbes of hard corals. PLoS ONE 6, e21195. https://doi.org/10.1371/journal.pone.0021195
Szabo, J.G., Meiners, G., Heckman, L., Rice, E.W., Hall, J., 2017. Decontamination of *Bacillus* spores adhered to iron and cement-mortar drinking water infrastructure in a model system using disinfectants. J. Environ. Manage. 187, 1–7. https://doi.org/10.1016/j.jenvman.2016.11.024
Szwetkowski, K.J., Falkinham, J.O., 2020. *Methylobacterium* spp. as emerging opportunistic premise plumbing pathogens. Pathogens 9, 149. https://doi.org/10.3390/pathogens9020149

Tahrioui, A., Schwab, M., Quesada, E., Llamas, I., 2013. Quorum sensing in some representative species of *Halomonadaceae*. Life 3, 260–275. https://doi.org/10.3390/life3010260
Tailliez, P., Pagès, S., Ginibre, N., Boemare, N., 2006. New insight into diversity in the genus *Xenorhabdus*, including the description of ten novel species. Int. J. Syst. Evol. Microbiol. 56, 2805–2818. https://doi.org/10.1099/ijs.0.64287-0
Tang, K., Zhang, Y., Yu, M., Shi, X., Coenye, T., Bossier, P., Zhang, X.-H., 2013. Evaluation of a new high-throughput method for identifying quorum quenching bacteria. Sci. Rep. 3, 2935. https://doi.org/10.1038/srep02935
Taylor, G.T., Zheng, D., Lee, M., Troy, P.J., Gyananath, G., Sharma, S.K., 1997. Influence of surface properties on accumulation of conditioning films and marine bacteria on substrata exposed to oligotrophic waters. Biofouling 11, 31–57. https://doi.org/10.1080/08927019709378319
Teasdale, M.E., Liu, J., Wallace, J., Akhlaghi, F., Rowley, D.C., 2009. Secondary metabolites produced by the marine bacterium *Halobacillus salinus* that inhibit quorum sensing-controlled phenotypes in Gram-negative bacteria. Appl. Environ. Microbiol. 75, 567–572. https://doi.org/10.1128/AEM.00632-08
Telgmann, U., Horn, H., Morgenroth, E., 2004. Influence of growth history on sloughing and erosion from biofilms. Water Res. 38, 3671–3684. https://doi.org/10.1016/j.watres.2004.05.020
Thierbach, S., Wienhold, M., Fetzner, S., Hennecke, U., 2019. Synthesis and biological activity of methylated derivatives of the *Pseudomonas* metabolites HHQ, HQNO and PQS. Beilstein J. Org. Chem. 15, 187–193. https://doi.org/10.3762/bjoc.15.18
Thoendel, M., Kavanaugh, J.S., Flack, C.E., Horswill, A.R., 2011. Peptide signaling in the *Staphylococci*. Chem. Rev. 111, 117–151. https://doi.org/10.1021/cr100370n
Thomas, G.M., Poinar, G.O., 1979. *Xenorhabdus* gen. nov., a genus of entomopathogenic, nematophilic bacteria of the family *Enterobacteriaceae*. Int. J. Syst. Bacteriol. 29, 352–360. https://doi.org/10.1099/00207713-29-4-352
Thormann, K.M., Saville, R.M., Shukla, S., Spormann, A.M., 2005. Induction of rapid detachment in *Shewanella oneidensis* MR-1 biofilms. J. Bacteriol. 187, 1014–1021. https://doi.org/10.1128/JB.187.3.1014-1021.2005
Thygesen, M., Schullehner, J., Hansen, B., Sigsgaard, T., Voutchkova, D.D., Kristiansen, S.M., Pedersen, C.B., Dalsgaard, S., 2021. Trace elements in drinking water and the incidence of attention-deficit hyperactivity disorder. J. Trace Elem. Med. Biol. 68, 126828. https://doi.org/10.1016/j.jtemb.2021.126828
Tindall, B.J., 2003. The nomenclatural type of the genus *Deleya* and the consequences of *Deleya aesta* and *Alcaligenes aquamarinus* being synonyms. Int. J. Syst. Evol. Microbiol. 53, 1699–1700. https://doi.org/10.1099/ijs.0.02530-0
Tobias, N.J., Brehm, J., Kresovic, D., Brameyer, S., Bode, H.B., Heermann, R., 2020. New vocabulary for bacterial communication. ChemBioChem 21, 759–768. https://doi.org/10.1002/cbic.201900580
Tobias, N.J., Mishra, B., Gupta, D.K., Sharma, R., Thines, M., Stinear, T.P., Bode, H.B., 2016. Genome comparisons provide insights into the role of secondary metabolites in the pathogenic phase of the *Photorhabdus* life cycle. BMC Genomics 17, 537. https://doi.org/10.1186/s12864-016-2862-4

Tobias, N.J., Shi, Y.-M., Bode, H.B., 2018. Refining the natural product repertoire in entomopathogenic bacteria. Trends Microbiol. 26, 833–840. https://doi.org/10.1016/j.tim.2018.04.007
Tolker-Nielsen, T., Sternberg, C., 2014. Methods for studying biofilm formation: flow cells and confocal laser scanning microscopy, in: Filloux, A., Ramos, J.-L. (Eds.), *Pseudomonas* Methods and Protocols, Methods in Molecular Biology. Springer New York, New York, NY, pp. 615–629. https://doi.org/10.1007/978-1-4939-0473-0_47
Tolker-Nielsen, T., Sternberg, C., 2011. Growing and analyzing biofilms in flow chambers. Curr. Protoc. Microbiol. 21. https://doi.org/10.1002/9780471729259.mc01b02s21
Tomaras, A.P., Dorsey, C.W., Edelmann, R.E., Actis, L.A., 2003. Attachment to and biofilm formation on abiotic surfaces by *Acinetobacter baumannii*: involvement of a novel chaperone-usher pili assembly system. Microbiology 149, 3473–3484. https://doi.org/10.1099/mic.0.26541-0
Tong, S.Y.C., Davis, J.S., Eichenberger, E., Holland, T.L., Fowler, V.G., 2015. *Staphylococcus aureus* infections: epidemiology, pathophysiology, clinical manifestations, and management. Clin. Microbiol. Rev. 28, 603–661. https://doi.org/10.1128/CMR.00134-14
Torabi Delshad, S., Soltanian, S., Sharifiyazdi, H., Haghkhah, M., Bossier, P., 2018. Identification of *N*-acyl homoserine lactone-degrading bacteria isolated from rainbow trout (*Oncorhynchus mykiss*). J. Appl. Microbiol. 125, 356–369. https://doi.org/10.1111/jam.13891
Torelli, R., Cacaci, M., Papi, M., Paroni Sterbini, F., Martini, C., Posteraro, B., Palmieri, V., De Spirito, M., Sanguinetti, M., Bugli, F., 2017. Different effects of matrix degrading enzymes towards biofilms formed by *E. faecalis* and *E. faecium* clinical isolates. Colloids Surf. B Biointerfaces 158, 349–355. https://doi.org/10.1016/j.colsurfb.2017.07.010
Toyofuku, M., Inaba, T., Kiyokawa, T., Obana, N., Yawata, Y., Nomura, N., 2016. Environmental factors that shape biofilm formation. Biosci. Biotechnol. Biochem. 80, 7–12. https://doi.org/10.1080/09168451.2015.1058701
Tran, T.T.T., Kannoorpatti, K., Padovan, A., Thennadil, S., 2021. A study of bacteria adhesion and microbial corrosion on different stainless steels in environment containing *Desulfovibrio vulgaris*. R. Soc. Open Sci. 8, 201577. https://doi.org/10.1098/rsos.201577
Tuck, B., Watkin, E., Somers, A., Machuca, L.L., 2022. A critical review of marine biofilms on metallic materials. Npj Mater. Degrad. 6, 25. https://doi.org/10.1038/s41529-022-00234-4
Tümer, E.H., Erbil, H.Y., 2021. Extrusion-Based 3D printing applications of PLA composites: a review. Coatings 11, 390. https://doi.org/10.3390/coatings11040390
Tuon, F.F., Dantas, L.R., Suss, P.H., Tasca Ribeiro, V.S., 2022. Pathogenesis of the *Pseudomonas aeruginosa* biofilm: a review. Pathogens 11, 300. https://doi.org/10.3390/pathogens11030300
Turan, N.B., Engin, G.Ö., 2018. Quorum quenching, in: Comprehensive Analytical Chemistry. Elsevier, pp. 117–149. https://doi.org/10.1016/bs.coac.2018.02.003
Turki, Y., Mehri, I., Lajnef, R., Rejab, A.B., Khessairi, A., Cherif, H., Ouzari, H., Hassen, A., 2017. Biofilms in bioremediation and wastewater treatment: characterization of bacterial community structure and diversity during seasons in municipal wastewater treatment process. Environ. Sci. Pollut. Res. 24, 3519–3530. https://doi.org/10.1007/s11356-016-8090-2

Tuson, H.H., Weibel, D.B., 2013. Bacteria–surface interactions. Soft Matter 9, 4368. https://doi.org/10.1039/c3sm27705d
Uçkay, I., Pittet, D., Vaudaux, P., Sax, H., Lew, D., Waldvogel, F., 2009. Foreign body infections due to *Staphylococcus epidermidis*. Ann. Med. 41, 109–119. https://doi.org/10.1080/07853890802337045
Ulman, A., Ferrario, J., Forcada, A., Seebens, H., Arvanitidis, C., Occhipinti-Ambrogi, A., Marchini, A., 2019. Alien species spreading via biofouling on recreational vessels in the Mediterranean Sea. J. Appl. Ecol. 56, 2620–2629. https://doi.org/10.1111/1365-2664.13502
Uneputty, A., Dávila-Lezama, A., Garibo, D., Oknianska, A., Bogdanchikova, N., Hernández-Sánchez, J.F., Susarrey-Arce, A., 2022. Strategies applied to modify structured and smooth surfaces: a step closer to reduce bacterial adhesion and biofilm formation. Colloid Interface Sci. Commun. 46, 100560. https://doi.org/10.1016/j.colcom.2021.100560
Uppuluri, P., Chaturvedi, A.K., Srinivasan, A., Banerjee, M., Ramasubramaniam, A.K., Köhler, J.R., Kadosh, D., Lopez-Ribot, J.L., 2010. Dispersion as an important step in the *Candida albicans* biofilm developmental cycle. PLoS Pathog. 6, e1000828. https://doi.org/10.1371/journal.ppat.1000828
Uppuluri, P., Lopez-Ribot, J.L., 2016. Go forth and colonize: dispersal from clinically important microbial biofilms. PLOS Pathog. 12, e1005397. https://doi.org/10.1371/journal.ppat.1005397
Utari, P.D., Setroikromo, R., Melgert, B.N., Quax, W.J., 2018. PvdQ quorum quenching acylase attenuates *Pseudomonas aeruginosa* virulence in a mouse model of pulmonary infection. Front. Cell. Infect. Microbiol. 8, 119. https://doi.org/10.3389/fcimb.2018.00119
Vacheethasanee, K., Temenoff, J.S., Higashi, J.M., Gary, A., Anderson, J.M., Bayston, R., Marchant, R.E., 1998. Bacterial surface properties of clinically isolated *Staphylococcus epidermidis* strains determine adhesion on polyethylene. J. Biomed. Mater. Res. 42, 425–432. https://doi.org/10.1002/(SICI)1097-4636(19981205)42:3<425::AID-JBM12>3.0.CO;2-F
Vaksmaa, A., Knittel, K., Abdala Asbun, A., Goudriaan, M., Ellrott, A., Witte, H.J., Vollmer, I., Meirer, F., Lott, C., Weber, M., Engelmann, J.C., Niemann, H., 2021. Microbial communities on plastic polymers in the Mediterranean Sea. Front. Microbiol. 12, 673553. https://doi.org/10.3389/fmicb.2021.673553
Valentini, M., Filloux, A., 2016. Biofilms and cyclic di-GMP (c-di-GMP) signaling: lessons from *Pseudomonas aeruginosa* and other bacteria. J. Biol. Chem. 291, 12547–12555. https://doi.org/10.1074/jbc.R115.711507
Van Delden, C., Iglewski, B.H., 1998. Cell-to-cell signaling and *Pseudomonas aeruginosa* infections. Emerg. Infect. Dis. 4, 551–560. https://doi.org/10.3201/eid0404.980405
Van Dillewijn, P., Nojiri, H., Van Der Meer, J.R., Wood, T.K., 2009. Bioremediation, a broad perspective. Microb. Biotechnol. 2, 125–127. https://doi.org/10.1111/j.1751-7915.2009.00091.x
van Gestel, J., Vlamakis, H., Kolter, R., 2015. Division of labor in biofilms: the ecology of cell differentiation. Microbiol. Spectr. 3, 3.2.26. https://doi.org/10.1128/microbiolspec.MB-0002-2014
Van Houdt, R., Michiels, C.W., 2010. Biofilm formation and the food industry, a focus on the bacterial outer surface. J. Appl. Microbiol. 109, 1117–1131. https://doi.org/10.1111/j.1365-2672.2010.04756.x

Vandecandelaere, I., Segaert, E., Mollica, A., Faimali, M., Vandamme, P., 2008. *Leisingera aquimarina* sp. nov., isolated from a marine electroactive biofilm, and emended descriptions of *Leisingera methylohalidivorans* Schaefer et al. 2002, *Phaeobacter daeponensis* Yoon et al. 2007 and *Phaeobacter inhibens* Martens et al. 2006. Int. J. Syst. Evol. Microbiol. 58, 2788–2793. https://doi.org/10.1099/ijs.0.65844-0

Vandeputte, O.M., Kiendrebeogo, M., Rasamiravaka, T., Stévigny, C., Duez, P., Rajaonson, S., Diallo, B., Mol, A., Baucher, M., El Jaziri, M., 2011. The flavanone naringenin reduces the production of quorum sensing-controlled virulence factors in *Pseudomonas aeruginosa* PAO1. Microbiology 157, 2120–2132. https://doi.org/10.1099/mic.0.049338-0

VanEpps, J.S., Younger, J.G., 2016. Implantable device-related infection. Shock 46, 597–608. https://doi.org/10.1097/SHK.0000000000000692

Vartoukian, S.R., Palmer, R.M., Wade, W.G., 2010. Strategies for culture of 'unculturable' bacteria: culturing the unculturable. FEMS Microbiol. Lett. no-no. https://doi.org/10.1111/j.1574-6968.2010.02000.x

Vatanyoopaisarn, S., Nazli, A., Dodd, C.E.R., Rees, C.E.D., Waites, W.M., 2000. Effect of flagella on initial attachment of *Listeria monocytogenes* to stainless steel. Appl. Environ. Microbiol. 66, 860–863. https://doi.org/10.1128/AEM.66.2.860-863.2000

Vats, P., Kaur, U.J., Rishi, P., 2022. Heavy metal-induced selection and proliferation of antibiotic resistance: a review. J. Appl. Microbiol. 132, 4058–4076. https://doi.org/10.1111/jam.15492

Veerachamy, S., Yarlagadda, T., Manivasagam, G., Yarlagadda, P.K., 2014. Bacterial adherence and biofilm formation on medical implants: a review. Proc. Inst. Mech. Eng. [H] 228, 1083–1099. https://doi.org/10.1177/0954411914556137

Ventre, I., Ledgham, F., Prima, V., Lazdunski, A., Foglino, M., Sturgis, J.N., 2003. Dimerization of the quorum sensing regulator RhlR: development of a method using EGFP fluorescence anisotropy. Mol. Microbiol. 48, 187–198. https://doi.org/10.1046/j.1365-2958.2003.03422.x

Verbeke, F., De Craemer, S., Debunne, N., Janssens, Y., Wynendaele, E., Van de Wiele, C., De Spiegeleer, B., 2017. Peptides as quorum sensing molecules: measurement techniques and obtained levels *in vitro* and *in vivo*. Front. Neurosci. 11. https://doi.org/10.3389/fnins.2017.00183

Vestby, L.K., Grønseth, T., Simm, R., Nesse, L.L., 2020. Bacterial biofilm and its role in the pathogenesis of disease. Antibiotics 9, 59. https://doi.org/10.3390/antibiotics9020059

Villaverde-Hueso, A., Sánchez-Díaz, G., Molina-Cabrero, F.J., Gallego, E., Posada de la Paz, M., Alonso-Ferreira, V., 2019. Mortality Due to Cystic Fibrosis over a 36-Year Period in Spain: Time Trends and Geographic Variations. Int. J. Environ. Res. Public. Health 16, 119. https://doi.org/10.3390/ijerph16010119

Vishwakarma, V., 2019. Impact of environmental biofilms: industrial components and its remediation. J. Basic Microbiol. 60, 198–206. https://doi.org/10.1002/jobm.201900569

Vladimirov, N., Sourjik, V., 2009. Chemotaxis: how bacteria use memory. bchm 390, 1097–1104. https://doi.org/10.1515/BC.2009.130

von Bodman, S.B., Willey, J.M., Diggle, S.P., 2008. Cell-cell communication in bacteria: united we stand. J. Bacteriol. 190, 4377–4391. https://doi.org/10.1128/JB.00486-08

von Ohle, C., Gieseke, A., Nistico, L., Decker, E.M., deBeer, D., Stoodley, P., 2010. Real-time microsensor measurement of local metabolic activities in *ex vivo* dental biofilms exposed to sucrose and treated with chlorhexidine. Appl. Environ. Microbiol. 76, 2326–2334. https://doi.org/10.1128/AEM.02090-09
von Schnitzler, J., Eggers, R., 1999. Mass transfer in polymers in a supercritical CO_2-atmosphere. J. Supercrit. Fluids 16, 81–92. https://doi.org/10.1016/S0896-8446(99)00020-0
Voutchkov, N., 2017. Diagnostics of membrane fouling and scaling, in: Pretreatment for Reverse Osmosis Desalination. Elsevier, pp. 43–64. https://doi.org/10.1016/B978-0-12-809953-7.00003-6
Vozza, N.F., Abdian, P.L., Russo, D.M., Mongiardini, E.J., Lodeiro, A.R., Molin, S., Zorreguieta, A., 2016. A *Rhizobium leguminosarum* CHDL- (cadherin-like-) lectin participates in assembly and remodeling of the biofilm matrix. Front. Microbiol. 7. https://doi.org/10.3389/fmicb.2016.01608
Vukelic, G., Vizentin, G., Brnic, J., Brcic, M., Sedmak, F., 2021. Long-term marine environment exposure effect on butt-welded shipbuilding steel. J. Mar. Sci. Eng. 9, 491. https://doi.org/10.3390/jmse9050491
Waldrop, R., McLaren, A., Calara, F., McLemore, R., 2014. Biofilm growth has a threshold response to glucose *in vitro*. Clin. Orthop. 472, 3305–3310. https://doi.org/10.1007/s11999-014-3538-5
Walter, M., Safari, A., Ivankovic, A., Casey, E., 2013. Detachment characteristics of a mixed culture biofilm using particle size analysis. Chem. Eng. J. 228, 1140–1147. https://doi.org/10.1016/j.cej.2013.05.071
Wang, G., Zhao, G., Chao, X., Xie, L., Wang, H., 2020. The characteristic of virulence, biofilm and antibiotic resistance of *Klebsiella pneumoniae*. Int. J. Environ. Res. Public. Health 17, 6278. https://doi.org/10.3390/ijerph17176278
Wang, Hui, Xu, J., Du, X., Du, Z., Cheng, X., Wang, Haibo, 2021. A self-healing polyurethane-based composite coating with high strength and anti-corrosion properties for metal protection. Compos. Part B Eng. 225, 109273. https://doi.org/10.1016/j.compositesb.2021.109273
Wang, L., Hou, J., Liu, S., Carrier, A.J., Guo, T., Liang, Q., Oakley, D., Zhang, X., 2019. CuO nanoparticles as haloperoxidase-mimics: chloride-accelerated heterogeneous Cu-Fenton chemistry for H_2O_2 and glucose sensing. Sens. Actuators B Chem. 287, 180–184. https://doi.org/10.1016/j.snb.2019.02.030
Wang, Y., Chen, S., Sun, H., Li, W., Hu, C., Ren, K., 2018. Recent progresses in microfabricating perfluorinated polymers (teflons) and the associated new applications in microfluidics. Microphysiological Syst. 1, 1–1. https://doi.org/10.21037/mps.2018.08.02
Water Environment Federation (Ed.), 2014. Wastewater treatment process modeling, Second edition. ed, WEF manual of practice. WEF Press, Water Environment Federation ; McGraw-Hill Education, Alexandria, Virginia : New York.
Waterfield, N.R., Ciche, T., Clarke, D., 2009. *Photorhabdus* and a host of hosts. Annu. Rev. Microbiol. 63, 557–574. https://doi.org/10.1146/annurev.micro.091208.073507
Waters, C.M., Bassler, B.L., 2005. Quorum sensing: cell-to-cell communication in bacteria. Annu. Rev. Cell Dev. Biol. 21, 319–346. https://doi.org/10.1146/annurev.cellbio.21.012704.131001
Watnick, P., Kolter, R., 2000. Biofilm, city of microbes. J. Bacteriol. 182, 2675–2679. https://doi.org/10.1128/JB.182.10.2675-2679.2000

Watson, B., Currier, T.C., Gordon, M.P., Chilton, M.D., Nester, E.W., 1975. Plasmid required for virulence of *Agrobacterium tumefaciens*. J. Bacteriol. 123, 255–264. https://doi.org/10.1128/jb.123.1.255-264.1975
Watson, C., Senyo, S., 2019. All-in-one automated microfluidics control system. HardwareX 5, e00063. https://doi.org/10.1016/j.ohx.2019.e00063
Wei, H., Zhuo, R.-X., Zhang, X.-Z., 2013. Design and development of polymeric micelles with cleavable links for intracellular drug delivery. Prog. Polym. Sci. 38, 503–535. https://doi.org/10.1016/j.progpolymsci.2012.07.002
Weibel, D.B., DiLuzio, W.R., Whitesides, G.M., 2007. Microfabrication meets microbiology. Nat. Rev. Microbiol. 5, 209–218. https://doi.org/10.1038/nrmicro1616
Wetzstein, H.-G., 2005. Comparative mutant prevention concentrations of pradofloxacin and other veterinary fluoroquinolones indicate differing potentials in preventing selection of resistance. Antimicrob. Agents Chemother. 49, 4166–4173. https://doi.org/10.1128/AAC.49.10.4166-4173.2005
Whiteley, M., Bangera, M.G., Bumgarner, R.E., Parsek, M.R., Teitzel, G.M., Lory, S., Greenberg, E.P., 2001. Gene expression in *Pseudomonas aeruginosa* biofilms. Nature 413, 860–864. https://doi.org/10.1038/35101627
Whitney, J.C., Howell, P.L., 2013. Synthase-dependent exopolysaccharide secretion in Gram-negative bacteria. Trends Microbiol. 21, 63–72. https://doi.org/10.1016/j.tim.2012.10.001
Wi, Y.M., Patel, R., 2018. Understanding biofilms and novel approaches to the diagnosis, prevention, and treatment of medical device-associated infections. Infect. Dis. Clin. North Am. 32, 915–929. https://doi.org/10.1016/j.idc.2018.06.009
Wiechert, J., Filipchyk, A., Hünnefeld, M., Gätgens, C., Brehm, J., Heermann, R., Frunzke, J., 2020. Deciphering the rules underlying xenogeneic silencing and counter-silencing of Lsr2-like proteins using CgpS of *Corynebacterium glutamicum* as a model. mBio 11, e02273-19. https://doi.org/10.1128/mBio.02273-19
Wille, J., Coenye, T., 2020. Biofilm dispersion: the key to biofilm eradication or opening Pandora's box? Biofilm 2, 100027. https://doi.org/10.1016/j.bioflm.2020.100027
Williamson, K.S., Richards, L.A., Perez-Osorio, A.C., Pitts, B., McInnerney, K., Stewart, P.S., Franklin, M.J., 2012. Heterogeneity in *Pseudomonas aeruginosa* biofilms includes expression of ribosome hibernation factors in the antibiotic-tolerant subpopulation and hypoxia-induced stress response in the metabolically active population. J. Bacteriol. 194, 2062–2073. https://doi.org/10.1128/JB.00022-12
Wingender, J., Neu, T.R., Flemming, H.-C. (Eds.), 1999. Microbial extracellular polymeric substances. Springer Berlin Heidelberg, Berlin, Heidelberg. https://doi.org/10.1007/978-3-642-60147-7
Winson, M.K., Camara, M., Latifi, A., Foglino, M., Chhabra, S.R., Daykin, M., Bally, M., Chapon, V., Salmond, G.P., Bycroft, B.W., 1995. Multiple *N*-acyl-L-homoserine lactone signal molecules regulate production of virulence determinants and secondary metabolites in *Pseudomonas aeruginosa*. Proc. Natl. Acad. Sci. 92, 9427–9431. https://doi.org/10.1073/pnas.92.20.9427
Wolcott, R.D., Rhoads, D.D., Bennett, M.E., Wolcott, B.M., Gogokhia, L., Costerton, J.W., Dowd, S.E., 2010. Chronic wounds and the medical biofilm paradigm. J. Wound Care 19, 45–53. https://doi.org/10.12968/jowc.2010.19.2.46966

Wu, C.-M., Naseem, S., Chou, M.-H., Wang, J.-H., Jian, Y.-Q., 2019. Recent advances in tungsten-oxide-based materials and their applications. Front. Mater. 6, 49. https://doi.org/10.3389/fmats.2019.00049
Wu, L., Luo, Y., 2021. Bacterial quorum-sensing systems and their role in intestinal bacteria-host crosstalk. Front. Microbiol. 12, 611413. https://doi.org/10.3389/fmicb.2021.611413
Xavier, J.B., Foster, K.R., 2007. Cooperation and conflict in microbial biofilms. Proc. Natl. Acad. Sci. 104, 876–881. https://doi.org/10.1073/pnas.0607651104
Xu, F.-F., Morohoshi, T., Wang, W.-Z., Yamaguchi, Y., Liang, Y., Ikeda, T., 2014. Evaluation of intraspecies interactions in biofilm formation by *Methylobacterium* species isolated from pink-pigmented household biofilms. Microbes Environ. 29, 388–392. https://doi.org/10.1264/jsme2.ME14038
Xu, L.-C., Logan, B.E., 2005. Interaction forces between colloids and protein-coated surfaces measured using an atomic force microscope. Environ. Sci. Technol. 39, 3592–3600. https://doi.org/10.1021/es048377i
Xu, Y., He, Q., Liu, C., Huangfu, X., 2019. Are micro- or nanoplastics leached from drinking water distribution systems? Environ. Sci. Technol. 53, 9339–9340. https://doi.org/10.1021/acs.est.9b03673
Xu, Y., Liu, X., Zheng, Y., Li, C., Kwok Yeung, K.W., Cui, Z., Liang, Y., Li, Z., Zhu, S., Wu, S., 2021. Ag_3PO_4 decorated black urchin-like defective TiO_2 for rapid and long-term bacteria-killing under visible light. Bioact. Mater. 6, 1575–1587. https://doi.org/10.1016/j.bioactmat.2020.11.013
Yabuuchi, E., Yano, I., Oyaizu, H., Hashimoto, Y., Ezaki, T., Yamamoto, H., 1990. Proposals of *Sphingomonas paucimobilis* gen. nov. and comb. nov., *Sphingomonas parapaucimobilis* sp. nov., *Sphingomonas yanoikuyae* sp. nov., *Sphingomonas adhaesiva* sp. nov., *Sphingomonas capsulata* comb, nov., and Two Genospecies of the Genus *Sphingomonas*. Microbiol. Immunol. 34, 99–119. https://doi.org/10.1111/j.1348-0421.1990.tb00996.x
Yamashita, T., Yamamoto-Ikemoto, R., 2014. Nitrogen and phosphorus removal from wastewater treatment plant effluent via bacterial sulfate reduction in an anoxic bioreactor packed with wood and iron. Int. J. Environ. Res. Public. Health 11, 9835–9853. https://doi.org/10.3390/ijerph110909835
Yan, L., Boyd, K.G., Adams, D.R., Burgess, J.G., 2003. Biofilm-specific cross-species induction of antimicrobial compounds in *Bacilli*. Appl. Environ. Microbiol. 69, 3719–3727. https://doi.org/10.1128/AEM.69.7.3719-3727.2003
Yang, Z., Sun, Z., Ren, Y., Chen, X., Zhang, W., Zhu, X., Mao, Z., Shen, J., Nie, S., 2019. Advances in nanomaterials for use in photothermal and photodynamic therapeutics (review). Mol. Med. Rep. https://doi.org/10.3892/mmr.2019.10218
Yawata, Y., Nomura, N., Uchiyama, H., 2008. Development of a novel biofilm continuous culture method for simultaneous assessment of architecture and gaseous metabolite production. Appl. Environ. Microbiol. 74, 5429–5435. https://doi.org/10.1128/AEM.00801-08
Yin, W., Wang, Y., Liu, L., He, J., 2019. Biofilms: the microbial “protective clothing” in extreme environments. Int. J. Mol. Sci. 20, 3423. https://doi.org/10.3390/ijms20143423
Yoon, S.S., Hennigan, R.F., Hilliard, G.M., Ochsner, U.A., Parvatiyar, K., Kamani, M.C., Allen, H.L., DeKievit, T.R., Gardner, P.R., Schwab, U., Rowe, J.J., Iglewski, B.H., McDermott, T.R., Mason, R.P., Wozniak, D.J., Hancock, R.E.W., Parsek, M.R., Noah, T.L., Boucher, R.C., Hassett, D.J., 2002. *Pseudomonas aeruginosa* anaerobic respiration in biofilms: relationships to

cystic fibrosis pathogenesis. Dev. Cell 3, 593–603. https://doi.org/10.1016/S1534-5807(02)00295-2
Yougbaré, S., Mutalik, C., Krisnawati, D.I., Kristanto, H., Jazidie, A., Nuh, M., Cheng, T.-M., Kuo, T.-R., 2020. Nanomaterials for the photothermal killing of bacteria. Nanomaterials 10, 1123. https://doi.org/10.3390/nano10061123
Yu, P., Wang, C., Zhou, J., Jiang, L., Xue, J., Li, W., 2016. Influence of surface properties on adhesion forces and attachment of *Streptococcus mutans* to Zirconia *in vitro*. BioMed Res. Int. 2016, 1–10. https://doi.org/10.1155/2016/8901253
Zaferani, S.H., 2018. Introduction of polymer-based nanocomposites, in: Polymer-Based Nanocomposites for Energy and Environmental Applications. Elsevier, pp. 1–25. https://doi.org/10.1016/B978-0-08-102262-7.00001-5
Zamora-Lagos, M.-A., Eckstein, S., Langer, A., Gazanis, A., Pfeiffer, F., Habermann, B., Heermann, R., 2018. Phenotypic and genomic comparison of *Photorhabdus luminescens* subsp. *laumondii* TT01 and a widely used rifampicin-resistant *Photorhabdus luminescens* laboratory strain. BMC Genomics 19, 854. https://doi.org/10.1186/s12864-018-5121-z
Zelezniak, A., Andrejev, S., Ponomarova, O., Mende, D.R., Bork, P., Patil, K.R., 2015. Metabolic dependencies drive species co-occurrence in diverse microbial communities. Proc. Natl. Acad. Sci. 112, 6449–6454. https://doi.org/10.1073/pnas.1421834112
Zhang, J., Gong, F., Li, L., Zhao, M., Song, J., 2014. *Pseudomonas aeruginosa* quorum-sensing molecule *N*-(3-oxododecanoyl) homoserine lactone attenuates lipopolysaccharide-induced inflammation by activating the unfolded protein response. Biomed. Rep. 2, 233–238. https://doi.org/10.3892/br.2014.225
Zhang, T., Yang, H.C., Miyamoto, C.M., 2014. 3D printing: a cost effective and timely approach to manufacturing of low-thrust engines, in: 50th AIAA/ASME/SAE/ASEE Joint Propulsion Conference. Presented at the 50th AIAA/ASME/SAE/ASEE Joint Propulsion Conference, American Institute of Aeronautics and Astronautics, Cleveland, OH. https://doi.org/10.2514/6.2014-3502
Zhang, W., Li, C., 2016. Exploiting quorum sensing interfering strategies in Gram-negative bacteria for the enhancement of environmental applications. Front. Microbiol. 6. https://doi.org/10.3389/fmicb.2015.01535
Zhang, Y., Tseng, T.-M., Schlichtmann, U., 2021. Portable all-in-one automated microfluidic system (PAMICON) with 3D-printed chip using novel fluid control mechanism. Sci. Rep. 11, 19189. https://doi.org/10.1038/s41598-021-98655-9
Zhao, K., Tseng, B.S., Beckerman, B., Jin, F., Gibiansky, M.L., Harrison, J.J., Luijten, E., Parsek, M.R., Wong, G.C.L., 2013. Psl trails guide exploration and microcolony formation in *Pseudomonas aeruginosa* biofilms. Nature 497, 388–391. https://doi.org/10.1038/nature12155
Zhao, W., Dao, C., Karim, M., Gomez-Chiarri, M., Rowley, D., Nelson, D.R., 2016. Contributions of tropodithietic acid and biofilm formation to the probiotic activity of *Phaeobacter inhibens*. BMC Microbiol. 16, 1. https://doi.org/10.1186/s12866-015-0617-z
Zheng, Y., He, L., Asiamah, T.K., Otto, M., 2018. Colonization of medical devices by *staphylococci*. Environ. Microbiol. 20, 3141–3153. https://doi.org/10.1111/1462-2920.14129

Zhong, S., He, S., 2021. Quorum sensing inhibition or quenching in *Acinetobacter baumannii*: the novel therapeutic strategies for new drug development. Front. Microbiol. 12, 558003. https://doi.org/10.3389/fmicb.2021.558003
Zhou, L., Zhang, Y., Ge, Y., Zhu, X., Pan, J., 2020. Regulatory mechanisms and promising applications of quorum sensing-inhibiting agents in control of bacterial biofilm formation. Front. Microbiol. 11, 589640. https://doi.org/10.3389/fmicb.2020.589640
Zhu, J., Beaber, J.W., Moré, M.I., Fuqua, C., Eberhard, A., Winans, S.C., 1998. Analogs of the autoinducer 3-oxooctanoyl-homoserine lactone strongly inhibit activity of the TraR protein of *Agrobacterium tumefaciens*. J. Bacteriol. 180, 5398–5405. https://doi.org/10.1128/JB.180.20.5398-5405.1998
Zhu, Z., Shan, L., Hu, F., Li, Z., Zhong, D., Yuan, Y., Zhang, J., 2020. Biofilm formation potential and chlorine resistance of typical bacteria isolated from drinking water distribution systems. RSC Adv. 10, 31295–31304. https://doi.org/10.1039/D0RA04985A
Zimmerli, W., Sendi, P., 2017. Orthopaedic biofilm infections. APMIS 125, 353–364. https://doi.org/10.1111/apm.12687
Zogaj, X., Nimtz, M., Rohde, M., Bokranz, W., Romling, U., 2001. The multicellular morphotypes of *Salmonella typhimurium* and *Escherichia coli* produce cellulose as the second component of the extracellular matrix. Mol. Microbiol. 39, 1452–1463. https://doi.org/10.1046/j.1365-2958.2001.02337.x
Zschiedrich, C.P., Keidel, V., Szurmant, H., 2016. Molecular mechanisms of two-component signal transduction. J. Mol. Biol. 428, 3752–3775. https://doi.org/10.1016/j.jmb.2016.08.003

Supplements

Table S.1: The extracts used for the screening of the marine and drinking water bacteria.

No.	Strain	Modification	Reference
1	*Escherichia coli* DH10B MtaA-pCOLA-P_{ara}-P_{tacI}	Insertion of pCOLA with a P_{ara} and P_{tacI} promoter serving as a control	[redacted] (Goethe-Universität Frankfurt am Main)
2	*Escherichia coli* DH10B MtaA-pCX39	Insertion of pCX39 for the overproduction of secondary metabolite class xenortides	[redacted] (Goethe-Universität Frankfurt am Main)
3	*Escherichia coli* DH10B MtaA-pCX39	Insertion of pCX39 for the overproduction of secondary metabolite class of xenortides/tryptamines	[redacted] (Goethe-Universität Frankfurt am Main)
4	*Escherichia coli* DH10B MtaA-pCX4	Insertion of pCX4 for the overproduction of secondary metabolite class of nevaltophines	[redacted] (Goethe-Universität Frankfurt am Main)
5	*Escherichia coli* DH10B MtaA-pCX41	Insertion of pCX41 for the overproduction of secondary metabolite class of rhabdopeptides	[redacted] (Goethe-Universität Frankfurt am Main)
6	*Escherichia coli* DH10B MtaA-pCX41	Insertion of pCX41 for the overproduction of secondary metabolite class of rhabdopeptides/tryptamines	[redacted] (Goethe-Universität Frankfurt am Main)
7	*Escherichia coli* DH10B MtaA-pCX47	Insertion of pCX47 for the overproduction of secondary metabolite class of nematophines/tryptamines	[redacted] (Goethe-Universität Frankfurt am Main)
8	*Escherichia coli* DH10B MtaA-pCX65-pCX61	Insertion of pCX65 and pCX61 for the overproduction of secondary metabolite class of putrescines	[redacted] (Goethe-Universität Frankfurt am Main)
9	*Escherichia coli* DH10B MtaA-pCX71	Insertion of pCX71 for the overproduction of secondary metabolite class of leurhabdopeptides	[redacted] (Goethe-Universität Frankfurt am Main)

10	*Photorhabdus luminescens* subsp. *namnaonensis* PB45.5	Wild type	(Glaeser et al., 2017), (Machado et al., 2018)
11	*Photorhabdus luminescens* subsp. *namnaonensis* PB45.5 Δ*hfq*	Δ*hfq*	[redacted] (Goethe-Universität Frankfurt am Main)
12	*Photorhabdus luminescens* subsp. *namnaonensis* PB45.5 Δ*hfq* + pct83_145-147/1	Δ*hfq*; Production of secondary metabolite class of kollosins	[redacted] (Goethe-Universität Frankfurt am Main)
13	*Photorhabdus luminescens* subsp. *namnaonensis* PB45.5 Δhfq + pct87_6/1	Δ*hfq*; Production of so far unknown secondary metabolites	[redacted] (Goethe-Universität Frankfurt am Main)
14	*Photorhabdus luminescens* subsp. *namnaonensis* PB45.5 Δ*hfq* + pct87_7/1	Δ*hfq*; Production of so far unknown secondary metabolites	[redacted] (Goethe-Universität Frankfurt am Main)
15	*Photorhabdus luminescens* subsp. *namnaonensis* PB45.5 Δ*hfq* + pct87_8-10/2	Δ*hfq*; Production of so far unknown secondary metabolites	[redacted] (Goethe-Universität Frankfurt am Main)
16	*Photorhabdus luminescens* subsp. *laumondii* TT01	Wild type	(Fischer-Le Saux et al., 1999)
17	*Photorhabdus luminescens* subsp. *laumondii* TT01 + *antJ*+++	Overexpression of *antJ*	[redacted] (Goethe-Universität Frankfurt am Main)
18	*Photorhabdus luminescens* subsp. *laumondii* TT01 Δ*antJ*	Δ*antJ*	[redacted] (Goethe-Universität Frankfurt am Main)

19	*Photorhabdus luminescens* subsp. *laumondii* TT01 Δ*hfq*	Δ*hfq*	[redacted] (Goethe-Universität Frankfurt am Main)
20	*Photorhabdus luminescens* subsp. *laumondii* TT01 Δ*hfq* pCEP-KM-*plu2670*	Δ*hfq*; Production of the secondary metabolite class of kolossins	[redacted] (Goethe-Universität Frankfurt am Main)
21	*Photorhabdus luminescens* subsp. *laumondii* TT01 Δ*hfq* pCEP-KM-*plu3130*	Δ*hfq*; Production of so far unknown secondary metabolites	[redacted] (Goethe-Universität Frankfurt am Main)
22	*Photorhabdus luminescens* subsp. *laumondii* TT01 Δ*hfq* pCEP-*plu1881*	Δ*hfq*; Production of the secondary metabolite class of glidobactins	[redacted] (Goethe-Universität Frankfurt am Main)
23	*Photorhabdus luminescens* subsp. *laumondii* TT01 Δ*hfq* pCEP-*plu3123*	Δ*hfq*; Production of the secondary metabolite class of ririwpeptides	[redacted] (Goethe-Universität Frankfurt am Main)
24	*Photorhabdus luminescens* subsp. *laumondii* TT01 Δ*hfq* pCEP-*plu3263*	Δ*hfq*; Production of the secondary metabolite class of GameXPeptides	[redacted] (Goethe-Universität Frankfurt am Main)
25	*Xenorhabdus doucetiae* DSM 17909	Wild type	(Tailliez et al., 2006)
26	*Xenorhabdus doucetiae* DSM 17909 Δ*hfq*	Δ*hfq*	[redacted] (Goethe-Universität Frankfurt am Main)
27	*Xenorhabdus doucetiae* DSM 17909 Δ*hfq* pBAD 70082	Δ*hfq*; Production of so far unknown secondary metabolites	[redacted] (Goethe-Universität Frankfurt am Main)
28	*Xenorhabdus doucetiae* DSM 17909 Δ*hfq* pBAD DC	Δ*hfq*; Production of the secondary metabolite class of phenylethylamides/tryptamides	[redacted] (Goethe-Universität Frankfurt am Main)

29	*Xenorhabdus doucetiae* DSM 17909 Δ*hfq* pBAD *gxpsA*	Δ*hfq*; Production of the secondary metabolite class of GameXPeptides	[redacted] (Goethe-Universität Frankfurt am Main)
30	*Xenorhabdus doucetiae* DSM 17909 Δ*hfq* pBAD XabA	Δ*hfq*; Production of the secondary metabolite class of xenoamicins	[redacted] (Goethe-Universität Frankfurt am Main)
31	*Xenorhabdus doucetiae* DSM 17909 Δ*hfq* pBAD XacA	Δ*hfq*; Production of the secondary metabolite class of xenoautocins	[redacted] (Goethe-Universität Frankfurt am Main)
32	*Xenorhabdus doucetiae* DSM 17909 Δ*hfq* pBAD_PAX-KM	Δ*hfq*; Production of the secondary metabolite class of PAX peptides	[redacted] (Goethe-Universität Frankfurt am Main)
33	*Xenorhabdus doucetiae* DSM 17909 Δ*hfq* pBAD_*xcnA*-KM	Δ*hfq*; Production of the secondary metabolite class of xenocoumacins	[redacted] (Goethe-Universität Frankfurt am Main)
34	*Xenorhabdus doucetiae* DSM 17909 Δ*hfq* pBAD_*xrdA*-KM	Δ*hfq*; Production of the secondary metabolite class of xenorhabdins	[redacted] (Goethe-Universität Frankfurt am Main)
35	*Xenorhabdus nematophila* DSM 3370	Wild type	(Thomas and Poinar, 1979)
36	*Xenorhabdus nematophila* DSM 3370 Δ*hfq*	Δ*hfq*	[redacted] (Goethe-Universität Frankfurt am Main)
37	*Xenorhabdus nematophila* DSM 3370 Δ*hfq* PAX	Δ*hfq*; Production of the secondary metabolite class of PAX peptides	[redacted] (Goethe-Universität Frankfurt am Main)
38	*Xenorhabdus nematophila* DSM 3370 Δ*hfq* PAX	Δ*hfq*; Production of the secondary metabolite class of PAX peptides	[redacted] (Goethe-Universität Frankfurt am Main)

39	*Xenorhabdus nematophila* DSM 3370 Δ*hfq* pCEP-KM-Xenoamicine	Δ*hfq*; Production of the secondary metabolite class of PAX peptides	[redacted] (Goethe-Universität Frankfurt am Main)
40	*Xenorhabdus nematophila* DSM 3370 Δ*hfq* pCEP-KM-Xenocoumacine	Δ*hfq*; Production of the secondary metabolite class of xenocoumacins	[redacted] (Goethe-Universität Frankfurt am Main)
41	*Xenorhabdus nematophila* DSM 3370 Δ*hfq* pCEP-KM-Xenortide	Δ*hfq*; Production of the secondary metabolite class of xenortides	[redacted] (Goethe-Universität Frankfurt am Main)
42	*Xenorhabdus nematophila* DSM 3370 Δ*hfq* pCEP-KM-Xenotetrapeptide	Δ*hfq*; Production of the secondary metabolite class of xenotetrapeptides	[redacted] (Goethe-Universität Frankfurt am Main)
43	*Xenorhabdus szentirmaii* DSM 16338	Wild type	(Lengyel et al., 2005)
44	*Xenorhabdus szentirmaii* DSM 16338 Δ*hfq*	Δ*hfq*	[redacted] (Goethe-Universität Frankfurt am Main)
45	*Xenorhabdus szentirmaii* DSM 16338 Δ*hfq* pCEP-KM-0346	Δ*hfq*; Production of the secondary metabolite class of GameXPeptides	[redacted] (Goethe-Universität Frankfurt am Main)
46	*Xenorhabdus szentirmaii* DSM 16338 Δ*hfq* pCEP-KM-0377	Δ*hfq*; Production of so far unknown secondary metabolites	[redacted] (Goethe-Universität Frankfurt am Main)
47	*Xenorhabdus szentirmaii* DSM 16338 Δ*hfq* pCEP-KM-1979	Δ*hfq*; Production of the secondary metabolite class of dipeptides	[redacted] (Goethe-Universität Frankfurt am Main)
48	*Xenorhabdus szentirmaii* DSM 16338 Δ*hfq* pCEP-KM-3397	Δ*hfq*; Production of the secondary metabolite class of rhabdopeptides	[redacted] (Goethe-Universität Frankfurt am Main)

49	*Xenorhabdus szentirmaii* DSM 16338 Δ*hfq* pCEP-KM-3460	Δ*hfq*; Production of the secondary metabolite class of szentiamides	[redacted] (Goethe-Universität Frankfurt am Main)
50	*Xenorhabdus szentirmaii* DSM 16338 Δ*hfq* pCEP-KM-3663	Δ*hfq*; Production of so far unknown secondary metabolites	[redacted] (Goethe-Universität Frankfurt am Main)
51	*Xenorhabdus szentirmaii* DSM 16338 Δ*hfq* pCEP-KM-3680	Δ*hfq*; Production of the secondary metabolite class of xenobactins	[redacted] (Goethe-Universität Frankfurt am Main)
52	*Xenorhabdus szentirmaii* DSM 16338 Δ*hfq* pCEP-KM-3942	Δ*hfq*; Production of the secondary metabolite class of rhabduscins	[redacted] (Goethe-Universität Frankfurt am Main)
53	*Xenorhabdus szentirmaii* DSM 16338 Δ*hfq* pCEP-KM-5118	Δ*hfq*; Production of the secondary metabolite class of jenamidins	[redacted] (Goethe-Universität Frankfurt am Main)
54	*Xenorhabdus szentirmaii* DSM 16338 Δ*hfq* pCEP-KM-*fclC*	Δ*hfq*; Production of the secondary metabolite class of fabclavins	[redacted] (Goethe-Universität Frankfurt am Main)
55	*Xenorhabdus szentirmaii* DSM 16338 Δ*hfq* pCEP-KM-*xfsA*	Δ*hfq*; Production of the secondary metabolite class of xenofuranones	[redacted] (Goethe-Universität Frankfurt am Main)
56	*Xenorhabdus szentirmaii* DSM 16338 Δ*hfq*-hmwp2	Δ*hfq*; Production of the secondary metabolite class of yersiniabactins	[redacted] (Goethe-Universität Frankfurt am Main)

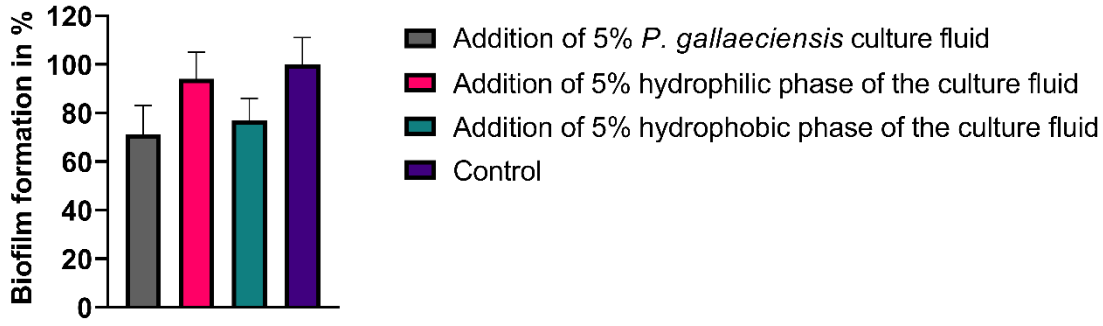

Fig. S.1 Effect of the hydrophilic and hydrophobic phase of culture fluid of *P. gallaeciensis* on biofilm of *P. aeruginosa*. The hydrophilic and hydrophobic phases were each diluted and tested for biofilm inhibitory effect in *P. aeruginosa*. The addition of only 5% 2216 medium served as a control. Error bars represent standard deviation of three biologically independently performed experiments.

Acknowledgements

Curriculum vitae